

INFORMATION TO USERS

This manuscript has been reproduced from the microfilm master. UMI films the text directly from the original or copy submitted. Thus, some thesis and dissertation copies are in typewriter face, while others may be from any type of computer printer.

The quality of this reproduction is dependent upon the quality of the copy submitted. Broken or indistinct print, colored or poor quality illustrations and photographs, print bleedthrough, substandard margins, and improper alignment can adversely affect reproduction.

In the unlikely event that the author did not send UMI a complete manuscript and there are missing pages, these will be noted. Also, if unauthorized copyright material had to be removed, a note will indicate the deletion.

Oversize materials (e.g., maps, drawings, charts) are reproduced by sectioning the original, beginning at the upper left-hand corner and continuing from left to right in equal sections with small overlaps.

Photographs included in the original manuscript have been reproduced xerographically in this copy. Higher quality 6" x 9" black and white photographic prints are available for any photographs or illustrations appearing in this copy for an additional charge. Contact UMI directly to order.

**ProQuest Information and Learning
300 North Zeeb Road, Ann Arbor, MI 48106-1346 USA
800-521-0600**

UMI[®]

Anisotropic Lattice Thermal Diffusivity in Olivines and Pyroxenes to High Temperatures

Michael Damian Harrell

**A dissertation submitted in partial fulfillment of the
requirements for the degree of**

Doctor of Philosophy

University of Washington

2002

Program Authorized to Offer Degree: The Department of Geological Sciences

UMI Number: 3053509

Copyright 2002 by
Harrell, Michael Damian

All rights reserved.

UMI[®]

UMI Microform 3053509

Copyright 2002 by ProQuest Information and Learning Company.
All rights reserved. This microform edition is protected against
unauthorized copying under Title 17, United States Code.

ProQuest Information and Learning Company
300 North Zeeb Road
P.O. Box 1346
Ann Arbor, MI 48106-1346

©Copyright 2002
Michael Damian Harrell

In presenting this dissertation in partial fulfillment of the requirements for the Doctoral degree at the University of Washington, I agree that the Library shall make its copies freely available for inspection. I further agree that extensive copying of the dissertation is allowable only for scholarly purposes, consistent with "fair use" as prescribed in the U.S. Copyright Law. Requests for copying or reproduction of this dissertation may be referred to Bell and Howell Information and Learning, 300 North Zeeb Road, Ann Arbor, MI 48106-1346, to whom the author has granted "the right to reproduce and sell (a) copies of the manuscript in microform and/or (b) printed copies of the manuscript made from microform."

Signature Michael Damian Hummel

Date 11 June 2002

University of Washington
Graduate School

This is to certify that I have examined this copy of a doctoral dissertation by

Michael Damian Harrell


and have found that it is complete and satisfactory in all respects,
and that any and all revisions required by the final
examining committee have been made.

Chair of Supervisory Committee:

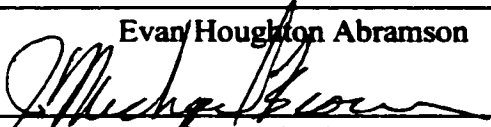


John Michael Brown

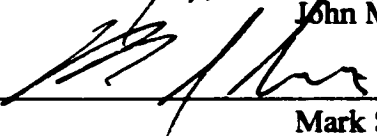
Reading Committee:



Evan Houghton Abramson



John Michael Brown



Mark Stefan Ghiorso

Date: 11 June 2002

University of Washington

Abstract

Anisotropic Lattice Thermal Diffusivity in Olivines and Pyroxenes to High Temperatures

Michael Damian Harrell

**Chair of the Supervisory Committee:
Professor John Michael Brown
The Department of Earth and Space Sciences**

The anisotropic lattice thermal diffusivity of three olivines (Fo_0 , Fo_{78} , and Fo_{91}), one orthopyroxene (En_{91}), and one clinopyroxene ($\text{Di}_{72}\text{He}_9\text{Jd}_3\text{Cr}_3\text{Ts}_{12}$) have been measured via impulsive stimulated light scattering, permitting the calculation of their lattice thermal diffusivity tensors to high temperatures. For Fo_0 olivine, measurements extend from room temperature to 600°C , for Fo_{78} to 900°C , and for Fo_{91} to 1000°C , all in steps of 100°C . The orthopyroxene also was taken in steps to 1000°C , while the clinopyroxene was measured at room temperature. A limited set of room-temperature measurements to 5 GPa on a fourth olivine (Fo_{89}) is also included. Diffusivities have been combined with calculations of density and specific heat to determine the lattice thermal conductivity tensors. An earlier theory that explains the observed behavior in terms of a positive lower bound on the phonon mean free path is discussed, and the data are used to constrain a model of thermal conductivity at high temperature. The relative contributions of optic and acoustic modes are evaluated from analysis of published dispersion curves.

Five conclusions are reached: First, the anisotropy of lattice thermal conductivity remains essentially unchanged over the observed range of temperatures, indicating that anisotropy remains significant under upper-mantle conditions, and, in regions displaying preferred alignment, may account for observed lateral variations in the geotherm. Second, thermal conductivity departs significantly from earlier predictions of its temperature dependence; this may be understood in terms of a phonon mean free path that cannot diminish below 1.75 times the mean interatomic spacing. Third, for olivine, the optic modes have group velocities that are approximately one-third those of the acoustic modes, and do not dominate lattice conduction despite their greater number. Fourth, impurity scattering is significant along the olivine Fe-Mg solid solution series, but is not appreciable near the endpoints and therefore likely does not play a major role in the upper mantle. Fifth, the historic underestimation of lattice thermal conductivity at temperature has led to an overestimation of radiative conductivity; radiative transport, although significant, plays an even smaller role in the upper mantle than has heretofore been assumed.

TABLE OF CONTENTS

	Page
List of Figures	iv
List of Tables	vi
Introduction.....	1
Materials:	
Sample Descriptions.....	5
Selection and Preparation of Single Crystals.....	8
Selection of Mineral Grains	8
Orientation of Single Crystals	9
Grinding, Polishing, and Coring.....	12
Methods:	
Measurement of Thermal Diffusivity.....	18
Theoretical Considerations.....	18
Traditional Techniques	20
Impulsive Stimulated Light Scattering	21
Generation of High Temperature	24
Main Vacuum Furnace.....	24
Auxiliary Furnace	26
Temperature Measurement and Control	28
Generation of High Pressure.....	29
Data Collection	30
General Procedures.....	30
Procedures Unique to the Collection of the Clinopyroxene Data ..	33
Results:	
Overview of the Analysis of Data.....	36
Individual Measurements	37
Methanol Standards	37
Thermal Diffusivities.....	38
Anisotropic Thermal Diffusivity Tensors.....	41
General Practices in Calculating the Tensors.....	41
Further Calculations for KH-CPX.....	44
Anisotropic Thermal Conductivity Tensors	46

Discussion:	Features of Interest in the Data	83
	The Degree of Anisotropy in Thermal Diffusivity	83
	Deviations from a Simple Inverse Dependence on Temperature	85
	Preferred Model for Thermal Conductivity	86
	Preferred Model	87
	Potential Refinement of the Model	90
	Contribution of Optic Modes	90
	High-Pressure Olivine	93
	The Forsterite-Fayalite Solid Solution in Olivine	95
	Radiative Heat Transport	97
	Directions for Future Work	98
List of References		121
Appendix A: Complete Set of Thermal Diffusivity Measurements		130
	KH-OLV	131
	6 August 1999	131
	11 August 1999	132
	14 August 1999	132
	19 August 1999, first set (a)	135
	19 August 1999, second set (b)	135
	24 August 1999	136
	15 September 1999	139
	17 September 1999	140
	20 September 1999	141
	22 September 1999	142
	28 September 1999	143
	1 October 1999	143
	4 October 1999	144
	6 October 1999	149
	18 October 1999	150
	SC73-10	153
	19 September 2000	153
	20 September 2000	155
	21 September 2000	156
	23 September 2000	160
	28 September 2000	161
	2 October 2000	162
	FA-147337	166
	29 March 2000	166
	30 March 2000	167
	31 March 2000	168
	5 April 2000	169
	6 April 2000	170
	7 April 2000	171
	10 April 2000	173

	Page
17 April 2000.....	174
18 April 2000.....	175
KH-OPX	176
20 October 1999	176
21 October 1999	179
26 October 1999	183
28 October 1999	184
29 October 1999	184
KH-CPX	192
26 March 1998, first set (a)	192
26 March 1998, second set (b)	192
27 March 1998.....	192
31 March 1998.....	193
1 April 1998	194
15 April 1998, a° -normal	194
15 April 1998, b -normal.....	195
16 July 1998	196
17 July 1998	197
22 July 1998	197
23 July 1998	198
SCchai	199
10 October 2000, room pressure	199
10 October 2000, P1(R1) 3.22, P1(R2) 3.24, P2(R1) 3.21, P2(R2) 3.23 GPa	200
11 October 2000, room pressure	201
18 October 2000, 3.22 GPa	202
18 October 2000, P(R1) 5.09, P(R2) 5.08 GPa	203
19 October 2000, P(R1) 5.09, P(R2) 5.13 GPa	203
19 October 2000, room pressure	203
Appendix B: MATLAB Files Used in Processing the Data.....	205

LIST OF FIGURES

Figure Number	Page
1. Machine Drawings for Auxiliary Furnace	35
2. Processing of a Methanol Standard	49
3. Measurement of Thermal Diffusivity in a Single Direction	50
4. Extraction of Characteristic Time from the Data	51
5. Round of Data Within a Crystallographic Plane	52
6. Unexpected Rotation of a Sample with Increasing Temperature.....	53
7. Anisotropic Lattice Thermal Diffusivities for KH-OLV to 1000°C	54
8. Anisotropic Lattice Thermal Diffusivities for SC73-10 to 900°C	55
9. Anisotropic Lattice Thermal Diffusivities for FA-147337 to 600°C	56
10. Anisotropic Lattice Thermal Diffusivities for KH-OPX to 1000°C	57
11. Isotropic Average Lattice Thermal Diffusivities for KH-OLV to 1000°C.....	58
12. Isotropic Average Lattice Thermal Diffusivities for SC73-10 to 600°C.....	59
13. Isotropic Average Lattice Thermal Diffusivities for FA-147337 to 400°C.....	60
14. Isotropic Average Lattice Thermal Diffusivities for KH-OPX to 1000°C	61
15. Representation of Thermal Diffusivity in the a - c Plane of KH-CPX.....	62
16. Anisotropic Lattice Thermal Conductivities for KH-OLV to 1000°C	63
17. Anisotropic Lattice Thermal Conductivities for SC73-10 to 900°C	64

Figure Number	Page
18. Anisotropic Lattice Thermal Conductivities for FA-147337 to 600°C	65
19. Anisotropic Lattice Thermal Conductivities for KH-OPX to 1000°C	66
20. Comparison of KH-OLV Diffusivities with Calculations for $\alpha = 1.75$	101
21. Comparison of SC73-10 Diffusivities with Calculations for $\alpha = 2.25$	102
22. Comparison of SC73-10 Diffusivities with Calculations for $\alpha = 1.75$	103
23. Comparison of FA-147337 Diffusivities with Calculations for $\alpha = 1.75$	104
24. Comparison of KH-OPX Diffusivities with Calculations for $\alpha = 1.75$	105
25. Comparison of KH-OLV Conductivities with Calculations for $\alpha = 1.75$	106
26. Comparison of SC73-10 Conductivities with Calculations for $\alpha = 2.25$	107
27. Comparison of FA-147337 Conductivities with Calculations for $\alpha = 1.75$	108
28. Comparison of KH-OPX Conductivities with Calculations for $\alpha = 1.75$	109
29. Group Velocities for the Optic Modes of Forsterite.....	110
30. Group Velocities for the Optic Modes of Fayalite	111
31. Mean Group Velocities for the Optic Modes of Forsterite	112
32. Mean Group Velocities for the Optic Modes of Fayalite	113
33. Contribution of Optic Modes to Thermal Conductivity in Forsterite.....	114
34. Anisotropic Lattice Thermal Conductivities for SCchai to 5.09 GPa	115
35. Thermal Conductivity Along the Fe-Mg Olivine Solid Solution Series	116
36. Thermal Resistivity Along the Fe-Mg Olivine Solid Solution Series	117
37. KH-OLV and Measurements of Total Thermal Conductivity	118

LIST OF TABLES

Table Number	Page
1. Composition of KH-CPX.....	15
2. Composition of SC73-10	16
3. Composition of FA-147337	17
4. Individual Thermal Diffusivities for KH-OLV	67
5. Individual Thermal Diffusivities for SC73-10	70
6. Individual Thermal Diffusivities for FA-147337	71
7. Individual Thermal Diffusivities for KH-OPX	72
8. Individual Thermal Diffusivities for KH-CPX	74
9. Thermal Diffusivity and Conductivity Tensors for KH-OLV	75
10. Thermal Diffusivity and Conductivity Tensors for SC73-10	76
11. Thermal Diffusivity and Conductivity Tensors for FA-147337	77
12. Thermal Diffusivity and Conductivity Tensors for KH-OPX.....	78
13. Thermal Diffusivity and Conductivity Tensors for KH-CPX.....	79
14. Thermal Diffusivities and Conductivities for SCchai	80
15. Specific Heats and Volumes of Phases.....	81
16. Normalized Tensor Values of Thermal Diffusivities	119

Dedication

To Professor Leon Judah Slutsky

Introduction

"There is, perhaps, no scientific inquiry more full of human interest than the study of the nature of heat, and the manner in which matter in general is affected by it. No branch of physical science is so intimately connected with the everyday occupations of life, and, consequently, none of them interests mankind more closely. ...It is not surprising, therefore, that an agent at once so powerful and so serviceable, so beneficent and yet sometimes so terrible, should have become a subject of adoration and worship among the inhabitants of the earth, but at first sight it may seem more than surprising that its study in early times should have been so much neglected."

(Preston, 1919, p. 1)

Despite the governing role of thermal transport in constraining the behavior of Earth's interior (Roufousse and Jeanloz, 1983), only a few determinations of thermal conductivity in mantle minerals have been reported, most of which have been sharply limited in scope (see Chai et al., 1996 for a review). This longstanding paucity of information in such a fundamental field of study may be attributed to the interplay of two causes: First, measurements of thermal conductivity have proven to be surprisingly difficult to perform (Clauser and Huenges, 1995). Second, most geodynamic models have not been aimed at resolving such sufficiently detailed observations that a better constrained set of material properties was necessary. Recent models (e.g. Hearn et al., 1997), however, have drawn upon a more detailed knowledge of the anisotropic thermal behavior of mantle minerals at high pressure and temperature, and have demonstrated that further measurements of this sort are now needed as a basis for an advanced understanding of the upper mantle.

Inhomogeneities in thermal conductivity within the upper mantle most directly affect the local geotherm, in that, for a given incoming heat flux from below, a less conductive region will develop and maintain a steeper temperature gradient than will its more conductive surroundings. The direct detection and interpretation of such inhomogeneities is restricted to drilling depths of about 10 km, however (Pollack and Chapman, 1977). Below this

accessible region, lateral variations in the geotherm may be inferred from changes in seismic wave velocities, but a simple change in velocities alone does not lend itself to unambiguous interpretation, since seismic velocities are sensitive not only to temperature but also to composition. Even for regions within which it is reasonable to expect uniform composition, it would be difficult on this basis alone to distinguish between variable conductivity within the upper mantle and variable heat flux from below. Fortunately, the upper mantle is not merely inhomogeneous with respect to seismic velocities, but anisotropic as well. It is through the correlation of this seismic anisotropy with its related thermal anisotropy that the effects of the latter may be distinguished, and this correlation is brought about via an understanding of the mineralogy and fabric of the rocks at these depths.

Seismic anisotropy throughout many regions within the upper mantle is well documented, and the measurement of both its degree and extent may be determined by a variety of techniques, each sensitive to different depths and resolutions. Compressional waves refracted along the interface between the crust and mantle, known as P_n waves, serve to characterize the azimuthal anisotropy of the uppermost mantle, which in the western U.S. may vary by up to 7.5% (Hearn, 1996). A vertically-integrated measure of anisotropy to greater depths is provided by observations of shear wave splitting of SKS and SKKS phases (Silver and Kaneshima, 1993), so that a comparison of the results of these two methods for a similar area may serve to indicate the overall depth to which that part of the mantle is anisotropic (Hearn, 1996). Finally, a broader, coarser determination of anisotropy may be derived from azimuthal variation in the propagation of surface waves that are sensitive to properties of the upper 200 to 300 km (Babuška et al., 1993).

Once the upper mantle's seismic anisotropy is known, the next task is to identify the underlying petrologic properties of the mantle which give rise to it. This has been accomplished for oceanic regions by the petrographic examination of oriented samples from ophiolites, which have shown a preferred orientation of the a -axes of olivine and c -axes of

orthopyroxene along the former direction of spreading, with the olivine *c*-axes and orthopyroxene *b*-axes vertical (Christensen, 1984). This is in accord with experimental determinations of the mechanism of lattice preferred orientation for these minerals when strained, and results in a degree of anisotropy comparable to what is observed in the mantle (Nicolas and Christensen, 1987).

Of particular interest as an application of data on thermal anisotropy is the effect on heat transport under oceanic crust arising from flow-induced deformation (Schärmeli, 1982; and Hearn et al., 1997). The earlier work concluded that the growing contribution of radiative transfer would reduce the effective thermal anisotropy of olivine to 0.98 for the *a*- versus *b*-axes and 1.10 for *a* versus *c*, thus diminishing its contribution to models of sea-floor spreading (Schärmeli, 1982). The more recent study, however, found that the combination of anisotropy in both thermal diffusivities and in viscosities led to higher heat flow and greater shear heating than would otherwise be expected. Thus, their model produced "higher surface heat flow, shallower ocean basins, weaker asthenosphere, and slightly thinner lithosphere" than one based on an isotropic half-space, and is more representative of field observations (Hearn et al., 1997). Clearly, both the extent and the effects of anisotropy in thermal conductivity on mantle behavior must continue to be addressed.

More generally, the pressure and temperature dependencies of thermal conductivity in mantle minerals are of concern in determining heat flow both at boundary layers and within convection cells. At both compositional (Chai et al., 1996) and thermal (Roufosse and Jeanloz, 1983) boundary layers, conduction is perforce the predominant means of heat transfer. Even in a dominantly convective environment, thermal conductivity must be known in order to determine, for example, the Rayleigh number of the system (Chai et al., 1996). Therefore, as mantle modelers strive to incorporate more realistic parameters into their codes, they must continue to move away from simple assumptions of "scalar and nearly

constant" thermal conductivity based on tenuously supported extrapolations of measurements at ambient conditions (Chai et al., 1996).

To address these matters, measurements of the lattice component of anisotropic thermal diffusivity as a function of composition, temperature, and to a limited extent, pressure, have been performed on a set of olivines and pyroxenes, and are herein presented and discussed. These measurements, made with impulsive stimulated light scattering, differ from those of all previous high-temperature and high-pressure studies of these minerals, in that this technique specifically measures the lattice thermal diffusivity; other methods provide only a measure of either the total diffusivity (lattice plus radiative) or the total conductivity, from which the individual lattice and radiative contributions must be extracted via modeling. Thus, this new set of data not only provides a direct basis for a quantitative discussion of the role of lattice vibrations in the transport of heat, but also provides a benchmark from which previous and future models of the lattice and radiative components may be checked, and with which all other measurements of total diffusivity and conductivity may, with greater confidence, be analyzed.

It should be noted at the outset that all measurements were performed by the author except the work at high pressure, which was done by Research Associate Professor Evan H. Abramson of the Department of Chemistry. Professor Abramson generously agreed to make available his laboratory notebook and raw data files for the author's analysis and inclusion in this study. All of the thermal diffusivity data were collected in the High Pressure Mineral Physics Laboratory, 263 Johnson Hall, at the University of Washington.

Materials

"Haveing thus premised and intimated, from what Terrestriall *phaenomena's*, and philosophicall *Postulatas*, the ensueing discourse, is drawn and Established; I now come to consider, what that Materiall substance was, whereof the Heavens, or at least the Earth, were made; and of what it did Originally consist; according to the words of *Moses*, and our observations in naturall things to this Day."

(Hobbs, 1715, p. 51)

Sample Descriptions

The set of minerals selected for study consists of four olivines of different composition, one orthopyroxene, and one clinopyroxene. The olivines were selected so as to span as much of the forsterite-fayalite solid solution as possible, within the limitations both of the availability of samples of adequate optical quality and of the need for sufficient iron content to generate a usable signal with the chosen technique. One olivine (Fo_{91}) and both pyroxenes were extracted from an ultramafic xenolith from Kilbourne Hole, New Mexico, and have been designated KH-OLV, KH-OPX, and KH-CPX. The second olivine (Fo_{78}) is from a xenolith from San Carlos, Arizona, described in detail by Irving (1980) under the name SC73-10; this designation is herein adopted for the olivine from that specimen. The third olivine (Fo_0) is a synthetic fayalite (Finch et al., 1980) which was given the label FA-147337, following the acquisition number, 147337, assigned it by the Smithsonian Museum of Natural History. The remaining olivine (Fo_{89}), used only in the high-pressure runs, is also from a San Carlos xenolith, and is designated SCchai to indicate that it was prepared by Dr. Mu Chai, a former graduate student in the laboratory. It is from the same specimen examined in Chai et al. (1996).

The ultramafic xenolith from Kilbourne Hole has been used by the High Pressure Mineral Physics Laboratory for a number of years as a source of representative upper

mantle material. It is a group I spinel lherzolite, irregularly shaped, approximately 15 cm on a side, encased in a rind of porphyritic vesicular basalt from 0.5 to 1 cm thick. The specimen has been cut from a larger mass, thereby exposing an entire face for examination and removal of mineral grains. The lherzolite displays a xenomorphic granular texture, with grain sizes of 1 to 2 mm, and is readily friable by hand, contributing to the ease of selecting single crystals for study. The sample is approximately 70% olivine, 20% orthopyroxene, and 5% each of clinopyroxene and spinel. The clinopyroxene and spinel phases occur only as fine grains (1 mm or less), which is why only its olivine and orthopyroxene grains were hand-picked for high-temperature measurements.

The Kilbourne Hole olivine has a composition of $\text{Fo}_{91}\text{Fa}_9$, from microprobe analyses performed on the department's JEOL 733 Superprobe. The composition of the Kilbourne Hole orthopyroxene is from similarly-acquired microprobe analyses in Chai et al. (1996), as their sample was taken from the same homogeneous xenolith. The composition is $(\text{Mg}_{1.63}\text{Fe}_{0.17}\text{Ca}_{0.04}\text{Mn}_{0.01})(\text{Cr}_{0.01}\text{Al}_{0.12})(\text{Si}_{1.89}\text{Al}_{0.11})\text{O}_6$, which is that of an aluminous enstatite (En_{91}). Similarly, the composition of the Kilbourne Hole clinopyroxene comes from Collins and Brown (1998). Their 36 microprobe analyses of three grains yield a composition of $\text{Di}_{-2}\text{He}_9\text{Jd}_3\text{Cr}_3\text{Ts}_{12}$ expressed with respect to the end-members diopside, hedenbergite, jadeite, cosmochlor, and the hypothetical Mg-Tschermak component. Table 1 reproduces the elemental abundances listed in their Table 1.

The San Carlos xenolith is described in Irving (1980) as follows, and is depicted in color in Irving's Plate 1:

"SC73-10. San Carlos. Group II spinel clinopyroxenite veins invading dunite....In this sample, subparallel but also cross-linked spinel clinopyroxenite veins of various widths cut yellow-green olivine-rich rock, which is largely dunite with variable but minor amounts (≤ 5 percent) of orthopyroxene and spinel. Some parts of the dunite are surrounded entirely by spinel clinopyroxenite...."

In consultation with Professor Irving, this sample was selected for the iron-poor olivine present in the dunite portion of the rock, the olivine presumably having been altered by metasomatism brought on by the injection of the clinopyroxenite. The specimen is a polished slab of approximate dimensions 14 x 7 x 1.5 cm, and the dunite sections are of 2 mm to 2 cm in width. Fifteen points on a polished thin section from this sample were subjected to electron probe microanalysis; the results are listed in Table 2. The recalculated composition for the olivine is $(\text{Mg}_{1.57}\text{Fe}_{0.44}\text{Mn}_{0.002}\text{Ni}_{0.0013}\text{Ca}_{0.0017})\text{Si}_{0.99}\text{O}_4$, which corresponds to Fo_{78} . Individual olivine grains are from 0.5 to 2 mm in diameter. The olivine grains selected for this study specifically were not taken from the light green protrusion along the right-hand side of the sample when the rock is oriented as in Irving's Plate 1. The olivine in this small part of the xenolith is much closer in color to that of a typical Fo_{90} mantle olivine, whereas the rest has a distinct brownish-yellow cast in aggregate, and so this part presumably is not of the desired low iron content. This section is joined to the main body of the composite xenolith by a layer of what appears to be the host basalt, and almost certainly is of separate origin.

The synthetic fayalite, FA-147337, was grown at Oak Ridge National Laboratory by Cabell B. Finch, who identified the sample as ORNL CBF 16029. It was grown from a melt using the Czochralski technique at 1200°C and 10^{-12} bar O_2 , conditions which were sufficiently reducing to limit the production of ferric iron in the sample (Finch et al., 1980). Personal communication with Mr. Finch indicates that it is nearly identical to specimens which were grown under the same conditions and further characterized in Kopp and Abraham (1982) and Robie et al. (1982). Fifteen microprobe analyses of fragments of this sample are listed in Table 3, and give a composition of $(\text{Mg}_{0.009}\text{Fe}_{2.02})\text{Si}_{0.98}\text{O}_4$, or effectively Fo_0 .

The remaining San Carlos olivine, SCchai, was taken from one of several polished thin sections of a large (1 cm diameter) single crystal archived in the laboratory by Dr. Chai after completion of his dissertation (Chai, 1996). This is believed to be the same crystal from which the samples in Chai et al. (1996) were taken, though perhaps not the same slice. Nonetheless, the San Carlos material is of highly uniform composition, therefore the published composition of $(\text{Mg}_{0.89}\text{Fe}_{0.11})_2\text{SiO}_4$ has been taken as representative. It is a *c*-normal cut that was ground and polished to a thickness of 49 μm on 3 June 1996, and is so labeled for archival purposes. Several disks of diameter 200 μm , suitable for loading into the diamond-anvil cell, had already been cored from the crystal but not removed from the slide, so no further preparation of this sample was necessary beyond dissolving the underlying cyanoacrylate and cleaning the disks in an ultrasonic bath, first in acetone, then in methanol.

Selection and Preparation of Single Crystals

Selection of Mineral Grains

For the samples taken from whole rocks, approximately 1 cm^3 of material was chipped at a time from each rock with a rock hammer, then manually disaggregated with an alumina mortar and pestle. The finer material was removed in stages from the bottom of the mortar to minimize the amount lost to powdering. A firm rocking motion of the pestle against the sample was found to be the most effective technique for separating the grains without unduly reducing their size. This was done until only single-crystal grains remained. The largest grains were removed and individually examined under a 10-40x binocular microscope to find those which were free of cracks, inclusions, or other visible defects. The

typical yield was three or four potentially usable olivine crystals from both the Kilbourne Hole and the San Carlos xenoliths. Large, clean orthopyroxene and clinopyroxene crystals were considerably scarcer; several batches from the Kilbourne Hole xenolith had to be processed to acquire two or three grains of each.

The synthetic fayalite arrived from the Smithsonian in the form of approximately twenty slightly elongate sand-sized splinters, the result of a curator's attempt to break a part of the original boule for use in this study at the personal request of Professor J. Michael Brown. The three largest splinters were chosen for orientation and polishing; after preparation, only two were still large enough to be clamped into the high-temperature furnace.

Orientation of Single Crystals

In order to calculate the thermal diffusivity tensor from a set of single-crystal measurements, one must know the crystallographic orientation of the sample at the time each measurement is made. Although the full thermal diffusivity tensor could, in theory, be calculated from a series of measurements made in any two noncoincident planes of known orientation, in practice smaller uncertainties are obtained if the chosen planes are orthogonal, due to the minimization of cross-correlation in their fitting parameters. Furthermore, for materials of higher than triclinic symmetry, it is convenient to select orthogonal planes that contain two crystallographic axes, so that the normal then is either the third axis or at least an axis of the reciprocal lattice. Olivine and orthopyroxene are both orthorhombic and clinopyroxene is monoclinic, so the samples were oriented accordingly, with two axes contained within the plane of each final, tabular shape.

The former laboratory practice for acquiring oriented samples was to pot fifty to sixty candidate grains in epoxy on a round glass slide, grind and polish all of them to the desired thickness, then find those grains which chanced to have nearly the desired orientation. This

involved the examination of all the polished grains under a petrographic microscope to find those with axes approximately normal to the slide surface, followed by the removal of likely specimens and verification of their orientations on the lab's 1960's-era Norelco XRG 5000 x-ray generator with a Nonius precession camera using Polaroid filmstock. This was a tedious procedure which often required several hours of labor and many tens of somewhat expensive exposures to acquire and characterize a single satisfactory crystal, and was immensely wasteful of sample material. A further objection was that the normal direction for even the acceptable samples often was 10° or more away from the desired direction, and therefore required additional care in processing the data. This was, nonetheless, the method used for the clinopyroxene crystals, though the experience made it abundantly clear that another way had to be found.

For subsequent orientation of the other minerals, each crystal was mounted with cyanoacrylate to the end of a short (2 cm) glass fiber attached to a standard x-ray post. Once mounted, the crystals were taken to the X-ray Crystallography Laboratory maintained by the Department of Chemistry in the Chemistry Library Building. Here, each crystal was oriented on a Nonius KappaCCD x-ray diffractometer with a fully automated goniometer head. As these were samples of known structure, no detailed description of the collection routine or automated analysis will be presented, beyond noting that the software did not choose the standard crystallographic setting for either olivine or orthopyroxene. It was necessary to transpose the *b* and *c* axes for olivine and the *a* and *c* axes for orthopyroxene in order to comply with convention. Throughout this work the conventional axes are used.

Once the orientation was known, the sample was rotated via automation such that each axis in turn was facing the side of the diffractometer. This permitted visual inspection to determine which axis-normal should be chosen in order to preserve the largest cross-section in the sample after grinding and polishing.

The transfer of each sample from the goniometer head to a frosted glass slide for grinding, while maintaining its orientation, required the design and construction of a jig that would be compatible with the diffractometer, one that would bring a slide against the sample vertically, rather than requiring that the sample be lowered against a horizontal slide, as had been done with older diffractometers. Such a jig was fabricated in the form of an upright tee-shaped aluminum superstructure mounted on a Newport low profile precision ball bearing translation stage, Model 423, with a micrometer actuator tip. The height of the tee coincided with the height of the sample on the goniometer head, approximately 47 cm above the tabletop surface of the diffractometer, and the two arms of the tee were of unequal length, 22 and 27 cm apiece, each of correct length to reach the sample from one side of the instrument or the other, depending on the configuration of the instrument that day. The ends of the tee were machined flat and vertical to hold a 2.54 cm round glass slide, and were fitted with a pair of leaf springs to retain the slide. Attached to the underside of the translation stage was an aluminum block designed to register against the side of the goniometer's base, thus aligning the normal of the slide with the normal of the sample. Once the jig was in place, the micrometer could be advanced to bring the slide nearly into contact with the sample while the glass fiber to which the sample was attached was monitored to assure that no actual contact, and consequent flexure of the glass fiber, occurred. The sample was centered on the slide to the degree permitted by the position of the goniometer; in a few cases the sample had to be attached near the edge of the slide, but such samples later were recentered after a small flat had been ground into each sample to preserve its orientation.

With the slide and sample nearly touching, a drop of high-viscosity cyanoacrylate adhesive (Extra Thick Maxi-Cure) was applied to the slide above the sample and allowed to flow down over it. Once the sample had been wetted in this fashion, the adhesive was set with a catalyst (Insta-Set Accelerator). This procedure was found to be necessary after the

first attempt, in which ordinary cyanoacrylate was used. That material proved to be too runny to apply to a vertical glass slide without fear of it dropping onto the instrument below, and often would not set on such clean, dry surfaces even after the passage of ten to fifteen minutes. Both the adhesive and catalyst are products of Bob Smith Industries, of Atascadero, California, though similar products are available from other suppliers to the toy and hobby trade.

After the adhesive had set, the glass fiber was cut with a small pair of scissors, freeing the slide for removal and immediate labeling with a diamond scribe. More cyanoacrylate was added to encase the crystal completely, then the perimeter of the slide was sprinkled with coarse olivine sand to act as support and a plug of quick-setting two-part clear epoxy was poured over the entire surface in preparation for the initial grinding and polishing operations. The epoxy was permitted to cure for at least 24 hours before proceeding.

Grinding, Polishing, and Coring

The epoxy plug and sample were ground flat on an Ingram Model 400 thin section grinder in the departmental thin section preparation room. Enough material was removed to leave a ring of epoxy and olivine sand of about 1 mm thickness surrounding the exposed cyanoacrylate and sample crystal. Further grinding proceeded slowly with frequent examination of progress under a binocular microscope until a satisfactorily large cross-section of the sample was presented.

The slide next was transferred to a Buehler Minimet polisher, and the crystal polished using Texmet polishing cloth and diamond grit of progressively finer size: 6, 3, 1, and finally 0.25 μm diameter, each lubricated with five drops of Tapmatic cutting oil, refreshed as needed. One to two hours of polishing at each grit size on the slowest speed and with an

applied backing pressure corresponding to four o'clock on the unmarked dial indicator produced the best results, though some plugs took several hours to polish, presumably because of high elasticity in a poorly mixed batch of epoxy.

With the first side polished to the point of showing no pits or scratches under 40x magnification, the cyanoacrylate was dissolved with acetone and the sample removed. The remaining epoxy then could be scraped from the slide with a razor without fear of damaging or losing the sample. Poor results had been achieved in earlier attempts to dissolve the epoxy with commercially available epoxy solvents, so the method of encasing the sample entirely in cyanoacrylate was adopted to avoid contact between the epoxy and the sample at all stages of processing. The crystal was remounted, face down, in a centered spot of the thinnest achievable layer of cyanoacrylate so that it could be pushed firmly against the slide to assure the new second surface would be parallel with the first. More cyanoacrylate was added to cover the sample, then potting, grinding, and polishing proceeded as before. It is worth emphasizing that the glass slide must be frosted before use, as the sample, cyanoacrylate, and entire plug are too easily pulled from an unfrosted slide by the grinder or, more rarely, by the polisher, generally resulting in the loss or destruction of the sample.

This method of preparing oriented, double-polished, single-crystal slabs produced samples with less than 2° of wedging between front and back, as determined by comparing the reflections of a HeNe laser returned from both surfaces. The axis-normal orientation was preserved to within 2° as well. This was measured by fixing each polished crystal on the goniometer of the lab's precession camera such that the reflection of a HeNe laser passing through the collimator returned through the collimator, then taking a precession photo of the sample in this position using an unfiltered source. The slight distortion in the circle defining the limit of the zero-level reciprocal lattice net was easily distinguished, and the sample was rotated until this circle was centered on the image, following the technique described in Stout and Jensen (1989, pp. 129-132). A comparison of the goniometer

settings in the initial, face-normal and final, centered positions provided a measure of the angular difference between the actual normal and the crystallographic axis. For all the samples except KH-CPX, this difference was small, 2° or less, so it was disregarded in calculating the thermal diffusivity tensors for the orthorhombic minerals.

The final step in preparing each sample was to shape a disc of the appropriate diameter from the polished slab. This was achieved by using a small drill press into which a blunted hypodermic needle had been chucked. The needle was spun against the face of the sample (once again mounted on a frosted glass slide) while surrounded by a slurry of one-micron diamond powder and Tapmatic cutting fluid. This operation ground away the sample under the needle, leaving a raised disc in the center. For small samples, the disc was necessarily incomplete, but it was sufficient if only a small part of the sample was as wide as the inner diameter of the needle. The furnace which held the samples, described in detail below, was designed to accept the discs cut by a 14 gauge needle (0.0820 to 0.0840" OD, 0.0610 to 0.0650" ID). The needle was allowed to cut completely through the sample and well into the underlying glass slide to avoid any taper on the edge of the disc that might have interfered with loading the disc into the furnace.

Table 1 Composition of KH-CPX

Element	Atoms PFU (basis of six O)
Si	1.8756(10)
Ti	0.0129(1)
Al	0.2833(7)
Cr	0.0275(1)
Fe	0.0907(3)
Ni	0.0001(0)
Mn	0.0026(1)
Mg	0.8513(19)
Ca	0.7596(8)
Na	0.1050(5)

Table 2 Composition of SC73-10

Pt#	SiO ₂	FeO	MnO	NiO	MgO	CaO	Total
16	38.45	20.5	0.1035	0.0767	41.09	0.0482	100.27
17	38.61	20.56	0.0685	0.0678	41.06	0.072	100.43
18	38.66	20.76	0.0603	0.0438	41.02	0.0621	100.61
19	38.38	20.45	0.0767	0.0502	41.14	0.0788	100.17
20	38.42	20.87	0.0694	0.042	40.88	0.0692	100.35
21	38.46	20.65	0.096	0.044	41.06	0.076	100.39
22	38.59	20.72	0.0749	0.068	41.16	0.0461	100.66
23	38.29	20.54	0.1316	0.0396	41.04	0.055	100.09
24	38.26	20.79	0.0971	0.06	40.96	0.0616	100.23
25	38.34	20.59	0.0861	0.0932	40.77	0.0562	99.93
26	38.76	20.36	0.1285	0.0953	41.05	0.0691	100.47
27	38.55	20.54	0.0849	0.0573	41.03	0.0586	100.32
28	38.63	20.47	0.0881	0.079	41.1	0.0667	100.44
29	38.77	20.74	0.1015	0.0902	41.05	0.0478	100.8
30	38.53	20.44	0.1082	0.0662	41.01	0.0755	100.23
avg	38.513	20.599	0.092	0.065	41.028	0.063	100.359
sd	0.159	0.149	0.021	0.019	0.098	0.011	0.225

Table 3 Composition of FA-147337

Pt#	SiO ₂	FeO	MnO	NiO	MgO	CaO	Total
1	28.89	70.94	0	0	0.1717	0.0087	100.01
2	28.96	70.66	0	0	0.1844	0.0062	99.81
3	28.95	71.59	0	0	0.1714	0.006	100.72
4	28.88	71.13	0	0	0.1774	0	100.18
5	28.96	70.96	0	0.0227	0.1664	0	100.11
6	28.75	71.21	0	0.0049	0.1613	0	100.13
7	28.91	70.96	0	0	0.1559	0	100.02
8	28.94	71.11	0	0	0.1516	0	100.2
9	29.08	71.08	0	0	0.1642	0	100.32
10	28.74	71.67	0	0	0.1417	0	100.54
11	29.1	71.32	0	0.0144	0.1882	0	100.62
12	29.16	71.3	0	0	0.1915	0.0093	100.66
13	29.12	71.13	0	0.0104	0.1726	0	100.43
14	28.61	71.04	0	0.0112	0.1995	0.0042	99.86
15	28.76	71.45	0	0	0.1525	0	100.37
avg	28.921	71.170	0.000	0.004	0.170	0.002	100.265
sd	0.157	0.264	0.000	0.007	0.016	0.004	0.287

Methods

"The question is now asked whether a secular judge may allow a witch to be submitted to a common purgation in the manner in which a civil defendant is allowed the trial by ordeal, as, for example, that by red-hot iron. And it may seem that he may do so."

(Kramer and Sprenger, 1484,
Section III, Question XVII)

Measurement of Thermal Diffusivity

Theoretical Considerations

Both thermal conductivity and thermal diffusivity are defined by the relationship between an imposed temperature difference and the resulting heat flow. Restricting the discussion to one-dimensional heat flow, thermal conductivity, K , is the factor of proportionality relating the heat flux, J , to the temperature gradient, assuming all heat transfer is via conduction:

$$J = -K \frac{\partial T}{\partial x}$$

whereas thermal diffusivity, D , relates the change in temperature at a point to variations in the temperature gradient:

$$\frac{\partial T}{\partial t} = D \frac{\partial^2 T}{\partial x^2}.$$

The two are proportional to one another via the density, ρ , and specific heat, C_p of the material.

$$D = \frac{K}{\rho C_p}$$

so from an experimentalist's viewpoint the choice of one over the other is a question of determining which set of relationships comprises quantities that are more readily measured. The available experimental technique, impulsive stimulated scattering, monitors the change of the temperature-dependent index of refraction during the decay of an imposed temperature gradient, therefore the observed quantity is thermal diffusivity.

One concern in determining thermal diffusivity arises from the fact that the thermal gradient and the heat flow are vectorial quantities which, in an anisotropic medium, are not necessarily parallel to one another; therefore thermal diffusivity must be expressed as a second-order tensor (Nye, 1985, p. 195). Its number of independent coefficients depends upon the symmetry of the material (Nye, 1985, pp. 22-24), which varies considerably among the common mantle minerals. Garnet is cubic, and thus isotropic, so a single measurement will suffice to determine its lone coefficient at a given pressure and temperature. Olivine and orthopyroxene are both orthorhombic, so three coefficients must be resolved, but the three principal directions of the tensor are constrained to lie along the three crystallographic axes of each mineral. These may be identified beforehand as an aid to orienting one's samples for measurement, as described in the previous chapter. The thermal diffusivity of phases of lower symmetry, such as clinopyroxene, may also be expressed in terms of three principal coefficients, but the corresponding principal directions are not as well constrained *a priori* by considerations of symmetry, so that in general measurements in more directions are necessary to identify them: a total of four for monoclinic crystals and six for triclinic. This can pose a considerable obstacle when using many experimental techniques, in light of the amount of work involved in performing even a single measurement along one direction at one pressure and temperature.

Of further concern is the observation that heat flow can take place via several mechanisms, the relative contributions of which vary with temperature. At low temperatures, thermal diffusion through lattice vibration is the primary mode of transport, and is of

greatest interest in determining the behavior of single crystals under mantle conditions (Chai et al., 1996). At higher temperatures, including perhaps those found through most of the mantle, radiative transfer may contribute nearly as much to overall flow (Roufosse and Jeanloz, 1983), but much of its long-range effectiveness is constrained by behavior at grain boundaries, so that ideally this would be studied separately in polycrystalline samples once the single-crystal lattice contribution is known independently. Finally, at the highest temperatures, heat flow from electron transfer must be considered, although this is unlikely to be important outside of the core and deepest mantle (Roufosse and Jeanloz, 1983). The precise significance of each of these modes across the full range of mantle conditions has yet to be determined experimentally, although the increasing contribution of radiative transfer in olivine at 2.5 GPa from 150°C to 1230°C and the implications of this for models of the sea floor have been examined (Schärmeli, 1982).

Traditional Techniques

Historic methods of measuring anisotropic thermal conductivity have long been known to produce results "of no great accuracy" (Wooster, 1936). The method cited involved coating an oriented crystal face with wax, then touching a hot needle to it so as to melt an elliptical portion of the coating. The axes of this ellipse determined the relative anisotropy of conductivity in that plane. Although admirably clever, this technique displayed great limitations. Not only did it fail to provide the absolute magnitudes of the thermal coefficients, but clearly it also was not readily adaptable to high-pressure measurements, although a range of high temperatures presumably could have been achieved with an appropriate choice of coatings in place of wax.

Most subsequent studies of thermal anisotropy have employed an oriented mineral slab clamped between two plates held at different initial temperatures, which furthermore may be

loaded into a piston-cylinder apparatus to observe the effects of elevated pressure (Schärmeli, 1982). Axial heat flow across the slab is monitored by thermocouples attached to its opposite faces. This technique relies on the availability of large (several-mm scale) gem-quality crystals that can be oriented and cut for loading. Such samples are readily available for Mg-rich olivine, but are scarce for other phases of mantle composition. One additional drawback lies in the great care that must be taken to prepare the intricate and, of necessity, disposable sample assembly in order to approximate a nearly homogeneous one-dimensional heat flow, both through the radially symmetric arrangement of cell components and through the application of highly-conducting materials along the sample faces. Not only must the high-PT behavior of these component materials be ascertained separately, but thorough numerical modeling of the geometry of the sample environment also is required to interpret the results, particularly in separating the contributions of lattice and radiative transport. (Schärmeli, 1982).

Impulsive Stimulated Light Scattering

One method for alleviating some of the above difficulties is a type of transient grating spectroscopy (Zaug et al., 1992) known under a variety of names, but herein called impulsive stimulated light scattering (ISLS). For this, a small (as little as 200 μm diameter by 20 μm thick), oriented sample disk is mounted so as to permit the passage of laser pulses that are used both to stimulate and to probe the sample. Two pulses crossing within the sample impose a set of parallel planes of alternating constructive and destructive interference; these planes are normal to the sample surface. The wavelength of the pulses is chosen such that the sample is weakly absorbent in that range, so that in the regions of constructive interference the sample suddenly is heated by a few degrees and rapidly expands, thereby changing its index of refraction relative to the adjacent regions of

destructive interference. This alternating pattern constitutes an optical grating within the sample, from which a probe beam, entering at the appropriate Bragg angle, may be diffracted. By observing the intensity of the diffracted signal through time, the rate at which the perturbations in the sample relax through thermal diffusion is obtained. For grating spacings of only a few microns, the heat flow is almost entirely one-dimensional, perpendicular to the planes of the grating; end effects are insubstantial (Chai et al., 1996). The method is attractive for several reasons: Small, gem-quality single crystals are readily obtainable. The probed region is entirely within the sample, so no interfaces with other materials need be considered. The observed component of the direction of propagation is both well defined and contained within the plane of the sample, so a number of directions may be examined merely by rotating the sample about the axis of the cell, thereby reducing to no more than two the number of specimens that must be prepared and loaded for each mineral. Finally, by varying the angle at which the excitation pulses converge, the grating spacing may be changed, which permits the explicit separation of diffusive and nondiffusive components via the relationship

$$\frac{1}{\tau} = \frac{4\pi^2 D}{d^2} + A$$

in which τ is the relaxation time, D the thermal diffusivity in the direction of the observed component of propagation, d the grating spacing, and A the non-diffusive radiative transfer. Thus, if a plot of $1/\tau$ versus $1/d^2$ takes the form of a line passing through the origin, the nondiffusive component is negligibly small (Chai et al., 1996) and the results may be taken as a measurement of the lattice component of thermal diffusivity. As shall be shown in subsequent sections, for the measurements in this work at all temperatures this relationship holds true—the phonon mean free paths are sufficiently short (tens of Ångstroms or less) and the photon mean free paths are sufficiently long (tenths of millimeters or more), that only the phonon processes behave diffusively on the scale of the experiment.

Shortcomings of the method include the need to select samples with suitable absorption spectra, although Fe-bearing mantle phases work well in conjunction with the 1064 nm output of a Nd:YAG laser for excitation and either frequency-doubled Nd:YAG or a separate Ar-ion laser (488 nm) as the probe. Also, at high temperatures, appropriate bandpass filters may be needed as an aid in separating the signal from background thermal radiation. Weak signals may be lost altogether at these higher temperatures. Fortunately, all of the materials in this study produced strong signals at high temperatures, so no such filters were required. It is worth noting that the signal-to-noise ratio actually increased for all samples at elevated temperatures, which is an indication of a stronger modulation of the index of refraction of each material under these conditions. Whether this is entirely due to greater absorption of the infrared pulses or to a greater temperature-sensitivity of the index of refraction was not investigated.

This same experimental arrangement is also of use in measuring a sample's speed of sound in the direction normal to the planes of the imposed grating, inasmuch as the rapid expansion of the heated regions will launch sound waves that also modulate the index of refraction of the material. For the silicates in this study these sound speeds are so fast that the resulting signal cannot be resolved properly with the available electronics, but this feature is of use in the case of methanol at room pressure and temperature. Methanol's much slower speed of sound can be measured and used as a calibration point for accurate determination of the convergence angle of the infrared pulses. This angle must be known well in order to calculate the spacing of the imposed grating, and thereby interpret the characteristic time of the decay of the signal in terms of thermal diffusivity.

In this work the infrared pulses were supplied by a Quantronix Model 416 Nd:YAG laser with mode locking and Q-switching, producing pulses at 1064 nm of 100 ps duration, each with 80 μ J of energy, for a peak power of 800 kW. Before September 1999, the

continuous probe was provided by a Cytofluorograf Ar⁺ laser manufactured by Bio/Physics Systems, Inc. This failed and was replaced by an Ar⁺ laser from Ion Laser Technology, Model 5500BSL-00. Both lasers operated at 488 nm and, for the latter system, at up to 100 mW, though much lower power levels sufficed in practice.

The diffracted signal was directed into a Pacific Instruments 3150 photomultiplier tube powered by a Power Designs Pacific Model 2K-10 power supply. The output was captured by a Tektronix 2430 digital oscilloscope that performed the initial signal averaging before passing the results to an Apple Macintosh II for collection and storage. The Mac II controlled all aspects of the timing of the experiment through the program LabVIEW 2.2.

Generation of High Temperature

The experimental portion of this work consists of a series of measurements of thermal diffusivity in oriented single crystals of olivine, orthopyroxene and clinopyroxene at temperatures up to 1000°C. These temperatures were achieved in a small, auxiliary furnace which fits within the laboratory's vacuum furnace, permitting the two to act in concert, thereby allowing the use of preexisting power supplies, temperature controllers, and positional translators for the assembly.

Main Vacuum Furnace

The main vacuum furnace was designed at Los Alamos National Laboratory (LANL), and is designated "Ultra-High-Temperature/High-Pressure Cell for Brillouin Scattering" as illustrated in LANL technical drawing number DS055. It is of cylindrical shape, with a cavity approximately 13 cm in diameter and 5 cm thick. At each end of the cylinder is a removable faceplate containing an oval silica window. One faceplate supports a series of

internal baffles and a recess for a Merrill-Bassett diamond-anvil cell, the other faceplate accommodates a feedthrough for powering either one or two heating elements and for inserting up to three thermocouples. The central body of the furnace houses a fitting for drawing a vacuum, and rests in a cradle which permits 195° of rotation about the furnace's horizontal main axis. This cradle sits on a turntable which allows slight rotation about a vertical axis, and it, in turn, is on an x-y translator. Tilt and height are controlled by adjusting the height of three screws which serve as legs for the entire assembly. The entire assembly thus permits the sample to be brought into translational position and rotational orientation as desired while allowing optical access for measurement.

Vacuum is drawn via a TurboTronic NT 50 turbomolecular pump backed by a Trivac D1-6B roughing pump. Pressure is measured on an Inficon CC3 electronic vacuum gauge that measures down to 10^{-4} torr and always bottoms out to zero during use, but the sensor is located next to the turbomolecular pump at the opposite end of a one-meter flexible bellows from the furnace itself, so the pressure inside the furnace may be higher than indicated by the gauge. A quantitative measure of the vacuum inside the furnace is of no importance to the experiment, however, as long as there is so little air inside that the laser paths are not noticeably distorted, the heating filaments do not fail prematurely, and the samples do not oxidize; the system meets these conditions. An example of the importance of avoiding oxidation of the sample is found in Holt (1975), in which polycrystalline olivine disks, originally green, turned red (oxidized) when heated in air to 1170 K during the application of a Pt coating, then black (reduced) when heated in vacuum to 1470 K, producing markedly anomalous trends in thermal diffusivity. Although the samples in the present study were found to be discolored by a metallic coating from the heating filaments, as were the other interior surfaces of the furnace, this coating was easily wiped away with a methanol-soaked cotton swab, revealing in every case an unaltered sample surface.

Auxiliary Furnace

One limitation of the main vacuum furnace is the difficulty in raising and holding its temperature above approximately 600°C. When driven at the high currents needed for this, the lifespan of its tungsten-rhenium heating filament drops to around an hour or less, which is not sufficient for the completion of a full experimental run. To reach and sustain higher temperatures, an auxiliary furnace and a set of baffles were designed to fit within the body of the main furnace. This auxiliary furnace mounts in the same space as the Merrill-Bassett diamond-anvil cells normally used at high temperatures, so no modification of the vacuum furnace was necessary.

The auxiliary furnace consists of the four machined parts shown in Figure 1, along with a filament, a retaining spring, and a few smaller pieces. The machined parts are radially symmetric to facilitate fabrication and to assure a uniform thermal environment for the sample. The central section of the furnace is a Mo tube with a stepped bore; sample discs fit against a shelf adjacent to the smallest point of constriction, halfway along the tube. Molybdenum was selected for its high thermal conductivity and its resistance to oxidation at high temperatures. This first property minimizes the difference between the temperature of the sample and the temperature measured by a thermocouple inserted in a separate bore approximately two millimeters away, while the second property eliminates the problem of surficial oxide flaking that developed in the stainless steel prototype.

The Mo tube sits in a ceramic cup which has a small hole in the center of its base for optical access to the sample. This cup also contains the heating filament which presses outward against the sidewall of the cup, thereby permitting the filament to wrap around the central tube without danger of contacting the tube and shorting out. A ceramic cap, also drilled for optical access, fits over the cup and tube. The leads from the heating filament pass through two small holes in this cap. The cup and cap are made of Macor, a

machineable ceramic from Corning, Inc., that does not require firing after shaping, so its machined dimensions are preserved. A machineable mullite ceramic of unknown composition was used for the prototype furnace, but this material melted at its points of contact with the filament. The Macor cap is reinforced with thinwalled tubes of a high-temperature mullite ceramic (Omega Engineering SH-1-24-100, 0.0625" OD, clearance for 24 AWG ID) at the feedthrough points for the filament leads.

The remaining machined piece is an outer ring of Inconel 600, a Ni-Cr-Fe alloy, that holds the other pieces together and provides a bearing surface for the setscrews of the main furnace. Tolerances on all the pieces are loose to allow for differences in thermal expansion, so the furnace must be held together manually with firm pressure while the setscrews are advanced to clamp it in place so that nothing is free to rattle after assembly. A loop of W-Re wire, bent in the shape of a wavy washer, sits between the Macor cap and an outer ridge on the central tube to take up the slack and permit limited along-axis relative movement during heating and cooling. This wire is the same material as the heating filament described below. Relative rotation of the pieces is prevented by friction and by the rigidity of the leads for the filament and thermocouple.

The heating filament is a length of W-Re thermocouple wire, 0.020" in diameter, trimmed to the desired length after it has been bent into its final shape. This shape is a series of thirteen tight bends, formed on a jig originally made for use in shaping the much longer filament of the main furnace. The wire is sold by Omega Engineering in matched lengths of W 5% Re and W 26% Re (i.e., spools of Type C thermocouple), but no difference was noted in the performances of the two compositions for this application. It should be noted that these alloys are brittle—a 25 to 50% rate of failure while bending the wire into shape is to be expected, and the filaments generally break during disassembly after four or five high-temperature runs. The straight leads of the filament extend through the baffles of the main furnace where they are bolted to thick copper wires (24 AWG) The

filament leads and the copper wires are sheathed in loose pieces of the same mullite tubing employed at the feedthroughs.

The final piece of the auxiliary furnace is the spring for retaining the sample. This is a Be-Cu alloy, 0.107" OD, purchased from Small Parts, Incorporated, in coils of 0.295" free length (part CS-59). Each spring must be manually rewound on a mandrel to form a tapered spring that fits snugly along the full length of the central tube of the furnace and simultaneously presses firmly against the sample. The Be-Cu loses much of its elasticity at elevated temperatures and must be discarded after a single use, but still prevents any measurable movement of the sample. One exception to this, in which it appears the sample was caught by the end of the spring and forced to rotate as the coil unwound during heating, must be mentioned as it was necessary to consider this rotation in fitting the data for that run.

Temperature Measurement and Control

Temperatures were measured with Omega Chromel-Alumel (Type K) thermocouples. These are commercially available as prefabricated units entirely enclosed in a flexible stainless steel sheath of 0.020" OD and 12" length (Omega part # KMQIN-020U-12), permitting them to be inserted around the internal baffles of the main furnace and to be brought into close proximity to the desired points. Two thermocouples, each with its own temperature reader, were used: one to monitor the temperature within two millimeters of the sample and the other to monitor the temperature near the filament of the main furnace. A third thermocouple was available as a spare, so that the furnace would not have to be disassembled and a new thermocouple soldered into place in the event of a single failure.

Each heating filament is powered by a 120 V variac with manual control of voltage. For temperatures at or below 500°C, the power to the variac running the primary filament was

regulated by an Omega CN8500 digital controller/thermocouple reader that measured the temperature near the primary filament, and the temperature at the sample was displayed on either an Omega DP 460 reader or an Omega DP41 controller/reader. At these temperatures the secondary filament was not used. For higher temperatures, the CN8500 controller regulated the secondary filament via the thermocouple near the sample and the primary filament was driven constantly.

Whenever new thermocouples were installed they were cross-checked against one another and were always found to agree to within 1°C (the resolution of the DP-460) or less at room temperature, in ice water, and in boiling water when a single reader was used. The DP41 reader disagreed with the other two by as much as 5°C, so its use was primarily restricted to determining when steady-state conditions had been achieved, as it is the only unit that displays temperatures to a precision of 0.01°C.

One attempt was made to calibrate the accuracy of the thermocouple measurements at high temperatures against the melting point of pure NaCl in vacuum, 801°C (Weast, 1987, p. B-130), but the salt sublimed long before melting temperatures were reached. No other suitable materials were found that would not either sublime or otherwise contaminate and possibly damage the furnace, so this effort was abandoned. The temperatures were accepted as displayed and assumed to be accurate to at least 5°C across the entire range. If true, this represents an insignificant contribution to the uncertainty in the determination of thermal diffusivity as a function of temperature, so in the end all temperatures were treated as being exactly equal to their nominal values.

Generation of High Pressure

The olivine SCchai was placed in a conventional Merrill-Bassett diamond-anvil cell with an Inconel 718 gasket and compressed in a medium of fluid Ar that was loaded under

cryogenic conditions. Pressures were measured by observing the shift in frequency of the R1 and R2 fluorescence peaks of ruby chips that were placed in the cell cavity along with the sample. The thermal diffusivities measured at high pressure are from a single experimental run conducted by Professor Evan H. Abramson primarily as a demonstration that such measurements could be made; for a detailed description of the use of diamond-anvil cells in the context of such measurements, see Chai (1996).

Data Collection

General Procedures

Each experimental run began only after the lasers and electronics had been permitted to operate for at least an hour so as to promote stability in the laser output and in the room temperature of the laboratory. Following this, the optics (lenses, mirrors, pinholes) on the ISLS table were adjusted to produce the strongest possible signal from a cuvet containing methanol, then left untouched until such time as the signal weakened by approximately 10% or more. The length of this interval varied in duration from somewhat under twenty minutes to slightly over three hours, after which a realignment was necessary.

The precise convergence angle of the infrared pulses was determined by measuring the temperature-dependent frequency of sound in room-temperature methanol, which was done using the same collection geometry and equipment as needed for the measurements of thermal diffusivity. The temperature of the methanol was taken to be the same as that of a calibrated glass Hg thermometer (Brooklyn P-M Thermo Co ASTM 37C 15691, -2°C to 52°C , 0.2°C divisions) suspended over the laser table within 0.5 m of the infrared convergent point. Measurements typically were made with between 500 and 800 V applied to the photomultiplier tube and the resolution of the oscilloscope set to between 2 and 20

mV per major division on the vertical axis and 10 ns per major division on the horizontal axis, since only the first few tens of nanoseconds of signal contained useful information about the speed of sound. The details of how these measurements were interpreted is discussed in the Results section.

Once the infrared convergence angle had been established, measurements proceeded on the mineral sample. Whenever possible, the voltage to the photomultiplier tube was kept the same between the methanol and the sample to minimize the effects of any non-ideal behavior in the electronics, though it was often necessary to increase the voltage to enhance a weak signal from the sample. Strong signals collected at several different voltages within the useful range always gave the same answer to within the experimental uncertainty, however. For the silicates the horizontal axis of the oscilloscope was set to between 100 and 500 ns per major division, depending upon the rapidity of the exponential decay of the signal. Care had to be taken to assure that a sufficiently long runout of the decay was collected in order to constrain the fit to the characteristic time of the decay; at the same time, too long of a baseline would have resulted in poor resolution of the initial steep decay of the signal.

For many of the samples, background measurements were made whenever any change was made in the instrument settings. These signals were collected under the same conditions as the diffusivity data but with one of the infrared beams blocked so that no thermal grating was imposed upon the sample. The background signals generally displayed a small packet of (presumably electronic) noise near zero time, followed by essentially a flat line. Once it had been established for each new material that the subtraction of this noise made no significant difference to the interpretation of the signals, this procedure was no longer rigorously followed.

After the signal had been collected and averaged for a period of between approximately two and fifteen minutes, depending on signal strength, the results were saved to a file

capable of being opened within the mathematical program MATLAB for later analysis. All files in a session were assigned uniform names with consecutively increasing file numbers, beginning at "thermalfile0" as an aid to automated processing. At this point the sample was rotated by $20^{\circ} \pm 0.5^{\circ}$ about its face-normal and the measurement repeated. This continued until, ideally, 160° of rotation were swept, but for some samples it was not possible to find an adequate signal, or indeed any signal, in all positions.

Whenever the signal strength fell significantly, or whenever the run was to be paused, another methanol standard was collected before the optics were touched or before the system was left unattended. This was later checked against the initial standard for that sequence to confirm that nothing had affected the infrared convergence angle during the course of collecting data. Another methanol standard was taken after each readjustment of the optics before taking data, then a final methanol standard at the conclusion of the entire run.

The room temperature data were collected with the sample in the furnace under vacuum and assigned a nominal temperature of 27°C , though a better estimate of temperatures may be extracted from the temperatures recorded for the methanol standards, if desired. At elevated temperatures, the furnace was allowed to reach steady-state, in which the temperature fluctuated by no more than $\pm 2^{\circ}\text{C}$, before proceeding. Stability of less than $\pm 1^{\circ}\text{C}$ was often observed. Temperatures were repeatedly checked during and after each measurement to catch any failure of the heater or controller. For each sample except the clinopyroxene, temperatures were methodically advanced until 1000°C was reached or the system failed, which usually occurred via shorting of one of the heating filaments. For some of the more vexing samples, no second attempt was made to reach 1000°C once a significant fraction of the temperature range had been covered.

Only one sample was measured during the course of any given experimental run, as the required disassembly and cleaning of the furnace after each run consumed too much time to permit resumption during a single session. Individual runs routinely covered 12, 24, or, in one instance, 50 continuous hours of operation, during which period the system required attention at intervals of approximately 20 minutes.

Procedures Unique to the Collection of the Clinopyroxene Data

Room-temperature thermal diffusivity measurements were completed on the samples of clinopyroxene, KH-CPX, approximately one year before measurements on the other samples began. Many of the procedures and pieces of equipment used in the later phase of data collection were developed during that year in order to address shortcomings discovered during the pioneering work on KH-CPX. Differences in the method of preparing samples already have been discussed, but there were additional differences in the way the data were collected.

The KH-CPX crystals were not mounted in the vacuum furnace, but were instead fastened to half of the frame of a Merrill-Bassett diamond-anvil cell by means of a vise designed to fit in the space normally occupied by the seat for one of the diamonds. This half-frame was then mounted in a rotation stage commonly used in the lab for diamond-anvil cell work at room temperature. The vise held the sample firmly between a rigid backing plate and a piece of steel shim stock, each containing a hole for optical access to the sample, but this arrangement was deemed inadequate for high-temperature work, as it did not provide any means of accommodating differential thermal expansion. It would hold crystals of much smaller size than the furnace insert that was later designed, however, which is why the KH-CPX dataset was not extended to elevated temperatures.

Infrared convergence angles were measured directly by removing the sample and its rotation stage, then inserting a post-mounted mirror at the point of convergence. The post was fixed to a horizontal rotation stage, by which means the mirror could be rotated to reflect first one, then the other infrared beam back upon itself. The amount of this rotation, measured to the nearest minute, equaled the convergence angle. This method demanded great care in several matters: attaching the mirror to the post such that its reflective surface contained the axis of rotation, placing the assembly on the laser table such that the axis of rotation intersected the point of infrared convergence, and rotating the mirror and reading the results without displacing any of the optics, to name three. The subsequent use of a methanol standard was much preferred.

Finally, in order to determine uniquely the orientation of the diffusivity tensor with respect to the crystallographic axes for KH-CPX from only two samples, it was necessary to record the absolute position of each sample with respect to one of two corresponding datasets of anisotropic sound velocities recorded from the same samples. These velocities were referenced against the tensor of elastic constants developed by Collins and Brown (1998) to determine the orientation of the two crystals, from which the orientation of the diffusivity tensor followed. This is discussed further in Results.

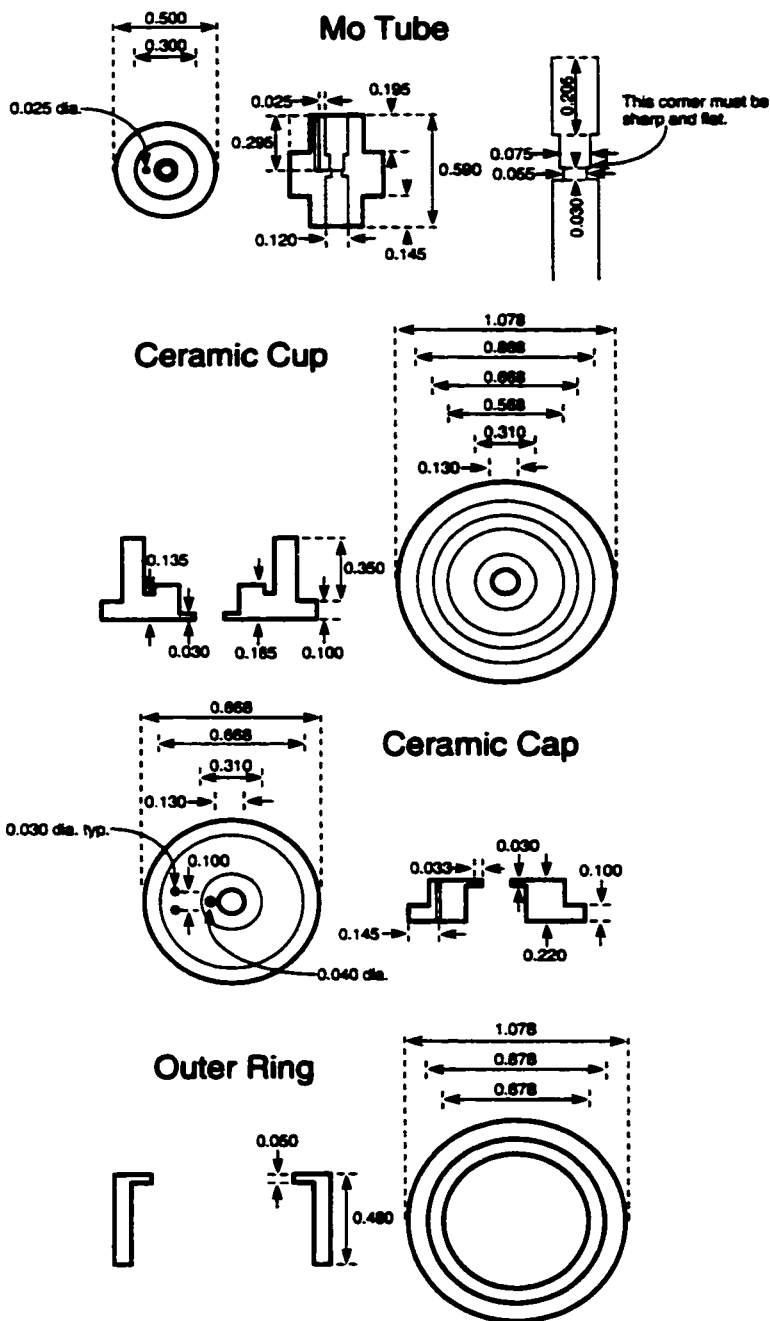


Figure 1 Machine Drawings for Auxiliary Furnace

The Mo Tube is made of molybdenum, the Ceramic Cup and Cap of Macor, and the Outer Ring of stainless steel, one each per furnace. Inside corners are radiused 0.020" and the edge break is 0.015". All dimensions are in inches.

Results

"Philonous. Sensible things therefore are nothing else but so many sensible qualities, or combinations of sensible qualities?

Hylas. Nothing else.

Phil. Heat is then a sensible thing?

Hyl. Certainly.

Phil. Doth the reality of sensible things consist in being perceived? or, is it something distinct from their being perceived, and that bears no relation to the mind?

Hyl. To exist is one thing, and to be *perceived* is another."
(Berkeley, 1713, p. 13)

Overview of the Analysis of Data

Each data file contains several variables that fall into two groups: a time-domain record of signal strength and a set of comments. Individual files first are processed to extract either an infrared convergence angle, in the case of methanol standards, or a characteristic time of exponential decay, in the case of thermal diffusivity files. Taken together, these convergence angles and characteristic times permit the calculation of the mineral's thermal diffusivity in the given directions, as preserved in the comments. Next, each coplanar set of thermal diffusivity vectors at a single temperature is fit by an elliptical curve, the major and minor axes of which correspond to two of the three principal values of the thermal diffusivity tensor. (This last statement is true only for the case of data collected from materials of orthorhombic or higher symmetry in which each slab is chosen to contain two crystallographic axes. Analysis of the more general case proceeds similarly, however.) Once this has been done for slabs of two different orientations, the entire thermal diffusivity tensor is known at each observed temperature. Finally, when this is combined with

independent determinations of specific heat and density, the material's temperature-dependent thermal conductivity tensor also may be calculated.

Individual Measurements

Methanol Standards

The time-domain record from a typical methanol file is shown in the upper left quarter of Figure 2. It comprises 1024 points at regular intervals of time, and represents the mean of a succession of waveforms (typically 150) dumped from the oscilloscope to the Mac II. Each waveform from the oscilloscope was itself was a running average of 512 successive signals from the photomultiplier tube.

The waveform begins at a time before the infrared pulses have reached the sample. Their arrival is indicated by the jump in signal intensity near 50 ns. Following this, the signal decays slightly between 50 and 150 ns, indicative of a structural relaxation in the methanol (Zaug, 1994), then flattens out to a level significantly above the original baseline, corresponding to the signal from the thermal component of the grating, which decays over the course of several microseconds. Superimposed on all this is a sinusoidal component that represents the acoustic signal; it is formed by the passage of two counterpropagating compressional waves across the thermal grating. The acoustic waves and the thermal grating have the same wavelength; peaks in the signal are formed when the acoustic and thermal components are in phase, and troughs when they are out of phase.

Both ends of the signal are manually truncated, leaving only the section that shows a large acoustic signal (Figure 2, upper right). This is Fourier transformed (Figure 2, lower

left), and the maximum of the single prominent peak in the transform is taken as the acoustic frequency, ν . This is related to the sound velocity, c , and the grating spacing, d , by

$$d = \frac{c}{\nu}$$

where c of methanol is calculated at temperature T from the relationship

$$c = 1103 \text{ ms}^{-1} - (3.2 \text{ ms}^{-1}\text{°C}^{-1})(T - 25\text{°C})$$

from Weast (1987, p. E-43). Once d is known, the convergence angle θ is given by

$$\sin \theta = \frac{\lambda}{2d}$$

in which λ is 1064 nm, the wavelength of the infrared pulses.

The results from all the methanol standards taken during a session were written to a single text file that contained the file number, date, time, temperature, sound velocity, and convergence angle for each measurement. This facilitated the automatic selection of the appropriate standards for the next step, the processing of each thermal diffusivity file. For KH-CPX, dummy text files were written in the same format but using the directly measured convergence angles so that the same software routines could be used for fitting all the data.

Thermal Diffusivities

Figure 3 displays the time-domain record of a typical measurement of the exponential decay in diffracted signal strength that arises from the dissipation, via thermal diffusion, of the imposed holographic grating. The signal was collected in the same manner as the methanol standards but with a much longer time base. As with the methanol standards, the record begins before the arrival of the infrared pulses, and shows a sharp increase at the time the grating is formed. Following this is a monotonic decrease in signal back to the

baseline; oscillations arising from acoustic waves are not seen, in part because of the relative weakness of the acoustic signal in silicates, and in part because of the chosen timescale.

Fitting each record of signal strength, s , versus time, t , with an exponential curve of the form

$$s = Ae^{\frac{-t}{\tau}}$$

in order to extract its characteristic time, τ , is straightforward, but the method of estimating the uncertainty in τ relies upon an empirical approach developed by Professor Abramson that requires a detailed explanation. The principle is to truncate the curve at various points and compare the resulting fits. A true exponential decay is self-similar, so no variation in characteristic times should be seen among the several fits. Any observed variation therefore becomes a measure of the uncertainty with which the characteristic time may be determined. An illustration of the technique is given in Figure 4. First, two points are automatically selected: the point of maximum signal and the point at which the signal has fallen to ten percent of this maximum. Next, four additional points are selected between these two points, evenly spaced along the temporal axis. Each of these six points is used in turn as the start of a least-squares fit to the data, from that point through the tail end of the curve. In the figure, the characteristic time for each such fit is plotted as an asterisk; the horizontal position marks the beginning of the fitting interval and the vertical position is the characteristic time in inverse microseconds. The points at each end are circled to indicate that they are not considered further: the initial point, in general, is skewed by electronic noise near the beginning of the imposition of the grating, and the final point is a fit to too short a section of data. They are plotted merely as a visual check to assure the data are not too grossly distorted at either end. The remaining four points are averaged together to give the mean, percent uncertainty, misfit, and 2σ error for the final determination of characteristic time. As with the methanol standards, these values for all the measurements

made during a single run, indexed by file number, were saved to a single text file for further processing.

From the characteristic time, τ , and the grating spacing, d , the thermal diffusivity, D , is calculated using the relationship

$$D = \frac{d^2}{4\pi^2\tau}$$

in which the grating spacing is the average of the methanol standards taken immediately before and immediately after the set of diffusivity measurements containing the file in question. The change in grating spacing was usually less than 0.5% from start to finish; a larger drift in the optics would have been cause to discard the dataset and repeat the measurements. All the diffusivities, uncertainties, comments, and other variables generated during the fitting process were placed into a ".mat" file for use in generating diffusivity tensors in MATLAB.

In the course of these experiments, 195 independent measurements of thermal diffusivity were made on KH-OLV from room temperature to 1000°C, 222 on SC73-10 to 900°C, 139 on FA-147337 to 600°C, 147 on KH-OPX to 1000°C, and 97 on KH-CPX at room temperature. Professor Abramson collected 35 measurements from SCchai at room pressure and an additional 35 at high pressure. The results of all of these measurements are listed in Appendix A. The number of entries in these tables exceeds the totals just given; file numbers above 100 indicate files from which a background measurement has been subtracted, *i.e.*, thermalfile114 is the same measurement as thermalfile14 of the same date, less the background. Another 31 measurements (13 for KH-OLV, 10 for FA-147337, and 8 for KH-CPX) were collected and processed but are not included. These consist of sets for which too few points were taken to constrain the tensor values, a set examining the effect of changing the bandwidth of the oscilloscope, an examination of sample homogeneity, and a set collected while the conditions of acquisition were deliberately varied.

Anisotropic Thermal Diffusivity Tensors

General Practices in Calculating the Tensors

From each set of thermal diffusivity measurements made on a sample at a single temperature, there are three parameters of interest: the two along-axis diffusivities and the orientation of these axes within the plane of the sample. The first two numbers represent two of the three principal values of the full diffusivity tensor, and the third provides a check of the consistency both of the sample's behavior and of the adequacy of the fitting routine from set to set. These parameters were extracted by fitting an elliptical curve to the points.

During the collection of thermal diffusivity data, no attempt was made to identify precisely the directions of the crystallographic axes within the plane of the sample except, as has been noted, in the case of KH-CPX; instead, the data were collected at fixed intervals of sample rotation. Mathematically, the values at any three noncoincident points along its curve will uniquely constrain an ellipse; in practice, a minimum of four points at 20° intervals proved adequate, in light of the generally observed low scatter and small uncertainties. Whenever possible, however, six or more points were taken. Typically the points span one crystallographic axis and closely approach the other, as it was often the case that the signal strength was greatly affected by the orientation of the sample, such that collection along both axes would not have been possible even if desired. This phenomenon is reflected in the varying size of the uncertainties associated with individual points within the same set, as in Figure 5.

A series of MATLAB routines were written (borrowing some code from routines long in use in the laboratory) to automatically group all points by temperature for each day's files, then apply a least-squares fit to each group, in which the orientation of the sample's normal

was read from the comments in each file. Each fit was weighted by the uncertainties previously calculated for each point. The results were the two principal diffusivities, with uncertainties, an r.m.s. misfit, and the orientation of the sample within the plane. This last parameter is listed in Tables 4-8 as an offset angle between an imposed 0° direction and the direction of the major axis of the ellipse.

The offset angle has no permanent physical significance with respect to the sample (except, as is explained in the following section, for KH-CPX), as it merely describes the rotational position of the sample's axes as measured by the scale inscribed on the outside of the cradle for the vacuum furnace. This changed each time the sample was removed and reinserted. Furthermore, the recorded rotation angles often had to be shifted during processing so as to fall between 0° and 180° to accommodate the preferences of the software—this is shown by the dual horizontal scale on Figure 5. The general utility of the offset angle is that it provides a common point of reference from set to set throughout a day's run. If the offset angle remained the same to within $\pm 1^\circ$, this was taken as an indication that the sample had not shifted as the furnace was removed from and replaced on the laser table, nor as the furnace was rotated, nor as the temperature was increased. It also served as an indication that each set of points adequately constrained the fit with respect to this free parameter. For a number of sets that contained too few points in the rotation, however, the offset angle was held fixed to permit the fitting routine to converge, once the offset had been determined from the more extensive sets collected on the same day.

The data collected from the α -normal cut of SC73-10 on 21 September 2000 require additional comment with respect to offset angle. From 100°C to 900°C the best-fit offset angle systematically advanced by 61.1° , as shown in Figure 6. At the lower temperatures, seven points at 20° intervals were measured, and from 700°C to 900°C nine points were taken, all leading to good fits and consistent values of diffusivity at each temperature. Given

this, the most reasonable conclusion is that the sample physically rotated inside the furnace as the temperature was advanced. The only plausible mechanism for this is that it was driven by its retaining spring as that spring unwound while undergoing thermal expansion. The direction of rotation was consistent with the handedness of the coil spring, and a calculation of the amount of expansion to be expected from the Be-Cu alloy, approximated as pure Cu, accounted for just the amount of rotation observed. As the results at each temperature are entirely self-consistent, it is assumed that all motion occurred as the temperature advanced, not after steady-state had been reached. Although this anomalous behavior was recognized during the course of the experiment, it was not possible to take measurements as the furnace cooled, nor at room temperature, to check for evidence of permanent rotation or of reversibility—the surface of the sample became covered with opaque deposits from the heating filament as soon as it was permitted to cool with respect to the surrounding interior surfaces of the furnace, as was the case in all runs. Upon removal of the secondary furnace, it was observed that the end of the coil spring was pressing against the side of the sample, which did not fill the entire circular recess of the furnace. Presumably on other days the end of the spring merely slipped across the face of the sample as the spring unwound.

The complete set of tensor values of thermal diffusivity at all temperatures are listed in Tables 4-8. For KH-OLV, data were collected to high temperatures at the two nominal infrared convergence angles of 10° and 15° to ascertain whether the corresponding range of grating spacings were within the limits of one-dimensional lattice thermal diffusivity. The two bodies of data produced the same results, confirming this. All other measurements were made at a nominal 15° convergence angle.

For each composition, one axis is shared between the two chosen cuts, and the results along this duplicated direction are in agreement in all cases. To calculate the final set of thermal diffusivity tensors, the results for each composition at each temperature (and, for

KH-OLV, each convergence angle) were combined into weighted averages. An isotropic value also has been calculated at each temperature, following

$$D_{\text{iso}} = \frac{D_{11} + D_{22} + D_{33}}{3}$$

in which D_{11} is the diffusivity along the a axis, D_{22} along b , and D_{33} along c for the orthorhombic minerals; for KH-CPX, average is calculated from the diagonalized tensor described in the following section. These averages (Figures 7-10) and isotropic values (Figures 11-14) are recorded in Tables 9-14, and form the basis for all further calculations and discussion.

Further Calculations for KH-CPX

Two additional steps were required in processing the data from KH-CPX, the first to account for the larger difference between the nominal orientation and actual orientation of each cut than was observed in the other materials, and the second to orient the diffusivity tensor with respect to the monoclinic axes of the clinopyroxene. In anticipation of these requirements, a set of measurements of sound velocity and a set of cell parameters were acquired for the material.

The sound velocities were measured in essentially the same manner as that used for the methanol standards, except that a string of frequency-doubled pulses from the Nd:YAG was used as the probe instead of the output of a separate CW laser. Each pulse gives one point on the time-domain curve, which was pieced together by the Mac II from a series of runs in which the arrival of the probe is successively delayed by increasing its path length. This obviates the need of an oscilloscope for collecting traces at the expense of drastically increasing the time needed to collect a single curve, but the advantages lie in the much greater intensity of the pulsed probe, and the much finer resolution of the first few tens of

nanoseconds in the evolution of the grating. The details of this method, used routinely in this laboratory, are presented in Zaug (1994).

As KH-CPX is acoustically anisotropic, each record from the two rotation studies could have contained information on both the quasilongitudinal and the two quasitransverse waves for the given propagation direction. For most directions, however, only the quasilongitudinal and, at best, a single quasitransverse branch were observed. Nevertheless, these were sufficient to permit the two samples to be oriented with respect to the tensor of elastic constants in Collins and Brown (1998). From this, it was discovered that the nominally a^* -normal sample had an actual normal that was rotated from the a^* axis by 7.8° towards b and 0.2° towards c , while the normal of the nominally b -normal sample was rotated 4.4° away from a and 0.1° away from c . These directions are with respect to the convention of adopting a right-handed set of axes in which the angle between the positive a and c axes is obtuse, as is assumed in all further discussion. For both samples, the smaller tilt angle was deemed negligible, but the coordinates of the diffusivity tensors were rotated from the laboratory (sample) reference frame to the crystallographic reference frame to account for the larger tilts.

This action alone permitted the correct calculation of the magnitude of the thermal diffusivity tensor, but was not sufficient to constrain uniquely the orientation of the tensor with respect to the crystallographic axes. Despite the few degrees of tilt, the two orientations were still so close to their nominal values that, essentially, the a^* -normal cut provided the diffusivities along b and c , while the b -normal cut provided the major and minor axes of the thermal diffusivity ellipse within the a - c plane. Considerations of symmetry constrain one axis of the diffusivity tensor, D_{22} , to lie along b , but the other two axes may assume any pair of orthogonal directions within the a - c plane. For the determination of the value along the maximum principal axis and the determination along the c axis to be compatible, however, the maximum must be separated from c by 16.0° .

Only with reference to the preserved rotation angles of the sample stage is it possible to distinguish between a positive and a negative offset between the two, though this would not have been necessary had a third, c^* -normal cut also been examined. By comparing the laboratory rotation angles with the rotation angles of the sound velocity datasets, which differ by a recorded, fixed amount, it is seen that the offset is negative, which is to say D_{33} of the diagonalized tensor lies within the acute a - c angle, 16.0° from c , illustrated in Figure 15. To complete the description, it must be added that X-ray crystallographic data indicate $\beta = 106.5^\circ$, $a = 9.738 \text{ \AA}$, $b = 8.884 \text{ \AA}$, and $c = 5.280 \text{ \AA}$, from which the diffusivity with respect to any crystallographic direction may be calculated, if desired. In Table 13, both the principle values of the diagonalized thermal diffusivity tensor and the values with respect to the conventional orthogonal axes (a^* , b , and c) are given. The latter expression has an off-diagonal term, D_{13} ($= D_{31}$). The two representations are equivalent via the 16.0° rotation, but the former is more useful in summarizing the extrema of the diffusivity ellipsoid, visualizing its physical orientation with respect to the crystallographic axes, and performing calculations for which the precise crystallographic orientation is not important, whereas the latter is appropriate for calculations made with strict respect to the crystallographic axes.

Anisotropic Thermal Conductivity Tensors

For many applications involving heat flow within Earth or other terrestrial bodies, it is more convenient to work with the thermal conductivity of materials than their thermal diffusivity. As was noted earlier, the conversion of one quantity to the other requires a knowledge of heat capacities and densities under the conditions of interest. For this work, heat capacities and densities were calculated on the MELTS Supplemental Calculator, which uses the internally consistent thermodynamic model of Berman (1988) as presented by

Ghiorso and Sack (1995). The version employed is, as of this writing, maintained on-line by Professor Ghiorso at <http://www.geology.washington.edu/~ghiorso/MeltsCALC/> for remote use, though it also may be acquired for local use as part of the larger MELTS software package.

For the calculation of thermodynamic properties, the MELTS Supplemental Calculator requires that the composition of a selected phase be expressed as mole fractions of end-member components of a solid-solution series, though it will also calculate these mole fractions separately if given the weight percents of the constituent oxides. A pressure and temperature also are required; for all phases in this study, the high-temperature calculations were performed for a pressure of 0 bar, and the high-pressure calculations assumed a temperature of 27°C.

The olivines were modeled along the forsterite ($\text{Fo} = \text{Mg}_2\text{SiO}_4$) to fayalite ($\text{Fa} = \text{Fe}_2\text{SiO}_4$) solid solution. KH-OLV was entered as $\text{Fo}_{91}\text{Fa}_9$, SCchai as $\text{Fo}_{89}\text{Fa}_{11}$, SC73-10 as $\text{Fo}_{78}\text{Fa}_{22}$, and FA-147337 as Fa_{100} . The pyroxenes were modeled by the phases diopside ($\text{Di} = \text{CaMgSi}_2\text{O}_6$), enstatite ($\text{En} = \text{Mg}_2\text{Si}_2\text{O}_6$), hedenbergite ($\text{He} = \text{CaFeSi}_2\text{O}_6$), aluminobuffonite ($\text{ABu} = \text{Ca}(\text{Ti},\text{Mg})\text{AlSiO}_6$), buffonite ($\text{Bu} = \text{Ca}(\text{Ti},\text{Fe})\text{AlSiO}_6$), esseneite ($\text{Es} = \text{CaFeAlSiO}_6$), and jadeite ($\text{Jd} = \text{NaAlSi}_2\text{O}_6$). This resulted in a composition for KH-CPX of $\text{Di}_{56}\text{En}_{14}\text{He}_7\text{ABu}_8\text{Bu}_5\text{Es}_{10}\text{Jd}_{10}$ and for KH-OPX of $\text{Di}_{25}\text{En}_{96}\text{He}_{17}\text{Es}_{12}$. The more restrictive model for orthopyroxene, in which KH-OPX was rendered as $\text{En}_{91}\text{Fs}_9$ (ferrosilite = $\text{Fs} = \text{Fe}_2\text{Si}_2\text{O}_6$), also was used, but its results did not significantly differ from those of the more general pyroxene model below 900°C. Around 1000°C, however, enstatite converts to protoenstatite (985°C for En_{100} , Deer et al., 1966, p. 108) which produces a discontinuity in the model. As no evidence of this phase change was observed in the experiment, nor was it to be expected for the actual composition under these conditions, the otherwise interchangeable results of the general pyroxene model were used exclusively.

The specific heats and molar volumes of all phases at the observed pressures and temperatures are listed in Table 15, along with the molecular weights. The anisotropic thermal conductivities, K , produced by combining these with the corresponding diffusivities, D , from Tables 9-14 according to

$$K = D\rho C_p$$

are given at the ends of Tables 9-14 and, except for KH-CPX, are represented in Figures 16-19. As with the diffusivities, isotropic values also are given in the tables, and both representations of the tensor are included for KH-CPX.

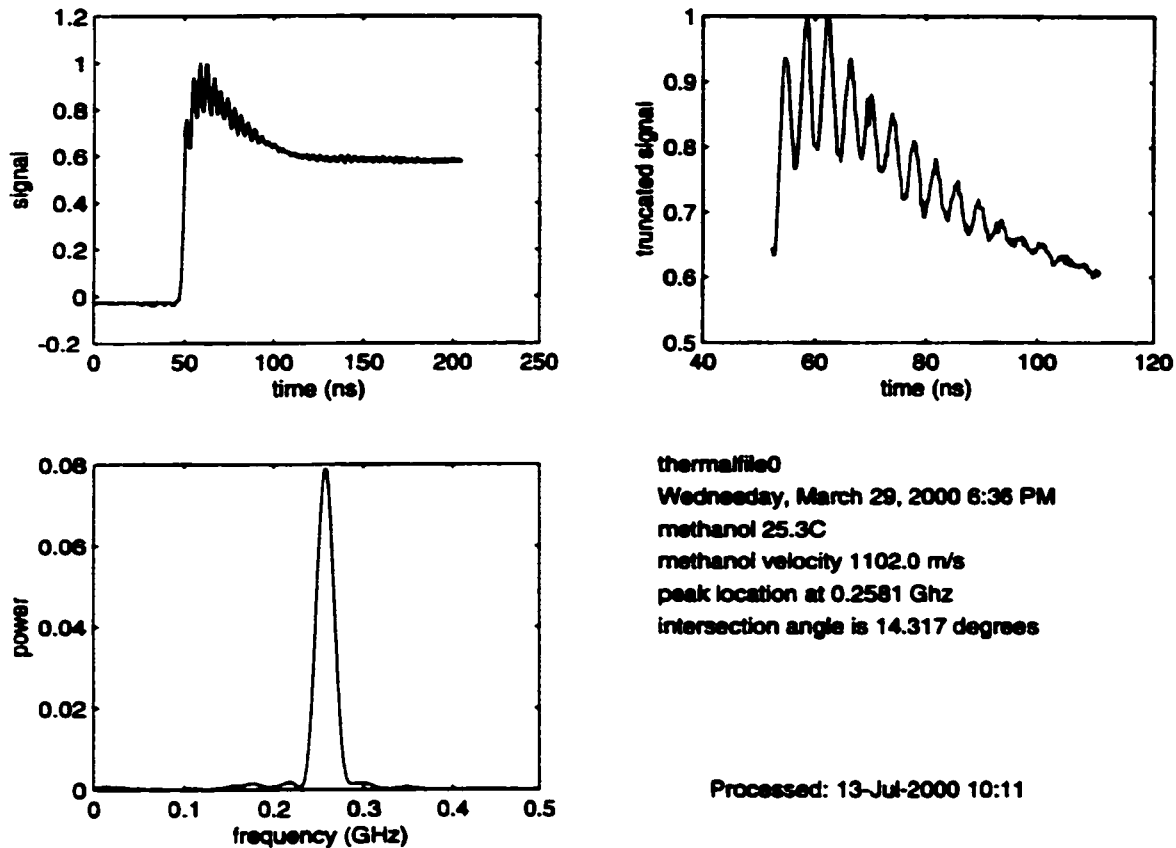


Figure 2 Processing of a Methanol Standard

The original signal (upper left) is manually truncated so as to isolate the acoustic signal (upper right). The Fourier transform of this (lower left) features a prominent peak at the frequency of the compressional wave. From this, the intersection angle of the infrared pulses is calculated, and is recorded at the lower right.

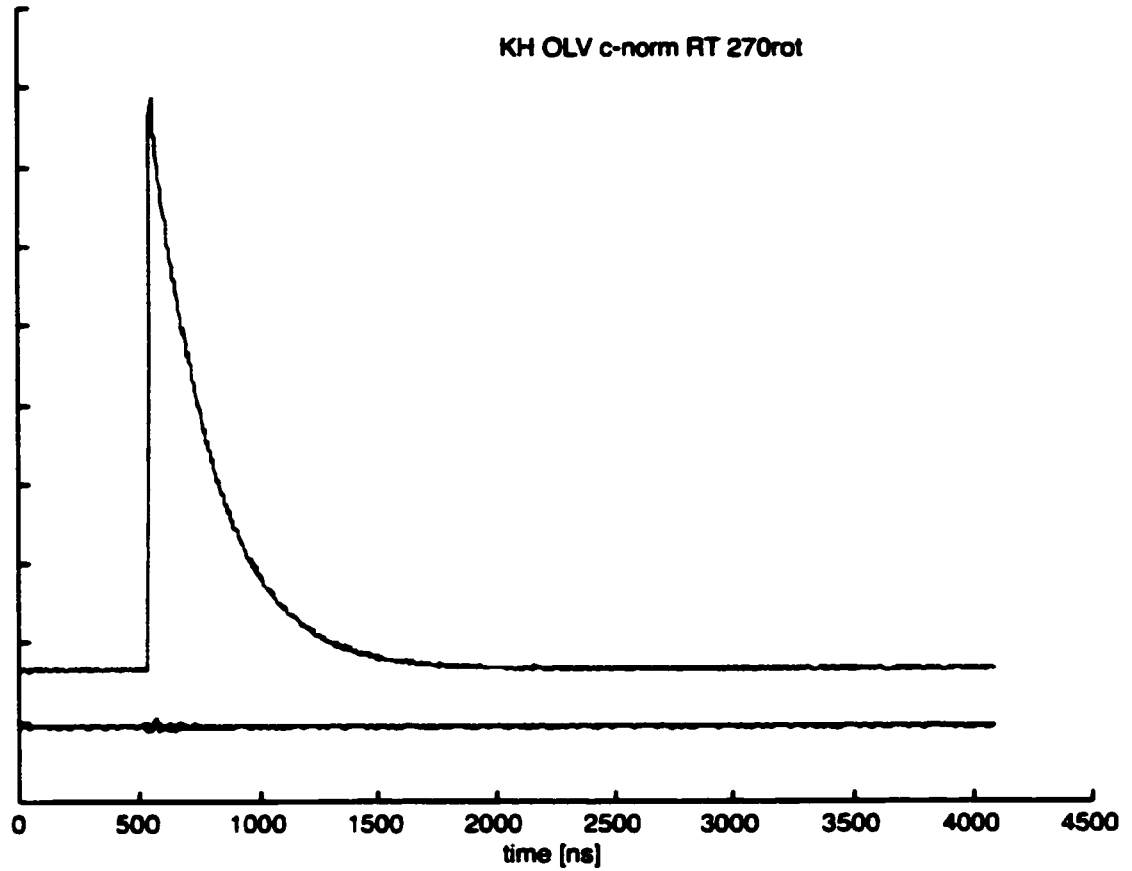


Figure 3 Measurement of Thermal Diffusivity in a Single Direction

The upper curve shows the sudden formation and exponential dissipation of the holographic thermal grating imposed upon the sample. The characteristic time of the decay is proportional to the component of thermal diffusivity in the direction normal to the planes of the grating. The lower curve was taken under the same conditions, but with one infrared pulse blocked so that no grating formed. The vertical scale is an arbitrary indication of intensity; the actual measurements were recorded as voltages.

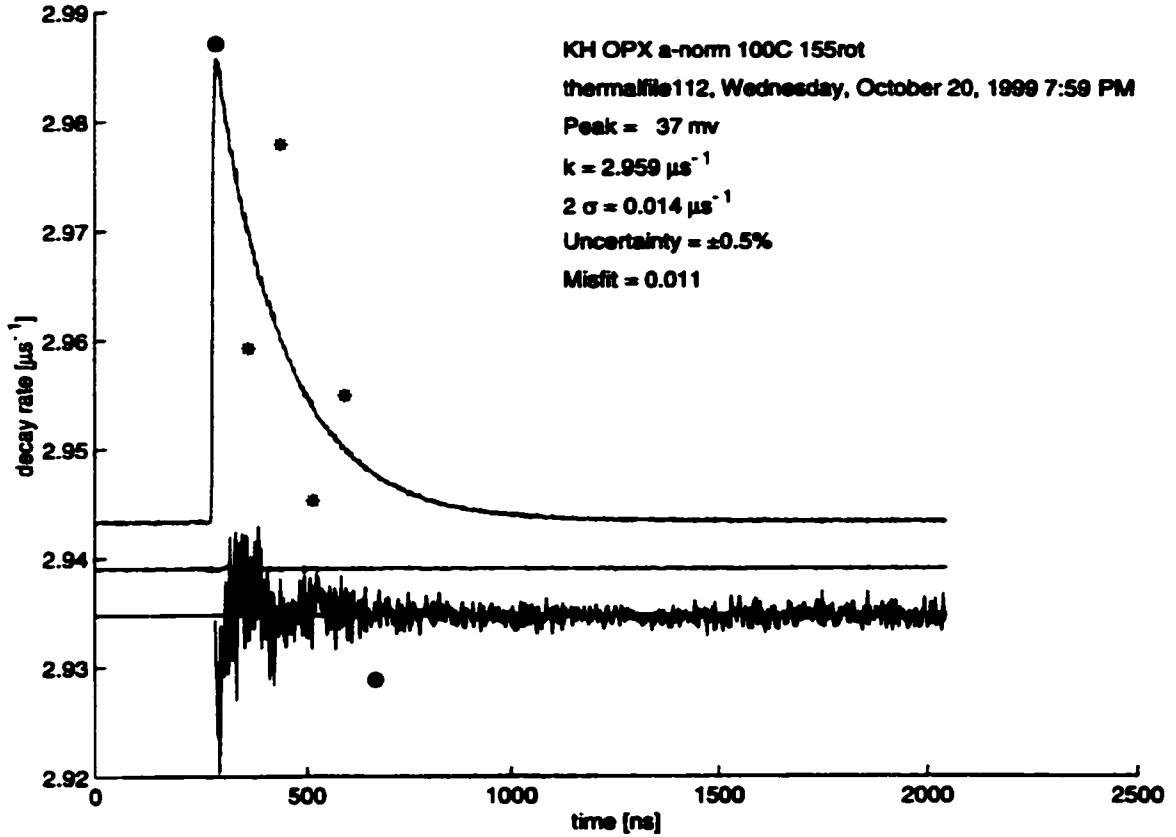


Figure 4 Extraction of Characteristic Time from the Data

The upper and middle curves are as in Figure 3. The six asterisks (two are circled) represent determinations of the decay rate as given by least-square fits to the exponential decay, the decay being fit from the horizontal position of each respective asterisk to the end of the data; the vertical position of each asterisk is the decay rate, shown along the vertical axis. The mean of the four central (non-circled) points is taken as the best representation. The difference between the curve generated by this mean value and the data is plotted as the lower, noisy curve; the difference has been multiplied by ten to facilitate visual identification of any systematic deviations.

KH OLV *a*-norm 27°C, thermalfiles 101 to 107
 Friday, September 17, 1999 11:22 AM

$D(2\sigma) = 2.02(0.08) \ 1.30(0.04) \text{ mm}^2\text{s}^{-1}$
 r.m.s. misfit = 0.007
 errorbar $2\sigma = 0.02$

offset = 23.7°

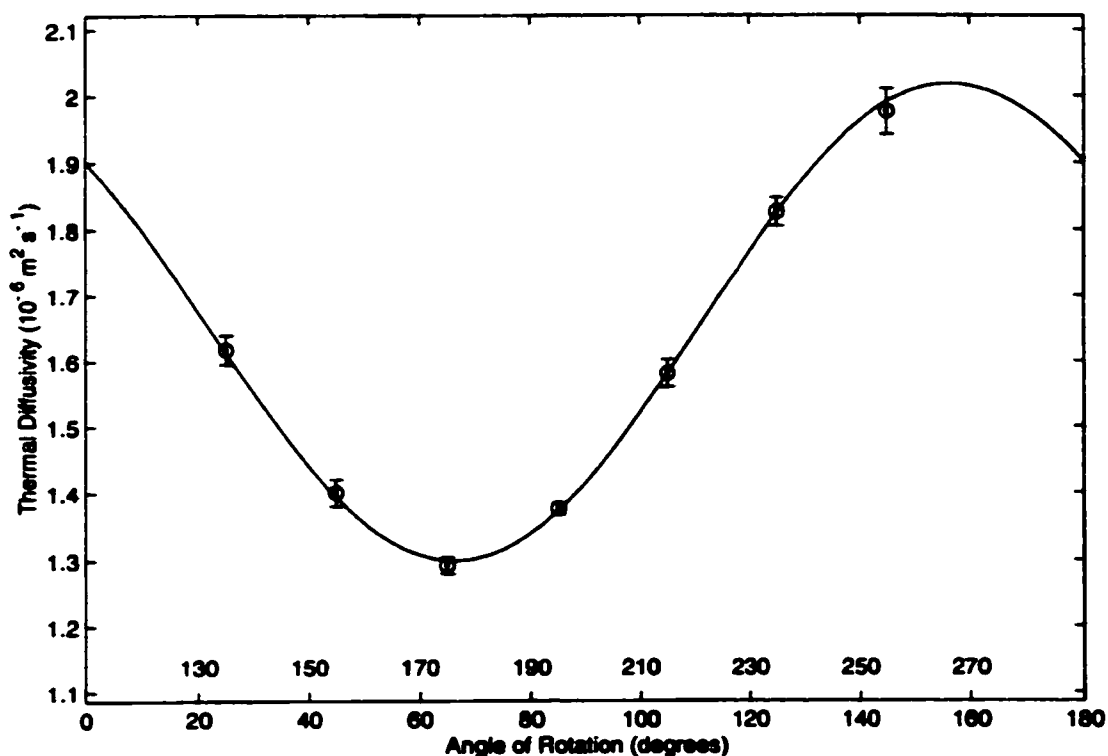


Figure 5 Round of Data Within a Crystallographic Plane

Each point and its uncertainty is derived from a measurement of the type shown in Figures 3 and 4; the sample is rotated about its normal between points. The curve is the weighted least-squares fit of an ellipse. The axes of the ellipse, represented here by the minimum and maximum of the curve, correspond to the two in-plane principal values of the thermal diffusivity tensor. In this case, since the sample contains the *b* and *c* axes (and therefore is described as *a*-normal), the values are D_{22} and D_{33} .

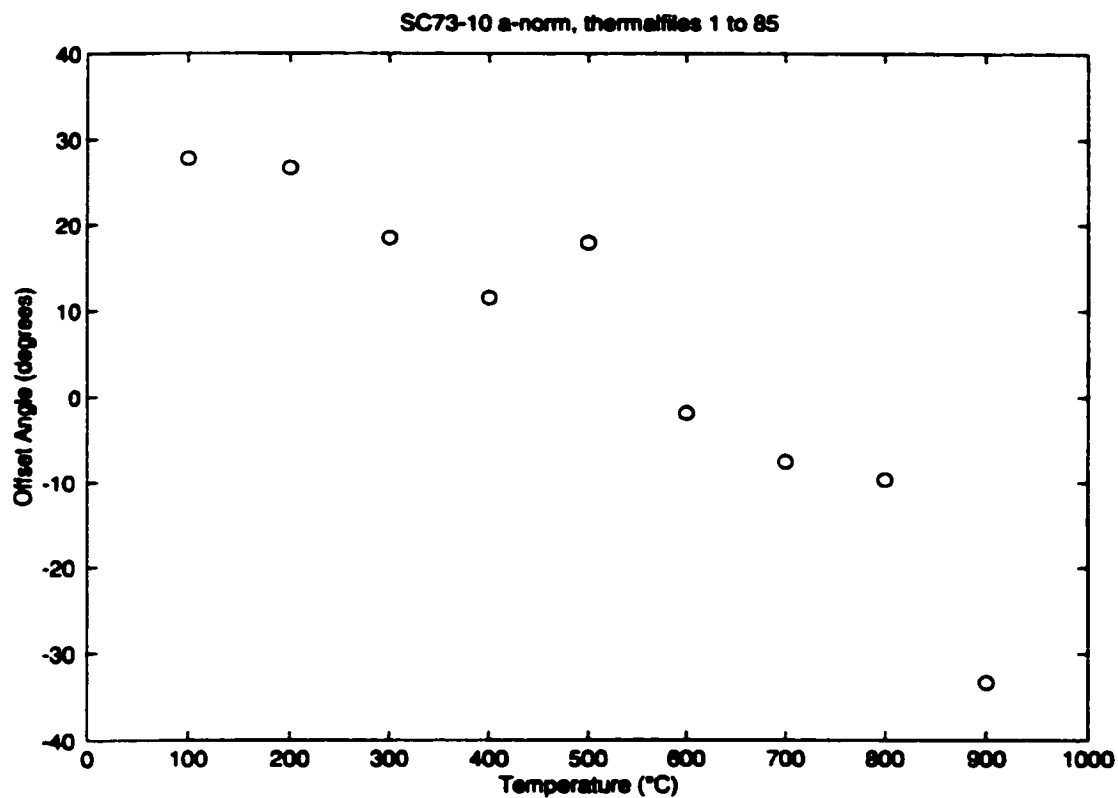


Figure 6 Unexpected Rotation of Sample with Increasing Temperature

For a single high-temperature run, the sample apparently rotated within the furnace as the temperature advanced. The amount and direction of rotation is consistent with the unwinding of the Be-Cu retaining spring as it underwent thermal expansion. For all other runs, the offset angle remained fixed to within 1° of rotation.

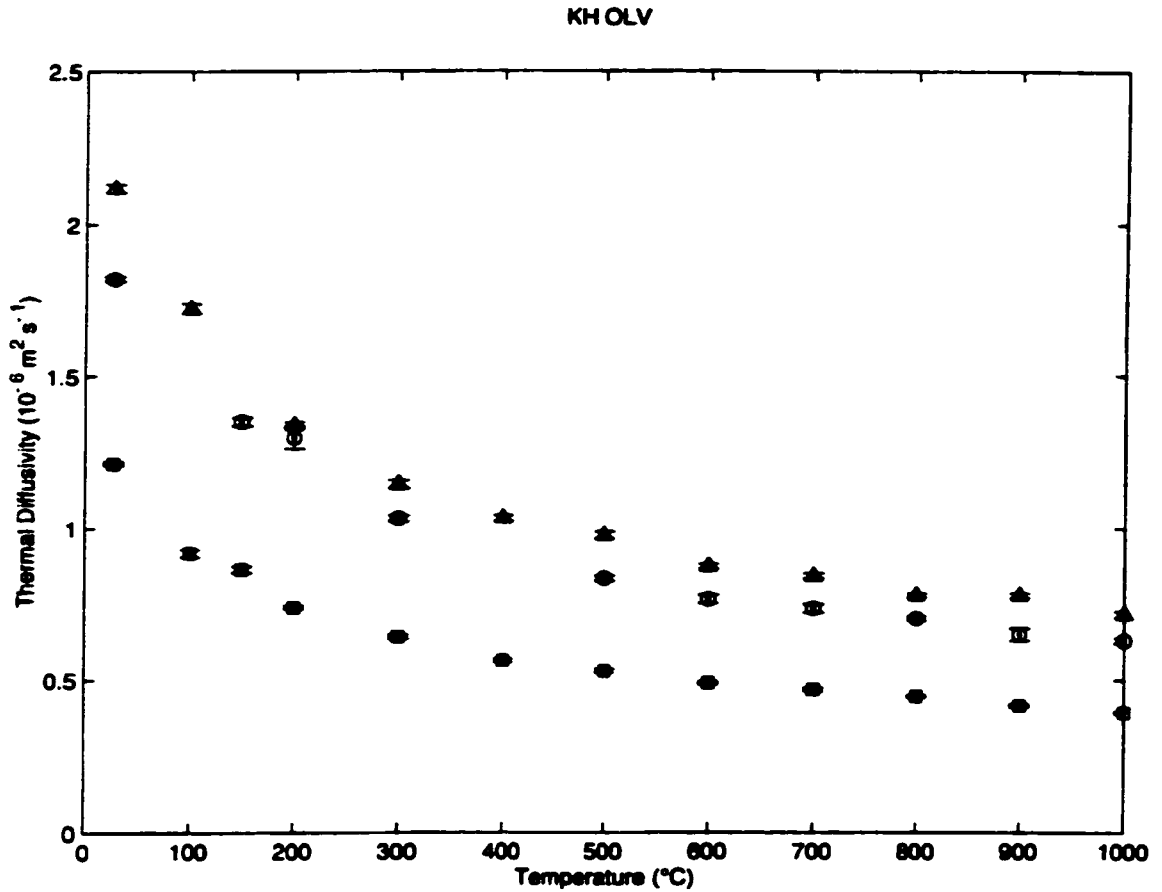


Figure 7 Anisotropic Lattice Thermal Diffusivities for KH-OLV to 1000°C

The points are the principal values of the lattice thermal diffusivity tensor, with uncertainties, as determined at each temperature. Multiple determinations are combined into weighted means. Triangles (at top) are D_{11} , squares (at bottom) are D_{22} , and circles (middle) are D_{33} . Gaps at 100, 150, 200, and 400°C are a consequence of measurements being made for only one sample (i.e. for only one orientation) at these temperatures.

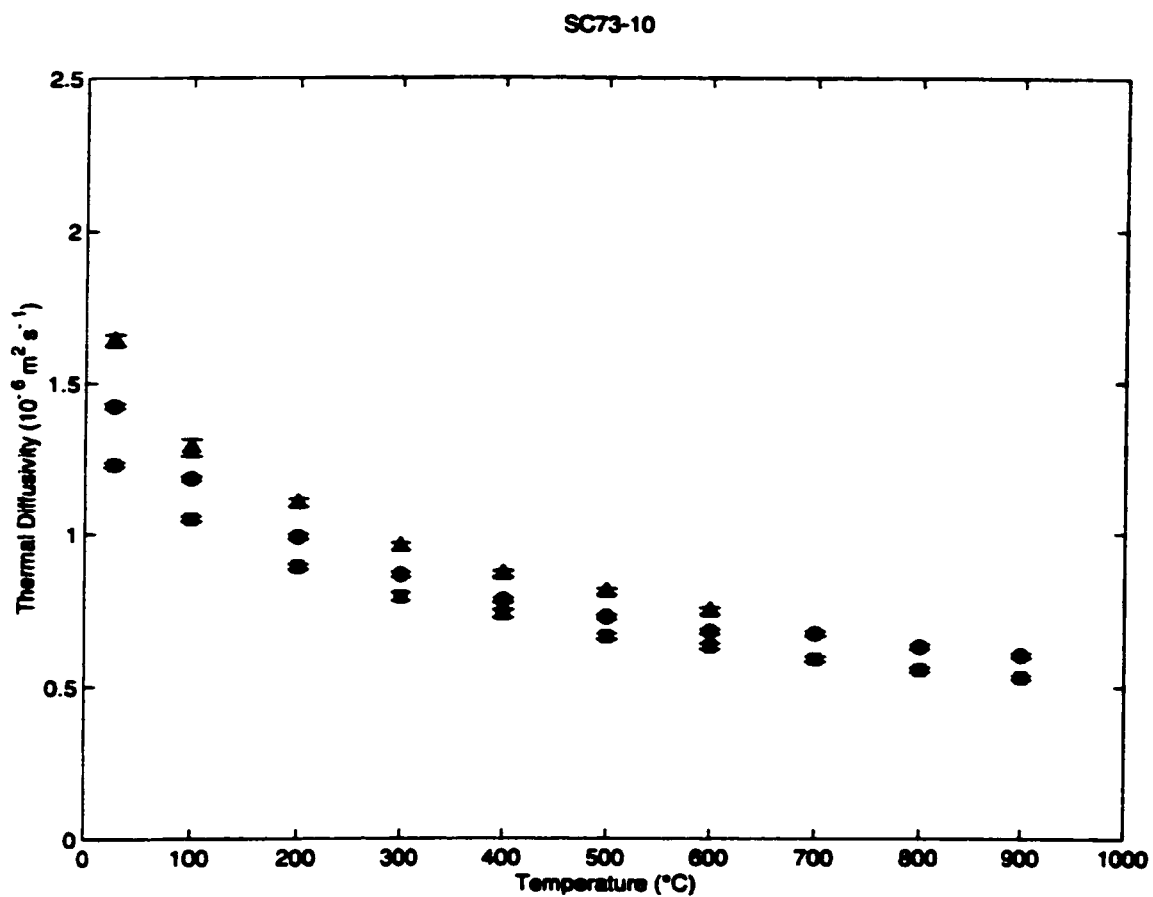


Figure 8 Anisotropic Lattice Thermal Diffusivities for SC73-10 to 900°C

The points are the principal values of the lattice thermal diffusivity tensor, with uncertainties, as determined at each temperature. Multiple determinations are combined into weighted means. Triangles (at top) are D_{11} , squares (at bottom) are D_{22} , and circles (middle) are D_{33} . Gaps at 700, 800, and 900°C are a consequence of measurements being made for only one sample (i.e. for only one orientation) at these temperatures.

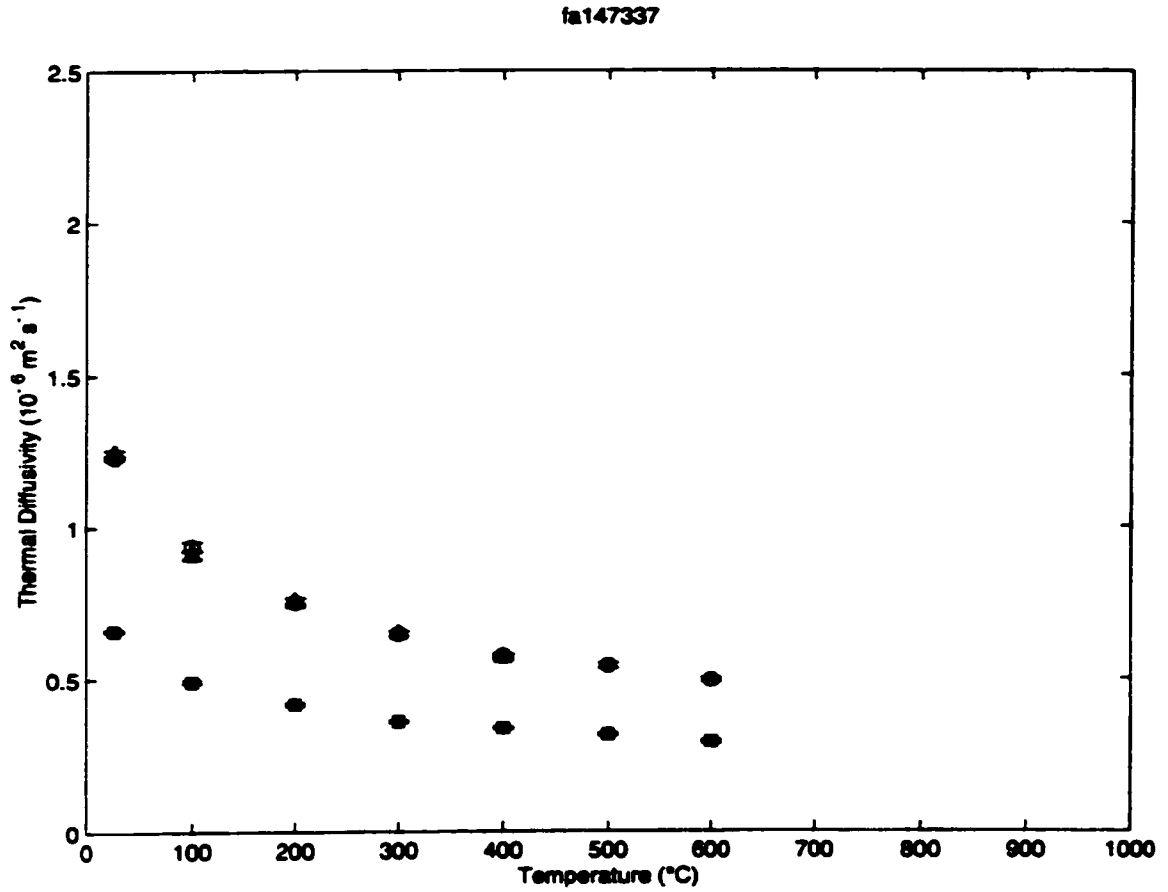


Figure 9 Anisotropic Lattice Thermal Diffusivities for FA-147337 to 600°C

The points are the principal values of the lattice thermal diffusivity tensor, with uncertainties, as determined at each temperature. Multiple determinations are combined into weighted means. Triangles (at top) are D_{11} , squares (at bottom) are D_{22} , and circles (also at top) are D_{33} . The sample is essentially isotropic in the a - c plane, as shown by the almost exact overlap of the points for D_{11} and D_{33} , both of which are plotted at all temperatures up to 400°C.

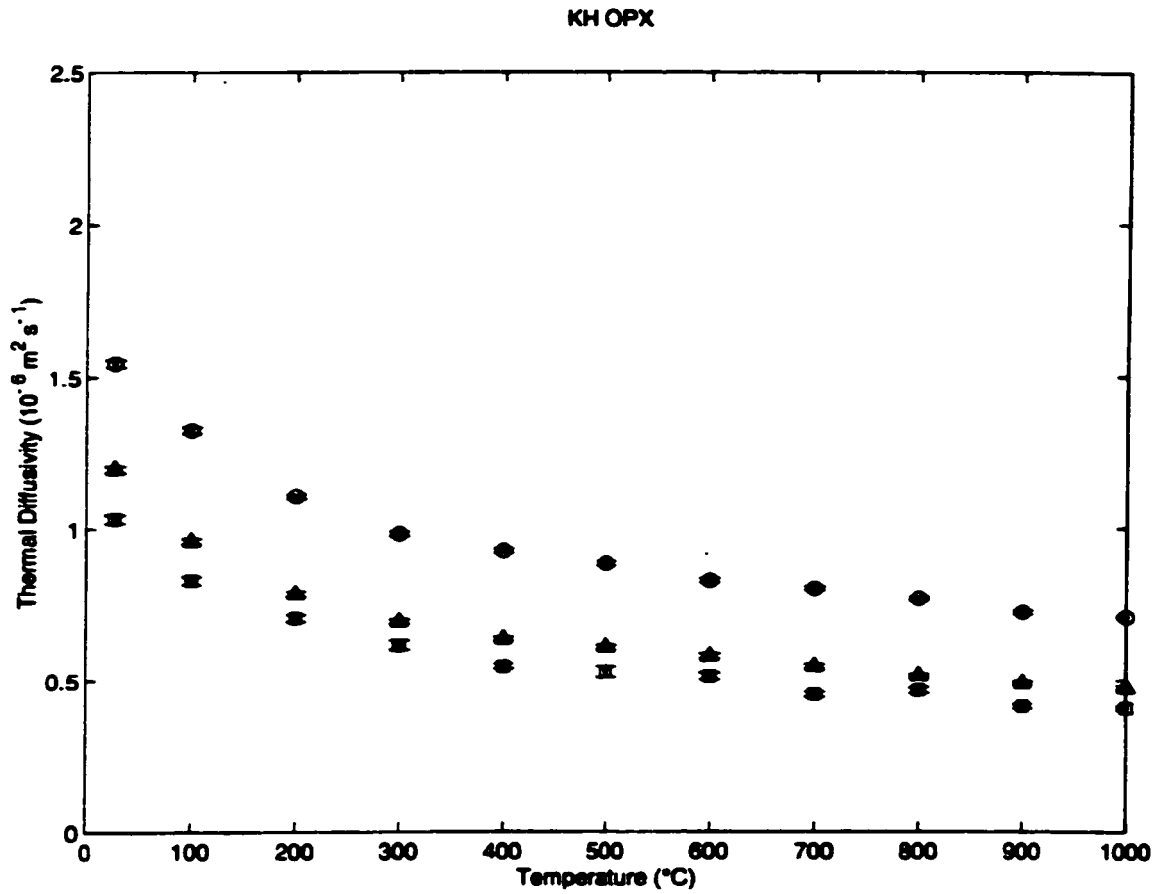


Figure 10 Anisotropic Lattice Thermal Diffusivities for KH-OPX to 1000°C

The points are the principal values of the lattice thermal diffusivity tensor, with uncertainties, as determined at each temperature. Multiple determinations are combined into weighted means. Triangles (middle) are D_{11} , squares (at bottom) are D_{22} , and circles (at top) are D_{33} .

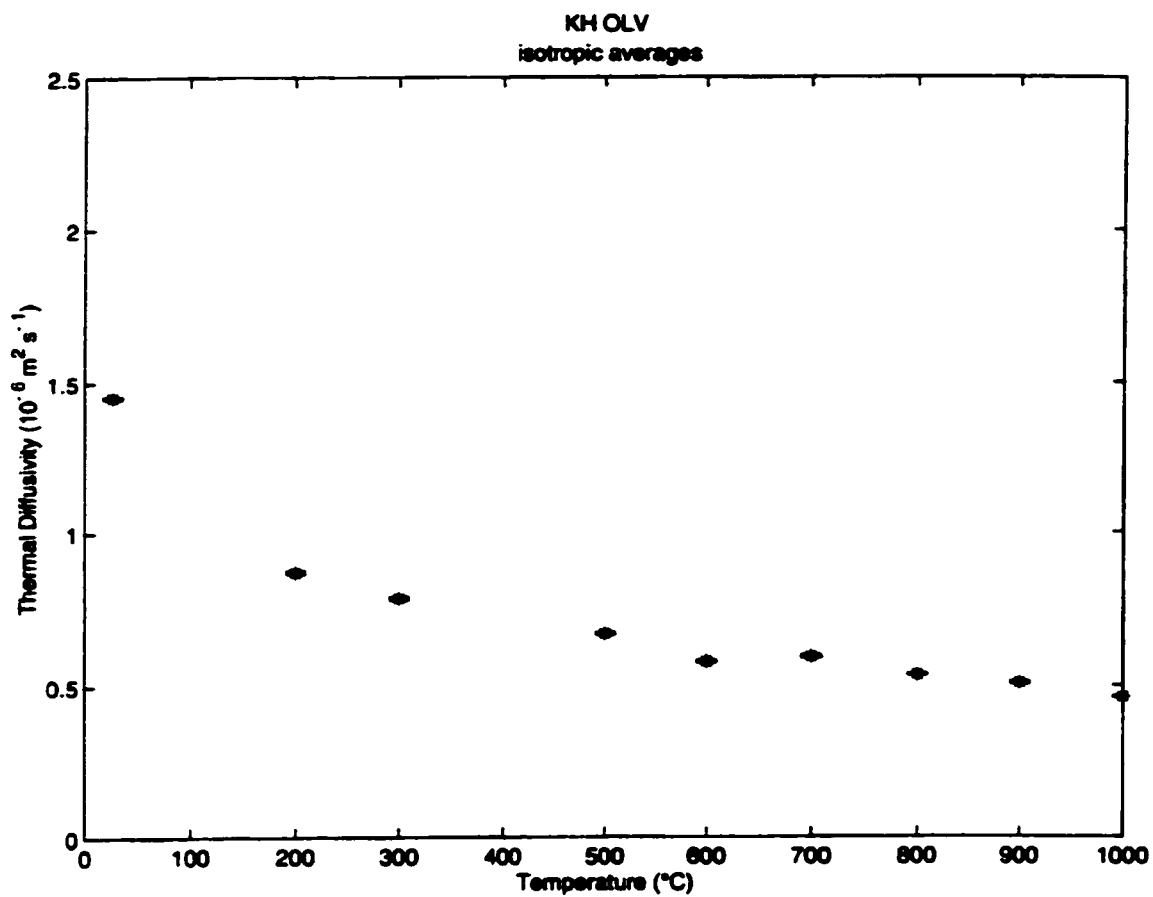


Figure 11 Isotropic Average Lattice Thermal Diffusivities for KH-OLV to 1000°C

The asterisks are the mean values of the lattice thermal diffusivity tensor, with uncertainties, as determined at each temperature. Gaps at 100, 150, 200, and 400°C are a consequence of measurements being made for only one sample (i.e. for only one orientation) at these temperatures.

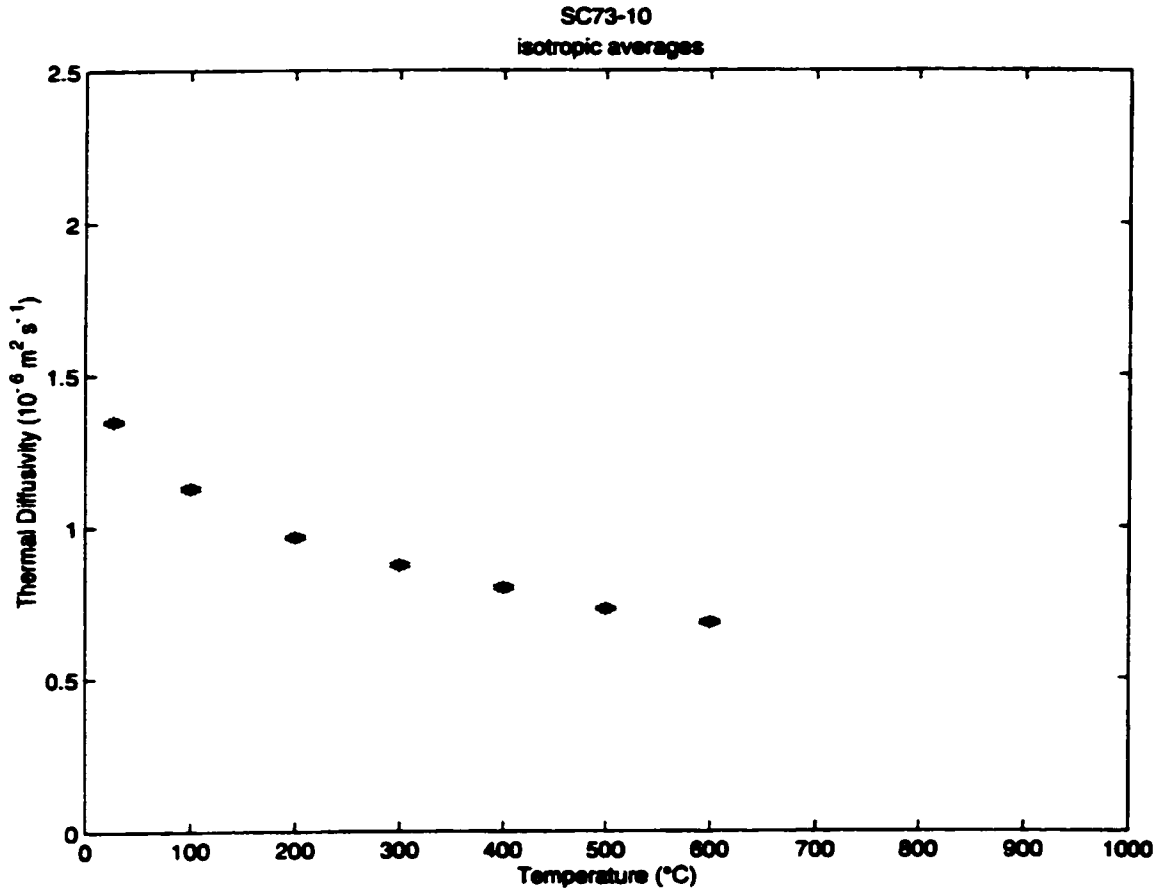


Figure 12 Isotropic Average Lattice Thermal Diffusivities for SC73-10 to 600°C

The asterisks are the mean values of the lattice thermal diffusivity tensor, with uncertainties, as determined at each temperature. The absence of points beyond 600°C is a consequence of measurements being made for only one sample (i.e. for only one orientation) above that temperature.

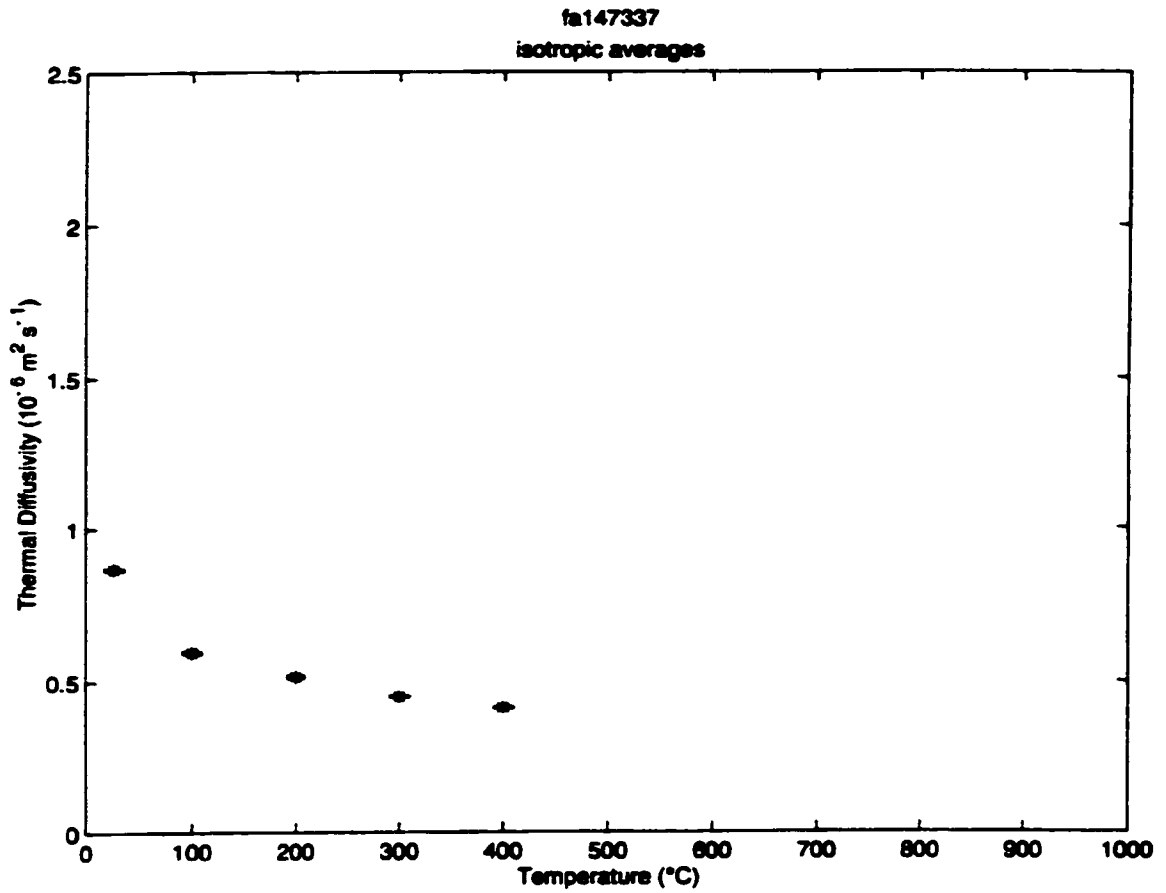


Figure 13 Isotropic Average Lattice Thermal Diffusivities for FA-147337 to 400°C

The asterisks are the mean values of the lattice thermal diffusivity tensor, with uncertainties, as determined at each temperature. The absence of points beyond 400°C is a consequence of measurements being made for only one sample (i.e. for only one orientation) above that temperature.

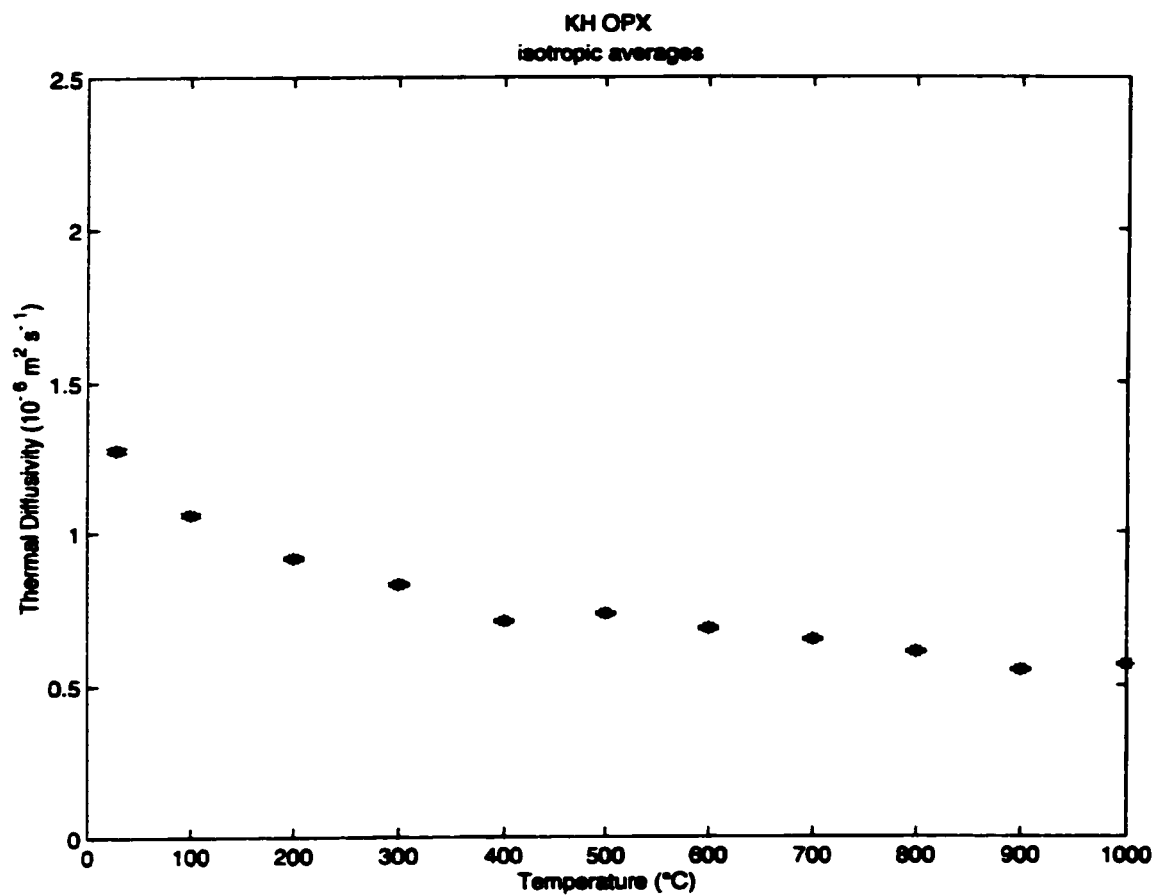


Figure 14 Isotropic Average Lattice Thermal Diffusivities for KH-OPX to 1000°C

The asterisks are the mean values of the lattice thermal diffusivity tensor, with uncertainties, as determined at each temperature.

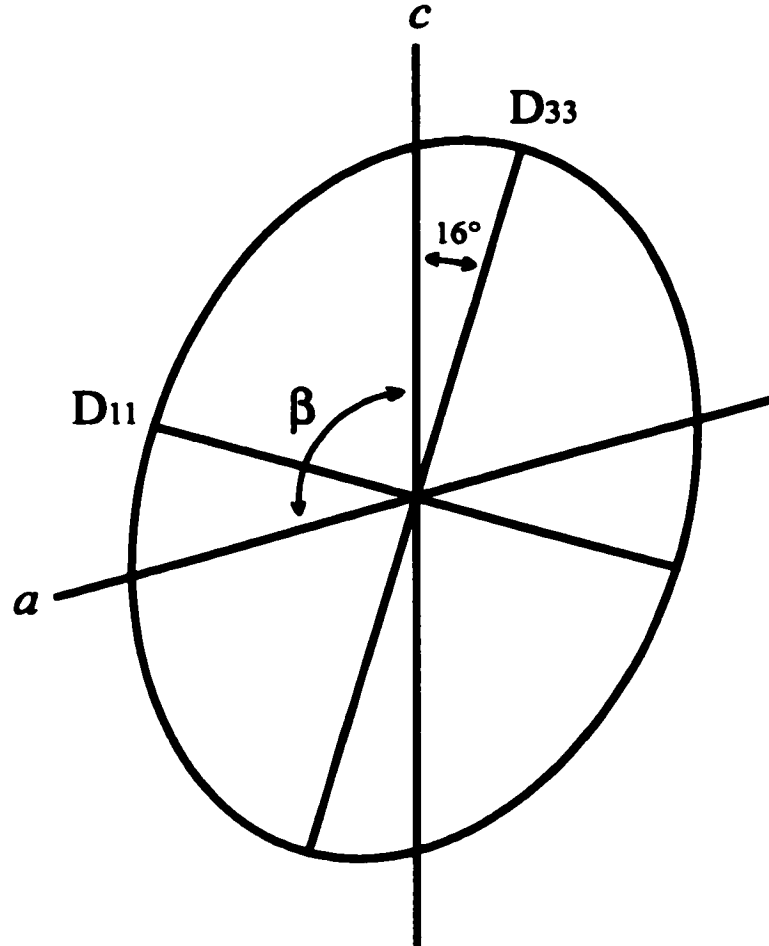


Figure 15 Representation of Thermal Diffusivity in the a - c Plane of KH-CPX

The thermal diffusivity ellipsoid is free to assume any orientation within the a - c plane for monoclinic crystals, though its third axis must be coincident with the b axis. In the case of KH-CPX, D_{33} is 16.0° away from c in the direction of the acute a - c angle. By convention, the angle between a and c , designated β , is always taken as the obtuse angle, and here is equal to 106.5° .

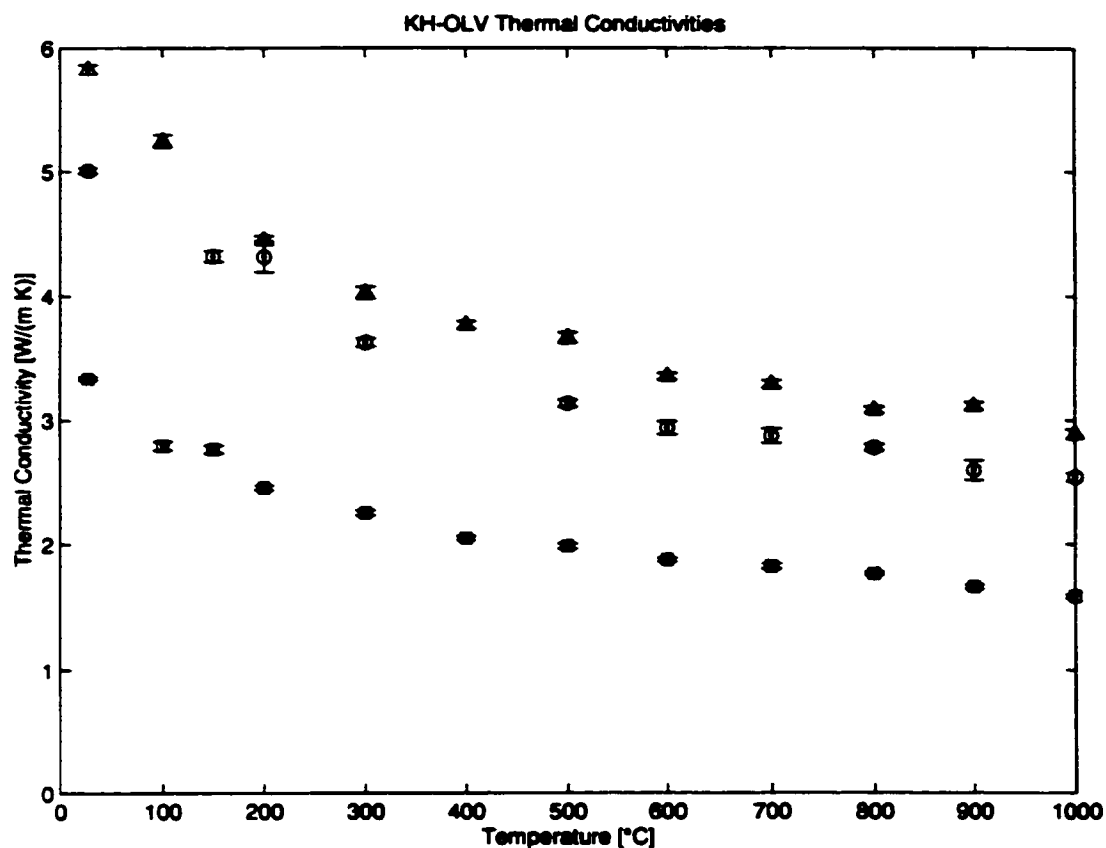


Figure 16 Anisotropic Lattice Thermal Conductivities for KH-OLV to 1000°C

The points are the principal values of the lattice thermal conductivity tensor, with uncertainties, as determined at each temperature. Triangles (at top) are K_{11} , squares (at bottom) are K_{22} , and circles (middle) are K_{33} . Gaps at 100, 150, 200, and 400°C are a consequence of measurements being made for only one sample (i.e. for only one orientation) at these temperatures.

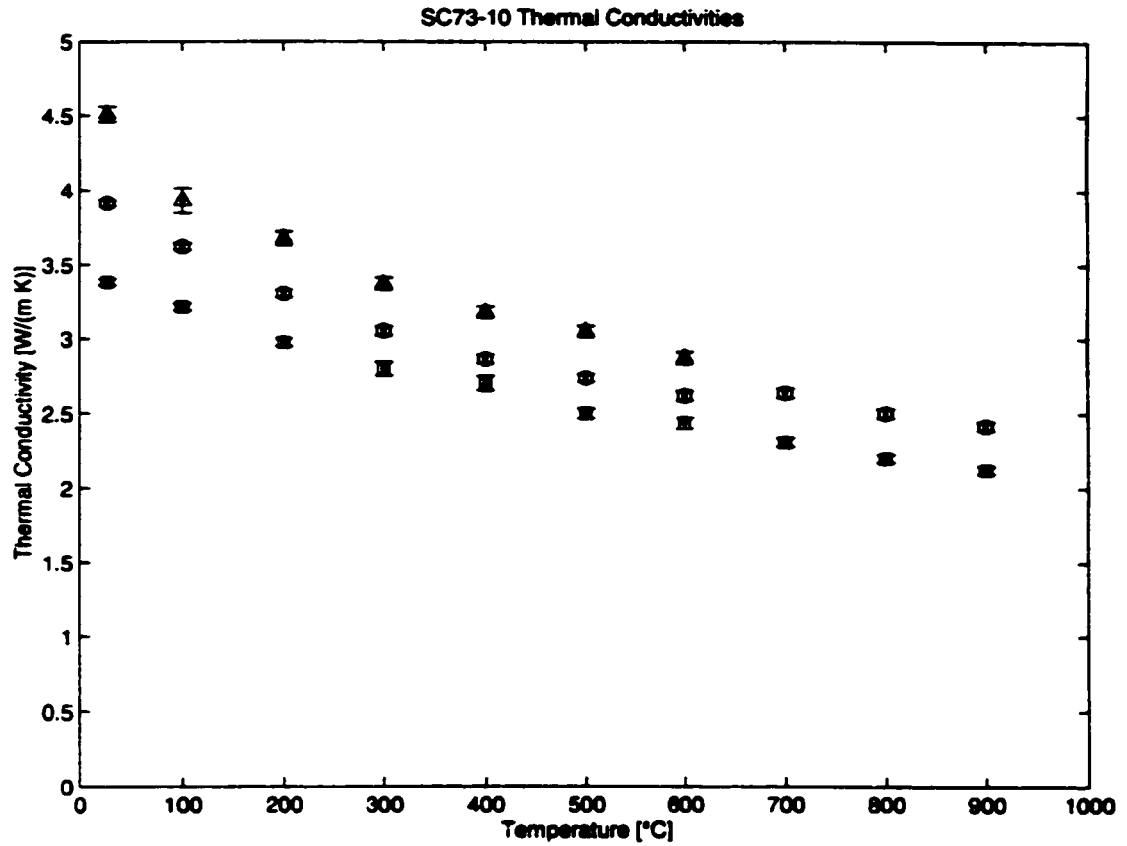


Figure 17 Anisotropic Lattice Thermal Conductivities for SC73-10 to 900°C

The points are the principal values of the lattice thermal conductivity tensor, with uncertainties, as determined at each temperature. Triangles (at top) are K_{11} , squares (at bottom) are K_{22} , and circles (middle) are K_{33} . Gaps at 700, 800, and 900°C are a consequence of measurements being made for only one sample (i.e. for only one orientation) at these temperatures.

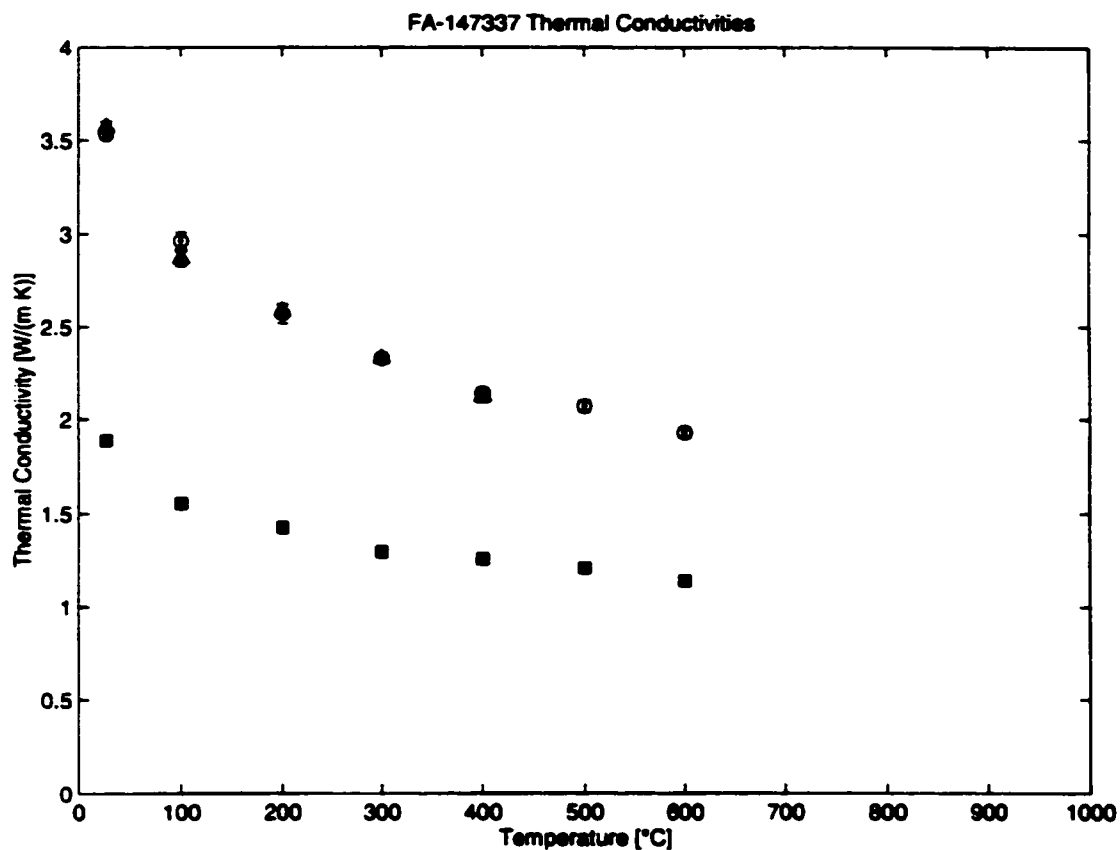


Figure 18 Anisotropic Lattice Thermal Conductivities for FA-147337 to 600°C

The points are the principal values of the lattice thermal conductivity tensor, with uncertainties, as determined at each temperature. Triangles (at top) are K_{11} , squares (at bottom) are K_{22} , and circles (also at top) are K_{33} . The sample is essentially isotropic in the a - c plane, as shown by the almost exact overlap of the points for K_{11} and K_{33} , both of which are plotted at all temperatures up to 400°C.

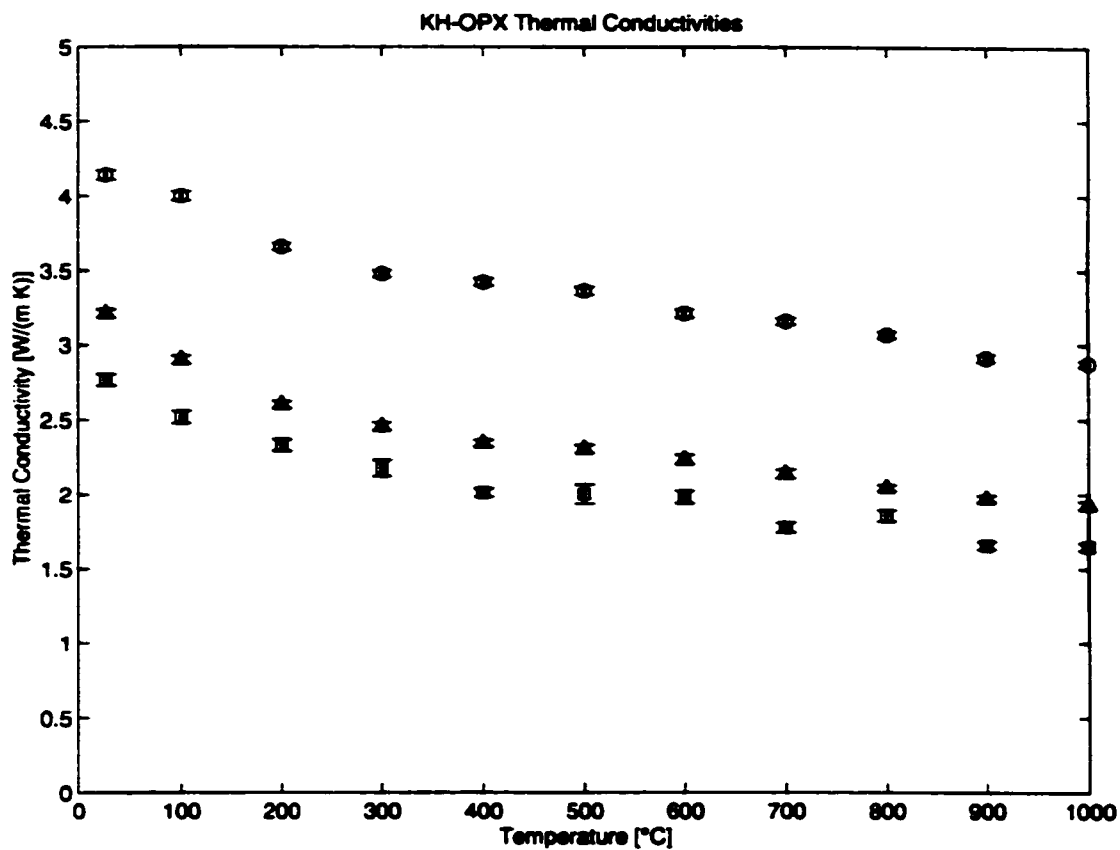


Figure 19 Anisotropic Lattice Thermal Conductivities for KH-OPX to 1000°C

The points are the principal values of the lattice thermal conductivity tensor, with uncertainties, as determined at each temperature. Triangles (middle) are K_{11} , squares (at bottom) are K_{22} , and circles (at top) are K_{33} .

Table 4 Individual Thermal Diffusivities for KH-OLV

Individual determinations of the in-plane components of the thermal diffusivity tensor, along with offset for conversion between laboratory and crystallographic orientation.

Temp [°C]	D_{11} [mm ² s ⁻¹]	D_{22} [mm ² s ⁻¹]	D_{33} [mm ² s ⁻¹]	Offset [°]	$2\sigma D_{11}$	$2\sigma D_{22}$	$2\sigma D_{33}$
27	2.0734	1.1875		-4.1	0.0343	0.0181	
200	1.3203	0.7528		-4.1	0.018	0.013	
400	1.0199	0.5682		-4.1	0.0149	0.008	
600	0.8652	0.4916		-4.1	0.0131	0.0067	
800	0.7707	0.4367		-4.1	0.0121	0.0066	
27	2.0716	1.187		-4.1	0.0344	0.0183	
200	1.3197	0.7549		-4.1	0.018	0.0131	
400	1.0227	0.5685		-4.1	0.0154	0.0082	
600	0.8639	0.4881		-4.1	0.0127	0.0067	
800	0.7706	0.437		-4.1	0.0122	0.0068	
27	2.1377	1.217		36.8	0.0245	0.0207	
27	2.1376	1.2185		36.8	0.0246	0.0217	
100	1.7221	0.9188		40.0	0.0223	0.016	
200	1.3607	0.7317		40.0	0.0217	0.0122	
300	1.1466	0.6174		40.0	0.0192	0.0144	
400	1.043	0.5536		40.0	0.0184	0.0093	
500	0.9756	0.5356		40.0	0.0157	0.0093	
600	0.8871	0.4889		40.0	0.0152	0.0081	
700	0.8431	0.4683		40.0	0.0109	0.0079	
800	0.7895	0.4612		40.0	0.0128	0.008	
100	1.7206	0.9161		40.0	0.0224	0.0177	
200	1.3607	0.7316		40.0	0.0215	0.0122	
300	1.1462	0.6187		40.0	0.019	0.0136	
400	1.0505	0.5529		40.0	0.0165	0.0093	
500	0.9766	0.5346		40.0	0.016	0.0092	
600	0.8875	0.488		40.0	0.0152	0.0081	
700	0.8426	0.4683		40.0	0.0109	0.0079	
800	0.7885	0.4613		40.0	0.0128	0.008	
900	0.7791	0.4178		38.0	0.0102	0.0067	
1000	0.7225	0.3826		38.0	0.014	0.0065	
900	0.7791	0.4178		38.0	0.0102	0.0067	
1000	0.7115	0.3854		38.0	0.0125	0.0064	
27		1.1448	1.6501	102.3		0.0252	0.0594
27		1.1242	1.6604	102.3		0.0186	0.0447
300		0.6231	0.9926	106.8		0.0159	0.0235

Table 4 continued

Temp [°C]	$D_{1,1}$ [mm ² s ⁻¹]	$D_{2,2}$ [mm ² s ⁻¹]	$D_{3,3}$ [mm ² s ⁻¹]	Offset [°]	$2\sigma D_{11}$	$2\sigma D_{22}$	$2\sigma D_{33}$
500		0.5276	0.8131	106.8		0.0266	0.0208
600		0.4899	0.7652	106.8		0.0224	0.0203
700		0.4673	0.7349	106.8		0.0215	0.0229
800		0.4505	0.6936	106.8		0.0134	0.0278
900		0.4136	0.6491	106.8		0.0127	0.0293
300		0.6311	0.9806	106.8		0.0253	0.0259
500		0.5132	0.8147	106.8		0.0189	0.0196
600		0.4819	0.7657	106.8		0.0162	0.0183
700		0.4625	0.7362	106.8		0.0156	0.0194
800		0.4495	0.6935	106.8		0.0127	0.0268
900		0.4107	0.6494	106.8		0.0099	0.0271
27		0.9833	1.6519	109.3		0.1474	0.033
27		0.997	1.5512	109.3		0.1162	0.0567
27		1.2615	1.8756	126.1		0.0418	0.0444
200		0.738	1.3078	126.1		0.0143	0.0523
27		1.2577	1.8756	126.1		0.0356	0.0433
200		0.7294	1.2874	126.1		0.0105	0.0516
27		1.2235	1.8402	125.0		0.0235	0.0224
150		0.8646	1.3492	125.0		0.0138	0.019
300		0.6604	1.0504	125.0		0.0106	0.0153
500		0.5201	0.841	125.0		0.0109	0.0121
800		0.4429	0.6822	125.0		0.0295	0.0152
27		1.2241	1.8349	125.0		0.0234	0.0218
150		0.8648	1.3499	125.0		0.0138	0.019
300		0.6581	1.0517	125.0		0.0106	0.0157
500		0.508	0.8453	125.0		0.0214	0.0131
800		0.4391	0.6844	125.0		0.0305	0.0164
27		1.2757	1.914	30.1		0.1109	0.2591
27		1.1709	1.8026	105.6		0.0255	0.0246
27		1.1531	1.8053	105.6		0.024	0.0223
27		1.2995	2.0205	23.8		0.0187	0.042
800		0.4443	0.716	23.8		0.0084	0.0124
1000		0.4095	0.636	23.8		0.0077	0.0111
27		1.2993	2.0178	23.8		0.0184	0.0407
800		0.4433	0.7171	23.8		0.0084	0.0124
1000		0.4051	0.6243	23.8		0.0077	0.0111
27		1.1446	1.8179	21.0		0.0183	0.0384
27		1.1489	1.8121	20.9		0.0236	0.0507
27		1.27	1.8309	67.7		0.0189	0.0236

Table 4 continued

Temp [°C]	D_{11} [mm ² s ⁻¹]	D_{22} [mm ² s ⁻¹]	D_{33} [mm ² s ⁻¹]	Offset [°]	$2\sigma D_{11}$	$2\sigma D_{22}$	$2\sigma D_{33}$
27		1.2623	1.8466	67.7		0.0187	0.0216
27	2.1441	1.2544		37.2	0.0355	0.0175	

Table 5 Individual Thermal Diffusivities for SC73-10

Individual determinations of the in-plane components of the thermal diffusivity tensor, along with offset for conversion between laboratory and crystallographic orientation.

Temp [°C]	D_{11} [mm ² s ⁻¹]	D_{22} [mm ² s ⁻¹]	D_{33} [mm ² s ⁻¹]	Offset [°]	$2\sigma D_{11}$	$2\sigma D_{22}$	$2\sigma D_{33}$
27	1.6367		1.4898	76.2	0.037		0.0192
100	1.2847		1.1998	76.2	0.0273		0.0159
200	1.1019		0.9681	76.2	0.0133		0.0115
300	0.9571		0.8518	76.2	0.0115		0.0101
400	0.868		0.7659	76.2	0.0098		0.009
500	0.8102		0.7114	76.2	0.0092		0.0086
600	0.7478		0.6646	76.2	0.0099		0.0101
27	1.6389		1.4284	76.2	0.0212		0.019
27		1.2644	1.3607	27.9		0.018	0.0223
100		1.0297	1.1396	27.9		0.0132	0.011
27		1.23	1.4041	39.9		0.0099	0.0118
100		1.0334	1.1894	27.8		0.0142	0.0176
200		0.882	0.995	26.7		0.0106	0.0131
300		0.7947	0.8888	18.5		0.013	0.0126
400		0.738	0.8173	11.5		0.0131	0.0128
500		0.6643	0.7524	17.9		0.0085	0.0106
600		0.6331	0.7059	-1.9		0.0092	0.0126
700		0.5913	0.6745	-7.6		0.0073	0.0077
800		0.5562	0.6317	-9.7		0.0066	0.0076
900		0.5313	0.6047	56.7		0.0064	0.0069
27		1.1476	1.2968	124.9		0.0155	0.0246
27		1.3629	1.5616	128.4		0.0249	0.0231
100		1.0871	1.2549	128.4		0.0138	0.0163
200		0.9044	1.0209	128.4		0.0119	0.0149

Table 6 Individual Thermal Diffusivities for FA-147337

Individual determinations of the in-plane components of the thermal diffusivity tensor, along with offset for conversion between laboratory and crystallographic orientation.

Temp [°C]	D_{11} [mm ² s ⁻¹]	D_{22} [mm ² s ⁻¹]	D_{33} [mm ² s ⁻¹]	Offset [°]	$2\sigma D_{11}$	$2\sigma D_{22}$	$2\sigma D_{33}$
27		0.721	1.3687	117.7		0.0125	0.0175
27		0.719	1.3697	117.7		0.0124	0.0171
27	1.3018	0.6572		92.4	0.0156	0.0091	
27		0.5602	1.0772	18.2		0.0113	0.0122
27	1.2091	0.623		109.7	0.0123	0.0117	
100	0.9084	0.4774		-3.1	0.0119	0.0076	
200	0.756	0.4177		-3.1	0.0092	0.0067	
300	0.6482	0.3585		-3.1	0.0075	0.0048	
400	0.5694	0.3394		-3.1	0.0077	0.0055	
27		0.7382	1.3494	47.3		0.013	0.0196
27		0.7146	1.323	99.2		0.0097	0.0118
100		0.5024	0.9381	158.4		0.0067	0.0137
200		0.4148	0.7513	158.4		0.0076	0.0151
300		0.3497	0.641	158.4		0.0217	0.0133
27		0.5822	1.0431	159.5		0.0098	0.0149
300		0.3634	0.6504	159.5		0.0048	0.0079
400		0.3375	0.5743	159.5		0.0044	0.0069
500		0.3169	0.5418	159.5		0.0041	0.0075
600		0.2928	0.4949	159.5		0.0041	0.0059

Table 7 Individual Thermal Diffusivities for KH-OPX

Individual determinations of the in-plane components of the thermal diffusivity tensor, along with offset for conversion between laboratory and crystallographic orientation.

Temp [°C]	D_{11} [mm ² s ⁻¹]	D_{22} [mm ² s ⁻¹]	D_{33} [mm ² s ⁻¹]	Offset [°]	$2\sigma D_{11}$	$2\sigma D_{22}$	$2\sigma D_{33}$
27		1.0341	1.529	154.0		0.0205	0.0204
100		0.8434	1.3172	154.0		0.0229	0.0176
200		0.707	1.0896	154.0		0.0163	0.0128
300		0.6147	0.9689	154.0		0.0211	0.0136
400		0.5524	0.9346	154.0		0.0104	0.016
27		1.0305	1.5271	154.0		0.0204	0.0207
100		0.8268	1.3172	154.0		0.0161	0.0173
200		0.7045	1.0924	154.0		0.0166	0.0123
300		0.6176	0.968	154.0		0.0217	0.0137
400		0.5404	0.9348	154.0		0.0104	0.0165
500		0.5281	0.8736	152.1		0.0266	0.0215
600		0.5128	0.827	152.1		0.0154	0.018
700		0.4594	0.8083	152.1		0.0135	0.0123
800		0.4681	0.7727	152.1		0.0131	0.0122
900		0.414	0.717	152.1		0.009	0.0097
1000		0.4081	0.7039	152.1		0.0082	0.0081
500		0.5274	0.8725	152.1		0.0224	0.0211
600		0.5148	0.8265	152.1		0.0156	0.0182
700		0.4503	0.8127	152.1		0.0105	0.012
800		0.4677	0.7725	152.1		0.0125	0.0121
900		0.4132	0.7166	152.1		0.009	0.0096
1000		0.4075	0.7054	152.1		0.0082	0.008
27	1.2205		1.669	-14.6	0.0219		0.0878
27	1.1899		1.5697	39.6	0.016		0.03
27	1.1905		1.574	39.6	0.0159		0.0279
100	0.9611		1.3417	40.7	0.0125		0.0266
200	0.7874		1.1291	40.7	0.01		0.0148
300	0.695		0.9941	40.7	0.0098		0.0121
400	0.6361		0.9253	40.7	0.0082		0.0113
500	0.6081		0.8898	40.7	0.0099		0.0109
600	0.5797		0.8333	40.7	0.011		0.0115
700	0.5462		0.8006	40.7	0.0105		0.0111
800	0.5158		0.7711	40.7	0.0067		0.0094
900	0.4916		0.7511	40.7	0.0081		0.0158
1000	0.4764		0.7222	40.7	0.0093		0.011

Table 7 continued

Temp [°C]	D_{11} [mm ² s ⁻¹]	D_{22} [mm ² s ⁻¹]	D_{33} [mm ² s ⁻¹]	Offset [°]	$2\sigma D_{11}$	$2\sigma D_{22}$	$2\sigma D_{33}$
100	0.9592		1.3304	40.7	0.0124		0.023
200	0.7867		1.1307	40.7	0.0101		0.0156
300	0.6938		0.9963	40.7	0.0098		0.0121
400	0.6361		0.9261	40.7	0.0082		0.0113
500	0.6081		0.8904	40.7	0.0101		0.0109
600	0.5795		0.8337	40.7	0.011		0.0115
700	0.5459		0.8001	40.7	0.0105		0.0111
800	0.5148		0.772	40.7	0.0066		0.0096
900	0.4914		0.7504	40.7	0.0079		0.0156
1000	0.4761		0.7219	40.7	0.0093		0.0108

Table 8 Individual Thermal Diffusivities for KH-CPX

Individual determinations of the in-plane components of the thermal diffusivity tensor (with respect to the principal axes), along with offset for conversion between laboratory and crystallographic orientation.

Temp [°C]	D_{11} [mm ² s ⁻¹]	D_{22} [mm ² s ⁻¹]	D_{33} [mm ² s ⁻¹]	Offset [°]	$2\sigma D_{11}$	$2\sigma D_{22}$	$2\sigma D_{33}$
27		0.9302	1.2573	123.7		0.1347	0.0349
27		0.8241	1.1965	32.3		0.0414	0.1232
27		0.8561	1.3015	123.5		0.0604	0.0288
27		0.8765	1.2732	123.2		0.0198	0.0334
27		0.8442	1.2756	92.0		0.0119	0.0289
27		0.8745	1.2508	121.3		0.0308	0.0523
27		0.8668	1.2732	49.7		0.0109	0.0161
27		0.7499	1.1615	90.6		0.0406	0.1331
27	0.866		1.292	20.8	0.0197		0.0336
27	0.8963		1.3582	121.2	0.0173		0.0218
27	0.7757		1.2022	20.8	0.0546		0.1209

Table 9 Thermal Diffusivity and Conductivity Tensors for KH-OLV

Temp [°C]	D_{11} [mm ² s ⁻¹]	D_{22} [mm ² s ⁻¹]	D_{33} [mm ² s ⁻¹]	$2\sigma D_{11}$	$2\sigma D_{22}$	$2\sigma D_{33}$	D_{iso} [mm ² s ⁻¹]	$2\sigma D_{iso}$
27	2.1195	1.2138	1.8207	0.0131	0.0048	0.0077	1.718	0.0159
100	1.7214	0.9176		0.0158	0.0119			
150		0.8647	1.3495		0.0098	0.0134		
200	1.3367	0.7386	1.2975	0.0098	0.0051	0.0367	1.1243	0.0383
300	1.1464	0.6412	1.0329	0.0135	0.0055	0.0093	0.9402	0.0173
400	1.0325	0.5618		0.0081	0.0043			
500	0.9761	0.5284	0.8349	0.0112	0.0051	0.0075	0.7798	0.0144
600	0.8741	0.489	0.7655	0.007	0.0035	0.0136	0.7095	0.0157
700	0.8429	0.4676	0.7356	0.0077	0.0051	0.0148	0.682	0.0175
800	0.7793	0.4463	0.7026	0.0062	0.0029	0.0065	0.6428	0.0095
900	0.7791	0.4162	0.6493	0.0072	0.004	0.0199	0.6148	0.0215
1000	0.7164	0.3936	0.6302	0.0094	0.0035	0.0079	0.58	0.0127

Temp [°C]	K_{11} [Wm ⁻¹ K ⁻¹]	K_{22} [Wm ⁻¹ K ⁻¹]	K_{33} [Wm ⁻¹ K ⁻¹]	$2\sigma K_{11}$	$2\sigma K_{22}$	$2\sigma K_{33}$	K_{iso} [Wm ⁻¹ K ⁻¹]
27	5.8275	3.3373	5.0059	0.036	0.0132	0.0212	4.7236
100	5.2418	2.7942		0.0481	0.0362		
150		2.7665	4.3176		0.0314	0.0429	
200	4.4427	2.4548	4.3124	0.0326	0.017	0.122	3.7366
300	4.0271	2.2524	3.6284	0.0474	0.0193	0.0327	3.3027
400	3.7696	2.0511		0.0296	0.0157		
500	3.6662	1.9847	3.1359	0.0421	0.0192	0.0282	2.9289
600	3.3549	1.8769	2.9381	0.0269	0.0134	0.0522	2.7233
700	3.2901	1.8252	2.8713	0.0301	0.0199	0.0578	2.6622
800	3.0827	1.7655	2.7793	0.0245	0.0115	0.0257	2.5425
900	3.1149	1.664	2.596	0.0288	0.016	0.0796	2.4583
1000	2.8886	1.5871	2.5411	0.0379	0.0141	0.0319	2.3389

Table 10 Thermal Diffusivity and Thermal Conductivity Tensors for SC73-10

Temp [°C]	D_{11} [mm ² s ⁻¹]	D_{22} [mm ² s ⁻¹]	D_{33} [mm ² s ⁻¹]	$2\sigma D_{11}$	$2\sigma D_{22}$	$2\sigma D_{33}$	D_{iso} [mm ² s ⁻¹]	$2\sigma D_{iso}$
27	1.6384	1.2289	1.4222	0.0184	0.0073	0.0074	1.4298	0.0211
100	1.2847	1.0498	1.183	0.0273	0.0079	0.0072	1.1725	0.0293
200	1.1019	0.8919	0.9902	0.0133	0.0079	0.0075	0.9947	0.0172
300	0.9571	0.7947	0.8661	0.0115	0.013	0.0079	0.8727	0.0191
400	0.868	0.738	0.7828	0.0098	0.0131	0.0074	0.7963	0.0179
500	0.8102	0.6643	0.7277	0.0092	0.0085	0.0067	0.7341	0.0142
600	0.7478	0.6331	0.6809	0.0099	0.0092	0.0079	0.6873	0.0156
700		0.5913	0.6745		0.0073	0.0077		
800		0.5562	0.6317		0.0066	0.0076		
900		0.5313	0.6047		0.0064	0.0069		

Temp [°C]	K_{11} [Wm ⁻¹ K ⁻¹]	K_{22} [Wm ⁻¹ K ⁻¹]	K_{33} [Wm ⁻¹ K ⁻¹]	$2\sigma K_{11}$	$2\sigma K_{22}$	$2\sigma K_{33}$	K_{iso} [Wm ⁻¹ K ⁻¹]
27	4.5084	3.3815	3.9135	0.0506	0.0201	0.0204	3.9345
100	3.9316	3.2128	3.6204	0.0835	0.0242	0.022	3.5883
200	3.6758	2.9753	3.3032	0.0444	0.0264	0.025	3.3181
300	3.3718	2.7997	3.0512	0.0405	0.0458	0.0278	3.0742
400	3.1763	2.7006	2.8645	0.0359	0.0479	0.0271	2.9138
500	3.0489	2.4998	2.7384	0.0346	0.032	0.0252	2.7624
600	2.8746	2.4337	2.6175	0.0381	0.0354	0.0304	2.6419
700		2.3111	2.6363		0.0285	0.0301	
800		2.2027	2.5017		0.0261	0.0301	
900		2.1263	2.4201		0.0256	0.0276	

Table 11 Thermal Diffusivity and Conductivity Tensors for FA-147337

Temp [°C]	D_{11} [mm ² s ⁻¹]	D_{22} [mm ² s ⁻¹]	D_{33} [mm ² s ⁻¹]	$2\sigma D_{11}$	$2\sigma D_{22}$	$2\sigma D_{33}$	D_{iso} [mm ² s ⁻¹]	$2\sigma D_{iso}$
27	1.2449	0.6588	1.2316	0.0097	0.0039	0.006	1.0451	0.012
100	0.9084	0.4914	0.9381	0.0119	0.005	0.0137	0.7793	0.0188
200	0.756	0.4164	0.7513	0.0092	0.005	0.0151	0.6412	0.0184
300	0.6482	0.3607	0.6479	0.0075	0.0033	0.0068	0.5523	0.0106
400	0.5694	0.3382	0.5743	0.0077	0.0034	0.0069	0.494	0.0109
500		0.3169	0.5418		0.0041	0.0075		
600		0.2928	0.4949		0.0041	0.0059		

Temp [°C]	K_{11} [Wm ⁻¹ K ⁻¹]	K_{22} [Wm ⁻¹ K ⁻¹]	K_{33} [Wm ⁻¹ K ⁻¹]	$2\sigma K_{11}$	$2\sigma K_{22}$	$2\sigma K_{33}$	K_{iso} [Wm ⁻¹ K ⁻¹]
27	3.5688	1.8886	3.5307	0.0278	0.0112	0.0172	2.9961
100	2.8716	1.5534	2.9654	0.0376	0.0158	0.0433	2.4635
200	2.5863	1.4245	2.5703	0.0315	0.0171	0.0517	2.1937
300	2.3312	1.2972	2.3301	0.027	0.0119	0.0245	1.9862
400	2.1203	1.2594	2.1386	0.0287	0.0127	0.0257	1.8394
500		1.2107	2.07		0.0157	0.0287	1.7835
600		1.1408	1.9282		0.016	0.023	1.6657

Table 12 Thermal Diffusivity and Conductivity Tensors for KH-OPX

Temp [°C]	D_{11} [mm ² s ⁻¹]	D_{22} [mm ² s ⁻¹]	D_{33} [mm ² s ⁻¹]	$2\sigma D_{11}$	$2\sigma D_{22}$	$2\sigma D_{33}$	D_{iso} [mm ² s ⁻¹]	$2\sigma D_{iso}$
27	1.1965	1.0323	1.5451	0.01	0.0144	0.0117	1.258	0.0211
100	0.9601	0.8323	1.3232	0.0088	0.0132	0.0101	1.0385	0.0188
200	0.787	0.7058	1.1068	0.0071	0.0116	0.0068	0.8665	0.0152
300	0.6944	0.6161	0.9834	0.0069	0.0151	0.0064	0.7646	0.0178
400	0.6361	0.5464	0.9286	0.0058	0.0074	0.0066	0.7037	0.0114
500	0.6081	0.5277	0.8865	0.0071	0.0171	0.0069	0.6741	0.0198
600	0.5796	0.5138	0.8315	0.0078	0.011	0.0069	0.6417	0.0151
700	0.5461	0.4537	0.8049	0.0074	0.0083	0.0058	0.6016	0.0126
800	0.5153	0.4679	0.7719	0.0047	0.0091	0.0053	0.585	0.0115
900	0.4915	0.4136	0.7261	0.0056	0.0063	0.0058	0.5437	0.0103
1000	0.4763	0.4078	0.7108	0.0065	0.0058	0.0046	0.5316	0.0099

Temp [°C]	K_{11} [Wm ⁻¹ K ⁻¹]	K_{22} [Wm ⁻¹ K ⁻¹]	K_{33} [Wm ⁻¹ K ⁻¹]	$2\sigma K_{11}$	$2\sigma K_{22}$	$2\sigma K_{33}$	K_{iso} [Wm ⁻¹ K ⁻¹]
27	3.2086	2.7682	4.1434	0.0268	0.0386	0.0314	3.3734
100	2.9036	2.5171	4.0017	0.0266	0.0399	0.0305	3.1408
200	2.6011	2.3327	3.658	0.0235	0.0383	0.0225	2.8639
300	2.4561	2.1791	3.4782	0.0244	0.0534	0.0226	2.7045
400	2.3438	2.0133	3.4216	0.0214	0.0273	0.0243	2.5929
500	2.307	2.002	3.3633	0.0269	0.0649	0.0262	2.5574
600	2.2372	1.9833	3.2096	0.0301	0.0425	0.0266	2.4767
700	2.1422	1.7798	3.1575	0.029	0.0326	0.0228	2.3598
800	2.0474	1.8591	3.067	0.0187	0.0362	0.0211	2.3245
900	1.9732	1.6605	2.9151	0.0225	0.0253	0.0233	2.1829
1000	1.9286	1.6513	2.8782	0.0263	0.0235	0.0186	2.1527

Table 13 Thermal Diffusivity and Conductivity Tensors for KH-CPX**Principal Axes**

Temp [°C]	D_{11} [mm ² s ⁻¹]	D_{22} [mm ² s ⁻¹]	D_{33} [mm ² s ⁻¹]	$2\sigma D_{11}$	$2\sigma D_{22}$	$2\sigma D_{33}$
27	0.8774		1.3356	0.0127		0.0181
		0.856	1.2737		0.007	0.0109

Temp [°C]	K_{11} [Wm ⁻¹ K ⁻¹]	K_{22} [Wm ⁻¹ K ⁻¹]	K_{33} [Wm ⁻¹ K ⁻¹]	$2\sigma K_{11}$	$2\sigma K_{22}$	$2\sigma K_{33}$
27	2.2622		3.4436	0.0327		0.0467
27		2.207	3.284		0.018	0.0281

Crystallographic Axes

Temp [°C]	D_{11} [mm ² s ⁻¹]	D_{22} [mm ² s ⁻¹]	D_{33} [mm ² s ⁻¹]	D_{13} [mm ² s ⁻¹]
27	0.91	0.86	1.3	-0.12

Temp [°C]	K_{11} [Wm ⁻¹ K ⁻¹]	K_{22} [Wm ⁻¹ K ⁻¹]	K_{33} [Wm ⁻¹ K ⁻¹]	K_{13} [Wm ⁻¹ K ⁻¹]
27	2.35	2.22	3.35	-0.31

Table 14 Thermal Diffusivities and Conductivities for SCchai**Individual Determinations**

Pressure [GPa]	D_{11} [mm ² s ⁻¹]	D_{22} [mm ² s ⁻¹]	$2\sigma D_{11}$	$2\sigma D_{22}$
0	2.17	1.29	0.06	0.06
0	2.45	1.38	0.05	0.04
0	2.38	1.36	0.06	0.03
3.22	2.91	1.71	0.07	0.04
3.22	2.62	1.77	0.09	0.06
5.09	2.83	1.76	0.09	0.04

Weighted Averages

Pressure [GPa]	D_{11} [mm ² s ⁻¹]	D_{22} [mm ² s ⁻¹]	$2\sigma D_{11}$	$2\sigma D_{22}$
0	2.3483	1.3566	0.0323	0.0223
3.22	2.8007	1.7285	0.0553	0.0333
5.09	2.83	1.76	0.09	0.04

Pressure [GPa]	K_{11} [Wm ⁻¹ K ⁻¹]	K_{22} [Wm ⁻¹ K ⁻¹]	$2\sigma K_{11}$	$2\sigma K_{22}$
0	6.426	3.7123	0.0884	0.061
3.22	7.8038	4.8163	0.1541	0.0928
5.09	7.9612	4.9511	0.2532	0.1125

Table 15 Specific Heats and Volumes of PhasesKH-OLV (Fo₉₁ Fa₉, mw = 146.371)

Temp [°C]	C _p [Jmol ⁻¹ K ⁻¹]	Volume [cm ³ mol ⁻¹]
27	120.770	43.925
100	134.047	44.021
150	141.054	44.088
200	146.764	44.158
300	155.634	44.304
400	162.311	44.457
500	167.586	44.618
600	171.896	44.786
700	175.507	44.963
800	178.591	45.147
900	181.266	45.338
1000	183.616	45.538

SC-OLV (Fo₇₈ Fa₂₂, mw = 154.572)

27	121.886	44.295
100	135.849	44.390
200	148.537	44.527
300	157.376	44.672
400	164.027	44.824
500	169.279	44.984
600	173.570	45.152
700	177.164	45.327
800	180.234	45.510
900	182.896	45.700

FA-147337 (Fa₁₀₀, mw = 203.778)

27	132.737	46.302
100	146.657	46.394
200	159.170	46.526
300	167.830	46.666
400	174.321	46.813
500	179.438	46.967
600	183.613	47.128

Table 15 continued

KH-OPX (Di₂₅ En₉₆ He₁₇ Es₁₂, mw = 210.424)

Temp [°C]	C _p [Jmol ⁻¹ K ⁻¹]	Volume [cm ³ mol ⁻¹]
27	169.058	63.043
100	191.044	63.171
200	209.389	63.354
300	224.748	63.543
400	234.857	63.739
500	242.587	63.942
600	247.625	64.152
700	252.519	64.372
800	256.671	64.599
900	260.291	64.835
1000	263.519	65.079

KH-CPX (Di₅₆ En₁₄ He₇ ABu₃ Bu_{.5} Es₁₀ Jd₁₀, mw = 216.672)

27	167.926	65.131
----	---------	--------

SCchai (Fo₈₉ Fa₁₁, mw = 147.633)

Pressure [GPa]	C _p [Jmol ⁻¹ K ⁻¹]	Volume [cm ³ mol ⁻¹]
0	120.355	43.982
3.22	119.611	42.927
5.09	119.179	42.365

Discussion

"What can it mean?"

'Mean? It means something dreadful—what else?'

'That is nothing to the point; anybody knows that without the telling. But *what?*—that is the question.'

'It is a chance that he that bears it can answer as well as any that are here, if you can contain yourself....'"

(Clemens, 1896, p. 37)

Features of Interest in the Data

The aspects of the data which most significantly merit attention fall into four categories: the amount of anisotropy exhibited by the phases, the trends in diffusivity with temperature, the trends with pressure, and the trends with composition. Each of these shall be discussed in turn, and a model shall be presented which permits the calculation of thermal conductivity across the observed ranges of temperature and pressure for these phases, and is suitable for extrapolation as well, inasmuch as it is based on the fundamental (and independently observable) material properties of the minerals in question. Finally, in the concluding section, some of the unanswered questions that have come to light during the formulation of this discussion shall be presented in conjunction with a few reasonably promising directions for future work intended to address these issues.

The Degree of Anisotropy in Thermal Diffusivity

Not only do all the minerals in this study display significant anisotropy with respect to thermal diffusivity, but for all the olivines for which high-temperature measurements were made, the relative degree of anisotropy remains essentially unchanged at all temperatures.

This is illustrated in Table 16, in which the normalized tensor values of the diffusivities at each temperature are listed. Kobayashi (1974) reached the same conclusion from a set of total (lattice plus radiative) thermal diffusivity data with much greater scatter, and noted that this need not be the case for all minerals, as earlier workers (Birch and Clark, 1940; and Kanamori et al., 1968) had seen a decrease in anisotropy with temperature for quartz, though this change does not appear to be large (Beck et al., 1978). The orthopyroxene, KH-OPX, shows some evidence of a slight increase in anisotropy with temperature, though the anisotropy is pronounced throughout the range of temperatures. As the present measurements encompass those major upper-mantle phases for which such anisotropy is to be expected (garnet, for example, is cubic), and as such phases comprise the bulk of Earth's upper mantle, these findings support the conclusion that the effects of anisotropic thermal diffusivity are of importance in the high-temperature regime of the upper mantle, particularly for regions in which the petrologic fabric displays extensive crystallographic alignment, as suggested in Hearn et al., 1997, and the contribution of orthopyroxene may increase slightly with depth.

Although the measurements on KH-CPX were not extended to high temperatures, it is not unreasonable to suggest that its anisotropy also will remain noticeable, and perhaps even increase somewhat (by analogy to orthopyroxene) under these conditions, so an estimate of its effects on overall heat flow can be made on this basis. One point of concern in the case of clinopyroxene, however, is that the extrema of diffusivity in the *a-c* plane are not constrained by symmetry to maintain a fixed orientation, so the question of whether the tensor rotates significantly with respect to the crystallographic axes as a function of temperature (or pressure and composition, for that matter) remains open.

For each of the three compositions of olivine, the degree of anisotropy remains approximately constant with temperature, but the three differ from one another markedly.

This is addressed in the section which discusses overall behavior along the forsterite-fayalite solid solution series.

Deviations from a Simple Inverse Dependence on Temperature

A simple model for lattice thermal conductivity, in this case following the exposition of Klemens (1969), describes the propagation of phonons in a perfect crystal as analogous to the movement of particles in an ideal gas, giving rise to an equation for thermal conductivity of the form

$$K = \frac{1}{3} cvl$$

in which c , v , and l are the specific heat, velocity, and mean free path, respectively. In a complex crystal, each of these quantities is a function of the distribution of the phonon population among the various lattice modes. Within a model that approximates the distribution of lattice modes as a continuous function (e.g. the Debye model), in which modes are distributed between the limits of zero frequency and a cutoff frequency, ω_c , one may write

$$K = \frac{1}{3} \int_0^{\omega_c} c(\omega)v(\omega)l(\omega)d\omega$$

for which, at sufficiently high temperatures, specific heats and velocities are taken to be approximately independent of temperature. In this regime, the temperature dependence of K primarily is governed by the temperature dependence of the mean free path. Since the density of phonons, and hence the likelihood of collision, increases with temperature, the common expectation is to observe a decrease in lattice thermal conductivity proportional to T^{-1} . One frequently encountered refinement to this is an allowance for the existence of an

invariant number of imperfections, such as impurities or defects, from which the phonons also may scatter at all temperatures. This leads to the expression

$$K = \frac{1}{A + BT}$$

for which values of A and B have been tabulated for many rocks and rock-forming minerals (e.g. Clauser and Huenges, 1995). Unfortunately, this simple model does not account for the high-temperature behavior of the current set of data all that well, certainly not well enough for its use as a guide to extrapolation. Both the thermal diffusivities and, more significantly, the thermal conductivities exhibit marked, systematic deviations from an inverse dependence on temperature. Specifically, the diffusivities and conductivities are higher at high temperatures than the values given by a T^{-1} extrapolation of the lower-temperature values. The deviation becomes significant for temperatures above approximately 400°C and increases with temperature, and is believed to arise from two factors not incorporated into the preceding model: the data span both the low-temperature and high-temperature regimes (with respect to the behavior of specific heat) for these minerals, and, at high temperatures, the mean free path may not become arbitrarily small. A model which accounts for the observed behavior is presented in the following section.

Preferred Model for Thermal Conductivity

The preferred model, also a refinement of the Debye model, is an extension of the work of Roufosse and Klemens (1974), which, in turn, is a mineralogic application of an earlier, general theoretical examination of thermal conductivity in dielectric crystals by the same authors (Roufosse and Klemens, 1973). Their most significant contribution is a characterization of the effect of a positive lower bound on the phonon mean free path, which is a natural consequence of diffusion within a discrete lattice, as opposed to that within a

continuum approximation. The size of this minimum is to be determined empirically, but is expected to be a small multiple of the distance between neighboring atoms. The model does not address anisotropy, but this is not seen as a serious shortcoming in this context, for, as noted above, the isotropic and individual anisotropic trends with temperature are similar for these materials. Only the isotropic trends will be discussed, but the results for each mineral may be scaled by appropriately selected constants of proportionality to fit the anisotropic values.

Preferred Model

The model (Roufosse and Klemens, 1974) calculates the lattice thermal conductivity as a function of temperature and pressure from a small set of observable material properties and a single free parameter which limits the diminution of the mean free path. This parameter, α , is expressed as a factor by which a , the cube root of the average volume per atom, is multiplied. For the minerals in this study, α has a value near two, and remains fixed with respect to pressure and temperature. The other terms in the model are the phonon group velocity (v), the mean atomic mass (M), the number of atoms per unit cell (N), and the Grüneisen parameter (γ). This last term is defined by the relationship

$$\gamma = \frac{\alpha_v K_S}{\rho C_p} = \frac{\alpha_v K_T}{\rho C_v}$$

in which α_v is the volume thermal expansivity, K_S and K_T are the adiabatic and isothermal bulk moduli, ρ is the density, and C_p and C_v are the specific heats at constant pressure and at constant volume (Anderson and Isaak, 1995). Nearly all of the parameters in the model are, themselves, dependent upon pressure and temperature.

In the simplest form of the model, all phonon modes are assumed to have the same group velocity as an average of the acoustic modes, as given by

$$v = \sqrt[3]{\frac{2v_s^3 + v_p^3}{3}}$$

in which v_s and v_p are the isotropic shear and compressional sound velocities. Furthermore, the material is assumed to be above its Debye temperature, so that the specific heat is in the high-temperature limit.

The phonon mean free path is permitted to vary with phonon angular frequency (ω), though it is not allowed to decrease below a minimum, l_0 , given by

$$l_0 = \alpha a$$

for all frequencies. Above this minimum, the dependence of l on ω and temperature is expressed with respect to a reference frequency, ω_0 , a cutoff frequency, ω_c , and a reference temperature, T_1 , at which $l(\omega_D) = l_0$, where ω_D is the Debye frequency, given by

$$\omega_D = \frac{\sqrt[3]{6\pi^2} v}{a}.$$

The reference temperature is

$$T_1 = \frac{Mv^2 N^{2/3}}{101.2\gamma^2 K_B}$$

where K_B is the Boltzmann constant, and the reference frequency is then

$$\omega_0 = \omega_D \sqrt{\frac{T_0}{T}}.$$

The cutoff frequency is

$$\omega_c = \omega_D N^{-1/3}.$$

Below the reference frequency, the mean free path is

$$l(\omega) = \frac{\sqrt{2} M v^4}{3\pi a \omega^2 \gamma^2 K_B T}$$

and is l_0 above the reference frequency to the cutoff frequency. This leads to an expression for conductivity, as outlined in Roufosse and Klemens (1973), of the form

$$K = \frac{\sqrt{2}Mv^3}{\sqrt[3]{36\pi^4 a^2 \gamma^2 \omega_D T}} \left[\int_0^{\omega_0} d\omega + \int_{\omega_0}^{\omega_c} \frac{\omega^2}{\omega_0^2} d\omega \right]$$

which is equal to

$$K = \frac{\sqrt{2}Mv^3 \omega_c}{\sqrt[3]{36\pi^4 a^2 \gamma^2 \omega_D T}} \left[\frac{2}{3} \sqrt{\frac{T_1}{T}} + \frac{1}{3} \frac{T}{T_1} \right].$$

In an initial attempt to check the applicability of this model to the data, the appropriate physical properties were taken from Anderson and Isaak (1995) and Bass (1995), and the temperature dependencies of these properties were neglected. As the observed diffusivities span the transition from low-temperature to high-temperature behavior, a direct comparison between the model conductivities and the corresponding conductivity data shows that the model grossly overestimates the low-temperature conductivities. In undertaking the present analysis, it appeared that much of this difference could be ascribed to the change in specific heat, so a set of satisfactory fits was obtained by comparing the results of the model to the diffusivities instead, normalized by the respective room-temperature values. These fits are shown in Figures 20-24. The significance of the ability of the model to produce a satisfactory functional form for thermal diffusivity lies in the remarkably similar value of the free parameter, α , for the different minerals. For KH-OLV, KH-OPX, and FA-147337, the best fits are with $\alpha = 1.75 \pm 0.05$. SC73-10 required a slightly higher value of 2.25 ± 0.05 , which is shown in Figure 21, though the results for assuming $\alpha = 1.75$ for this sample are given in Figure 22 for comparison. For all these materials, α is physically reasonable, and it is remarkable that the same value is appropriate for this range of compositions and structures. These fits also captured the high-temperature trends in conductivity fairly well, both in terms of the magnitudes (except for FA-147337) and in terms of the temperature dependencies, as shown in Figures 25-28.

Potential Refinement of the Model

Three obvious shortcomings of the current approach require attention in order to produce a more satisfactory model of thermal conductivity across the entire temperature range. First, the known temperature dependencies of the underlying material properties must be incorporated into the calculations. Second, the behaviors of the individual vibrational modes below the Debye temperature must each have their own formulation. Third, the significant difference in group velocities and mean free paths, both between the acoustic and optic modes and among the various optic modes, also needs to be included. The first of these points may be addressed via recourse to high-temperature data available in the literature when available, and the second requires a knowledge of the characteristic temperature and low-temperature behavior of each mode, so only the third point shall be discussed here. A better estimate of the contribution the optic modes is derived and presented in the following section.

Contribution of Optic Modes

One shortcoming of the model lies in its assignment of the same group velocities to both acoustic and optic vibrational modes, which grossly overestimates the group velocities of most of the optic modes, and hence their contribution to thermal conductivity. As shall be shown, a more appropriate estimate of the mean group velocity for optic modes in olivines, certainly, and by analogy in pyroxenes, places it at one-third of the corresponding Debye velocity. This figure comes from an examination of phonon dispersion relations presented in Rao et al. (1988) and Ghose et al. (1991), and the categorization of the various modes by Chopelas (1990 and 1991).

Group velocities for vibrational modes may be derived from observations of phonon dispersion; specifically, the group velocity of a mode is given by the derivative of phonon energy versus phonon wave vector. Direct observation of the dispersion relations of all 84 vibrational modes of olivine (three acoustic and 81 optic) has not been achieved, but it is possible to observe and characterize the behavior of the acoustic and low-energy optic modes across nearly the entire span of the Brillouin zone by inelastic neutron scattering (Rao et al., 1988). For forsterite, the acoustic and 22 optic modes have been observed (Rao et al., 1988), while for fayalite, the total consists of the acoustic and nine of the optic modes (Ghose et al., 1991). In conjunction with these measurements, the respective authors developed rigid-ion lattice dynamic models for the olivine end-members, from which the behavior of all the modes was calculated, though only the dispersion relations of those modes which are of energies comparable to the experimentally observed modes were included in the figures. For the present study, the published figures of the model results were optically scanned and the slope of the curve for each mode was estimated from the values at the zone-center and zone-edge endpoints.

The group velocities for the optic modes of forsterite and fayalite are plotted in Figures 29 and 30, sorted by their respective zone-center frequencies. This sorting permits them to be categorized according to the type of motion each represents, following the classification scheme of Chopelas (1990), which uses fourteen vibrational categories, three acoustic and eleven optic, some of which overlap in their ranges of frequency. The categories consist of three transverse and longitudinal acoustic, two translational MO_6 , one translational and one rotational SiO_4 , and six internal SiO_4 groupings. Of these last six internal categories, the four categories of high-frequency internal modes of SiO_4 are not represented in the scanned figures, but these are generally viewed as having group velocities near zero, and so are assumed to contribute little to thermal conductivity. For forsterite, modes from all the other categories are included, therefore this subset of modes is taken as a reasonable

representation of the whole. The results for fayalite are not as extensive, in that optic modes from only three categories are included, but these three categories correspond to those categories which, in forsterite, span the greatest range of group velocities, and therefore also are taken as representative.

Mean group velocities within each category of modes are plotted in Figures 31 and 32. For forsterite, the averages of the low-wavenumber categories are raised by the effects of a small number of modes with very high group velocities, but the majority of modes, and the majority of categories, have lower group velocities than the acoustic modes. The overall average of 1997 ms^{-1} , or approximately one-third of the Debye velocity, is taken as the best representation for forsterite. For fayalite, the averages of the categories all fall below the acoustic group velocities, and again, the average of 1678 ms^{-1} , also approximately one-third of the Debye velocity, is adopted. Although no phonon dispersion data or calculations are available for orthopyroxene, this estimate of one-third of the Debye velocity is assumed for this mineral as well, as it seems to be a better estimate than the alternative of using the full Debye velocity for these modes.

An additional consideration is the potential for variability in mean free path from mode to mode. One method for assessing this is via examination of the Raman spectra of the materials, in that the spectral peak widths vary inversely with the lifetime of each corresponding mode (Hofmeister, 2001). For forsterite, measurements of seventy Raman peak widths (full width at half-maximum) have been made from the spectra reported in Chopelas (1991), though the author is grateful to Professor Chopelas for making available the original spectra, as the published figures both were much reduced and usually truncated the more intense peaks. The lifetimes, as with the velocities, were categorized according to Chopelas (1990), and a mean lifetime was calculated for each category. It was found that these lifetimes spanned a factor of two, generally decreasing towards higher frequency. By combining these measurements with the optic mode group velocities for each category, the

contribution of the optic modes to thermal conductivity was calculated using the model of Klemens (1999), which produces only a slight positive correction to an inverse-temperature model over this range. The results are shown in Figure 33.

As illustrated in Figure 33, the overall contribution of all optic modes to thermal conductivity (neglecting the high-frequency internal SiO₂ modes) is about 60% of the total conductivity at room temperature. This contribution decreases steadily to about 30% by 1000°C, though, which indicates that the contribution from the acoustic modes remains nearly constant across this range of temperatures.

The results of this analysis differ greatly from those of Hofmeister (2001), in which it was concluded that the optic modes were responsible for heat transport at room temperature. This difference arises from Hofmeister's explicit assumption that the acoustic and optic modes all have effectively the same group velocities (i.e., half the sum of the isotropic compressional and shear wave velocities), specific heats, and lifetimes.

High-Pressure Olivine

The results of the high-pressure measurements on SCchai, listed in Table 14 and plotted in Figure 34, fall nearly along a linearly increasing trend, though it should be noted that most of the increase occurs between the ambient and 3.22 GPa values; from 3.22 to 5.09 GPa the diffusivities and conductivities are essentially constant within their respective uncertainties. Previous experimental (Fujisawa et al., 1968; and Katsura, 1995) and theoretical (Mooney and Steg, 1969) studies suggest that both diffusivity and conductivity should depend linearly on pressure over this range, with slopes similar to those observed, so the linear fits have been adopted. In light of the comparatively large uncertainties of the high-pressure D_{11} values, no significance has been assigned to the slight difference in the slopes of the best fits along the two observed axes.

Many difficulties arise in the attempt to compare these results with those of previous studies, often related to the differences in sample selection (e.g., composition, single-crystal vs. aggregate, grain size, porosity) or experimental technique, since in all other methods the thermal properties of the sample and those of the apparatus cannot be considered separately. The authors (Fujisawa et al., 1968; Schloessin and Dvořák, 1972; Schärmeli, 1982; and Katsura, 1995) have gone to great lengths to account for the peculiarities of their respective sample geometries, presses, thermocouple placements, and heater arrangements, though it is often not easy to compensate fully for the effects each of these have on their results. Although many of these same problems arise in conventional measurements of thermal diffusivity under ambient conditions as well, they are mentioned here because the difficulties, too, increase with pressure. It seems most prudent to conclude that the results are not incompatible, within broad uncertainties.

One final point on this subject is that all previous measurements have been of total diffusivity or conductivity, not just of the lattice component. Discussion of most of the considerations involved in estimating the radiative contribution so that the lattice contribution may be derived, a universal problem with other techniques, shall be deferred to the section on radiative heat transport, but one aspect, unique to the high-pressure measurements, deserves mention here. The mean free path of thermal photons in olivine is limited, to a great extent, by the Fe^{2+} absorption band occurring at wavelengths near 1 μm , particularly as this band broadens with temperature (Fukao et al., 1968). The effect of increased pressure is to shift this band to lower wavelengths, thereby increasing the "thermal window" for transmission between 1 and 4 μm , but as Shankland (1970) has demonstrated, this effect is small in comparison with the corresponding thermal broadening of the band along any reasonable geotherm, so the net radiative contribution remains small at high pressures and temperatures. It remains difficult to model, however, and as Schärmeli (1982)

has pointed out, independent measurements of the lattice component, such as presented here, remain highly desirable so that the conventional assumptions used in the decomposition of total diffusivity and total conductivity may be tested.

The Forsterite-Fayalite Solid Solution in Olivine

The room-temperature subset of measurements spanning the Mg-Fe solid solution series in olivine may be compared directly with the work of Horai (1971), who measured the room-temperature isotropic thermal conductivities of 166 common minerals, including eight olivines ranging from Fo₄ to Fo₉₈, though all but two were above Fo₈₆. Horai's method was to create a 100 ml aqueous slurry of finely ground (< 0.05 mm) powder for each mineral, measure the total conductivity with the needle-probe method of Von Herzen and Maxwell (1959), then extract the conductivities of the components based on their volume fractions, using the estimates of upper and lower bounds of Hashin and Shtrikman (1962). The results, converted from the original units of mcal cm⁻¹ s⁻¹ °C⁻¹, are plotted in Figure 35, along with the room-temperature isotropic averages calculated from the present dataset. An unweighted second-order polynomial fit to the Horai data

$$K_{iso} = Fo^2 - 0.008Fo + 3.163$$

is quite similar to the unidentified curve in Horai's Figure 6*b*, though Horai's curve was constrained to pass directly through the points at Fo₄ and Fo₅₄, and so shows a more pronounced minimum near Fo₂₀. This same polynomial fit works well with the present data if lowered by approximately 0.2 W m⁻¹ K⁻¹.

Horai's explanation for the departure from a linear trend along the solid solution is that the mean free path decreases with the introduction of randomly-distributed substitutions that act as scattering centers; by contrast, the compressional velocities do vary linearly with

composition, indicating that changes in phonon velocity alone will not explain the trend. Horai presents a model of this effect based on Joffe (1956) and derives an estimate of the phonon mean free path in forsterite of 1.6 times the lattice constant, with impurities decreasing thermal conductivity by 16% for Fo_{90} . This effect is highlighted when the data are plotted in terms of thermal resistivity (K^{-1}), as in Figure 36. An unweighted linear fit to the Horai data passes through the cluster of points near the forsterite end-member, and, fortuitously, intersects the FA-147337 value. The two intermediate compositions, SC73-10 and Horai's Fo_{54} , however, are offset by about 0.03 m K/W , or a little over 10% of their total resistivities, which is an indication of the significance of the effect of mixing Fe and Mg on the crystallographic sites.

The present set of data permit this analysis to be extended to embrace the observed anisotropy as well, though only incompletely. For KH-OLV and FA-147337, the anisotropy is approximately proportional to that of the corresponding compressional velocities, which, for example, largely account for the nearly isotropic behavior of FA-147337 in the a - c plane. The case of SC73-10 is complicated by the observation that the diffusivity along b is essentially identical to that of KH-OLV, while the other two components are so much lower than those of KH-OLV that the resulting isotropic average falls on the expected trend. This suggests that, for SC73-10, the diffusivities are being affected by an agent with an anisotropic effect, whether this agent is the distribution of cations, vacancies, other defects, or perhaps the presence of OH. The sample has experienced a history of metasomatism, so it is not known whether its diffusivities are a reflection of some aspect of this process. No sound velocity measurements have been made on this material, so it cannot be stated whether the unusual anisotropy is related to similar behavior in the elastic constants, or whether it arises from anisotropic constraints on the mean free path. A detailed x-ray structural refinement also is not available. Both are of great interest for future study of this material.

Radiative Heat Transport

Although not directly the subject of this study, the radiative component of thermal transport deserves some mention, since both the measurements and the models herein presented do involve temperatures at which this phenomenon becomes significant. The quantitative characterization of the transfer of heat by radiation within mantle minerals presents a great number of difficulties in the range of temperatures and pressures of interest, many related to such extrinsic features as the effects of grain boundaries on scattering (Shankland et al., 1979), which make it difficult to translate laboratory results into an expectation of mantle behavior. Even within the limits of a strict consideration of the intrinsic single-crystal properties, however, an assessment of the efficiency of radiative transport must take into account the variable infrared opacity of these minerals.

Below approximately 400°C the radiative conductivity, K_R , is small, but increases rapidly with temperature, following to the relationship

$$K_R = \frac{16\sigma n^2 T^3}{3\langle\epsilon\rangle}$$

in which σ is the Stefan-Boltzmann constant, n is the refractive index, and $\langle\epsilon\rangle$ is the mean extinction coefficient of the material, weighted by the black-body distribution (Schatz and Simmons, 1972). For iron-bearing silicates such as olivine, the governing parameter is the peak in absorption that is present for wavelengths near 1 μm through its effect on $\langle\epsilon\rangle$.

(Indeed, this absorption feature makes possible the experiments reported in this dissertation.) As temperature increases, this absorption peak both broadens and becomes more intense (Shankland et al., 1979), which accounts for the observation of Schatz and Simmons (1972) that the radiative conductivity for Fo_{92} olivine increases only gradually for temperatures up to 1600°C, as shown in Figure 37. In light of the data in the present study,

it appears that the radiative contribution is even smaller in both magnitude and rate of growth than was reported by Schatz and Simmons, in that they assumed a simple inverse-temperature model for lattice thermal conductivity in order to interpret their measurements of total conductivity. Thus, they concluded that radiation accounted for approximately half of the heat conduction between 900 and 1600°C, whereas the larger current value for lattice conductivity reduces this to only about one-quarter of the total (Figure 37). A comparison with the measurements of Katsura (1995), scaled such that the measurements below 300°C fall on the same trend, gives similar results, also plotted in Figure 37. Since the effective radiative transport is expected to become even smaller for heterogeneous polycrystalline aggregates, it is concluded that the radiative component is a significant, but secondary, aspect of heat flow in the upper mantle, and does not appear to become much more important as temperatures or, as noted above, pressures increase.

Directions for Future Work

It is entirely too easy, because entirely too true, to suggest that more data are needed in order to span a greater range of pressures, temperatures, and compositions, and that, in conjunction with this effort, yet more will be needed in order to narrow the gaps between observations. It is, however, perhaps more useful to point out only those immediately realizable steps that appear likely to be the most fruitful, and to call particular attention to some foreseeable pitfalls.

The desirability of examining further the unusual anisotropy of SC73-10 with respect to its elastic behavior and detailed crystallographic structure has already been mentioned, and remains a priority. Indeed, it is hoped that such measurements may be completed in time for inclusion in the submission of this body of work for publication.

The extension of this technique to modestly higher temperatures, perhaps 1300°C, seems feasible, though some attention would have to be paid to the ceramics chosen for the secondary furnace. The present design should not be pushed beyond approximately 1100°C. It is not clear whether the additional points would contribute enough novelty to the understanding of the trends to make such an effort worthwhile.

A hitherto overlooked direction for study is towards lower temperatures. This is common practice in the study of metals, as it is a way of examining the effect of phonon scattering in a regime of infrequent three-phonon interaction (Klemens, 1969), but has received little attention in the study of silicate minerals. Dr. Jonathan C. Crowhurst designed and tested a cryostat for an unrelated project while working as a post-doctoral researcher in this laboratory which would be suited for this purpose. It operates while suspended within the main vacuum furnace and is cooled with liquid nitrogen; the furnace's vacuum not only serves as insulation, but prevents the sample from developing a layer of frost that would inhibit optical access. In limited tests, temperatures of -150°C were achieved and maintained, and the design can accept samples inside and outside of the diamond-anvil cell.

Finally, some effort was expended to develop a new reference material as a laboratory standard for thermal diffusivity, but was not brought to completion. The ideal standard should be isotropic, produce a large signal, be commercially available in a homogeneous, stable form that is easily shaped, be insensitive to small fluctuations near room temperature, and possess a thermal diffusivity similar to those of the minerals of interest. A good candidate for this is the OD 0.6 absorptive neutral density glass filter from Newport Corporation (FSR-OD60). Before this material can be used, however, it must be calibrated against a widely accepted standard for thermal conductivity, such as Corning Pyroceram 9606 (Gustafsson, 1991; Pillai and George, 1991; and Hisano et al., 1999). This latter material is opaque, and so cannot be of direct use in this laboratory. Adequate samples of

each have been obtained and measurements attempted on a guarded-hot-plate device constructed in accordance with ASTM standards C 177-97 (ASTM, 2000a) and D 5470-95 (ASTM, 2000b), but the results to date have been inconsistent and irreproducible.

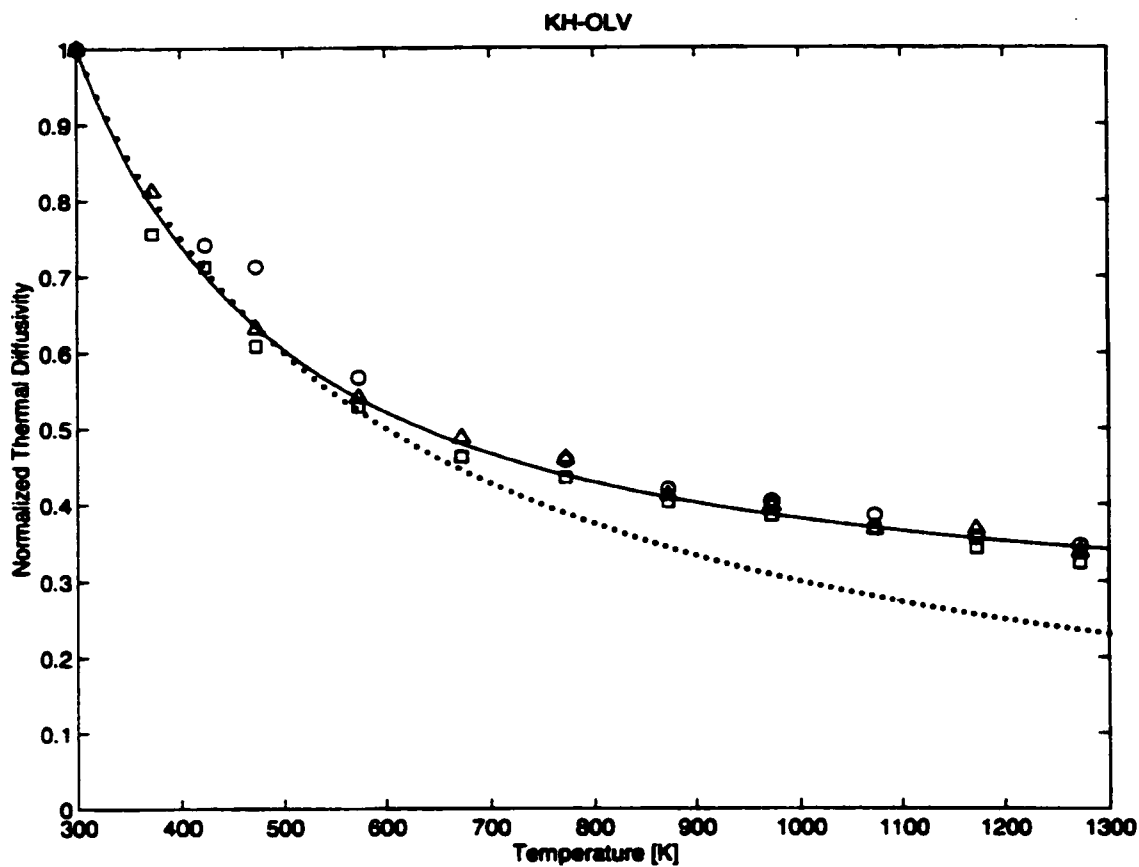


Figure 20 Comparison of KH-OLV Diffusivities with Calculations for $\alpha = 1.75$

The points are the principal values of the lattice thermal diffusivity tensor normalized by their respective values at room temperature. Triangles are D_{11} , squares are D_{22} , and circles are D_{33} . The solid curve shows the results of the preferred model for $\alpha = 1.75$, also normalized by its value at room temperature. The dotted curve shows the underestimate that results from assuming a simple inverse-temperature dependence for lattice thermal diffusivity.

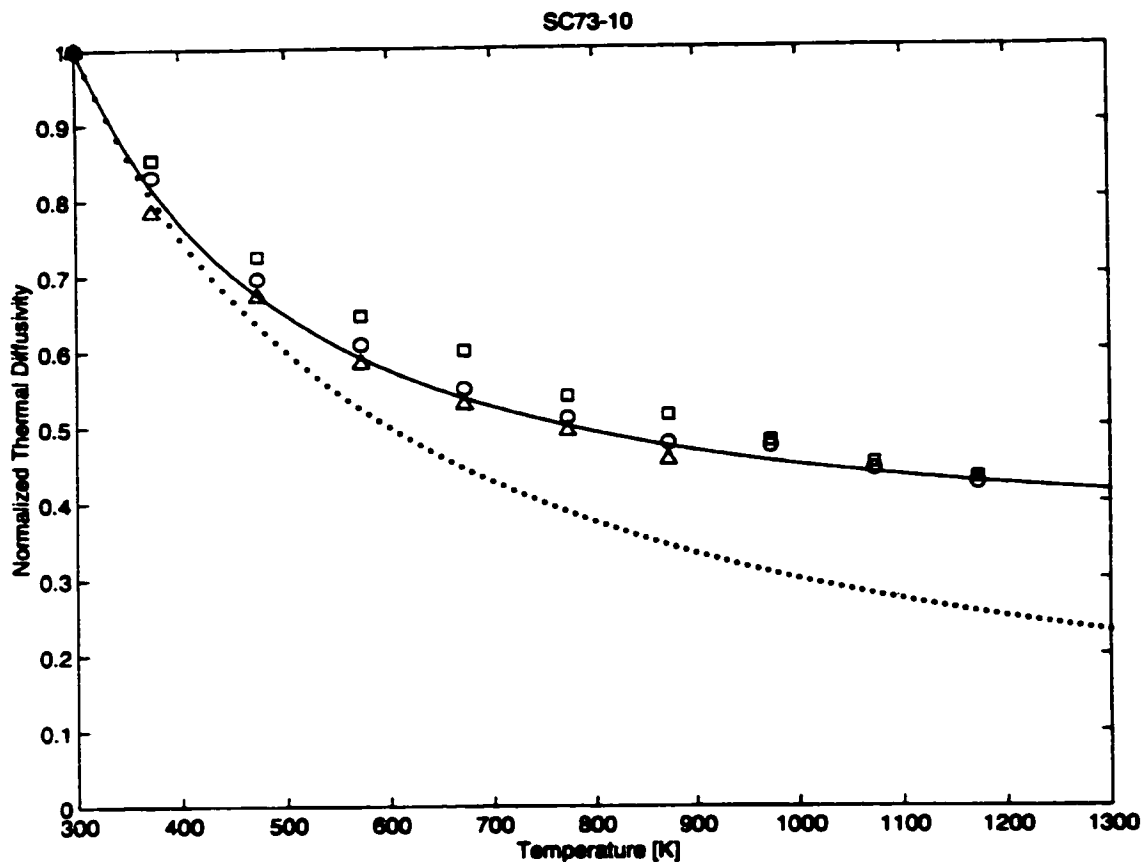


Figure 21 Comparison of SC73-10 Diffusivities with Calculations for $\alpha = 2.25$

The points are the principal values of the lattice thermal diffusivity tensor normalized by their respective values at room temperature. Triangles are D_{11} , squares are D_{22} , and circles are D_{33} . The solid curve shows the results of the preferred model for $\alpha = 2.25$, also normalized by its value at room temperature. The dotted curve shows the underestimate that results from assuming a simple inverse-temperature dependence for lattice thermal diffusivity.

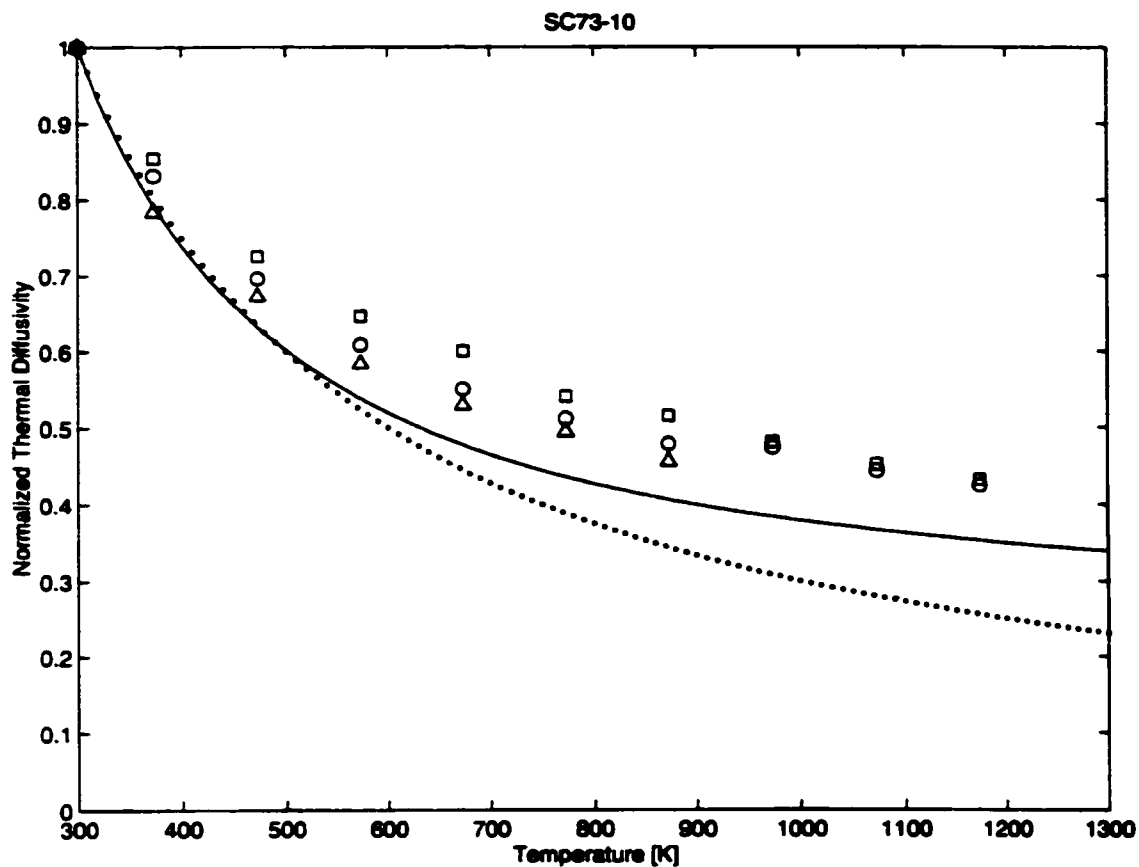


Figure 22 Comparison of SC73-10 Diffusivities with Calculations for $\alpha = 1.75$

The points are the principal values of the lattice thermal diffusivity tensor normalized by their respective values at room temperature. Triangles are D_{11} , squares are D_{22} , and circles are D_{33} . The solid curve shows the results of the preferred model for $\alpha = 1.75$, also normalized by its value at room temperature. For this sample, a larger value of α produces a better fit, shown in Figure 21. The dotted curve shows the underestimate that results from assuming a simple inverse-temperature dependence for lattice thermal diffusivity.

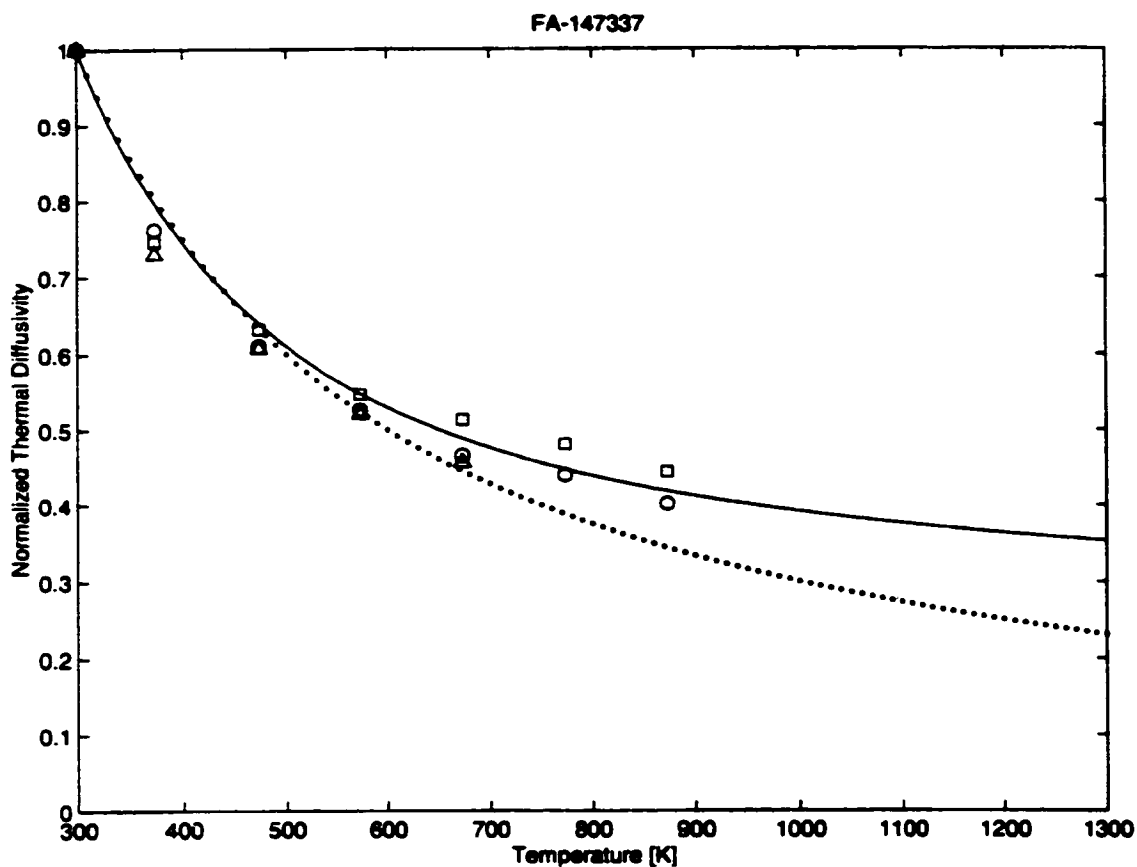


Figure 23 Comparison of FA-147337 Diffusivities with Calculations for $\alpha = 1.75$

The points are the principal values of the lattice thermal diffusivity tensor normalized by their respective values at room temperature. Triangles are D_{11} , squares are D_{22} , and circles are D_{33} . The solid curve shows the results of the preferred model for $\alpha = 1.75$, also normalized by its value at room temperature. The dotted curve shows the underestimate that results from assuming a simple inverse-temperature dependence for lattice thermal diffusivity.

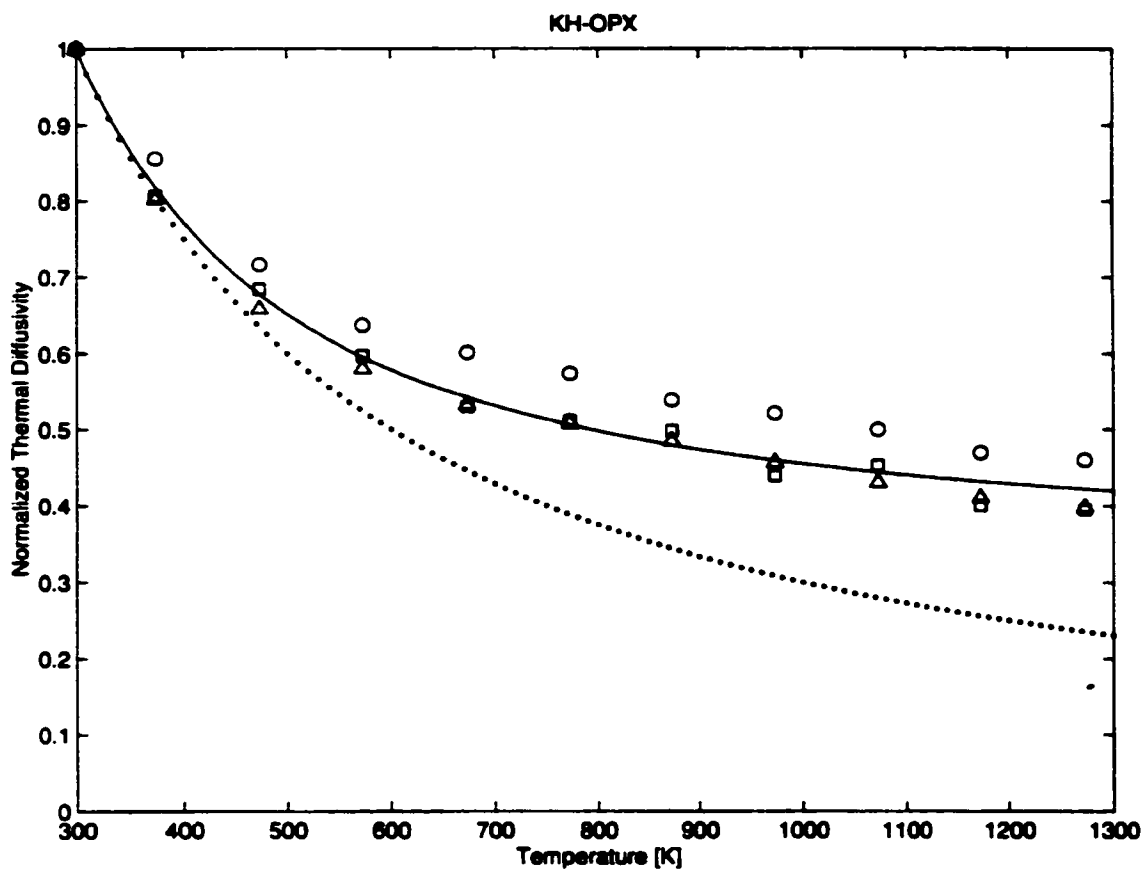


Figure 24 Comparison of KH-OPX Diffusivities with Calculations for $\alpha = 1.75$

The points are the principal values of the lattice thermal diffusivity tensor normalized by their respective values at room temperature. Triangles are D_{11} , squares are D_{22} , and circles are D_{33} . The solid curve shows the results of the preferred model for $\alpha = 1.75$, also normalized by its value at room temperature. The dotted curve shows the underestimate that results from assuming a simple inverse-temperature dependence for lattice thermal diffusivity.

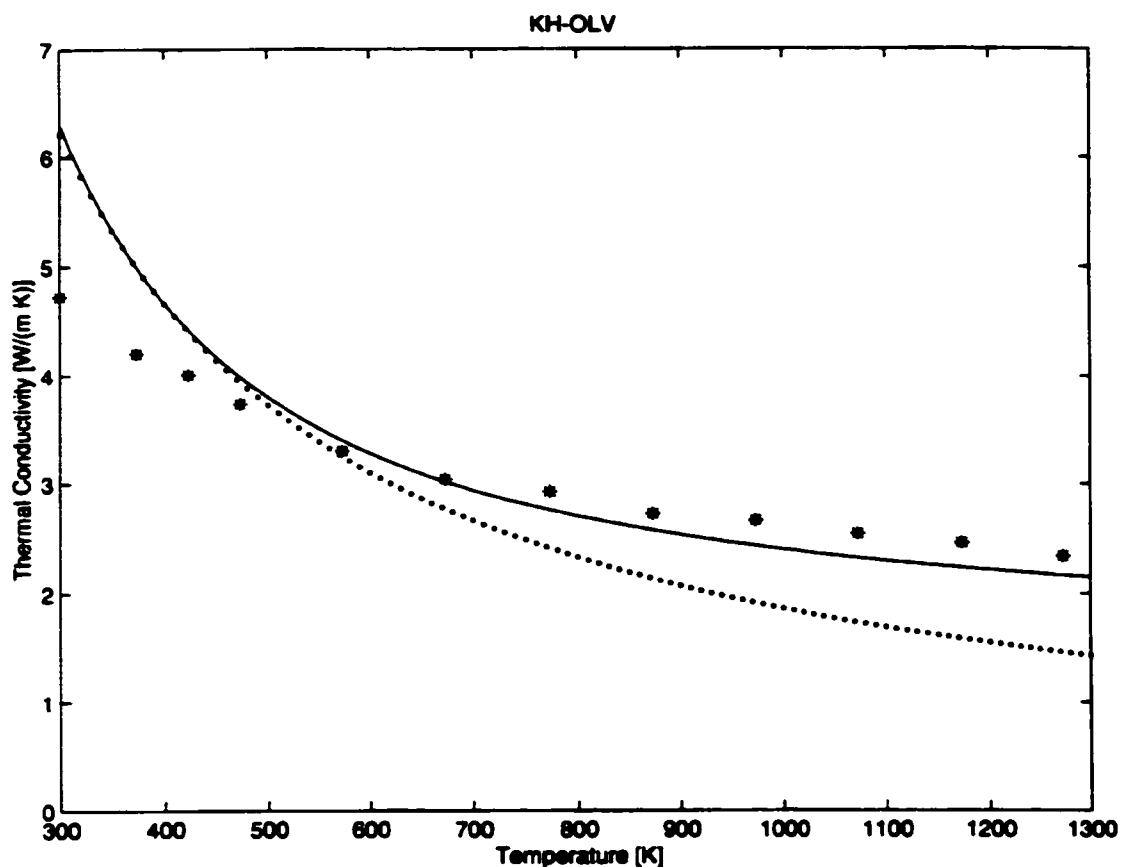


Figure 25 Comparison of KH-OLV Conductivities with Calculations for $\alpha = 1.75$

The asterisks are the isotropic average lattice thermal conductivities. The solid curve shows the results of the preferred model for $\alpha = 1.75$. Below the Debye temperature, the model uses an overestimate of specific heat, resulting in high conductivities. At high temperatures, however, it reproduces the measured values reasonably well. The dotted curve shows the underestimate that results from assuming a simple inverse-temperature dependence for lattice thermal conductivity.

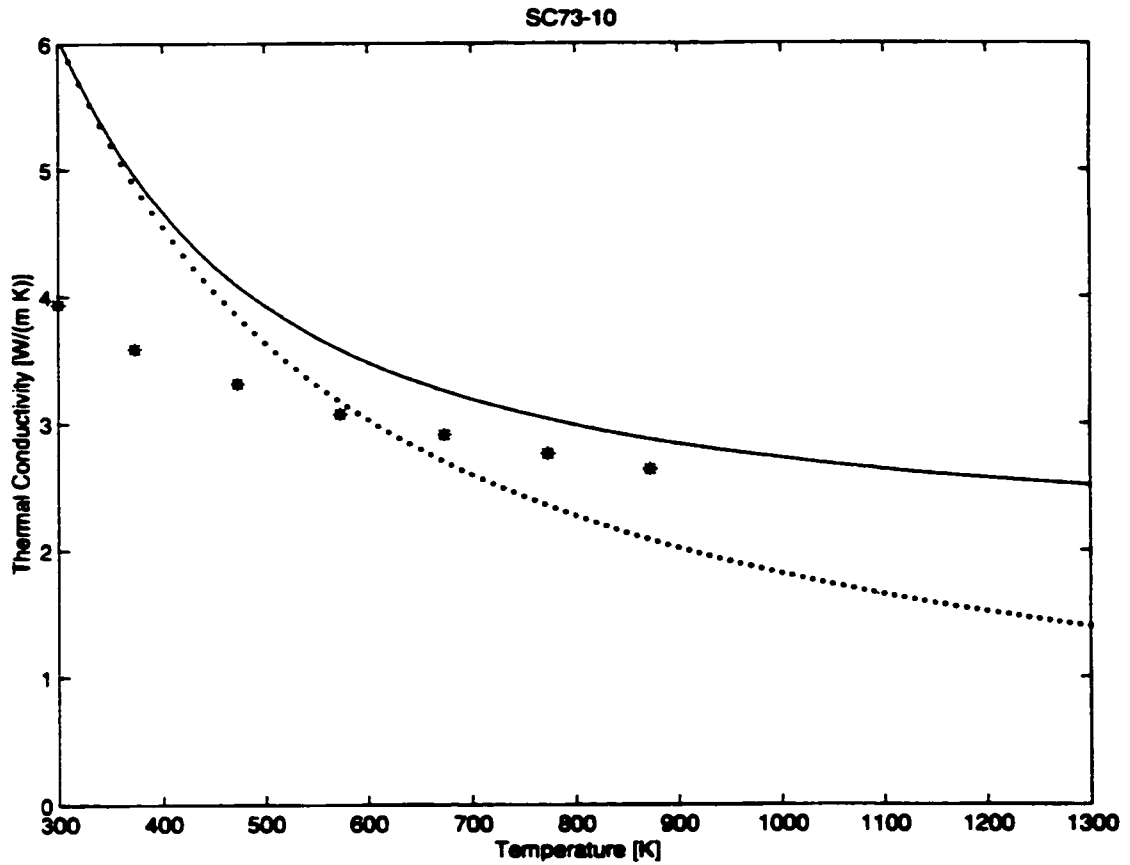


Figure 26 Comparison of SC73-10 Conductivities with Calculations for $\alpha = 2.25$

The asterisks are the isotropic average lattice thermal conductivities. The solid curve shows the results of the preferred model for $\alpha = 2.25$. Below the Debye temperature, the model uses an overestimate of specific heat, resulting in high conductivities. At high temperatures, however, it reproduces the apparent trend reasonably well. The dotted curve shows the underestimate that results from assuming a simple inverse-temperature dependence for lattice thermal conductivity.

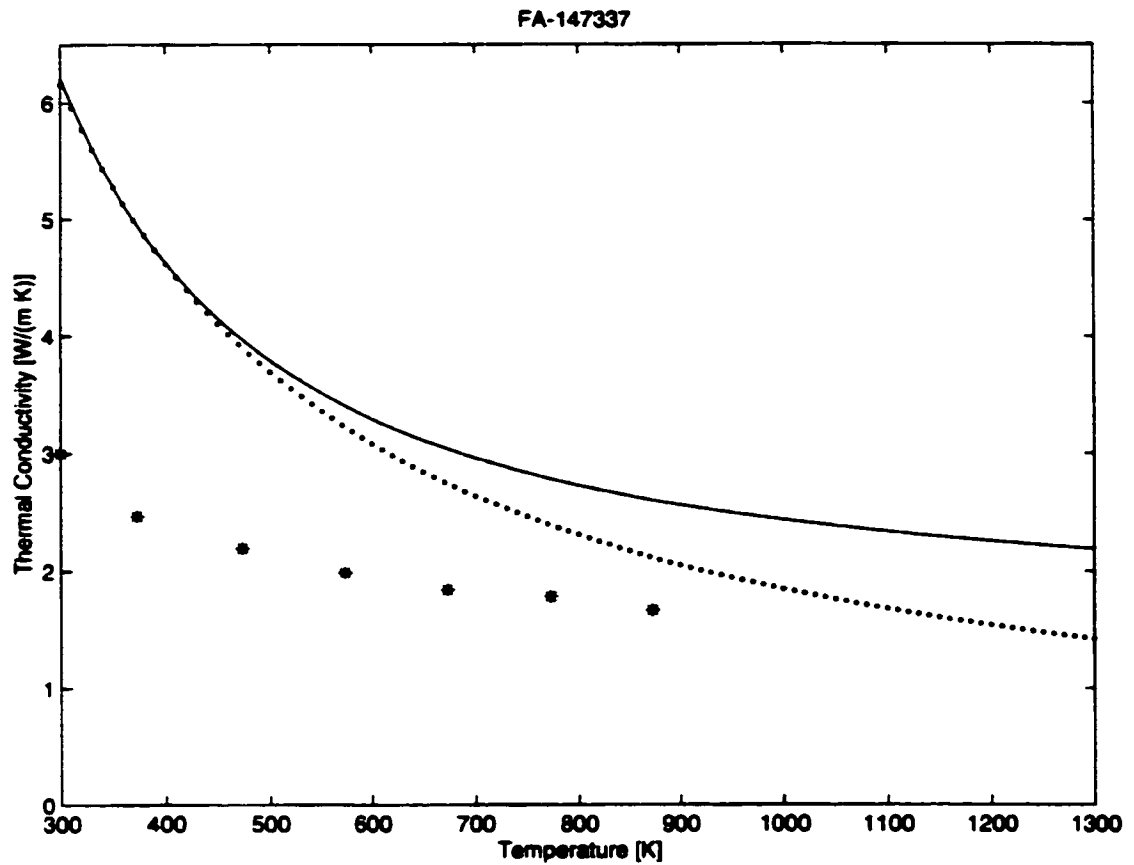


Figure 27 Comparison of FA-147337 Conductivities with Calculations for $\alpha = 1.75$

The asterisks are the isotropic average lattice thermal conductivities. The solid curve shows the results of the preferred model for $\alpha = 1.75$. At all temperatures, the model produces high conductivities, though at high temperatures it reproduces the apparent trend reasonably well with only a constant offset. The dotted curve shows the results from assuming a simple inverse-temperature dependence for lattice thermal conductivity.

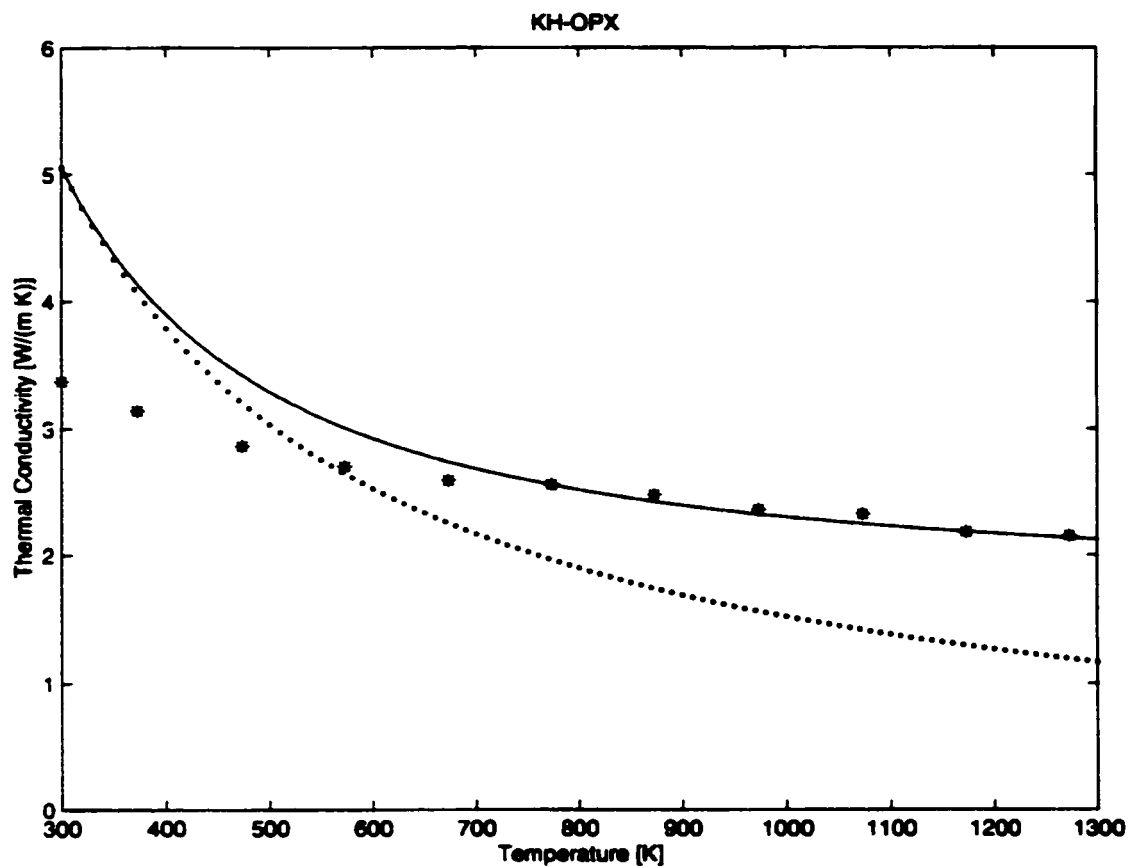


Figure 28 Comparison of KH-OPX Conductivities with Calculations for $\alpha = 1.75$

The asterisks are the isotropic average lattice thermal conductivities. The solid curve shows the results of the preferred model for $\alpha = 1.75$. Below the Debye temperature, the model uses an overestimate of specific heat, resulting in high conductivities. At high temperatures, however, it reproduces the apparent trend quite well. The dotted curve shows the underestimate that results from assuming a simple inverse-temperature dependence for lattice thermal conductivity.

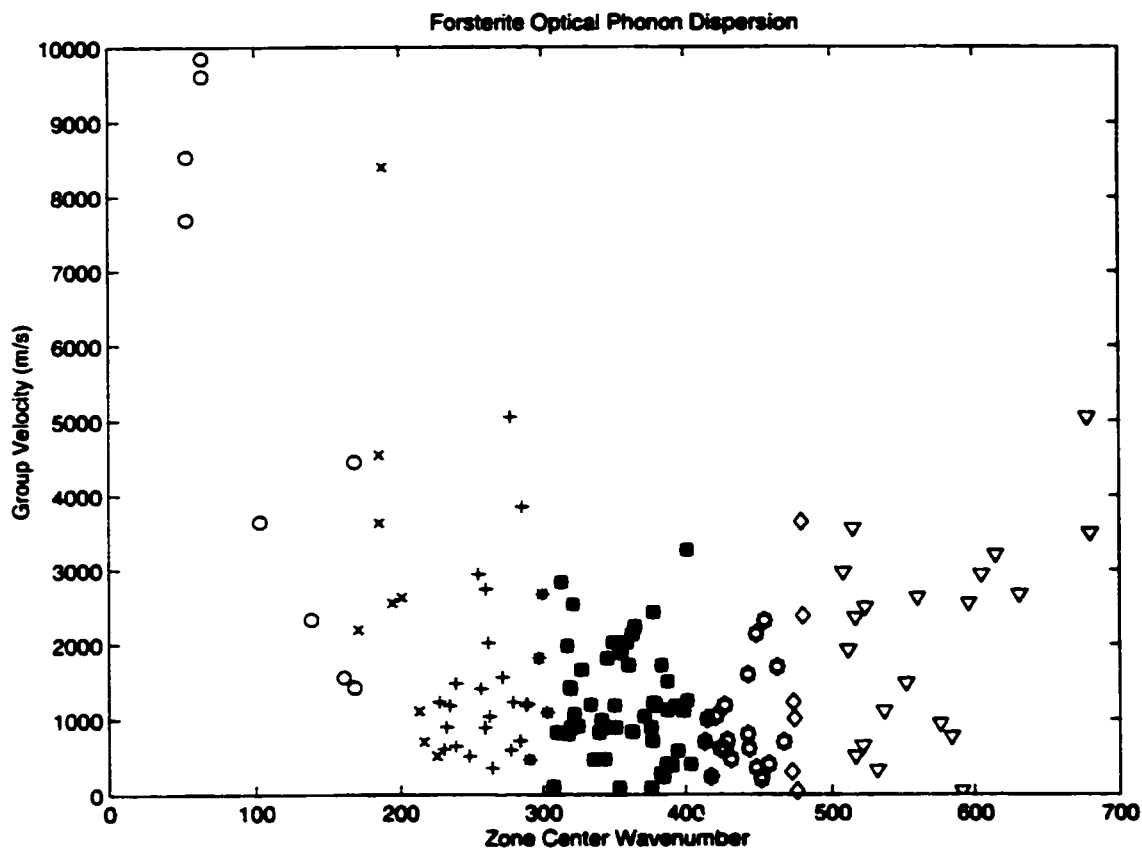


Figure 29 Group Velocities for the Optic Modes of Forsterite

The points are the estimated group velocities for each mode, categorized by type of vibration. Circles and x's represent those modes which fall in the range of transverse acoustic SiO_4 vibrations, crosses represent transverse acoustic $\text{M}(2)\text{O}_6$, asterisks represent transverse acoustic $\text{M}(1)\text{O}_6$, squares represent rotational SiO_4 , and diamonds and triangles represent ν_2 and ν_4 internal SiO_4 vibrations, respectively. A great deal of overlap in range of frequencies exists for some categories; since it was not possible to distinguish between the possible assignments with the available data, each ambiguous mode was assigned to both categories. In light of the clustering of velocities this is assumed to have no effect on calculating an average velocity for each category.

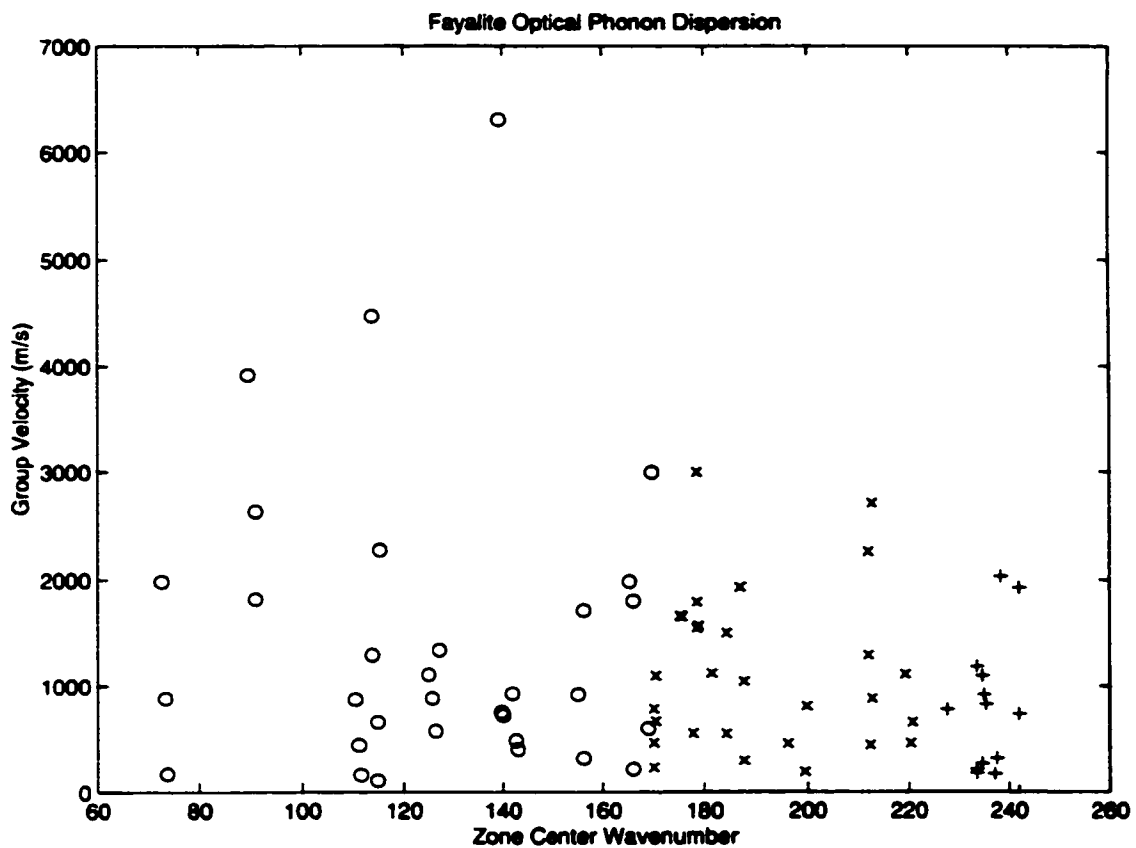


Figure 30 Group Velocities for the Optic Modes of Fayalite

The points are the estimated group velocities for each mode, categorized by type of vibration. Circles and x's represent those modes which fall in the range of transverse acoustic SiO₄ vibrations, and crosses represent transverse acoustic M(2)O₆ vibrations.

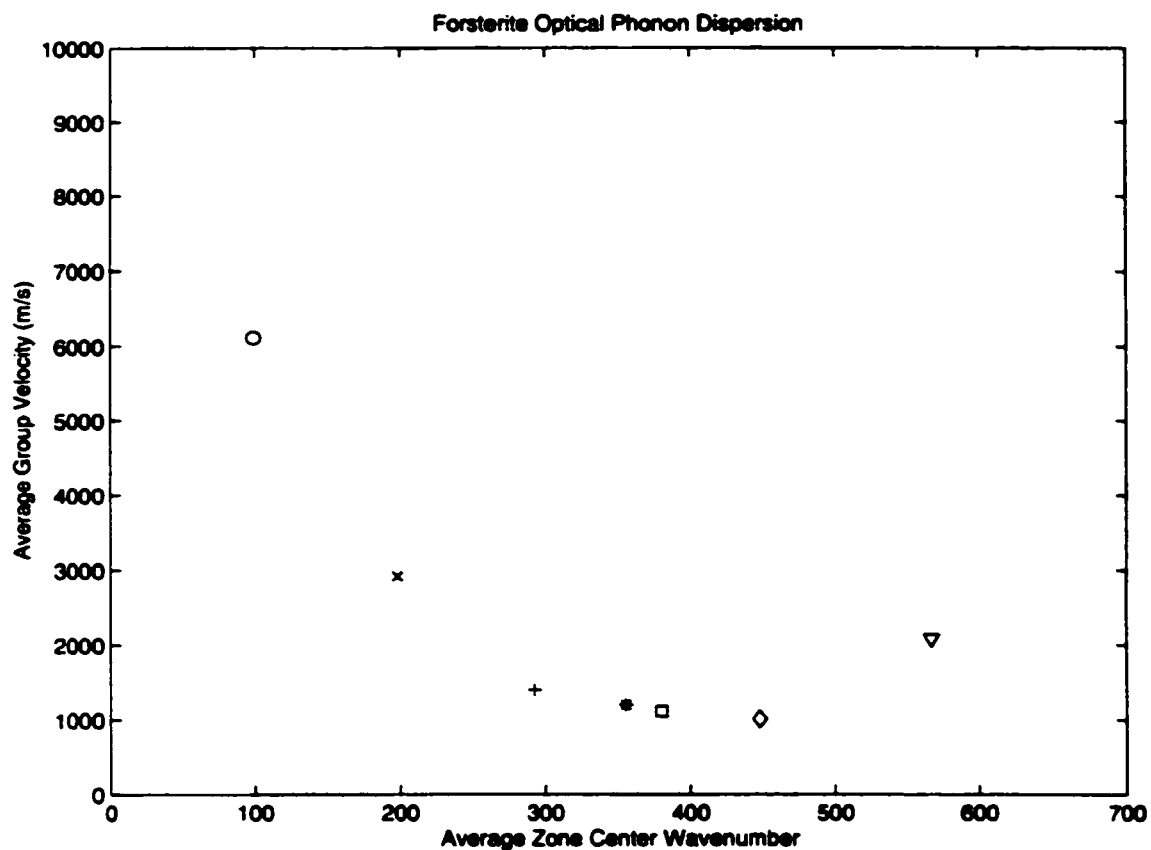


Figure 31 Mean Group Velocities for the Optic Modes of Forsterite

The points are the mean group velocities for each mode, categorized by type of vibration. The circle and the x represent those modes which fall in the range of transverse acoustic SiO_4 vibrations, the cross represents transverse acoustic $\text{M}(2)\text{O}_6$, the asterisk represents transverse acoustic $\text{M}(1)\text{O}_6$, the square represent rotational SiO_4 , and the diamond and the triangle represent v_2 and v_4 internal SiO_4 vibrations, respectively.

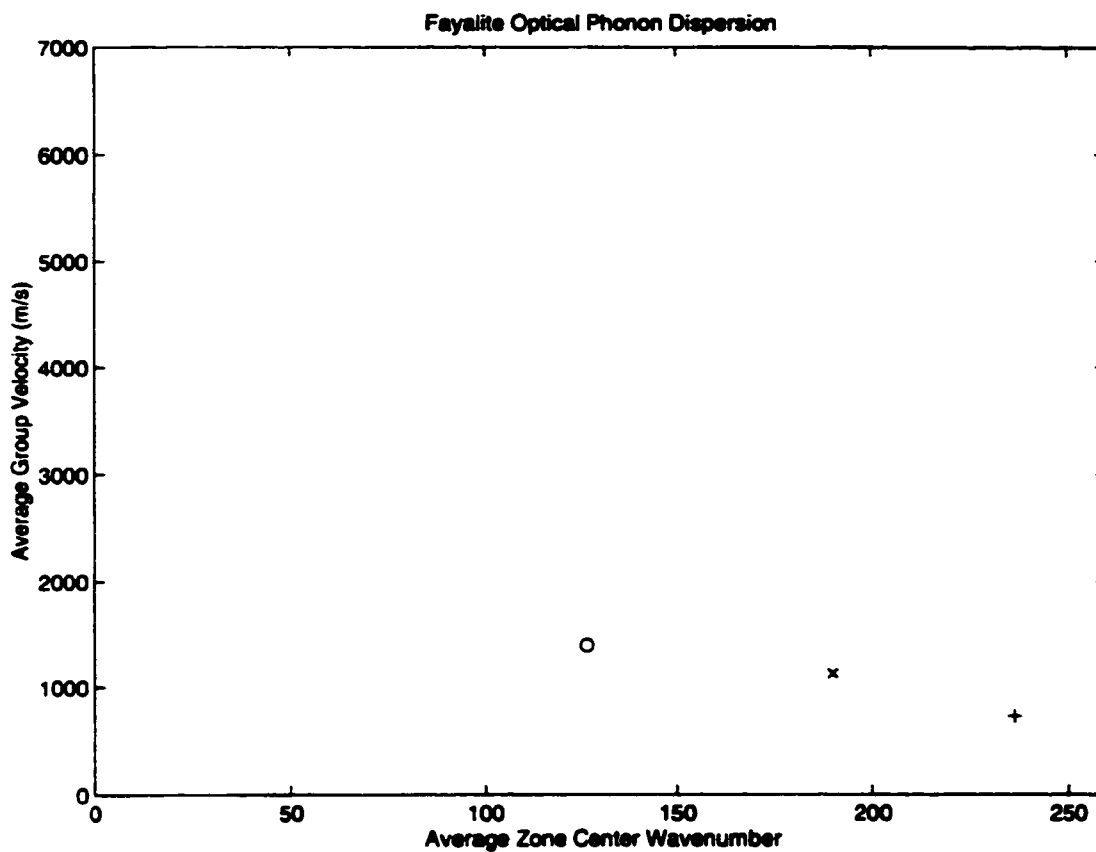


Figure 32 Mean Group Velocities for the Optic Modes of Fayalite

The points are the mean group velocities for each mode, categorized by type of vibration. The circle and the x represent those modes which fall in the range of transverse acoustic SiO_4 vibrations, and the cross represents transverse acoustic $\text{M}(2)\text{O}_6$ vibrations.

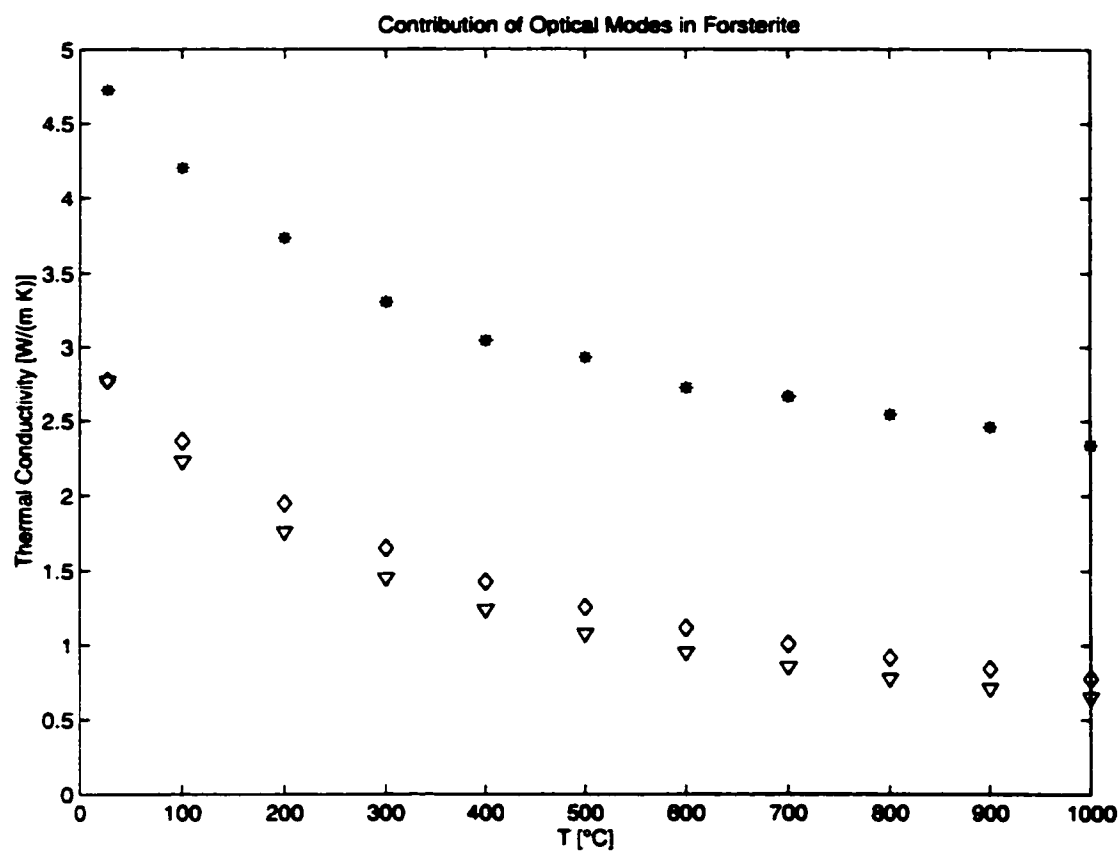


Figure 33 Contribution of Optic Modes to Thermal Conductivity in Forsterite

The asterisks are the isotropic average lattice thermal conductivity for KH-OLV, used here as a proxy for pure forsterite, which is expected to have somewhat higher conductivity. The diamonds show the total contribution of all optic modes for forsterite, following the theory of Klemens (1999), which differs only slightly from an inverse-temperature approximation for these modes (shown by the triangles).

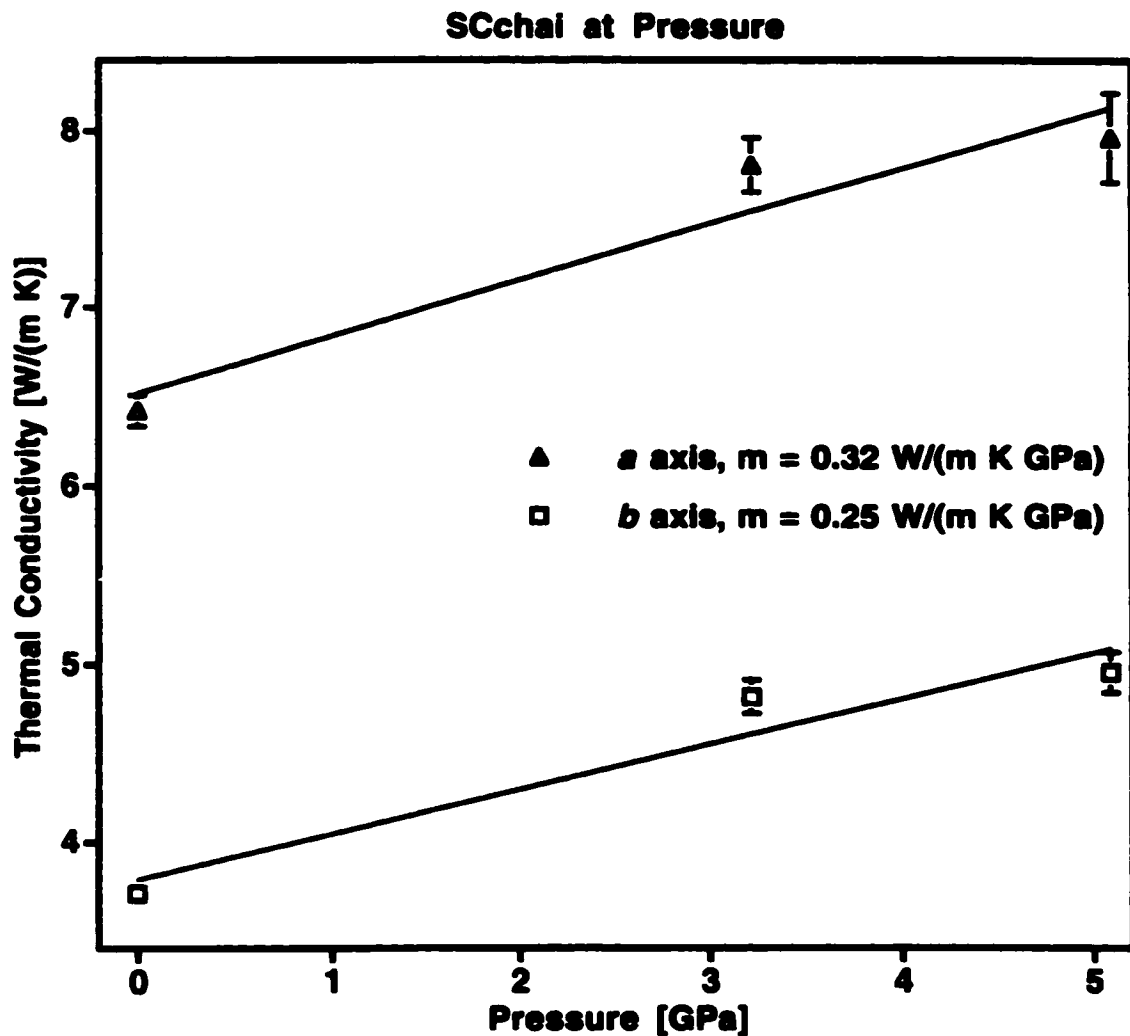


Figure 34 Anisotropic Lattice Thermal Conductivities for SCchai to 5.09 GPa

The points are two of the principal values of the lattice thermal conductivity tensor, with uncertainties, as determined at each pressure. Multiple determinations are combined into weighted means. Triangles (at top) are K_{11} and squares (at bottom) are K_{22} . The lack of data for K_{33} is a consequence of measurements being made for only one sample (i.e. for only one orientation) at these pressures. The solid lines are least-square linear fits of slope m .

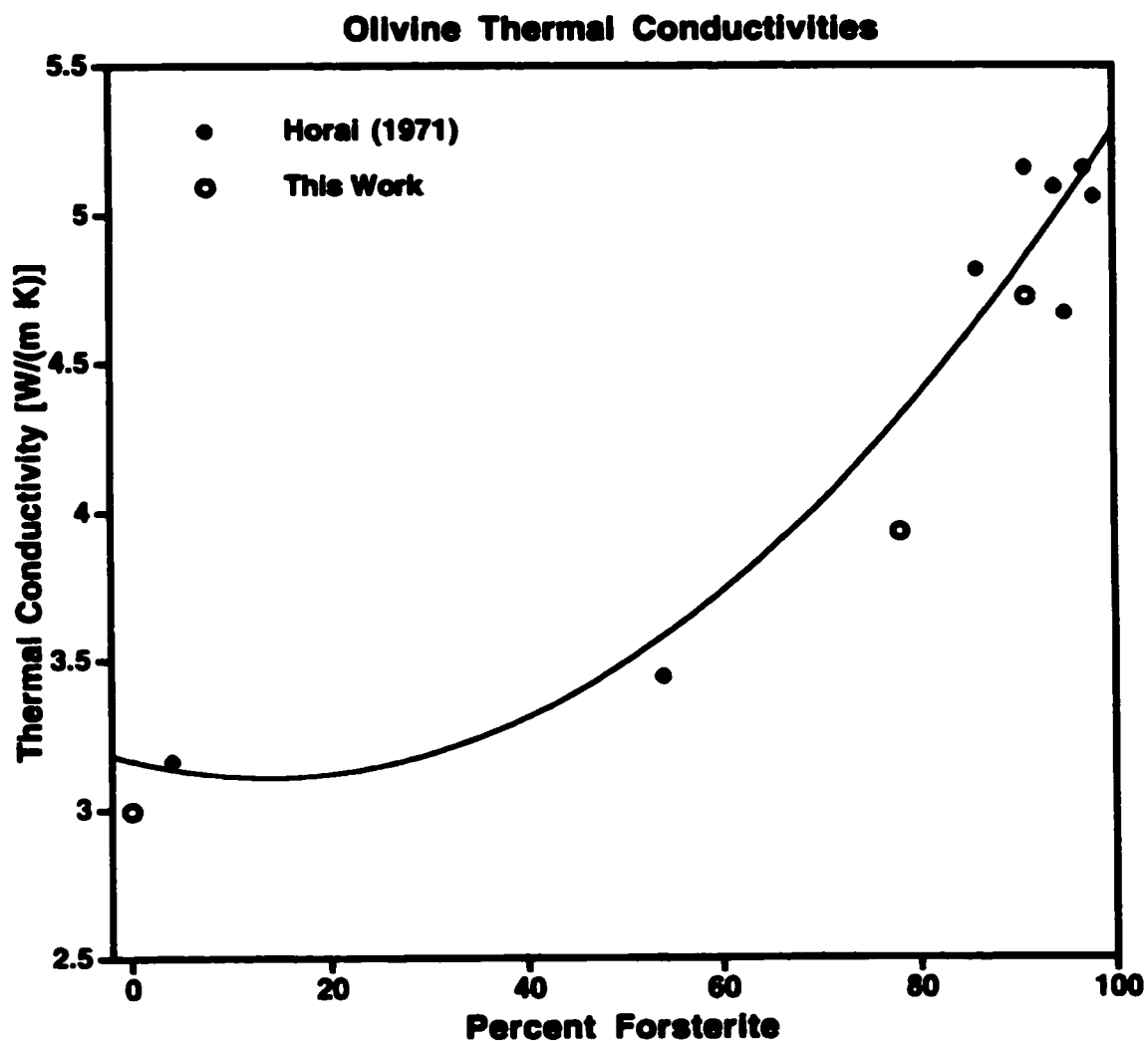


Figure 35 Thermal Conductivity Along the Fe-Mg Olivine Solid Solution Series

Solid circles are the room-temperature isotropic thermal conductivity data of Horai (1971), and open circles are the room-temperature isotropic average lattice thermal conductivities for FA-147337, SC73-10, and KH-OLV. The solid curve is a least-square quadratic fit to the Horai data.

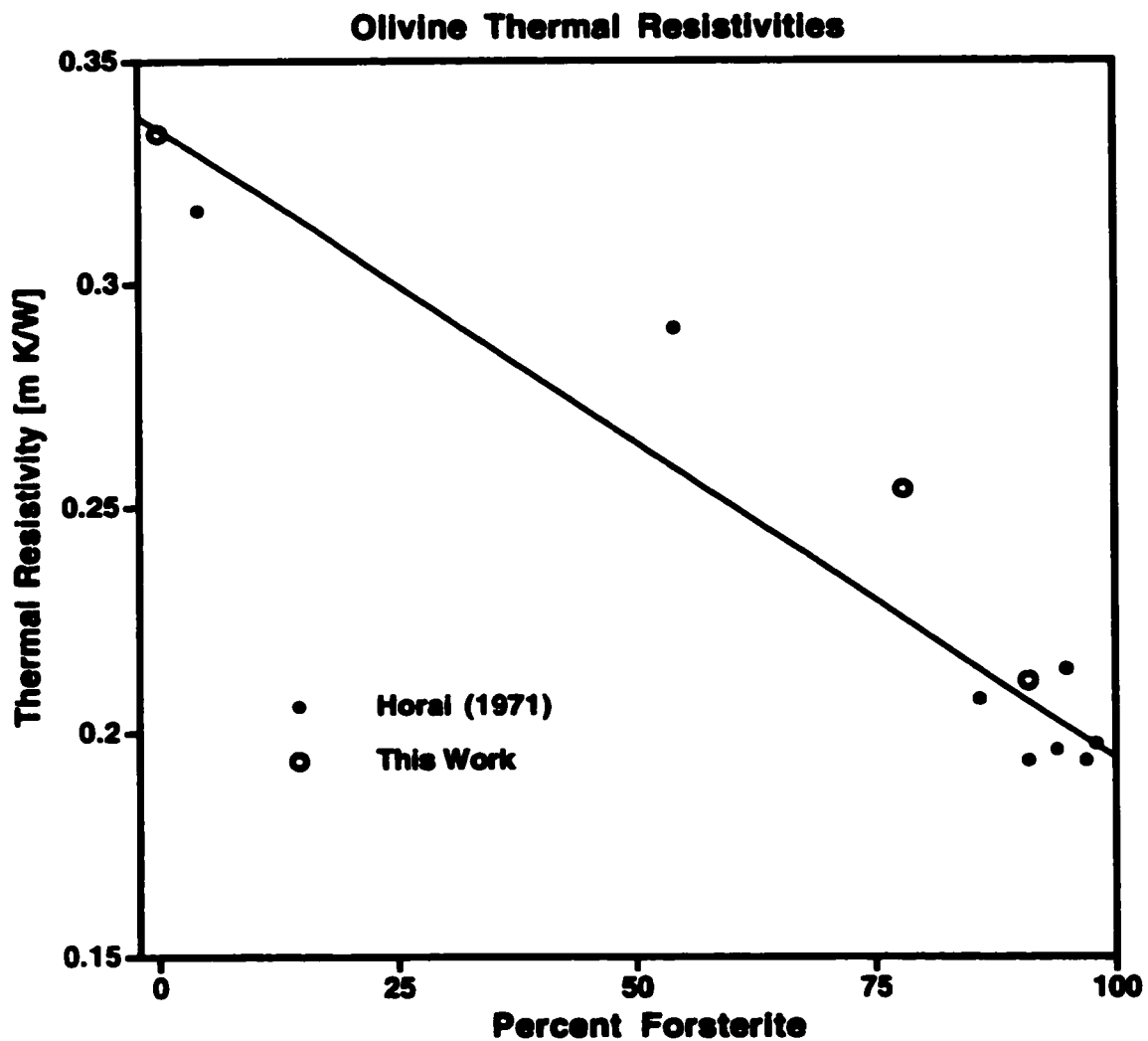


Figure 36 Thermal Resistivity Along the Fe-Mg Olivine Solid Solution Series

Solid circles are the room-temperature isotropic thermal resistivity data of Horai (1971), and open circles are the room-temperature isotropic average lattice thermal resistivities for FA-147337, SC73-10, and KH-OLV. The solid line is a least-square linear fit to the Horai data.

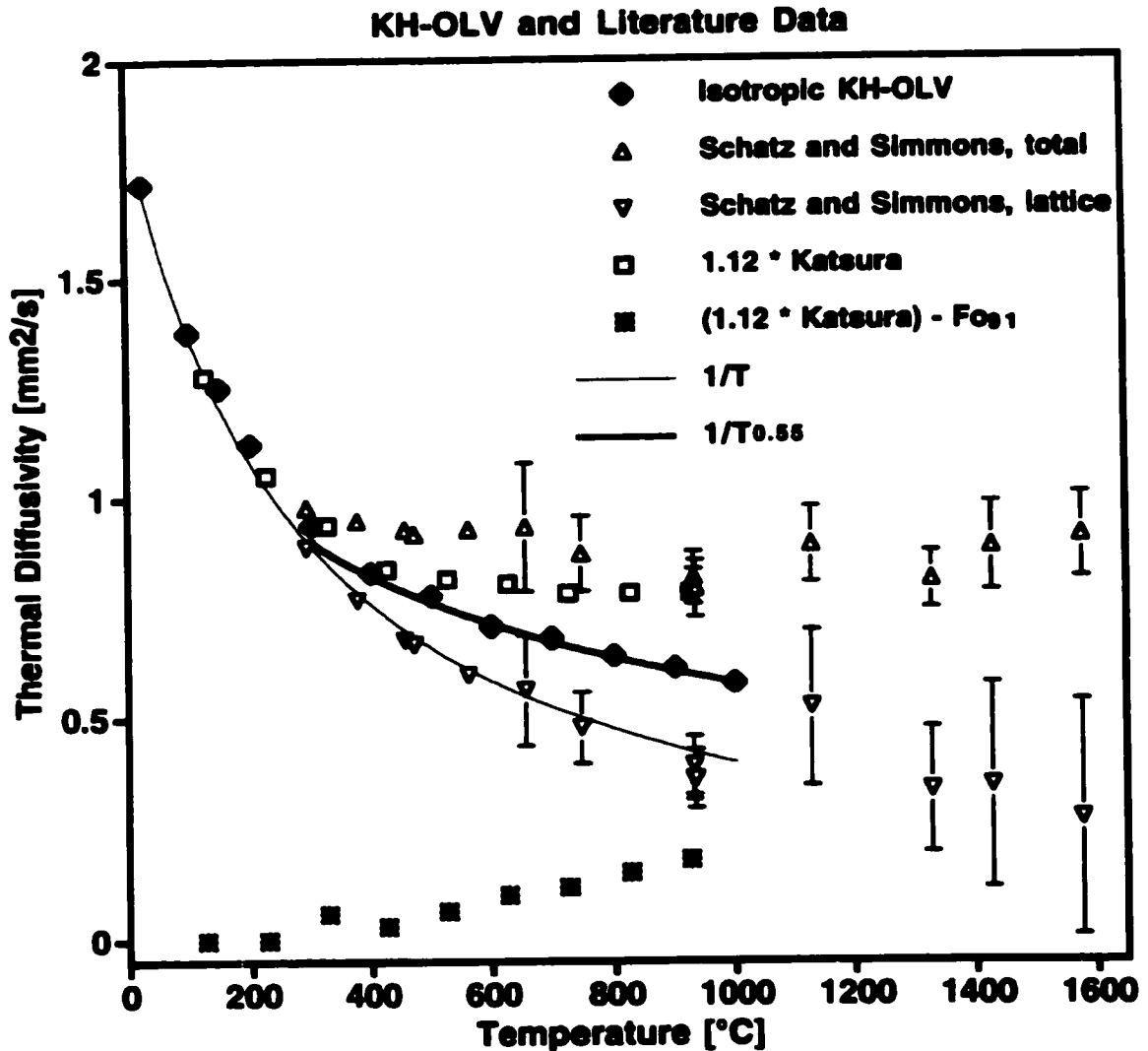


Figure 37 KH-OLV and Measurements of Total Thermal Diffusivity

The isotropic average lattice thermal diffusivity for KH-OLV is shown in solid diamonds along with an *ad hoc* interpolation of the form $T^{0.55}$ as a visual guide (thick solid curve) for its departure from T^{-1} (thin solid curve). The measurements of total diffusivity from Schatz and Simmons (1972) are plotted as upward-pointing triangles, along with their estimates for the lattice component as downward-pointing triangles, and their uncertainties on each. The measured total diffusivity of Katsura (1995), scaled by 1.12 to achieve agreement at low temperatures, is shown by the squares. The difference between the scaled Katsura values and the KH-OLV values, as represented by the asterisks, is an indication of the radiative component of thermal diffusivity at these temperatures.

Table 16 Normalized Tensor Values of Thermal Diffusivities**KH-OLV**

Temp [°C]	D_{11}/D_{11}	D_{22}/D_{11}	D_{33}/D_{11}
27	1	0.5727	0.859
200	1	0.5526	0.9707
300	1	0.5593	0.901
500	1	0.5413	0.8553
600	1	0.5594	0.8758
700	1	0.5548	0.8727
800	1	0.5727	0.9016
900	1	0.5342	0.8334
1000	1	0.5494	0.8797

SC73-10

27	1	0.7501	0.868
100	1	0.8172	0.9208
200	1	0.8094	0.8986
300	1	0.8303	0.9049
400	1	0.8502	0.9018
500	1	0.8199	0.8982
600	1	0.8466	0.9105

FA-147337

27	1	0.5292	0.9893
100	1	0.541	1.0327
200	1	0.5508	0.9938
300	1	0.5565	0.9995
400	1	0.594	1.0086

KH-OPX

Temp [°C]	D_{11}/D_{33}	D_{22}/D_{33}	D_{33}/D_{33}
27	0.7744	0.6681	1
100	0.7256	0.629	1
200	0.7111	0.6377	1

Table 16 continued

Temp [°C]	D_{11}/D_{33}	D_{22}/D_{33}	D_{33}/D_{33}
300	0.7061	0.6265	1
400	0.6850	0.5884	1
500	0.6860	0.5953	1
600	0.6971	0.6179	1
700	0.6785	0.5637	1
800	0.6676	0.6062	1
900	0.6769	0.5696	1
1000	0.6701	0.5737	1

List of References

"Where was that book you spoke of?" he asked.

'Here it is,' replied Bomba, producing it from his pouch. 'It is in a strange language and some of it is gone....'"

(Rockwood, 1929, p. 32)

Abramson, E.H., Brown, J.M., Slutsky, L.J., and Zaug, J. (1997) The elastic constants of San Carlos olivine to 17 GPa. Journal of Geophysical Research, 102(B6), 12,253-12,263.

Anderson, O.L., and Isaak, D.G. (1995) Elastic constants of mantle minerals at high temperature. In T.J. Ahrens, Ed., Mineral Physics and Crystallography: A Handbook of Physical Constants. American Geophysical Union, Washington, DC, pp. 64-97.

ASTM (2000a) Standard test method for steady-state heat flux measurements and thermal transmission properties by means of the guarded-hot-plate apparatus. In Annual Book of ASTM Standards 2000, Section 4 Construction, Volume 04.06. American Society for Testing and Materials, West Conshohocken, PA, pp. 20-41.

ASTM (2000b) Standard test methods for thermal transmission properties of thin thermally conductive solid electrical insulation materials. In Annual Book of ASTM Standards 2000, Section 10 Electrical Insulation and Electronics, Volume 10.02. American Society for Testing and Materials, West Conshohocken, PA, pp. 543-549.

- Babuška, V., Montagnet, J.-P., Plomerová, J., and Girardin, N. (1993) Age-dependent large-scale fabric of the mantle lithosphere as derived from surface-wave velocity anisotropy. *Pure and Applied Geophysics*, 151, 257-280.
- Bass, J.D. (1995) Elasticity of minerals, glasses, and melts. In T.J. Ahrens, Ed., *Mineral Physics and Crystallography: A Handbook of Physical Constants*. American Geophysical Union, Washington, DC, pp. 45-64.
- Beck, A.E., Darbha, D.M., and Schloessin, H.H. (1978) Lattice conductivities of single-crystal and polycrystalline materials at mantle pressures and temperatures. *Physics of the Earth and Planetary Interiors*, 17, 35-53.
- Berkeley, G. (1713) *Three Dialogues Between Hylas and Philonous*. G. James, London.
- Berman, R.G. (1988) Internally-consistent thermodynamic data for minerals in the system $\text{Na}_2\text{O}-\text{K}_2\text{O}-\text{CaO}-\text{MgO}-\text{FeO}-\text{Fe}_2\text{O}_3-\text{Al}_2\text{O}_3-\text{SiO}_2-\text{TiO}_2-\text{H}_2\text{O}-\text{CO}_2$. *Journal of Petrology*, 29(2), 445-522.
- Bierce, A. (1911) *The Collected Works of Ambrose Bierce, Volume VII, The Devil's Dictionary*. Neale Publishing, New York.
- Birch, A.F., and Clark, H. (1940) The thermal conductivity of rocks and its dependence upon temperature and composition. *American Journal of Science*, 238(8), Part 2, 529-558.
- Chai, M. (1996) *Physical Properties of Mantle Silicates Under Upper Mantle Pressures*. Ph.D. thesis, University of Washington, Seattle, 186 pp.
- Chai, M., Brown, J.M., and Slutsky, L.J. (1996) Thermal diffusivity of mantle minerals. *Physics and Chemistry of Minerals*, 23, 470-475.

- Chopelas, A. (1990) Thermal properties of forsterite at mantle pressures derived from vibrational spectroscopy. *Physics and Chemistry of Minerals*, 17, 149-156.
- Chopelas, A. (1991) Single crystal Raman spectra of forsterite, fayalite, and monticellite. *American Mineralogist*, 76, 1101-1109.
- Christensen, N.I. (1984) The magnitude, symmetry and origin of upper mantle anisotropy based on fabric analyses of ultramafic tectonites. *Geophysical Journal of the Royal Astronomical Society*, 76, 89-111.
- Clauser, C., and Huenges, E. (1995) Thermal conductivity of rocks and minerals. In T.J. Ahrens, Ed., *Rock Physics and Phase Relations: A Handbook of Physical Constants*. American Geophysical Union, Washington, DC, pp. 105-126.
- Clemens, S.L. as Twain, M. as Anonymous as Alden, J.F., Trans., as de Conte, L. (1896) *Personal Recollections of Joan of Arc*. Harper, New York.
- Collins, M.D., and Brown J.M. (1998) Elasticity of an upper mantle clinopyroxene. *Physics and Chemistry of Minerals*, 26, 7-13.
- Deer, W.A., Howie, R.A., and Zussman, J. (1966) *An Introduction to the Rock-Forming Minerals*. Longman, Burnt Mill, Harlow, Essex, UK.
- Finch, C.B., Clark, G.W., and Kopp, O.C. (1980) Czochralski growth of single-crystal fayalite under controlled oxygen fugacity conditions. *American Mineralogist*, 65, 381-389.
- Fujisawa, H., Fujii, N., Mizutani, H., Kanamori, H., and Akimoto, S.-I. (1968) Thermal diffusivity of Mg_2SiO_4 , Fe_2SiO_4 , and NaCl at high pressures and temperatures. *Journal of Geophysical Research*, 73(14), 4727-4733.

- Fukao, Y., Mizutani, H., and Uyeda, S. (1968) Optical absorption spectra at high temperatures and radiative thermal conductivity of olivines. *Physics of the Earth and Planetary Interiors*, 1, 57-62.
- Ghiorso, M.S., and Sack, R.O. (1995) Chemical mass transfer in magmatic processes IV. A revised and internally consistent thermodynamic model for the interpolation and extrapolation of liquid-solid equilibria in magmatic systems at elevated temperatures and pressures. *Contributions to Mineralogy and Petrology*, 119, 197-212.
- Ghose, S., Hastings, J.M., Choudhury, N., Chaprot, S.L., and Rao, K.R. (1991) Phonon dispersion relation in fayalite, Fe_2SiO_4 . *Physica B*, 174, 83-86.
- Gustafsson, S.E. (1991) Transient plane source techniques for thermal conductivity and thermal diffusivity measurements of solid materials. *Review of Scientific Instruments*, 62(3), 797-804.
- Hashin, Z., and Shtrikman, S. (1962) A variational approach to the theory of the effective magnetic permeability of multiphase materials. *Journal of Applied Physics*, 33, 3125-3131.
- Hearn, T.H. (1996) Anisotropic P_n tomography in the western United States. *Journal of Geophysical Research*, 101(B4), 8403-8414.
- Hearn, E.H., Humphreys, E.D., Chai, M., and Brown, J.M. (1997) Effect of anisotropy on oceanic upper mantle temperatures, structure, and dynamics. *Journal of Geophysical Research*, 102(B6), 11,943-11,956.
- Hisano, K., Sawai, S., and Morimoto, K. (1999) Simultaneous measurement of specific heat capacity [*sic*], thermal conductivity, and thermal diffusivity by thermal radiation

- calorimetry. *International Journal of Thermophysics*, 20(2), 733-742.
- Hobbs, W. (1715) *The Earth generated and anatomized*. In R. Porter, Ed., *The Earth Generated and Anatomized by William Hobbs; An Early Eighteenth Century Theory of the Earth*, Cornell University Press, Ithaca, NY, pp. 35-126.
- Hofmeister, A.M. (2001) Thermal conductivity of spinels and olivines from vibrational spectroscopy: Ambient conditions. *American Mineralogist*, 86, 1188-1208.
- Holt, J.B. (1975) Thermal diffusivity of olivine. *Earth and Planetary Science Letters*, 27, 404-408.
- Horai, K.-I. (1971) Thermal conductivity of rock-forming minerals. *Journal of Geophysical Research*, 76(5), 1278-1308.
- Irving, A.J. (1980) Petrology and geochemistry of composite ultramafic xenoliths in alkalic basalts and implications for magmatic processes within the mantle. *American Journal of Science*, 280-A, 389-426.
- Joffe, A.F. (1956) Heat transfer in semiconductors. *Canadian Journal of Physics*, 34, 1342-1355.
- Kanamori, H., Fujii, N., and Mizutani, H. (1968) Thermal diffusivity measurement of rock-forming minerals from 300° to 1,100°K [*sic*], *Journal of Geophysical Research*, 73, 595-605.
- Katsura, T. (1995) Thermal diffusivity of olivine under upper mantle conditions. *Geophysical Journal International*, 122, 63-69.
- Klemens, P.G. (1969) Theory of the thermal conductivity of solids. In R.P. Tye, Ed., *Thermal Conductivity, Volume 1*. Academic Press, London, pp. 1-68.

- Klemens, P.G. (1999) Role of optical modes in thermal conduction. In C. Uher and D. Morelli, Eds., *Thermal Conductivity 25 / Thermal Expansion 13*. CRC Press, Boca Raton, FL, pp. 291-299.
- Kobayashi, Y. (1974) Anisotropy of thermal diffusivity in olivine, pyroxene and dunite. *Journal of Physics of the Earth*, 22, 359-373.
- Kopp, O.C., and Abraham, M.M. (1982) Additional observations on the ferric ion (Fe^{3+}) content of melt-grown fayalite (Fe_2SiO_4). *American Mineralogist*, 67, 349.
- Kramer, H., and Sprenger, J. (1484) *Malleus maleficarum*. In M. Summers, Trans., *The Malleus Maleficarum of Heinrich Kramer and James Sprenger*, Dover, New York, pp. 1-275.
- Mooney, D.L., and Steg, R.G. (1969) Pressure dependence of the thermal conductivity and ultrasonic attenuation of non-metallic solids. *High Temperatures – High Pressures*, 1, 237-240.
- Nicolas, A., and Christensen, N.I. (1987) Formation of anisotropy in upper mantle peridotites—A review. In K. Fuchs, and C. Froidevaux, Eds., *Geodynamics Series*, 16, *Composition, Structure and Dynamics of the Lithosphere-Asthenosphere System*, American Geophysical Union, Washington, DC, pp. 111-123.
- Nye, J.F. (1985) *Physical Properties of Crystals: Their Representation by Tensors and Matrices*, Oxford University Press, Oxford.
- Pillai, C.G.S., and George, A.M. (1991) An improved comparative thermal conductivity apparatus for measurements at high temperatures. *International Journal of Thermophysics*, 12(3), 563-576.

- Pollack, H.N., and Chapman, D.S. (1977) The flow of heat from the Earth's interior. *Scientific American*, 237(2), 60-76.
- Preston, T. (1919) *The Theory of Heat (Third Edition)*. Macmillan, London.
- Rao, K.R., Chaplot, S.L., Choudhury, N., Ghose, S., Hastings, J.M., Corliss, L.M., and Price, D.L. (1988) Lattice dynamics and inelastic neutron scattering from forsterite, Mg_2SiO_4 : Phonon dispersion relation, density of states and specific heat. *Physics and Chemistry of Minerals*, 16, 83-97.
- Robie, R.A., Finch, C.B., and Hemingway, B.S. (1982) Heat capacity and entropy of fayalite (Fe_2SiO_4) between 5.1 and 383 K: comparison of calorimetric and equilibrium values for the QFM buffer reaction. *American Mineralogist*, 67, 463-469.
- Rockwood, R. [house pseudonym] (1929) *Bomba the Jungle Boy in the Swamp of Death; or, The Sacred Alligators of Abarago*. Cupples & Leon, New York.
- Roufousse, M.C., and Jeanloz, R. (1983) Thermal conductivity of minerals at high pressure: The effect of phase transitions. *Journal of Geophysical Research*, 88(B9), 7399-7409.
- Roufousse, M., and Klemens, P.G. (1973) Thermal conductivity of complex dielectric crystals. *Physical Review. B, Condensed Matter and Materials Physics*, 7(12), 5379-5386.
- Roufousse, M.C., and Klemens, P.G. (1974) Lattice thermal conductivity of minerals at high temperatures. *Journal of Geophysical Research*, 79(5), 703-705.
- Schärmeli, G.H. (1982) Anisotropy of olivine thermal conductivity at 2.5 GPa and up to

- 1500 K measured on optically non-thick samples. In W. Schreyer, Ed., *High-Pressure Researches in Geoscience*, E. Schweizerbart'sche Verlagbuchhandlung, Stuttgart, pp. 349-373.
- Schatz, J.F., and Simmons, G. (1972) Thermal conductivity of earth materials at high temperatures. *Journal of Geophysical Research*, 77(35), 6966-6983.
- Schloessin, H.H., and Dvořák, Z. (1972) Anisotropic lattice thermal conductivity in enstatite as a function of pressure and temperature. *Geophysical Journal of the Royal Astronomical Society*, 27(5), 499-516.
- Shankland, T.J. (1970) Pressure shift of infrared absorption bands in minerals and the effect on radiative heat transport. *Journal of Geophysical Research*, 75(2), 409-413.
- Shankland, T.J., Nitsan, U., and Duba, A.G. (1979) Optical absorption and radiative heat transport in olivine at high temperature. *Journal of Geophysical Research*, 84(B4), 1603-1610.
- Silver, P.G., and Kaneshima, S. (1993) Constraints on mantle anisotropy beneath Precambrian North America from a transportable teleseismic experiment. *Geophysical Research Letters*, 20(12), 1127-1130.
- Stout, G.H., and Jensen, L.H. (1989) *X-Ray Structure Determination: A Practical Guide (Second Edition)*. John Wiley & Sons, New York.
- Von Herzen, R., and Maxwell, A.E. (1959) The measurement of thermal conductivity of deep-sea sediments by a needle-probe method. *Journal of Geophysical Research*, 64, 1557-1563.
- Weast, R.C., Ed. (1987) *CRC Handbook of Chemistry and Physics (Sixty-Eighth*

- Edition). CRC Press, Boca Raton, FL.
- Westlind, D. (1996) *The Politics of Popular Identity: Understanding Recent Populist Movements in Sweden and the United States*. Lund University Press, Lund, Sweden.
- Wooster, W.A. (1936) Thermal conductivity in relation to crystal structure. *Zeitschrift für Kristallographie, Mineralogie und Petrographie*, 87, 138-149.
- Zaug, J.M. (1994) *Determination of Macroscopic Properties of Solids and Liquids up to Very High Pressure Using Impulsive Stimulated Light Scattering*. Ph.D. thesis, University of Washington, Seattle, 199 pp.
- Zaug, J., Abramson, E.H., Brown, J.M., and Slutsky, L.J. (1992) Elastic constants, equation of state and thermal diffusivity at high pressure. In Y. Syono and M.H. Manghnani, Eds., *High Pressure Research: Application to Earth and Planetary Sciences*, American Geophysical Union, Washington, DC.
- Zaug, J.M., Abramson, E.H., Brown, J.M., and Slutsky, L.J. (1993) Sound velocities in olivine at Earth mantle pressures. *Science*, 260, 1487-1489.

Appendix A: Complete Set of Thermal Diffusivity Measurements

"Oblivion, n. The state or condition in which the wicked cease from struggling and the dreary are at rest. Fame's eternal dumping ground. Cold storage for high hopes. A place where ambitious authors meet their works without pride and their betters without envy. A dormitory without an alarm clock."

(Bierce, 1911, p. 86)

The following is a comprehensive list of the thermal diffusivity measurements and standards used in constraining the tensor values reported in the body of this study. The list is divided by sample and subdivided by the date on which the data were collected; measurements are listed first, then standards. The appropriate interleaving of the two is indicated by the sequential "thermalfile" numbers assigned to each entry. The format is the same as is generated and used by the various MATLAB routines employed in processing the raw data (individual records of exponential decay), and consists of two lines of text per entry. For the measurements, the first line consists of the "thermalfile" number, sample identification code, axis-normal orientation, temperature ($^{\circ}\text{C}$, where RT is taken as 27°C), rotation stage angle in degrees, and the day, date, and time of collection. The second line repeats the file number, temperature, and rotation angle in strictly numeric format, followed by the intensity of the peak (mV), the characteristic time and its 2σ value (both in μs^{-1}), and the percent uncertainty and misfit. For the standards, the first line starts with the "thermalfile" number, followed by the word

"methanol," the room temperature to the nearest 0.1°C, and the day, date, and time of collection. The second line repeats the thermalfile number and temperature, followed by the calculated speed of sound in methanol and the infrared convergence angle in decimal degrees. Thermalfiles with numbers higher than 100 are from the same data as the corresponding thermalfile number from which 100 has been subtracted (i.e. thermalfile105 is thermalfile5), except that a background measurement has been subtracted from the data in the case of the higher number. For KH-CPX, dummy entries record the convergence angle determined from retroreflection measurements.

KH-OLV

6 August 1999

thermalfile0	KH OLV a-norm RT 195rot	Friday, August 6, 1999 12:36 PM
0 27	195 24 3.465 0.087 2.5 0.022	
thermalfile2	KH OLV a-norm RT 205rot	Friday, August 6, 1999 1:32 PM
2 27	205 8 3.669 0.101 2.7 0.030	
thermalfile3	KH OLV a-norm RT 215rot	Friday, August 6, 1999 2:16 PM
3 27	215 7 4.325 0.393 9.1 0.057	
thermalfile4	KH OLV a-norm RT 225rot	Friday, August 6, 1999 2:39 PM
4 27	225 16 4.383 0.323 7.4 0.032	
thermalfile7	KH OLV a-norm RT 245rot	Friday, August 6, 1999 4:50 PM
7 27	245 6 4.502 0.468 10.4 0.057	
thermalfile1	methanol 27.6C	Friday, August 6, 1999 1:21 PM
1 27.6	1094.7 15.322	
thermalfile5	methanol 28.2C	Friday, August 6, 1999 3:05 PM
5 28.2	1092.8 15.461	
thermalfile6	methanol 28.3C	Friday, August 6, 1999 3:31 PM
6 28.3	1092.4 15.337	

11 August 1999

thermalfile0	KH OLV a-norm RT 110rot	Wednesday, August 11, 1999 3:00 PM
0 27	110 2 2.943 0.039 1.3 0.097	
thermalfile1	KH OLV a-norm RT 130rot	Wednesday, August 11, 1999 4:09 PM
1 27	130 13 3.129 0.071 2.3 0.022	
thermalfile10	KH OLV a-norm RT 270rot	Wednesday, August 11, 1999 10:06 PM
10 27	270 5 2.838 0.063 2.2 0.109	
thermalfile100	KH OLV a-norm RT 110rot	Wednesday, August 11, 1999 3:00 PM
100 27	110 1 2.864 0.021 0.7 0.055	
thermalfile101	KH OLV a-norm RT 130rot	Wednesday, August 11, 1999 4:09 PM
101 27	130 12 3.132 0.066 2.1 0.019	
thermalfile102	KH OLV a-norm RT 150rot	Wednesday, August 11, 1999 4:41 PM
102 27	150 10 3.591 0.101 2.8 0.013	
thermalfile105	KH OLV a-norm RT 170rot	Wednesday, August 11, 1999 6:02 PM
105 27	170 4 3.973 0.124 3.1 0.035	
thermalfile106	KH OLV a-norm RT 190rot	Wednesday, August 11, 1999 7:06 PM
106 27	190 2 4.163 0.076 1.8 0.058	
thermalfile108	KH OLV a-norm RT 210rot	Wednesday, August 11, 1999 8:24 PM
108 27	210 4 3.943 0.131 3.3 0.032	
thermalfile109	KH OLV a-norm RT 250rot	Wednesday, August 11, 1999 9:18 PM
109 27	250 5 3.073 0.051 1.7 0.020	
thermalfile110	KH OLV a-norm RT 270rot	Wednesday, August 11, 1999 10:06 PM
110 27	270 2 2.802 0.043 1.5 0.031	
thermalfile2	KH OLV a-norm RT 150rot	Wednesday, August 11, 1999 4:41 PM
2 27	150 11 3.586 0.101 2.8 0.021	
thermalfile5	KH OLV a-norm RT 170rot	Wednesday, August 11, 1999 6:02 PM
5 27	170 4 4.000 0.118 2.9 0.049	
thermalfile6	KH OLV a-norm RT 190rot	Wednesday, August 11, 1999 7:06 PM
6 27	190 2 4.173 0.184 4.4 0.082	
thermalfile8	KH OLV a-norm RT 210rot	Wednesday, August 11, 1999 8:24 PM
8 27	210 6 4.004 0.123 3.1 0.091	
thermalfile9	KH OLV a-norm RT 250rot	Wednesday, August 11, 1999 9:18 PM
9 27	250 7 3.090 0.057 1.9 0.066	
thermalfile4	methanol 27.2C	Wednesday, August 11, 1999 5:31 PM
4 27.2	1096.0 15.342	
thermalfile7	methanol 27.5C	Wednesday, August 11, 1999 7:53 PM
7 27.5	1095.0 15.344	

14 August 1999

thermalfile106	KH OLV a-norm 300C 210rot	Saturday, August 14, 1999 10:38 PM
106	300 210 4 2.286 0.010 0.5	0.052
thermalfile107	KH OLV a-norm 300C 260rot	Saturday, August 14, 1999 11:10 PM
107	300 260 5 1.624 0.092 5.7	0.036
thermalfile109	KH OLV a-norm 300C 240rot	Sunday, August 15, 1999 12:25 AM
109	300 240 7 1.850 0.019 1.0	0.029
thermalfile11	KH OLV a-norm 500C 210rot	Sunday, August 15, 1999 1:44 AM
11	500 210 25 1.896 0.019 1.0	0.020
thermalfile111	KH OLV a-norm 500C 210rot	Sunday, August 15, 1999 1:44 AM
111	500 210 23 1.890 0.016 0.8	0.016
thermalfile112	KH OLV a-norm 500C 270rot	Sunday, August 15, 1999 2:12 AM
112	500 270 4 1.273 0.027 2.1	0.044
thermalfile113	KH OLV a-norm 500C 240rot	Sunday, August 15, 1999 2:40 AM
113	500 240 16 1.556 0.030 1.9	0.024
thermalfile115	KH OLV a-norm 600C 240rot	Sunday, August 15, 1999 4:12 AM
115	600 240 20 1.453 0.026 1.8	0.023
thermalfile116	KH OLV a-norm 600C 210rot	Sunday, August 15, 1999 4:41 AM
116	600 210 27 1.776 0.016 0.9	0.018
thermalfile117	KH OLV a-norm 600C 270rot	Sunday, August 15, 1999 5:07 AM
117	600 270 4 1.200 0.023 1.9	0.034
thermalfile119	KH OLV a-norm 700C 270rot	Sunday, August 15, 1999 6:06 AM
119	700 270 6 1.143 0.023 2.0	0.035
thermalfile12	KH OLV a-norm 500C 270rot	Sunday, August 15, 1999 2:12 AM
12	500 270 5 1.309 0.043 3.3	0.064
thermalfile120	KH OLV a-norm 700C 240rot	Sunday, August 15, 1999 6:37 AM
120	700 240 11 1.401 0.022 1.6	0.042
thermalfile121	KH OLV a-norm 700C 210rot	Sunday, August 15, 1999 7:05 AM
121	700 210 26 1.702 0.019 1.1	0.020
thermalfile124	KH OLV a-norm 500C 210rot	Sunday, August 15, 1999 8:17 AM
124	500 210 11 1.937 0.015 0.8	0.027
thermalfile125	KH OLV a-norm 500C 270rot	Sunday, August 15, 1999 8:43 AM
125	500 270 4 1.325 0.016 1.2	0.027
thermalfile127	KH OLV a-norm 800C 270rot	Sunday, August 15, 1999 9:45 AM
127	800 270 5 1.118 0.017 1.5	0.031
thermalfile128	KH OLV a-norm 800C 210rot	Sunday, August 15, 1999 10:09 AM
128	800 210 14 1.596 0.028 1.8	0.039
thermalfile129	KH OLV a-norm 800C 240rot	Sunday, August 15, 1999 10:27 AM
129	800 240 12 1.364 0.025 1.8	0.036
thermalfile13	KH OLV a-norm 500C 240rot	Sunday, August 15, 1999 2:40 AM
13	500 240 18 1.559 0.032 2.0	0.026
thermalfile131	KH OLV a-norm 900C 240rot	Sunday, August 15, 1999 11:23 AM
131	900 240 9 1.255 0.024 1.9	0.031
thermalfile132	KH OLV a-norm 900C 270rot	Sunday, August 15, 1999 11:49 AM
132	900 270 4 1.027 0.013 1.3	0.033

thermalfile133	KH OLV a-norm 900C 210rot	Sunday, August 15, 1999 12:07 PM
133	900 210 14 1.488 0.029 2.0	0.052
thermalfile136	KH OLV a-norm 1000C 210rot	Sunday, August 15, 1999 2:19 PM
136	1000 210 2 1.489 0.029 2.0	0.031
thermalfile137	KH OLV a-norm 1000C 270rot	Sunday, August 15, 1999 3:02 PM
137	1000 270 3 1.034 0.026 2.5	0.036
thermalfile15	KH OLV a-norm 600C 240rot	Sunday, August 15, 1999 4:12 AM
15	600 240 21 1.456 0.027 1.9	0.026
thermalfile16	KH OLV a-norm 600C 210rot	Sunday, August 15, 1999 4:41 AM
16	600 210 28 1.780 0.019 1.1	0.020
thermalfile17	KH OLV a-norm 600C 270rot	Sunday, August 15, 1999 5:07 AM
17	600 270 6 1.215 0.036 2.9	0.061
thermalfile19	KH OLV a-norm 700C 270rot	Sunday, August 15, 1999 6:06 AM
19	700 270 7 1.153 0.032 2.7	0.054
thermalfile20	KH OLV a-norm 700C 240rot	Sunday, August 15, 1999 6:37 AM
20	700 240 12 1.410 0.030 2.1	0.039
thermalfile21	KH OLV a-norm 700C 210rot	Sunday, August 15, 1999 7:05 AM
21	700 210 27 1.704 0.022 1.3	0.020
thermalfile24	KH OLV a-norm 500C 210rot	Sunday, August 15, 1999 8:17 AM
24	500 210 11 1.943 0.018 0.9	0.028
thermalfile25	KH OLV a-norm 500C 270rot	Sunday, August 15, 1999 8:43 AM
25	500 270 4 1.345 0.030 2.2	0.037
thermalfile27	KH OLV a-norm 800C 270rot	Sunday, August 15, 1999 9:45 AM
27	800 270 6 1.120 0.018 1.6	0.031
thermalfile28	KH OLV a-norm 800C 210rot	Sunday, August 15, 1999 10:09 AM
28	800 210 14 1.597 0.029 1.8	0.040
thermalfile29	KH OLV a-norm 800C 240rot	Sunday, August 15, 1999 10:27 AM
29	800 240 12 1.366 0.026 1.9	0.034
thermalfile31	KH OLV a-norm 900C 240rot	Sunday, August 15, 1999 11:23 AM
31	900 240 9 1.259 0.026 2.0	0.030
thermalfile32	KH OLV a-norm 900C 270rot	Sunday, August 15, 1999 11:49 AM
32	900 270 5 1.031 0.017 1.7	0.031
thermalfile33	KH OLV a-norm 900C 210rot	Sunday, August 15, 1999 12:07 PM
33	900 210 14 1.490 0.031 2.1	0.049
thermalfile36	KH OLV a-norm 1000C 210rot	Sunday, August 15, 1999 2:19 PM
36	1000 210 2 1.488 0.025 1.7	0.046
thermalfile37	KH OLV a-norm 1000C 270rot	Sunday, August 15, 1999 3:02 PM
37	1000 270 4 1.031 0.021 2.0	0.034
thermalfile6	KH OLV a-norm 300C 210rot	Saturday, August 14, 1999 10:38 PM
6	300 210 7 2.300 0.018 0.8	0.084
thermalfile7	KH OLV a-norm 300C 260rot	Saturday, August 14, 1999 11:10 PM
7	300 260 7 1.595 0.023 1.5	0.085
thermalfile9	KH OLV a-norm 300C 240rot	Sunday, August 15, 1999 12:25 AM
9	300 240 9 1.850 0.010 0.5	0.067

thermalfile0 methanol 24.8C Saturday, August 14, 1999 5:20 PM
 0 24.8 1103.6 15.449
 thermalfile1 methanol 25.2C Saturday, August 14, 1999 6:13 PM
 1 25.2 1102.4 15.420
 thermalfile10 methanol 25.9C Sunday, August 15, 1999 1:26 AM
 10 25.9 1100.1 15.427
 thermalfile23 methanol 26.1C Sunday, August 15, 1999 8:05 AM
 23 26.1 1099.5 15.431
 thermalfile35 methanol 26.6C Sunday, August 15, 1999 1:42 PM
 35 26.6 1097.9 15.436
 thermalfile5 methanol 26.0C Saturday, August 14, 1999 10:21 PM
 5 26.0 1099.8 15.430

19 August 1999, first set (a)

thermalfile1 KH OLV a-norm RT 210rot Thursday, August 19, 1999 5:07 PM
 1 27 210 2 3.620 0.054 1.5 0.110
 thermalfile101 KH OLV a-norm RT 210rot Thursday, August 19, 1999 5:07 PM
 101 27 210 2 3.559 0.060 1.7 0.071
 thermalfile102 KH OLV a-norm RT 230rot Thursday, August 19, 1999 5:46 PM
 102 27 230 1 3.072 0.120 3.9 0.092
 thermalfile103 KH OLV a-norm RT 250rot Thursday, August 19, 1999 6:16 PM
 103 27 250 0 2.685 0.164 6.1 0.124
 thermalfile105 KH OLV a-norm RT 190rot Thursday, August 19, 1999 7:36 PM
 105 27 190 1 3.847 0.094 2.5 0.053
 thermalfile2 KH OLV a-norm RT 230rot Thursday, August 19, 1999 5:46 PM
 2 27 230 1 2.368 1.580 66.7 0.141
 thermalfile3 KH OLV a-norm RT 250rot Thursday, August 19, 1999 6:16 PM
 3 27 250 1 3.115 0.206 6.6 0.167
 thermalfile5 KH OLV a-norm RT 190rot Thursday, August 19, 1999 7:36 PM
 5 27 190 2 4.140 0.038 0.9 0.125
 thermalfile0 methanol 26.1C Thursday, August 19, 1999 4:32 PM
 0 26.1 1099.5 15.406

19 August 1999, second set (b)

thermalfile10 KH OLV a-norm RT 250rot Friday, August 20, 1999 12:02 AM
 10 27 250 8 1.276 0.034 2.6 0.031
 thermalfile107 KH OLV a-norm RT 190rot Thursday, August 19, 1999 11:12 PM
 107 27 190 54 1.760 0.016 0.9 0.017

thermalfile108 KH OLV a-norm RT 210rot Thursday, August 19, 1999 11:26 PM
 108 27 210 52 1.572 0.025 1.6 0.021
 thermalfile109 KH OLV a-norm RT 230rot Thursday, August 19, 1999 11:40 PM
 109 27 230 12 1.356 0.020 1.4 0.033
 thermalfile110 KH OLV a-norm RT 250rot Friday, August 20, 1999 12:02 AM
 110 27 250 8 1.270 0.026 2.1 0.028
 thermalfile113 KH OLV a-norm 200C 250rot Friday, August 20, 1999 1:29 AM
 113 200 250 4 0.730 0.003 0.5 0.026
 thermalfile114 KH OLV a-norm 200C 250rot Friday, August 20, 1999 1:29 AM
 114 200 250 4 0.730 0.003 0.5 0.026
 thermalfile115 KH OLV a-norm 200C 210rot Friday, August 20, 1999 2:23 AM
 115 200 210 56 0.995 0.012 1.2 0.027
 thermalfile13 KH OLV a-norm 200C 250rot Friday, August 20, 1999 1:29 AM
 13 200 250 5 0.737 0.003 0.5 0.024
 thermalfile14 KH OLV a-norm 200C 230rot Friday, August 20, 1999 1:57 AM
 14 200 230 5 0.891 0.015 1.6 0.030
 thermalfile15 KH OLV a-norm 200C 210rot Friday, August 20, 1999 2:23 AM
 15 200 210 57 0.996 0.012 1.2 0.026
 thermalfile7 KH OLV a-norm RT 190rot Thursday, August 19, 1999 11:12 PM
 7 27 190 55 1.761 0.016 0.9 0.017
 thermalfile8 KH OLV a-norm RT 210rot Thursday, August 19, 1999 11:26 PM
 8 27 210 53 1.573 0.026 1.7 0.021
 thermalfile9 KH OLV a-norm RT 230rot Thursday, August 19, 1999 11:40 PM
 9 27 230 13 1.359 0.022 1.6 0.032
 thermalfile12 methanol 26.9C Friday, August 20, 1999 1:11 AM
 12 26.9 1096.9 9.760
 thermalfile6 methanol 26.6C Thursday, August 19, 1999 10:56 PM
 6 26.6 1097.9 9.701

24 August 1999

thermalfile10 KH OLV a-norm 150C 250rot Tuesday, August 24, 1999 8:31 PM
 10 150 250 4 0.875 0.007 0.8 0.028
 thermalfile102 KH OLV a-norm RT 210rot Tuesday, August 24, 1999 4:04 PM
 102 27 210 26 1.540 0.006 0.5 0.010
 thermalfile103 KH OLV a-norm RT 190rot Tuesday, August 24, 1999 4:25 PM
 103 27 190 16 1.798 0.033 1.8 0.013
 thermalfile104 KH OLV a-norm RT 170rot Tuesday, August 24, 1999 5:00 PM
 104 27 170 20 1.851 0.021 1.2 0.011
 thermalfile105 KH OLV a-norm RT 150rot Tuesday, August 24, 1999 5:22 PM
 105 27 150 10 1.807 0.006 0.5 0.008
 thermalfile106 KH OLV a-norm RT 140rot Tuesday, August 24, 1999 5:37 PM

106	27	140	13	1.750	0.013	0.7	0.010	
thermalfile108	KH	OLV	a-norm	RT	250rot	Tuesday, August 24, 1999 6:48 PM		
108	27	250	7	1.242	0.011	0.9	0.025	
thermalfile11	KH	OLV	a-norm	150C	230rot	Tuesday, August 24, 1999 8:44 PM		
11	150	230	7	0.960	0.007	0.7	0.022	
thermalfile110	KH	OLV	a-norm	150C	250rot	Tuesday, August 24, 1999 8:31 PM		
110	150	250	3	0.875	0.008	0.9	0.024	
thermalfile111	KH	OLV	a-norm	150C	230rot	Tuesday, August 24, 1999 8:44 PM		
111	150	230	6	0.960	0.007	0.7	0.021	
thermalfile112	KH	OLV	a-norm	150C	210rot	Tuesday, August 24, 1999 8:58 PM		
112	150	210	6	1.113	0.007	0.6	0.018	
thermalfile113	KH	OLV	a-norm	150C	190rot	Tuesday, August 24, 1999 9:16 PM		
113	150	190	7	1.288	0.010	0.8	0.016	
thermalfile114	KH	OLV	a-norm	150C	170rot	Tuesday, August 24, 1999 9:36 PM		
114	150	170	11	1.348	0.010	0.8	0.014	
thermalfile117	KH	OLV	a-norm	300C	170rot	Tuesday, August 24, 1999 11:11 PM		
117	300	170	19	1.061	0.009	0.8	0.016	
thermalfile118	KH	OLV	a-norm	300C	190rot	Tuesday, August 24, 1999 11:32 PM		
118	300	190	17	0.988	0.012	1.2	0.018	
thermalfile119	KH	OLV	a-norm	300C	210rot	Tuesday, August 24, 1999 11:50 PM		
119	300	210	9	0.857	0.005	0.6	0.019	
thermalfile12	KH	OLV	a-norm	150C	210rot	Tuesday, August 24, 1999 8:58 PM		
12	150	210	7	1.113	0.007	0.7	0.020	
thermalfile120	KH	OLV	a-norm	300C	230rot	Wednesday, August 25, 1999 12:09 AM		
120	300	230	6	0.735	0.005	0.6	0.021	
thermalfile121	KH	OLV	a-norm	300C	250rot	Wednesday, August 25, 1999 12:28 AM		
121	300	250	3	0.666	0.004	0.6	0.022	
thermalfile124	KH	OLV	a-norm	500C	250rot	Wednesday, August 25, 1999 1:44 AM		
124	500	250	2	0.514	0.037	7.2	0.042	
thermalfile125	KH	OLV	a-norm	500C	230rot	Wednesday, August 25, 1999 2:11 AM		
125	500	230	6	0.580	0.012	2.0	0.026	
thermalfile126	KH	OLV	a-norm	500C	210rot	Wednesday, August 25, 1999 2:25 AM		
126	500	210	11	0.684	0.007	1.1	0.024	
thermalfile127	KH	OLV	a-norm	500C	190rot	Wednesday, August 25, 1999 2:49 AM		
127	500	190	19	0.796	0.005	0.6	0.019	
thermalfile128	KH	OLV	a-norm	500C	170rot	Wednesday, August 25, 1999 3:00 AM		
128	500	170	24	0.855	0.007	0.9	0.019	
thermalfile13	KH	OLV	a-norm	150C	190rot	Tuesday, August 24, 1999 9:16 PM		
13	150	190	8	1.288	0.012	0.9	0.018	
thermalfile132	KH	OLV	a-norm	800C	170rot	Wednesday, August 25, 1999 4:07 AM		
132	800	170	3	0.667	0.013	1.9	0.011	
thermalfile133	KH	OLV	a-norm	800C	190rot	Wednesday, August 25, 1999 4:23 AM		
133	800	190	2	0.645	0.002	0.5	0.018	
thermalfile134	KH	OLV	a-norm	800C	210rot	Wednesday, August 25, 1999 4:40 AM		

134	800	210	8	0.564	0.004	0.8	0.017	
thermalfile14	KH OLV a-norm 150C 170rot						Tuesday, August 24, 1999 9:36 PM	
14	150	170	12	1.349	0.011	0.8	0.015	
thermalfile17	KH OLV a-norm 300C 170rot						Tuesday, August 24, 1999 11:11 PM	
17	300	170	20	1.061	0.009	0.8	0.016	
thermalfile18	KH OLV a-norm 300C 190rot						Tuesday, August 24, 1999 11:32 PM	
18	300	190	18	0.988	0.011	1.1	0.018	
thermalfile19	KH OLV a-norm 300C 210rot						Tuesday, August 24, 1999 11:50 PM	
19	300	210	10	0.857	0.005	0.6	0.018	
thermalfile2	KH OLV a-norm RT 210rot						Tuesday, August 24, 1999 4:04 PM	
2	27	210	26	1.541	0.007	0.5	0.010	
thermalfile20	KH OLV a-norm 300C 230rot						Wednesday, August 25, 1999 12:09 AM	
20	300	230	7	0.736	0.006	0.8	0.022	
thermalfile21	KH OLV a-norm 300C 250rot						Wednesday, August 25, 1999 12:28 AM	
21	300	250	4	0.669	0.004	0.6	0.027	
thermalfile24	KH OLV a-norm 500C 250rot						Wednesday, August 25, 1999 1:44 AM	
24	500	250	3	0.538	0.009	1.7	0.032	
thermalfile25	KH OLV a-norm 500C 230rot						Wednesday, August 25, 1999 2:11 AM	
25	500	230	7	0.588	0.005	0.8	0.023	
thermalfile26	KH OLV a-norm 500C 210rot						Wednesday, August 25, 1999 2:25 AM	
26	500	210	12	0.684	0.004	0.6	0.020	
thermalfile27	KH OLV a-norm 500C 190rot						Wednesday, August 25, 1999 2:49 AM	
27	500	190	20	0.795	0.004	0.5	0.018	
thermalfile28	KH OLV a-norm 500C 170rot						Wednesday, August 25, 1999 3:00 AM	
28	500	170	25	0.854	0.005	0.6	0.017	
thermalfile3	KH OLV a-norm RT 190rot						Tuesday, August 24, 1999 4:25 PM	
3	27	190	16	1.801	0.035	1.9	0.014	
thermalfile32	KH OLV a-norm 800C 170rot						Wednesday, August 25, 1999 4:07 AM	
32	800	170	4	0.668	0.011	1.7	0.014	
thermalfile33	KH OLV a-norm 800C 190rot						Wednesday, August 25, 1999 4:23 AM	
33	800	190	2	0.645	0.003	0.5	0.024	
thermalfile34	KH OLV a-norm 800C 210rot						Wednesday, August 25, 1999 4:40 AM	
34	800	210	8	0.564	0.005	0.8	0.017	
thermalfile4	KH OLV a-norm RT 170rot						Tuesday, August 24, 1999 5:00 PM	
4	27	170	20	1.853	0.023	1.2	0.011	
thermalfile5	KH OLV a-norm RT 150rot						Tuesday, August 24, 1999 5:22 PM	
5	27	150	11	1.812	0.009	0.5	0.011	
thermalfile6	KH OLV a-norm RT 140rot						Tuesday, August 24, 1999 5:37 PM	
6	27	140	13	1.753	0.015	0.9	0.012	
thermalfile8	KH OLV a-norm RT 250rot						Tuesday, August 24, 1999 6:48 PM	
8	27	250	7	1.243	0.012	0.9	0.020	
thermalfile0	methanol 26.1C		1099.5		9.800		Tuesday, August 24, 1999 3:01 PM	
0	26.1							
thermalfile1	methanol 26.4C							Tuesday, August 24, 1999 3:44 PM

1	26.4	1098.5	9.747	
thermalfile16	methanol	27.7C		Tuesday, August 24, 1999 11:01 PM
16	27.7	1094.4	9.765	
thermalfile23	methanol	28.0C		Wednesday, August 25, 1999 1:29 AM
23	28.0	1093.4	9.753	
thermalfile30	methanol	28.2C		Wednesday, August 25, 1999 3:51 AM
30	28.2	1092.8	9.821	
thermalfile9	methanol	27.6C		Tuesday, August 24, 1999 8:09 PM
9	27.6	1094.7	9.742	

15 September 1999

thermalfile1	KH OLV a-norm	RT 195rot		Wednesday, September 15, 1999 12:02 PM
1	27	195	28 1.819 0.028	1.6 0.018
thermalfile101	KH OLV a-norm	RT 195rot		Wednesday, September 15, 1999 12:02 PM
101	27	195	28 1.815 0.023	1.3 0.017
thermalfile102	KH OLV a-norm	RT 175rot		Wednesday, September 15, 1999 12:17 PM
102	27	175	33 1.796 0.019	1.1 0.014
thermalfile103	KH OLV a-norm	RT 155rot		Wednesday, September 15, 1999 12:30 PM
103	27	155	28 1.627 0.007	0.5 0.014
thermalfile104	KH OLV a-norm	RT 135rot		Wednesday, September 15, 1999 12:43 PM
104	27	135	20 1.447 0.012	0.8 0.018
thermalfile105	KH OLV a-norm	RT 215rot		Wednesday, September 15, 1999 1:02 PM
105	27	215	15 1.602 0.015	0.9 0.017
thermalfile106	KH OLV a-norm	RT 235rot		Wednesday, September 15, 1999 1:18 PM
106	27	235	12 1.470 0.016	1.1 0.021
thermalfile107	KH OLV a-norm	RT 255rot		Wednesday, September 15, 1999 1:31 PM
107	27	255	7 1.214 0.005	0.5 0.028
thermalfile2	KH OLV a-norm	RT 175rot		Wednesday, September 15, 1999 12:17 PM
2	27	175	33 1.802 0.023	1.3 0.015
thermalfile3	KH OLV a-norm	RT 155rot		Wednesday, September 15, 1999 12:30 PM
3	27	155	28 1.632 0.009	0.6 0.015
thermalfile4	KH OLV a-norm	RT 135rot		Wednesday, September 15, 1999 12:43 PM
4	27	135	20 1.454 0.015	1.1 0.018
thermalfile5	KH OLV a-norm	RT 215rot		Wednesday, September 15, 1999 1:02 PM
5	27	215	15 1.611 0.012	0.7 0.016
thermalfile6	KH OLV a-norm	RT 235rot		Wednesday, September 15, 1999 1:18 PM
6	27	235	12 1.485 0.024	1.6 0.021
thermalfile7	KH OLV a-norm	RT 255rot		Wednesday, September 15, 1999 1:31 PM
7	27	255	7 1.229 0.008	0.7 0.025
thermalfile0	methanol	26.2C		Wednesday, September 15, 1999 11:46 AM
0	26.2	1099.2	9.722	

thermalfile9 methanol 27.3C Wednesday, September 15, 1999 1:57 PM
 9 27.3 1095.6 9.654

17 September 1999

thermalfile1 KH OLV a-norm RT 135rot Friday, September 17, 1999 11:22 AM
 1 27 135 26 1.603 0.023 1.4 0.016
 thermalfile101 KH OLV a-norm RT 135rot Friday, September 17, 1999 11:22 AM
 101 27 135 26 1.601 0.022 1.3 0.015
 thermalfile102 KH OLV a-norm RT 155rot Friday, September 17, 1999 11:39 AM
 102 27 155 17 1.386 0.020 1.5 0.017
 thermalfile103 KH OLV a-norm RT 175rot Friday, September 17, 1999 11:51 AM
 103 27 175 15 1.279 0.012 0.9 0.013
 thermalfile104 KH OLV a-norm RT 195rot Friday, September 17, 1999 12:06 PM
 104 27 195 11 1.362 0.008 0.6 0.015
 thermalfile105 KH OLV a-norm RT 215rot Friday, September 17, 1999 12:24 PM
 105 27 215 20 1.565 0.021 1.3 0.015
 thermalfile106 KH OLV a-norm RT 235rot Friday, September 17, 1999 12:37 PM
 106 27 235 21 1.807 0.021 1.1 0.013
 thermalfile107 KH OLV a-norm RT 255rot Friday, September 17, 1999 12:49 PM
 107 27 255 15 1.956 0.034 1.8 0.013
 thermalfile11 KH OLV a-norm 800C 175rot Friday, September 17, 1999 3:11 PM
 11 800 175 7 0.434 0.001 0.5 0.016
 thermalfile111 KH OLV a-norm 800C 175rot Friday, September 17, 1999 3:11 PM
 111 800 175 7 0.433 0.001 0.5 0.016
 thermalfile112 KH OLV a-norm 800C 220rot Friday, September 17, 1999 3:22 PM
 112 800 220 18 0.572 0.002 0.5 0.015
 thermalfile113 KH OLV a-norm 800C 265rot Friday, September 17, 1999 3:31 PM
 113 800 265 10 0.692 0.003 0.5 0.014
 thermalfile117 KH OLV a-norm 1000C 265rot Friday, September 17, 1999 4:17 PM
 117 1000 265 11 0.626 0.002 0.5 0.019
 thermalfile118 KH OLV a-norm 1000C 220rot Friday, September 17, 1999 4:25 PM
 118 1000 220 22 0.496 0.001 0.5 0.017
 thermalfile119 KH OLV a-norm 1000C 175rot Friday, September 17, 1999 4:38 PM
 119 1000 175 8 0.402 0.001 0.5 0.021
 thermalfile12 KH OLV a-norm 800C 220rot Friday, September 17, 1999 3:22 PM
 12 800 220 18 0.572 0.002 0.5 0.015
 thermalfile13 KH OLV a-norm 800C 265rot Friday, September 17, 1999 3:31 PM
 13 800 265 10 0.691 0.003 0.5 0.014
 thermalfile17 KH OLV a-norm 1000C 265rot Friday, September 17, 1999 4:17 PM
 17 1000 265 11 0.626 0.001 0.5 0.019
 thermalfile18 KH OLV a-norm 1000C 220rot Friday, September 17, 1999 4:25 PM

18	1000	220	22	0.497	0.001	0.5	0.017	
thermalfile19		KH OLV a-norm	1000C 175rot					Friday, September 17, 1999 4:38 PM
19	1000	175	8	0.403	0.000	0.5	0.022	
thermalfile2		KH OLV a-norm	RT 155rot					Friday, September 17, 1999 11:39 AM
2	27	155	17	1.387	0.022	1.6	0.017	
thermalfile3		KH OLV a-norm	RT 175rot					Friday, September 17, 1999 11:51 AM
3	27	175	15	1.281	0.010	0.8	0.014	
thermalfile4		KH OLV a-norm	RT 195rot					Friday, September 17, 1999 12:06 PM
4	27	195	11	1.365	0.011	0.8	0.015	
thermalfile5		KH OLV a-norm	RT 215rot					Friday, September 17, 1999 12:24 PM
5	27	215	20	1.568	0.024	1.5	0.015	
thermalfile6		KH OLV a-norm	RT 235rot					Friday, September 17, 1999 12:37 PM
6	27	235	21	1.808	0.021	1.2	0.014	
thermalfile7		KH OLV a-norm	RT 255rot					Friday, September 17, 1999 12:49 PM
7	27	255	15	1.957	0.036	1.9	0.013	
thermalfile0		methanol 23.9C						Friday, September 17, 1999 11:03 AM
0	23.9	1106.5		9.682				
thermalfile10		methanol 26.5C						Friday, September 17, 1999 2:56 PM
10	26.5	1098.2		9.647				
thermalfile15		methanol 26.7C						Friday, September 17, 1999 3:46 PM
15	26.7	1097.6		9.625				
thermalfile16		methanol 26.8C						Friday, September 17, 1999 4:09 PM
16	26.8	1097.2		9.593				
thermalfile21		methanol 27.2C						Friday, September 17, 1999 4:52 PM
21	27.2	1096.0		9.673				
thermalfile9		methanol 25.7C						Friday, September 17, 1999 1:05 PM
9	25.7	1100.8		9.601				

20 September 1999

thermalfile1		KH OLV a-norm	RT 220rot					Monday, September 20, 1999 3:01 PM
1	27	220	17	1.404	0.017	1.2	0.021	
thermalfile101		KH OLV a-norm	RT 220rot					Monday, September 20, 1999 3:01 PM
101	27	220	17	1.403	0.016	1.2	0.020	
thermalfile102		KH OLV a-norm	RT 265rot					Monday, September 20, 1999 3:15 PM
102	27	265	3	1.779	0.030	1.7	0.031	
thermalfile103		KH OLV a-norm	RT 175rot					Monday, September 20, 1999 3:30 PM
103	27	175	4	1.134	0.017	1.5	0.030	
thermalfile104		KH OLV a-norm	RT 155rot					Monday, September 20, 1999 3:50 PM
104	27	155	6	1.232	0.012	0.9	0.022	
thermalfile2		KH OLV a-norm	RT 265rot					Monday, September 20, 1999 3:15 PM
2	27	265	3	1.782	0.021	1.2	0.027	

thermalfile3	KH OLV a-norm RT 175rot	Monday, September 20, 1999 3:30 PM
3 27	175 4 1.128 0.010 0.9 0.027	
thermalfile4	KH OLV a-norm RT 155rot	Monday, September 20, 1999 3:50 PM
4 27	155 6 1.230 0.006 0.5 0.021	
thermalfile0	methanol 26.5C	Monday, September 20, 1999 2:42 PM
0 26.5	1098.2 9.605	
thermalfile6	methanol 27.4C	Monday, September 20, 1999 4:16 PM
6 27.4	1095.3 9.629	

21 September 1999

thermalfile1	KH OLV a-norm RT 135rot	Tuesday, September 21, 1999 3:15 PM
1 27	135 7 1.271 0.012 1.0 0.026	
thermalfile10	KH OLV a-norm RT 270rot	Tuesday, September 21, 1999 5:14 PM
10 27	270 7 1.535 0.005 0.5 0.019	
thermalfile101	KH OLV a-norm RT 135rot	Tuesday, September 21, 1999 3:15 PM
101 27	135 7 1.271 0.012 0.9 0.028	
thermalfile102	KH OLV a-norm RT 155rot	Tuesday, September 21, 1999 3:32 PM
102 27	155 8 1.345 0.008 0.6 0.022	
thermalfile103	KH OLV a-norm RT 175rot	Tuesday, September 21, 1999 3:47 PM
103 27	175 7 1.560 0.016 1.1 0.022	
thermalfile104	KH OLV a-norm RT 195rot	Tuesday, September 21, 1999 3:59 PM
104 27	195 10 1.758 0.023 1.3 0.019	
thermalfile105	KH OLV a-norm RT 215rot	Tuesday, September 21, 1999 4:14 PM
105 27	215 5 1.801 0.017 1.0 0.025	
thermalfile106	KH OLV a-norm RT 235rot	Tuesday, September 21, 1999 4:25 PM
106 27	235 5 1.839 0.021 1.1 0.033	
thermalfile109	KH OLV a-norm RT 255rot	Tuesday, September 21, 1999 5:05 PM
109 27	255 5 1.705 0.015 0.9 0.030	
thermalfile110	KH OLV a-norm RT 270rot	Tuesday, September 21, 1999 5:14 PM
110 27	270 7 1.531 0.007 0.5 0.022	
thermalfile2	KH OLV a-norm RT 155rot	Tuesday, September 21, 1999 3:32 PM
2 27	155 8 1.345 0.009 0.7 0.020	
thermalfile3	KH OLV a-norm RT 175rot	Tuesday, September 21, 1999 3:47 PM
3 27	175 7 1.567 0.019 1.2 0.021	
thermalfile4	KH OLV a-norm RT 195rot	Tuesday, September 21, 1999 3:59 PM
4 27	195 10 1.763 0.027 1.5 0.019	
thermalfile5	KH OLV a-norm RT 215rot	Tuesday, September 21, 1999 4:14 PM
5 27	215 5 1.806 0.009 0.5 0.019	
thermalfile6	KH OLV a-norm RT 235rot	Tuesday, September 21, 1999 4:25 PM
6 27	235 5 1.842 0.025 1.3 0.026	
thermalfile9	KH OLV a-norm RT 255rot	Tuesday, September 21, 1999 5:05 PM

9	27	255	4	1.714	0.021	1.2	0.023
thermalfile0	methanol 26.7C			Tuesday, September 21, 1999 2:55 PM			
0	26.7	1097.6	9.686				
thermalfile12	methanol 28.4C			Tuesday, September 21, 1999 5:40 PM			
12	28.4	1092.1	9.749				
thermalfile7	methanol 27.9C			Tuesday, September 21, 1999 4:41 PM			
7	27.9	1093.7	9.826				
thermalfile8	methanol 28.0C			Tuesday, September 21, 1999 4:56 PM			
8	28.0	1093.4	9.745				

28 September 1999

thermalfile1	KH OLV c-norm RT 135rot			Tuesday, September 28, 1999 12:51 PM			
1	27	135	31	1.462	0.031	2.1	0.020
thermalfile2	KH OLV c-norm RT 155rot			Tuesday, September 28, 1999 1:04 PM			
2	27	155	20	1.252	0.011	0.9	0.021
thermalfile3	KH OLV c-norm RT 175rot			Tuesday, September 28, 1999 1:18 PM			
3	27	175	13	1.291	0.013	1.0	0.023
thermalfile4	KH OLV c-norm RT 195rot			Tuesday, September 28, 1999 1:39 PM			
4	27	195	12	1.494	0.004	0.5	0.019
thermalfile7	KH OLV c-norm RT 215rot			Tuesday, September 28, 1999 3:21 PM			
7	27	215	8	1.781	0.016	0.9	0.016
thermalfile8	KH OLV c-norm RT 235rot			Tuesday, September 28, 1999 3:32 PM			
8	27	235	6	2.043	0.015	0.8	0.023
thermalfile0	methanol 24.8C			Tuesday, September 28, 1999 12:37 PM			
0	24.8	1103.6	9.671				
thermalfile5	methanol 26.1C			Tuesday, September 28, 1999 1:49 PM			
5	26.1	1099.5	9.672				
thermalfile6	methanol 26.8C			Tuesday, September 28, 1999 3:10 PM			
6	26.8	1097.2	9.663				

1 October 1999

thermalfile1	KH OLV c-norm RT 270rot			Friday, October 1, 1999 1:20 PM			
1	27	270	22	2.054	0.016	0.8	0.012
thermalfile101	KH OLV c-norm RT 270rot			Friday, October 1, 1999 1:20 PM			
101	27	270	22	2.055	0.015	0.7	0.011
thermalfile102	KH OLV c-norm RT 255rot			Friday, October 1, 1999 1:30 PM			
102	27	255	14	2.064	0.006	0.5	0.011
thermalfile103	KH OLV c-norm RT 235rot			Friday, October 1, 1999 1:45 PM			

103	27	235	14	1.970	0.007	0.5	0.011	
thermalfile104	KH OLV c-norm RT 210rot							Friday, October 1, 1999 2:01 PM
104	27	210	22	1.670	0.017	1.0	0.017	
thermalfile105	KH OLV c-norm RT 185rot							Friday, October 1, 1999 2:11 PM
105	27	185	15	1.336	0.023	1.7	0.023	
thermalfile106	KH OLV c-norm RT 165rot							Friday, October 1, 1999 2:20 PM
106	27	165	5	1.199	0.021	1.7	0.031	
thermalfile107	KH OLV c-norm RT 145rot							Friday, October 1, 1999 2:35 PM
107	27	145	10	1.256	0.008	0.6	0.024	
thermalfile2	KH OLV c-norm RT 255rot							Friday, October 1, 1999 1:30 PM
2	27	255	14	2.063	0.005	0.5	0.012	
thermalfile3	KH OLV c-norm RT 235rot							Friday, October 1, 1999 1:45 PM
3	27	235	14	1.970	0.010	0.5	0.011	
thermalfile4	KH OLV c-norm RT 210rot							Friday, October 1, 1999 2:01 PM
4	27	210	22	1.670	0.016	1.0	0.017	
thermalfile5	KH OLV c-norm RT 185rot							Friday, October 1, 1999 2:11 PM
5	27	185	15	1.336	0.022	1.7	0.023	
thermalfile6	KH OLV c-norm RT 165rot							Friday, October 1, 1999 2:20 PM
6	27	165	5	1.197	0.018	1.5	0.031	
thermalfile7	KH OLV c-norm RT 145rot							Friday, October 1, 1999 2:35 PM
7	27	145	10	1.255	0.007	0.5	0.024	
thermalfile0	methanol 26.2C							Friday, October 1, 1999 1:07 PM
0	26.2	1099.2		9.588				
thermalfile9	methanol 27.0C							Friday, October 1, 1999 2:59 PM
9	27.0	1096.6		9.519				

4 October 1999

thermalfile1	KH OLV c-norm 100C 255rot							Monday, October 4, 1999 1:20 PM
1	100	255	45	1.710	0.008	0.5	0.013	
thermalfile10	KH OLV c-norm 200C 185rot							Monday, October 4, 1999 2:59 PM
10	200	185	82	0.829	0.006	0.7	0.027	
thermalfile101	KH OLV c-norm 100C 255rot							Monday, October 4, 1999 1:20 PM
101	100	255	45	1.708	0.008	0.5	0.013	
thermalfile102	KH OLV c-norm 100C 235rot							Monday, October 4, 1999 1:27 PM
102	100	235	43	1.660	0.010	0.6	0.014	
thermalfile103	KH OLV c-norm 100C 210rot							Monday, October 4, 1999 1:37 PM
103	100	210	52	1.362	0.010	0.8	0.018	
thermalfile104	KH OLV c-norm 100C 185rot							Monday, October 4, 1999 1:49 PM
104	100	185	39	1.049	0.009	0.9	0.025	
thermalfile105	KH OLV c-norm 100C 165rot							Monday, October 4, 1999 2:03 PM
105	100	165	17	0.932	0.012	1.3	0.032	

thermalfile109	KH OLV c-norm 200C 165rot	Monday, October 4, 1999 2:49 PM
109	200 165 52 0.745 0.007 0.9	0.026
thermalfile11	KH OLV c-norm 200C 210rot	Monday, October 4, 1999 3:06 PM
11	200 210 80 1.097 0.018 1.7	0.025
thermalfile110	KH OLV c-norm 200C 185rot	Monday, October 4, 1999 2:59 PM
110	200 185 82 0.829 0.006 0.7	0.026
thermalfile111	KH OLV c-norm 200C 210rot	Monday, October 4, 1999 3:06 PM
111	200 210 80 1.096 0.018 1.7	0.025
thermalfile112	KH OLV c-norm 200C 235rot	Monday, October 4, 1999 3:11 PM
112	200 235 52 1.341 0.020 1.5	0.020
thermalfile113	KH OLV c-norm 200C 255rot	Monday, October 4, 1999 3:17 PM
113	200 255 47 1.349 0.006 0.5	0.014
thermalfile117	KH OLV c-norm 300C 255rot	Monday, October 4, 1999 4:22 PM
117	300 255 68 1.214 0.035 2.9	0.019
thermalfile118	KH OLV c-norm 300C 235rot	Monday, October 4, 1999 4:30 PM
118	300 235 94 1.102 0.006 0.6	0.013
thermalfile119	KH OLV c-norm 300C 210rot	Monday, October 4, 1999 4:44 PM
119	300 210 146 0.896 0.007 0.8	0.020
thermalfile12	KH OLV c-norm 200C 235rot	Monday, October 4, 1999 3:11 PM
12	200 235 52 1.342 0.021 1.5	0.020
thermalfile120	KH OLV c-norm 300C 185rot	Monday, October 4, 1999 4:50 PM
120	300 185 105 0.704 0.008 1.2	0.022
thermalfile121	KH OLV c-norm 300C 165rot	Monday, October 4, 1999 4:57 PM
121	300 165 62 0.626 0.009 1.5	0.022
thermalfile125	KH OLV c-norm 400C 165rot	Monday, October 4, 1999 5:35 PM
125	400 165 46 0.563 0.002 0.5	0.015
thermalfile126	KH OLV c-norm 400C 185rot	Monday, October 4, 1999 5:44 PM
126	400 185 93 0.633 0.002 0.5	0.018
thermalfile127	KH OLV c-norm 400C 210rot	Monday, October 4, 1999 5:50 PM
127	400 210 93 0.849 0.016 1.8	0.021
thermalfile128	KH OLV c-norm 400C 235rot	Monday, October 4, 1999 5:58 PM
128	400 235 56 1.029 0.014 1.3	0.016
thermalfile129	KH OLV c-norm 400C 255rot	Monday, October 4, 1999 6:05 PM
129	400 255 49 1.069 0.009 0.9	0.013
thermalfile13	KH OLV c-norm 200C 255rot	Monday, October 4, 1999 3:17 PM
13	200 255 47 1.349 0.006 0.5	0.014
thermalfile133	KH OLV c-norm 500C 255rot	Monday, October 4, 1999 6:59 PM
133	500 255 64 0.958 0.008 0.8	0.014
thermalfile134	KH OLV c-norm 500C 235rot	Monday, October 4, 1999 7:10 PM
134	500 235 143 0.936 0.015 1.6	0.022
thermalfile135	KH OLV c-norm 500C 210rot	Monday, October 4, 1999 7:22 PM
135	500 210 144 0.786 0.017 2.1	0.026
thermalfile136	KH OLV c-norm 500C 185rot	Monday, October 4, 1999 7:29 PM
136	500 185 80 0.602 0.007 1.1	0.019

thermalfile137	KH OLV c-norm 500C 165rot	Monday, October 4, 1999 7:37 PM
137	500 165 37 0.530 0.001 0.5	0.017
thermalfile141	KH OLV c-norm 600C 165rot	Monday, October 4, 1999 8:56 PM
141	600 165 65 0.487 0.002 0.5	0.016
thermalfile142	KH OLV c-norm 600C 185rot	Monday, October 4, 1999 9:02 PM
142	600 185 107 0.560 0.005 0.9	0.017
thermalfile143	KH OLV c-norm 600C 210rot	Monday, October 4, 1999 9:12 PM
143	600 210 138 0.740 0.009 1.2	0.023
thermalfile144	KH OLV c-norm 600C 235rot	Monday, October 4, 1999 9:19 PM
144	600 235 83 0.845 0.016 1.9	0.012
thermalfile145	KH OLV c-norm 600C 255rot	Monday, October 4, 1999 9:25 PM
145	600 255 100 0.864 0.010 1.2	0.012
thermalfile149	KH OLV c-norm 700C 255rot	Monday, October 4, 1999 10:10 PM
149	700 255 112 0.828 0.005 0.6	0.019
thermalfile150	KH OLV c-norm 700C 235rot	Monday, October 4, 1999 10:19 PM
150	700 235 112 0.813 0.004 0.5	0.015
thermalfile151	KH OLV c-norm 700C 210rot	Monday, October 4, 1999 10:30 PM
151	700 210 125 0.693 0.005 0.7	0.018
thermalfile152	KH OLV c-norm 700C 185rot	Monday, October 4, 1999 10:37 PM
152	700 185 83 0.534 0.006 1.1	0.015
thermalfile153	KH OLV c-norm 700C 165rot	Monday, October 4, 1999 10:44 PM
153	700 165 35 0.465 0.004 0.9	0.016
thermalfile157	KH OLV c-norm 800C 165rot	Tuesday, October 5, 1999 12:30 AM
157	800 165 89 0.443 0.005 1.1	0.017
thermalfile158	KH OLV c-norm 800C 185rot	Tuesday, October 5, 1999 12:38 AM
158	800 185 125 0.525 0.004 0.7	0.023
thermalfile159	KH OLV c-norm 800C 210rot	Tuesday, October 5, 1999 12:44 AM
159	800 210 108 0.684 0.007 1.0	0.021
thermalfile160	KH OLV c-norm 800C 235rot	Tuesday, October 5, 1999 1:04 AM
160	800 235 80 0.813 0.020 2.5	0.023
thermalfile161	KH OLV c-norm 800C 255rot	Tuesday, October 5, 1999 1:21 AM
161	800 255 48 0.779 0.002 0.5	0.014
thermalfile17	KH OLV c-norm 300C 255rot	Monday, October 4, 1999 4:22 PM
17	300 255 68 1.215 0.035 2.8	0.019
thermalfile18	KH OLV c-norm 300C 235rot	Monday, October 4, 1999 4:30 PM
18	300 235 93 1.102 0.006 0.6	0.013
thermalfile19	KH OLV c-norm 300C 210rot	Monday, October 4, 1999 4:44 PM
19	300 210 146 0.896 0.007 0.8	0.020
thermalfile2	KH OLV c-norm 100C 235rot	Monday, October 4, 1999 1:27 PM
2	100 235 43 1.662 0.010 0.6	0.015
thermalfile20	KH OLV c-norm 300C 185rot	Monday, October 4, 1999 4:50 PM
20	300 185 105 0.704 0.008 1.2	0.023
thermalfile21	KH OLV c-norm 300C 165rot	Monday, October 4, 1999 4:57 PM
21	300 165 62 0.626 0.010 1.5	0.022

thermalfile25	KH OLV c-norm 400C 165rot	Monday, October 4, 1999 5:35 PM
25 400	165 45 0.563 0.002 0.5	0.015
thermalfile26	KH OLV c-norm 400C 185rot	Monday, October 4, 1999 5:44 PM
26 400	185 93 0.633 0.002 0.5	0.018
thermalfile27	KH OLV c-norm 400C 210rot	Monday, October 4, 1999 5:50 PM
27 400	210 93 0.849 0.016 1.8	0.021
thermalfile28	KH OLV c-norm 400C 235rot	Monday, October 4, 1999 5:58 PM
28 400	235 56 1.031 0.016 1.5	0.016
thermalfile29	KH OLV c-norm 400C 255rot	Monday, October 4, 1999 6:05 PM
29 400	255 49 1.071 0.012 1.1	0.013
thermalfile3	KH OLV c-norm 100C 210rot	Monday, October 4, 1999 1:37 PM
3 100	210 52 1.362 0.010 0.8	0.018
thermalfile33	KH OLV c-norm 500C 255rot	Monday, October 4, 1999 6:59 PM
33 500	255 64 0.957 0.007 0.7	0.013
thermalfile34	KH OLV c-norm 500C 235rot	Monday, October 4, 1999 7:10 PM
34 500	235 143 0.935 0.014 1.5	0.022
thermalfile35	KH OLV c-norm 500C 210rot	Monday, October 4, 1999 7:22 PM
35 500	210 144 0.786 0.016 2.1	0.026
thermalfile36	KH OLV c-norm 500C 185rot	Monday, October 4, 1999 7:29 PM
36 500	185 79 0.603 0.007 1.2	0.019
thermalfile37	KH OLV c-norm 500C 165rot	Monday, October 4, 1999 7:37 PM
37 500	165 38 0.531 0.002 0.5	0.017
thermalfile4	KH OLV c-norm 100C 185rot	Monday, October 4, 1999 1:49 PM
4 100	185 38 1.050 0.009 0.9	0.025
thermalfile41	KH OLV c-norm 600C 165rot	Monday, October 4, 1999 8:56 PM
41 600	165 65 0.488 0.002 0.5	0.016
thermalfile42	KH OLV c-norm 600C 185rot	Monday, October 4, 1999 9:02 PM
42 600	185 107 0.560 0.005 0.9	0.017
thermalfile43	KH OLV c-norm 600C 210rot	Monday, October 4, 1999 9:12 PM
43 600	210 138 0.740 0.009 1.2	0.023
thermalfile44	KH OLV c-norm 600C 235rot	Monday, October 4, 1999 9:19 PM
44 600	235 83 0.845 0.016 1.9	0.012
thermalfile45	KH OLV c-norm 600C 255rot	Monday, October 4, 1999 9:25 PM
45 600	255 100 0.864 0.010 1.2	0.012
thermalfile49	KH OLV c-norm 700C 255rot	Monday, October 4, 1999 10:10 PM
49 700	255 112 0.828 0.005 0.5	0.019
thermalfile5	KH OLV c-norm 100C 165rot	Monday, October 4, 1999 2:03 PM
5 100	165 17 0.932 0.010 1.0	0.032
thermalfile50	KH OLV c-norm 700C 235rot	Monday, October 4, 1999 10:19 PM
50 700	235 111 0.814 0.004 0.5	0.015
thermalfile51	KH OLV c-norm 700C 210rot	Monday, October 4, 1999 10:30 PM
51 700	210 125 0.693 0.005 0.7	0.018
thermalfile52	KH OLV c-norm 700C 185rot	Monday, October 4, 1999 10:37 PM
52 700	185 83 0.534 0.006 1.1	0.015

thermalfile53	KH OLV c-norm 700C 165rot	Monday, October 4, 1999 10:44 PM
53 700	165 35 0.465 0.004 0.8	0.016
thermalfile57	KH OLV c-norm 800C 165rot	Tuesday, October 5, 1999 12:30 AM
57 800	165 88 0.443 0.005 1.1	0.017
thermalfile58	KH OLV c-norm 800C 185rot	Tuesday, October 5, 1999 12:38 AM
58 800	185 125 0.525 0.004 0.7	0.023
thermalfile59	KH OLV c-norm 800C 210rot	Tuesday, October 5, 1999 12:44 AM
59 800	210 108 0.685 0.007 1.0	0.021
thermalfile60	KH OLV c-norm 800C 235rot	Tuesday, October 5, 1999 1:04 AM
60 800	235 80 0.814 0.021 2.5	0.023
thermalfile61	KH OLV c-norm 800C 255rot	Tuesday, October 5, 1999 1:21 AM
61 800	255 48 0.780 0.002 0.5	0.014
thermalfile9	KH OLV c-norm 200C 165rot	Monday, October 4, 1999 2:49 PM
9 200	165 52 0.745 0.007 0.9	0.026
thermalfile0	methanol 25.9C	Monday, October 4, 1999 12:55 PM
0 25.9	1100.1 9.668	
thermalfile15	methanol 26.9C	Monday, October 4, 1999 3:38 PM
15 26.9	1096.9 9.697	
thermalfile16	methanol 27.2C	Monday, October 4, 1999 4:12 PM
16 27.2	1096.0 9.590	
thermalfile23	methanol 27.4C	Monday, October 4, 1999 5:09 PM
23 27.4	1095.3 9.610	
thermalfile24	methanol 27.5C	Monday, October 4, 1999 5:26 PM
24 27.5	1095.0 9.691	
thermalfile31	methanol 27.6C	Monday, October 4, 1999 6:25 PM
31 27.6	1094.7 9.735	
thermalfile32	methanol 27.8C	Monday, October 4, 1999 6:48 PM
32 27.8	1094.0 9.574	
thermalfile39	methanol 28.0C	Monday, October 4, 1999 7:49 PM
39 28.0	1093.4 9.598	
thermalfile40	methanol 27.7C	Monday, October 4, 1999 8:44 PM
40 27.7	1094.4 9.638	
thermalfile47	methanol 27.3C	Monday, October 4, 1999 9:36 PM
47 27.3	1095.6 9.683	
thermalfile48	methanol 27.3C	Monday, October 4, 1999 10:00 PM
48 27.3	1095.6 9.676	
thermalfile55	methanol 27.2C	Monday, October 4, 1999 10:58 PM
55 27.2	1096.0 9.683	
thermalfile56	methanol 27.0C	Tuesday, October 5, 1999 12:18 AM
56 27.0	1096.6 9.686	
thermalfile63	methanol 27.0C	Tuesday, October 5, 1999 1:53 AM
63 27.0	1096.6 9.687	
thermalfile7	methanol 26.6C	Monday, October 4, 1999 2:21 PM
7 26.6	1097.9 9.644	

thermalfile8 methanol 26.6C Monday, October 4, 1999 2:34 PM
 8 26.6 1097.9 9.685

6 October 1999

thermalfile1 KH OLV c-norm 900C 255rot Wednesday, October 6, 1999 3:21 PM
 1 900 255 72 0.748 0.003 0.5 0.020
 thermalfile10 KH OLV c-norm 1000C 185rot Wednesday, October 6, 1999 4:29 PM
 10 1000 185 54 0.429 0.001 0.5 0.019
 thermalfile101 KH OLV c-norm 900C 255rot Wednesday, October 6, 1999 3:21 PM
 101 900 255 72 0.748 0.003 0.5 0.020
 thermalfile102 KH OLV c-norm 900C 235rot Wednesday, October 6, 1999 3:28 PM
 102 900 235 68 0.749 0.004 0.5 0.018
 thermalfile103 KH OLV c-norm 900C 210rot Wednesday, October 6, 1999 3:35 PM
 103 900 210 83 0.633 0.002 0.5 0.018
 thermalfile104 KH OLV c-norm 900C 185rot Wednesday, October 6, 1999 3:39 PM
 104 900 185 46 0.451 0.002 0.5 0.019
 thermalfile105 KH OLV c-norm 900C 165rot Wednesday, October 6, 1999 3:47 PM
 105 900 165 41 0.421 0.002 0.6 0.017
 thermalfile109 KH OLV c-norm 1000C 165rot Wednesday, October 6, 1999 4:19 PM
 109 1000 165 45 0.404 0.002 0.5 0.018
 thermalfile11 KH OLV c-norm 1000C 210rot Wednesday, October 6, 1999 4:35 PM
 11 1000 210 84 0.614 0.012 1.9 0.024
 thermalfile110 KH OLV c-norm 1000C 185rot Wednesday, October 6, 1999 4:29 PM
 110 1000 185 55 0.427 0.001 0.5 0.018
 thermalfile111 KH OLV c-norm 1000C 210rot Wednesday, October 6, 1999 4:35 PM
 111 1000 210 84 0.612 0.010 1.7 0.024
 thermalfile112 KH OLV c-norm 1000C 235rot Wednesday, October 6, 1999 4:42 PM
 112 1000 235 113 0.707 0.007 1.1 0.022
 thermalfile113 KH OLV c-norm 1000C 255rot Wednesday, October 6, 1999 4:47 PM
 113 1000 255 106 0.732 0.013 1.8 0.023
 thermalfile12 KH OLV c-norm 1000C 235rot Wednesday, October 6, 1999 4:42 PM
 12 1000 235 113 0.708 0.008 1.2 0.022
 thermalfile13 KH OLV c-norm 1000C 255rot Wednesday, October 6, 1999 4:47 PM
 13 1000 255 106 0.733 0.014 2.0 0.024
 thermalfile2 KH OLV c-norm 900C 235rot Wednesday, October 6, 1999 3:28 PM
 2 900 235 68 0.749 0.004 0.5 0.018
 thermalfile3 KH OLV c-norm 900C 210rot Wednesday, October 6, 1999 3:35 PM
 3 900 210 83 0.633 0.002 0.5 0.018
 thermalfile4 KH OLV c-norm 900C 185rot Wednesday, October 6, 1999 3:39 PM
 4 900 185 46 0.451 0.002 0.5 0.019
 thermalfile5 KH OLV c-norm 900C 165rot Wednesday, October 6, 1999 3:47 PM

5	900	165	41	0.421	0.002	0.6	0.017	
thermalfile9	KH OLV c-norm 1000C 165rot							Wednesday, October 6, 1999 4:19 PM
9	1000	165	45	0.406	0.003	0.8	0.021	
thermalfile0	methanol 28.6C							Wednesday, October 6, 1999 3:11 PM
0	28.6	1091.5		9.646				
thermalfile15	methanol 28.8C							Wednesday, October 6, 1999 4:54 PM
15	28.8	1090.8		9.700				
thermalfile7	methanol 28.6C							Wednesday, October 6, 1999 3:55 PM
7	28.6	1091.5		9.696				
thermalfile8	methanol 28.8C							Wednesday, October 6, 1999 4:10 PM
8	28.8	1090.8		9.682				

18 October 1999

thermalfile102	KH OLV c-norm RT 200rot							Monday, October 18, 1999 3:00 PM
102	27	200	84	2.805	0.033	1.2	0.012	
thermalfile103	KH OLV c-norm RT 220rot							Monday, October 18, 1999 3:09 PM
103	27	220	89	2.982	0.036	1.2	0.010	
thermalfile104	KH OLV c-norm RT 240rot							Monday, October 18, 1999 3:14 PM
104	27	240	101	3.530	0.031	0.9	0.007	
thermalfile105	KH OLV c-norm RT 260rot							Monday, October 18, 1999 3:23 PM
105	27	260	57	4.267	0.036	0.8	0.012	
thermalfile106	KH OLV c-norm RT 270rot							Monday, October 18, 1999 3:35 PM
106	27	270	43	4.541	0.043	0.9	0.015	
thermalfile108	KH OLV c-norm RT 180rot							Monday, October 18, 1999 3:53 PM
108	27	180	85	3.182	0.036	1.1	0.009	
thermalfile11	KH OLV c-norm 200C 115rot							Monday, October 18, 1999 5:31 PM
11	200	115	55	3.133	0.029	0.9	0.007	
thermalfile111	KH OLV c-norm 200C 115rot							Monday, October 18, 1999 5:31 PM
111	200	115	55	3.133	0.028	0.9	0.008	
thermalfile112	KH OLV c-norm 200C 135rot							Monday, October 18, 1999 5:41 PM
112	200	135	27	2.957	0.015	0.5	0.010	
thermalfile113	KH OLV c-norm 200C 155rot							Monday, October 18, 1999 5:51 PM
113	200	155	97	2.574	0.031	1.2	0.012	
thermalfile114	KH OLV c-norm 200C 175rot							Monday, October 18, 1999 6:02 PM
114	200	175	69	2.109	0.026	1.2	0.014	
thermalfile115	KH OLV c-norm 200C 195rot							Monday, October 18, 1999 6:14 PM
115	200	195	39	1.882	0.041	2.2	0.014	
thermalfile116	KH OLV c-norm 200C 215rot							Monday, October 18, 1999 6:24 PM
116	200	215	15	1.832	0.013	0.7	0.020	
thermalfile12	KH OLV c-norm 200C 135rot							Monday, October 18, 1999 5:41 PM
12	200	135	27	2.958	0.015	0.5	0.007	

thermalfile120	KH OLV c-norm 400C 215rot	Monday, October 18, 1999 7:22 PM
120	400 215 41 1.379 0.016 1.2	0.019
thermalfile121	KH OLV c-norm 400C 195rot	Monday, October 18, 1999 7:28 PM
121	400 195 50 1.376 0.013 0.9	0.016
thermalfile122	KH OLV c-norm 400C 175rot	Monday, October 18, 1999 7:39 PM
122	400 175 50 1.604 0.012 0.7	0.015
thermalfile123	KH OLV c-norm 400C 155rot	Monday, October 18, 1999 7:50 PM
123	400 155 62 1.989 0.027 1.3	0.013
thermalfile124	KH OLV c-norm 400C 135rot	Monday, October 18, 1999 8:01 PM
124	400 135 26 2.269 0.011 0.5	0.013
thermalfile125	KH OLV c-norm 400C 115rot	Monday, October 18, 1999 8:10 PM
125	400 115 55 2.516 0.031 1.2	0.011
thermalfile128	KH OLV c-norm 600C 115rot	Monday, October 18, 1999 9:33 PM
128	600 115 99 2.056 0.026 1.3	0.012
thermalfile129	KH OLV c-norm 600C 135rot	Monday, October 18, 1999 9:41 PM
129	600 135 93 1.935 0.014 0.7	0.010
thermalfile13	KH OLV c-norm 200C 155rot	Monday, October 18, 1999 5:51 PM
13	200 155 97 2.574 0.031 1.2	0.012
thermalfile130	KH OLV c-norm 600C 155rot	Monday, October 18, 1999 9:48 PM
130	600 155 70 1.661 0.019 1.1	0.012
thermalfile131	KH OLV c-norm 600C 175rot	Monday, October 18, 1999 9:58 PM
131	600 175 22 1.358 0.006 0.5	0.014
thermalfile132	KH OLV c-norm 600C 195rot	Monday, October 18, 1999 10:08 PM
132	600 195 18 1.182 0.005 0.5	0.012
thermalfile133	KH OLV c-norm 600C 215rot	Monday, October 18, 1999 10:18 PM
133	600 215 17 1.181 0.008 0.7	0.013
thermalfile137	KH OLV c-norm 800C 215rot	Monday, October 18, 1999 10:57 PM
137	800 215 46 1.069 0.015 1.4	0.017
thermalfile138	KH OLV c-norm 800C 195rot	Monday, October 18, 1999 11:03 PM
138	800 195 36 1.049 0.011 1.0	0.015
thermalfile139	KH OLV c-norm 800C 175rot	Monday, October 18, 1999 11:09 PM
139	800 175 81 1.209 0.010 0.8	0.017
thermalfile14	KH OLV c-norm 200C 175rot	Monday, October 18, 1999 6:02 PM
14	200 175 69 2.109 0.026 1.2	0.013
thermalfile140	KH OLV c-norm 800C 155rot	Monday, October 18, 1999 11:15 PM
140	800 155 73 1.494 0.029 1.9	0.019
thermalfile141	KH OLV c-norm 800C 135rot	Monday, October 18, 1999 11:21 PM
141	800 135 53 1.747 0.024 1.4	0.012
thermalfile142	KH OLV c-norm 800C 115rot	Monday, October 18, 1999 11:29 PM
142	800 115 42 1.816 0.003 0.5	0.006
thermalfile15	KH OLV c-norm 200C 195rot	Monday, October 18, 1999 6:14 PM
15	200 195 39 1.882 0.039 2.1	0.012
thermalfile16	KH OLV c-norm 200C 215rot	Monday, October 18, 1999 6:24 PM
16	200 215 15 1.829 0.010 0.5	0.013

thermalfile2	KH OLV c-norm RT 200rot	Monday, October 18, 1999 3:00 PM
2	27 200 84 2.806 0.032 1.1	0.012
thermalfile20	KH OLV c-norm 400C 215rot	Monday, October 18, 1999 7:22 PM
20	400 215 41 1.377 0.015 1.1	0.017
thermalfile21	KH OLV c-norm 400C 195rot	Monday, October 18, 1999 7:28 PM
21	400 195 50 1.375 0.012 0.9	0.015
thermalfile22	KH OLV c-norm 400C 175rot	Monday, October 18, 1999 7:39 PM
22	400 175 50 1.602 0.011 0.7	0.013
thermalfile23	KH OLV c-norm 400C 155rot	Monday, October 18, 1999 7:50 PM
23	400 155 62 1.988 0.025 1.3	0.012
thermalfile24	KH OLV c-norm 400C 135rot	Monday, October 18, 1999 8:01 PM
24	400 135 25 2.266 0.009 0.5	0.010
thermalfile25	KH OLV c-norm 400C 115rot	Monday, October 18, 1999 8:10 PM
25	400 115 55 2.515 0.029 1.2	0.010
thermalfile28	KH OLV c-norm 600C 115rot	Monday, October 18, 1999 9:33 PM
28	600 115 99 2.057 0.027 1.3	0.012
thermalfile29	KH OLV c-norm 600C 135rot	Monday, October 18, 1999 9:41 PM
29	600 135 93 1.936 0.015 0.8	0.010
thermalfile3	KH OLV c-norm RT 220rot	Monday, October 18, 1999 3:09 PM
3	27 220 90 2.984 0.036 1.2	0.010
thermalfile30	KH OLV c-norm 600C 155rot	Monday, October 18, 1999 9:48 PM
30	600 155 70 1.663 0.021 1.2	0.012
thermalfile31	KH OLV c-norm 600C 175rot	Monday, October 18, 1999 9:58 PM
31	600 175 22 1.362 0.011 0.8	0.014
thermalfile32	KH OLV c-norm 600C 195rot	Monday, October 18, 1999 10:08 PM
32	600 195 18 1.186 0.003 0.5	0.012
thermalfile33	KH OLV c-norm 600C 215rot	Monday, October 18, 1999 10:18 PM
33	600 215 17 1.186 0.011 0.9	0.013
thermalfile37	KH OLV c-norm 800C 215rot	Monday, October 18, 1999 10:57 PM
37	800 215 46 1.068 0.014 1.3	0.017
thermalfile38	KH OLV c-norm 800C 195rot	Monday, October 18, 1999 11:03 PM
38	800 195 36 1.048 0.010 0.9	0.016
thermalfile39	KH OLV c-norm 800C 175rot	Monday, October 18, 1999 11:09 PM
39	800 175 81 1.209 0.010 0.8	0.018
thermalfile4	KH OLV c-norm RT 240rot	Monday, October 18, 1999 3:14 PM
4	27 240 101 3.532 0.032 0.9	0.007
thermalfile40	KH OLV c-norm 800C 155rot	Monday, October 18, 1999 11:15 PM
40	800 155 73 1.494 0.028 1.9	0.019
thermalfile41	KH OLV c-norm 800C 135rot	Monday, October 18, 1999 11:21 PM
41	800 135 53 1.747 0.024 1.4	0.012
thermalfile42	KH OLV c-norm 800C 115rot	Monday, October 18, 1999 11:29 PM
42	800 115 42 1.816 0.004 0.5	0.006
thermalfile5	KH OLV c-norm RT 260rot	Monday, October 18, 1999 3:23 PM
5	27 260 58 4.270 0.034 0.8	0.011

thermalfile6	KH OLV c-norm RT 270rot	Monday, October 18, 1999 3:35 PM
6 27	270 43 4.545 0.041 0.9 0.015	
thermalfile8	KH OLV c-norm RT 180rot	Monday, October 18, 1999 3:53 PM
8 27	180 85 3.185 0.036 1.1 0.009	
thermalfile0	methanol 25.2C	Monday, October 18, 1999 1:35 PM
0 25.2	1102.4 14.972	
thermalfile1	methanol 25.5C	Monday, October 18, 1999 2:08 PM
1 25.5	1101.4 15.001	
thermalfile10	methanol 26.9C	Monday, October 18, 1999 5:12 PM
10 26.9	1096.9 14.962	
thermalfile18	methanol 26.9C	Monday, October 18, 1999 6:38 PM
18 26.9	1096.9 15.038	
thermalfile19	methanol 27.0C	Monday, October 18, 1999 7:08 PM
19 27.0	1096.6 15.030	
thermalfile27	methanol 27.1C	Monday, October 18, 1999 8:20 PM
27 27.1	1096.3 15.016	
thermalfile35	methanol 26.6C	Monday, October 18, 1999 10:31 PM
35 26.6	1097.9 14.990	
thermalfile36	methanol 26.5C	Monday, October 18, 1999 10:48 PM
36 26.5	1098.2 14.922	
thermalfile44	methanol 26.4C	Monday, October 18, 1999 11:45 PM
44 26.4	1098.5 14.942	
thermalfile45	methanol 26.4C	Tuesday, October 19, 1999 12:01 AM
45 26.4	1098.5 14.923	
thermalfile46	methanol 26.4C	Tuesday, October 19, 1999 12:24 AM
46 26.4	1098.5 14.947	
thermalfile9	methanol 26.4C	Monday, October 18, 1999 4:05 PM
9 26.4	1098.5 14.937	

SC73-10*19 September 2000*

thermalfile1	SC73-10 a-norm RT 200rot	Tuesday, September 19, 2000 3:19 PM
1 27	200 33 3.255 0.030 0.9 0.009	
thermalfile2	SC73-10 a-norm RT 180rot	Tuesday, September 19, 2000 3:29 PM
2 27	180 41 3.133 0.032 1.0 0.008	
thermalfile3	SC73-10 a-norm RT 160rot	Tuesday, September 19, 2000 3:36 PM
3 27	160 114 3.034 0.039 1.3 0.011	
thermalfile4	SC73-10 a-norm RT 140rot	Tuesday, September 19, 2000 3:44 PM
4 27	140 64 3.100 0.049 1.6 0.010	

thermalfile5	SC73-10 a-norm RT 120rot	Tuesday, September 19, 2000 3:51 PM
5 27	120 32 3.183 0.042 1.3 0.009	
thermalfile6	SC73-10 a-norm RT 110rot	Tuesday, September 19, 2000 3:59 PM
6 27	110 49 3.340 0.054 1.6 0.009	
thermalfile7	SC73-10 a-norm RT 220rot	Tuesday, September 19, 2000 4:10 PM
7 27	220 71 3.192 0.039 1.2 0.008	
thermalfile8	SC73-10 a-norm RT 240rot	Tuesday, September 19, 2000 4:17 PM
8 27	240 35 3.163 0.045 1.4 0.010	
thermalfile9	SC73-10 a-norm RT 260rot	Tuesday, September 19, 2000 4:26 PM
9 27	260 47 3.494 0.050 1.4 0.008	
thermalfile12	SC73-10 a-norm 100C 260rot	Tuesday, September 19, 2000 9:17 PM
12 100	260 60 2.783 0.027 1.0 0.007	
thermalfile13	SC73-10 a-norm 100C 240rot	Tuesday, September 19, 2000 9:27 PM
13 100	240 40 2.648 0.028 1.1 0.011	
thermalfile14	SC73-10 a-norm 100C 220rot	Tuesday, September 19, 2000 9:39 PM
14 100	220 56 2.628 0.027 1.0 0.009	
thermalfile15	SC73-10 a-norm 100C 200rot	Tuesday, September 19, 2000 9:49 PM
15 100	200 69 2.599 0.043 1.7 0.007	
thermalfile16	SC73-10 a-norm 100C 180rot	Tuesday, September 19, 2000 9:56 PM
16 100	180 76 2.535 0.019 0.7 0.006	
thermalfile17	SC73-10 a-norm 100C 160rot	Tuesday, September 19, 2000 10:04 PM
17 100	160 100 2.503 0.027 1.1 0.014	
thermalfile18	SC73-10 a-norm 100C 140rot	Tuesday, September 19, 2000 10:12 PM
18 100	140 103 2.546 0.039 1.5 0.017	
thermalfile20	SC73-10 a-norm 100C 200rot	Tuesday, September 19, 2000 10:56 PM
20 100	200 65 2.679 0.014 0.5 0.007	
thermalfile21	SC73-10 a-norm 100C 220rot	Tuesday, September 19, 2000 11:08 PM
21 100	220 47 2.763 0.030 1.1 0.008	
thermalfile22	SC73-10 a-norm 100C 220rot	Tuesday, September 19, 2000 11:13 PM
22 100	220 52 2.772 0.027 1.0 0.009	
thermalfile23	SC73-10 a-norm 100C 220rot	Tuesday, September 19, 2000 11:19 PM
23 100	220 49 2.770 0.038 1.4 0.010	
thermalfile24	SC73-10 a-norm 100C 260rot	Tuesday, September 19, 2000 11:44 PM
24 100	260 44 2.920 0.038 1.3 0.009	
thermalfile25	SC73-10 a-norm 100C 260rot	Tuesday, September 19, 2000 11:51 PM
25 100	260 38 2.935 0.067 2.3 0.012	
thermalfile26	SC73-10 a-norm 100C 260rot	Tuesday, September 19, 2000 11:51 PM
26 100	260 38 2.935 0.067 2.3 0.012	
thermalfile0	methanol 25.2C	Tuesday, September 19, 2000 2:25 PM
0 25.2	1102.4 15.219	
thermalfile10	methanol 25.9C	Tuesday, September 19, 2000 4:35 PM
10 25.9	1100.1 15.237	
thermalfile11	methanol 26.4C	Tuesday, September 19, 2000 9:02 PM
11 26.4	1098.5 15.238	

thermalfile19 methanol 26.4C Tuesday, September 19, 2000 10:20 PM
 19 26.4 1098.5 15.275

20 September 2000

thermalfile2 SC73-10 a-norm RT 260rot Wednesday, September 20, 2000 4:03 PM
 2 27 260 58 3.338 0.062 1.9 0.008
 thermalfile3 SC73-10 a-norm RT 240rot Wednesday, September 20, 2000 4:13 PM
 3 27 240 43 3.165 0.047 1.5 0.009
 thermalfile4 SC73-10 a-norm RT 220rot Wednesday, September 20, 2000 4:25 PM
 4 27 220 72 3.182 0.051 1.6 0.012
 thermalfile5 SC73-10 a-norm RT 200rot Wednesday, September 20, 2000 4:42 PM
 5 27 200 89 3.054 0.060 2.0 0.008
 thermalfile6 SC73-10 a-norm RT 180rot Wednesday, September 20, 2000 4:50 PM
 6 27 180 81 3.052 0.026 0.9 0.008
 thermalfile7 SC73-10 a-norm RT 160rot Wednesday, September 20, 2000 4:55 PM
 7 27 160 126 2.990 0.035 1.2 0.012
 thermalfile8 SC73-10 a-norm RT 140rot Wednesday, September 20, 2000 5:01 PM
 8 27 140 68 3.030 0.035 1.1 0.009
 thermalfile12 SC73-10 a-norm RT 130rot Wednesday, September 20, 2000 6:30 PM
 12 27 130 35 3.120 0.038 1.2 0.009
 thermalfile13 SC73-10 a-norm RT 140rot Wednesday, September 20, 2000 6:38 PM
 13 27 140 87 3.026 0.030 1.0 0.008
 thermalfile14 SC73-10 a-norm RT 150rot Wednesday, September 20, 2000 6:43 PM
 14 27 150 118 2.987 0.034 1.2 0.009
 thermalfile15 SC73-10 a-norm RT 160rot Wednesday, September 20, 2000 6:48 PM
 15 27 160 112 2.977 0.034 1.1 0.008
 thermalfile16 SC73-10 a-norm RT 170rot Wednesday, September 20, 2000 6:53 PM
 16 27 170 94 3.036 0.063 2.1 0.009
 thermalfile17 SC73-10 a-norm RT 180rot Wednesday, September 20, 2000 6:59 PM
 17 27 180 85 3.178 0.032 1.0 0.008
 thermalfile18 SC73-10 a-norm RT 190rot Wednesday, September 20, 2000 7:05 PM
 18 27 190 77 3.137 0.026 0.8 0.007
 thermalfile19 SC73-10 a-norm RT 200rot Wednesday, September 20, 2000 7:13 PM
 19 27 200 76 3.304 0.058 1.8 0.010
 thermalfile20 SC73-10 a-norm RT 210rot Wednesday, September 20, 2000 7:21 PM
 20 27 210 61 3.265 0.025 0.8 0.007
 thermalfile21 SC73-10 a-norm RT 220rot Wednesday, September 20, 2000 7:27 PM
 21 27 220 37 3.311 0.038 1.1 0.007
 thermalfile22 SC73-10 a-norm RT 230rot Wednesday, September 20, 2000 7:34 PM
 22 27 230 37 3.357 0.030 0.9 0.006
 thermalfile23 SC73-10 a-norm RT 240rot Wednesday, September 20, 2000 7:42 PM

23	27	240	35	3.410	0.031	0.9	0.008
thermalfile24	SC73-10	a-norm	RT 250rot	Wednesday, September 20, 2000 7:49 PM			
24	27	250	41	3.502	0.027	0.8	0.008
thermalfile25	SC73-10	a-norm	RT 260rot	Wednesday, September 20, 2000 7:53 PM			
25	27	260	42	3.526	0.029	0.8	0.008
thermalfile26	SC73-10	a-norm	RT 270rot	Wednesday, September 20, 2000 7:58 PM			
26	27	270	40	3.392	0.063	1.9	0.011
thermalfile0	methanol	24.5C		Wednesday, September 20, 2000 3:32 PM			
0	24.5	1104.6		15.184			
thermalfile10	methanol	25.0C		Wednesday, September 20, 2000 5:13 PM			
10	25.0	1103.0		15.185			
thermalfile11	methanol	25.1C		Wednesday, September 20, 2000 6:17 PM			
11	25.1	1102.7		15.242			
thermalfile27	methanol	25.2C		Wednesday, September 20, 2000 8:03 PM			
27	25.2	1102.4		15.219			

21 September 2000

thermalfile1	SC73-10	a-norm	100C 260rot	Wednesday, September 20, 2000 10:39 PM			
1	100	260	55	2.894	0.013	0.5	0.008
thermalfile2	SC73-10	a-norm	100C 240rot	Wednesday, September 20, 2000 10:45 PM			
2	100	240	48	2.864	0.020	0.7	0.008
thermalfile3	SC73-10	a-norm	100C 220rot	Wednesday, September 20, 2000 10:52 PM			
3	100	220	72	2.646	0.061	2.3	0.010
thermalfile4	SC73-10	a-norm	100C 200rot	Wednesday, September 20, 2000 10:58 PM			
4	100	200	82	2.562	0.050	1.9	0.009
thermalfile5	SC73-10	a-norm	100C 180rot	Wednesday, September 20, 2000 11:04 PM			
5	100	180	99	2.523	0.027	1.1	0.007
thermalfile6	SC73-10	a-norm	100C 160rot	Wednesday, September 20, 2000 11:10 PM			
6	100	160	146	2.547	0.019	0.7	0.009
thermalfile7	SC73-10	a-norm	100C 140rot	Wednesday, September 20, 2000 11:19 PM			
7	100	140	104	2.604	0.035	1.3	0.007
thermalfile10	SC73-10	a-norm	200C 150rot	Thursday, September 21, 2000 12:35 AM			
10	200	150	129	2.202	0.015	0.7	0.013
thermalfile11	SC73-10	a-norm	200C 170rot	Thursday, September 21, 2000 12:45 AM			
11	200	170	134	2.159	0.015	0.7	0.014
thermalfile12	SC73-10	a-norm	200C 190rot	Thursday, September 21, 2000 12:52 AM			
12	200	190	112	2.181	0.011	0.5	0.011
thermalfile13	SC73-10	a-norm	200C 210rot	Thursday, September 21, 2000 12:58 AM			
13	200	210	92	2.240	0.016	0.7	0.008
thermalfile14	SC73-10	a-norm	200C 230rot	Thursday, September 21, 2000 1:03 AM			
14	200	230	42	2.404	0.027	1.1	0.011

thermalfile15	SC73-10 a-norm 200C 250rot	Thursday, September 21, 2000 1:10 AM
15	200 250 39 2.415 0.014 0.6 0.008	
thermalfile16	SC73-10 a-norm 200C 270rot	Thursday, September 21, 2000 1:15 AM
16	200 270 40 2.426 0.017 0.7 0.008	
thermalfile19	SC73-10 a-norm 300C 270rot	Thursday, September 21, 2000 1:58 AM
19	300 270 63 2.183 0.020 0.9 0.008	
thermalfile20	SC73-10 a-norm 300C 250rot	Thursday, September 21, 2000 2:04 AM
20	300 250 51 2.147 0.014 0.6 0.008	
thermalfile21	SC73-10 a-norm 300C 230rot	Thursday, September 21, 2000 2:10 AM
21	300 230 63 2.067 0.014 0.7 0.009	
thermalfile22	SC73-10 a-norm 300C 210rot	Thursday, September 21, 2000 2:16 AM
22	300 210 92 2.019 0.035 1.7 0.013	
thermalfile23	SC73-10 a-norm 300C 190rot	Thursday, September 21, 2000 2:20 AM
23	300 190 74 1.963 0.030 1.5 0.013	
thermalfile24	SC73-10 a-norm 300C 170rot	Thursday, September 21, 2000 2:27 AM
24	300 170 101 1.960 0.027 1.4 0.015	
thermalfile25	SC73-10 a-norm 300C 150rot	Thursday, September 21, 2000 2:33 AM
25	300 150 114 1.998 0.022 1.1 0.013	
thermalfile28	SC73-10 a-norm 400C 150rot	Thursday, September 21, 2000 3:12 AM
28	400 150 90 1.873 0.032 1.7 0.015	
thermalfile29	SC73-10 a-norm 400C 170rot	Thursday, September 21, 2000 3:18 AM
29	400 170 105 1.816 0.030 1.7 0.016	
thermalfile30	SC73-10 a-norm 400C 190rot	Thursday, September 21, 2000 3:22 AM
30	400 190 102 1.800 0.026 1.4 0.015	
thermalfile31	SC73-10 a-norm 400C 210rot	Thursday, September 21, 2000 3:28 AM
31	400 210 80 1.857 0.031 1.7 0.016	
thermalfile32	SC73-10 a-norm 400C 230rot	Thursday, September 21, 2000 3:33 AM
32	400 230 61 1.900 0.020 1.1 0.011	
thermalfile33	SC73-10 a-norm 400C 250rot	Thursday, September 21, 2000 3:39 AM
33	400 250 39 1.942 0.012 0.6 0.008	
thermalfile34	SC73-10 a-norm 400C 270rot	Thursday, September 21, 2000 3:44 AM
34	400 270 47 2.000 0.010 0.5 0.009	
thermalfile37	SC73-10 a-norm 500C 270rot	Thursday, September 21, 2000 4:21 AM
37	500 270 68 1.837 0.010 0.5 0.009	
thermalfile38	SC73-10 a-norm 500C 250rot	Thursday, September 21, 2000 4:27 AM
38	500 250 40 1.805 0.005 0.5 0.009	
thermalfile39	SC73-10 a-norm 500C 230rot	Thursday, September 21, 2000 4:34 AM
39	500 230 58 1.733 0.005 0.5 0.009	
thermalfile40	SC73-10 a-norm 500C 210rot	Thursday, September 21, 2000 4:40 AM
40	500 210 108 1.680 0.012 0.7 0.014	
thermalfile41	SC73-10 a-norm 500C 190rot	Thursday, September 21, 2000 4:45 AM
41	500 190 126 1.626 0.014 0.9 0.016	
thermalfile42	SC73-10 a-norm 500C 170rot	Thursday, September 21, 2000 4:51 AM
42	500 170 140 1.639 0.021 1.3 0.019	

thermalfile43 SC73-10 a-norm 500C 150rotThursday, September 21, 2000 4:57 AM
 43 500 150 125 1.674 0.010 0.6 0.013
 thermalfile46 SC73-10 a-norm 600C 150rotThursday, September 21, 2000 5:58 AM
 46 600 150 55 1.663 0.005 0.5 0.011
 thermalfile47 SC73-10 a-norm 600C 170rotThursday, September 21, 2000 6:03 AM
 47 600 170 126 1.582 0.010 0.6 0.015
 thermalfile48 SC73-10 a-norm 600C 190rotThursday, September 21, 2000 6:08 AM
 48 600 190 147 1.557 0.019 1.2 0.021
 thermalfile49 SC73-10 a-norm 600C 210rotThursday, September 21, 2000 6:14 AM
 49 600 210 113 1.571 0.021 1.3 0.018
 thermalfile50 SC73-10 a-norm 600C 230rotThursday, September 21, 2000 6:19 AM
 50 600 230 88 1.590 0.008 0.5 0.013
 thermalfile51 SC73-10 a-norm 600C 250rotThursday, September 21, 2000 6:25 AM
 51 600 250 53 1.649 0.008 0.5 0.010
 thermalfile52 SC73-10 a-norm 600C 270rotThursday, September 21, 2000 6:30 AM
 52 600 270 39 1.687 0.014 0.8 0.009
 thermalfile55 SC73-10 a-norm 700C 270rotThursday, September 21, 2000 7:26 AM
 55 700 270 38 1.593 0.008 0.5 0.010
 thermalfile56 SC73-10 a-norm 700C 250rotThursday, September 21, 2000 7:33 AM
 56 700 250 71 1.562 0.019 1.2 0.017
 thermalfile57 SC73-10 a-norm 700C 230rotThursday, September 21, 2000 7:38 AM
 57 700 230 101 1.488 0.011 0.8 0.016
 thermalfile58 SC73-10 a-norm 700C 210rotThursday, September 21, 2000 7:43 AM
 58 700 210 96 1.440 0.008 0.6 0.015
 thermalfile59 SC73-10 a-norm 700C 190rotThursday, September 21, 2000 7:47 AM
 59 700 190 134 1.462 0.017 1.2 0.021
 thermalfile60 SC73-10 a-norm 700C 170rotThursday, September 21, 2000 7:52 AM
 60 700 170 73 1.516 0.013 0.9 0.015
 thermalfile61 SC73-10 a-norm 700C 150rotThursday, September 21, 2000 7:58 AM
 61 700 150 51 1.599 0.014 0.9 0.014
 thermalfile62 SC73-10 a-norm 700C 130rotThursday, September 21, 2000 8:04 AM
 62 700 130 58 1.639 0.007 0.5 0.012
 thermalfile63 SC73-10 a-norm 700C 110rotThursday, September 21, 2000 8:10 AM
 63 700 110 46 1.654 0.011 0.7 0.012
 thermalfile66 SC73-10 a-norm 800C 110rotThursday, September 21, 2000 9:21 AM
 66 800 110 48 1.539 0.007 0.5 0.011
 thermalfile67 SC73-10 a-norm 800C 130rotThursday, September 21, 2000 9:27 AM
 67 800 130 44 1.530 0.012 0.8 0.011
 thermalfile68 SC73-10 a-norm 800C 150rotThursday, September 21, 2000 9:33 AM
 68 800 150 48 1.502 0.009 0.6 0.012
 thermalfile69 SC73-10 a-norm 800C 170rotThursday, September 21, 2000 9:39 AM
 69 800 170 58 1.436 0.006 0.5 0.013
 thermalfile70 SC73-10 a-norm 800C 190rotThursday, September 21, 2000 9:48 AM
 70 800 190 119 1.379 0.010 0.7 0.017

thermalfile71 SC73-10 a-norm 800C 210rotThursday, September 21, 2000 9:55 AM
 71 800 210 109 1.363 0.008 0.6 0.017
 thermalfile72 SC73-10 a-norm 800C 230rotThursday, September 21, 2000 10:00 AM
 72 800 230 80 1.374 0.010 0.7 0.014
 thermalfile73 SC73-10 a-norm 800C 250rotThursday, September 21, 2000 10:05 AM
 73 800 250 70 1.444 0.011 0.8 0.016
 thermalfile74 SC73-10 a-norm 800C 270rotThursday, September 21, 2000 10:11 AM
 74 800 270 45 1.529 0.029 1.9 0.018
 thermalfile77 SC73-10 a-norm 900C 270rotThursday, September 21, 2000 11:24 AM
 77 900 270 35 1.364 0.007 0.5 0.014
 thermalfile78 SC73-10 a-norm 900C 250rotThursday, September 21, 2000 11:29 AM
 78 900 250 70 1.310 0.014 1.1 0.014
 thermalfile79 SC73-10 a-norm 900C 230rotThursday, September 21, 2000 11:33 AM
 79 900 230 101 1.306 0.009 0.7 0.017
 thermalfile80 SC73-10 a-norm 900C 210rotThursday, September 21, 2000 11:37 AM
 80 900 210 111 1.327 0.011 0.8 0.020
 thermalfile81 SC73-10 a-norm 900C 190rotThursday, September 21, 2000 11:42 AM
 81 900 190 62 1.381 0.009 0.7 0.015
 thermalfile82 SC73-10 a-norm 900C 170rotThursday, September 21, 2000 11:47 AM
 82 900 170 45 1.456 0.011 0.8 0.014
 thermalfile83 SC73-10 a-norm 900C 150rotThursday, September 21, 2000 11:51 AM
 83 900 150 52 1.476 0.005 0.5 0.012
 thermalfile84 SC73-10 a-norm 900C 130rotThursday, September 21, 2000 11:56 AM
 84 900 130 27 1.473 0.010 0.7 0.013
 thermalfile85 SC73-10 a-norm 900C 110rotThursday, September 21, 2000 12:01 PM
 85 900 110 34 1.430 0.010 0.7 0.015
 thermalfile0 methanol 24.8C Wednesday, September 20, 2000 10:28 PM
 0 24.8 1103.6 15.189
 thermalfile8 methanol 24.8C Wednesday, September 20, 2000 11:26 PM
 8 24.8 1103.6 15.192
 thermalfile17 methanol 25.0C Thursday, September 21, 2000 1:21 AM
 17 25.0 1103.0 15.223
 thermalfile9 methanol 24.9C Thursday, September 21, 2000 12:24 AM
 9 24.9 1103.3 15.213
 thermalfile18 methanol 24.9C Thursday, September 21, 2000 1:48 AM
 18 24.9 1103.3 15.225
 thermalfile26 methanol 24.9C Thursday, September 21, 2000 2:39 AM
 26 24.9 1103.3 15.228
 thermalfile27 methanol 24.9C Thursday, September 21, 2000 3:04 AM
 27 24.9 1103.3 15.224
 thermalfile35 methanol 25.0C Thursday, September 21, 2000 3:50 AM
 35 25.0 1103.0 15.211
 thermalfile36 methanol 24.9C Thursday, September 21, 2000 4:12 AM
 36 24.9 1103.3 15.190

thermalfile44	methanol 25.0C	Thursday, September 21, 2000 5:02 AM
44 25.0	1103.0 15.194	
thermalfile45	methanol 24.8C	Thursday, September 21, 2000 5:49 AM
45 24.8	1103.6 15.224	
thermalfile53	methanol 25.0C	Thursday, September 21, 2000 6:37 AM
53 25.0	1103.0 15.217	
thermalfile54	methanol 25.0C	Thursday, September 21, 2000 7:17 AM
54 25.0	1103.0 15.212	
thermalfile64	methanol 25.3C	Thursday, September 21, 2000 8:17 AM
64 25.3	1102.0 15.213	
thermalfile65	methanol 25.4C	Thursday, September 21, 2000 9:12 AM
65 25.4	1101.7 15.219	
thermalfile75	methanol 25.5C	Thursday, September 21, 2000 10:17 AM
75 25.5	1101.4 15.219	
thermalfile76	methanol 25.5C	Thursday, September 21, 2000 10:47 AM
76 25.5	1101.4 15.230	
thermalfile86	methanol 25.7C	Thursday, September 21, 2000 12:06 PM
86 25.7	1100.8 15.224	

23 September 2000

thermalfile1	SC73-10 a-norm RT 110rot	Saturday, September 23, 2000 3:00 PM
1 27	110 37 2.972 0.030 1.0 0.012	
thermalfile2	SC73-10 a-norm RT 130rot	Saturday, September 23, 2000 3:08 PM
2 27	130 28 3.054 0.028 0.9 0.011	
thermalfile3	SC73-10 a-norm RT 150rot	Saturday, September 23, 2000 3:15 PM
3 27	150 29 3.135 0.061 2.0 0.012	
thermalfile4	SC73-10 a-norm RT 170rot	Saturday, September 23, 2000 3:23 PM
4 27	170 45 3.110 0.064 2.0 0.015	
thermalfile5	SC73-10 a-norm RT 190rot	Saturday, September 23, 2000 3:28 PM
5 27	190 29 3.211 0.088 2.7 0.012	
thermalfile6	SC73-10 a-norm RT 210rot	Saturday, September 23, 2000 3:34 PM
6 27	210 39 3.027 0.047 1.5 0.014	
thermalfile7	SC73-10 a-norm RT 230rot	Saturday, September 23, 2000 3:42 PM
7 27	230 37 2.879 0.036 1.3 0.011	
thermalfile8	SC73-10 a-norm RT 250rot	Saturday, September 23, 2000 3:48 PM
8 27	250 31 2.811 0.028 1.0 0.009	
thermalfile9	SC73-10 a-norm RT 270rot	Saturday, September 23, 2000 3:56 PM
9 27	270 38 2.813 0.034 1.2 0.013	
thermalfile0	methanol 21.5C	Saturday, September 23, 2000 2:44 PM
0 21.5	1114.2 15.256	
thermalfile10	methanol 22.4C	Saturday, September 23, 2000 4:03 PM

10 22.4 1111.3 15.229

28 September 2000

thermalfile10	SC73-10 a-norm RT 250rot	Thursday, September 28, 2000 6:52 PM
10 27	250 28 3.367 0.061 1.8 0.014	
thermalfile11	SC73-10 a-norm RT 270rot	Thursday, September 28, 2000 7:02 PM
11 27	270 32 3.397 0.041 1.2 0.018	
thermalfile3	SC73-10 a-norm RT 110rot	Thursday, September 28, 2000 5:55 PM
3 27	110 28 3.569 0.067 1.9 0.012	
thermalfile4	SC73-10 a-norm RT 130rot	Thursday, September 28, 2000 6:05 PM
4 27	130 28 3.655 0.058 1.6 0.015	
thermalfile5	SC73-10 a-norm RT 150rot	Thursday, September 28, 2000 6:11 PM
5 27	150 35 3.821 0.023 0.6 0.012	
thermalfile6	SC73-10 a-norm RT 170rot	Thursday, September 28, 2000 6:18 PM
6 27	170 33 3.753 0.071 1.9 0.014	
thermalfile7	SC73-10 a-norm RT 190rot	Thursday, September 28, 2000 6:26 PM
7 27	190 28 3.738 0.045 1.2 0.014	
thermalfile8	SC73-10 a-norm RT 210rot	Thursday, September 28, 2000 6:44 PM
8 27	210 31 3.423 0.059 1.7 0.012	
thermalfile9	SC73-10 a-norm RT 230rot	Thursday, September 28, 2000 6:44 PM
9 27	230 31 3.423 0.059 1.7 0.012	
thermalfile14	SC73-10 a-norm 100C 270rot	Thursday, September 28, 2000 9:15 PM
14 100	270 56 2.709 0.012 0.5 0.007	
thermalfile15	SC73-10 a-norm 100C 250rot	Thursday, September 28, 2000 9:25 PM
15 100	250 65 2.683 0.016 0.6 0.007	
thermalfile16	SC73-10 a-norm 100C 230rot	Thursday, September 28, 2000 9:36 PM
16 100	230 95 2.699 0.040 1.5 0.008	
thermalfile17	SC73-10 a-norm 100C 210rot	Thursday, September 28, 2000 9:46 PM
17 100	210 56 2.864 0.026 0.9 0.007	
thermalfile18	SC73-10 a-norm 100C 190rot	Thursday, September 28, 2000 9:53 PM
18 100	190 60 2.971 0.040 1.3 0.008	
thermalfile19	SC73-10 a-norm 100C 170rot	Thursday, September 28, 2000 10:01 PM
19 100	170 67 3.046 0.036 1.2 0.008	
thermalfile20	SC73-10 a-norm 100C 150rot	Thursday, September 28, 2000 10:11 PM
20 100	150 23 3.101 0.027 0.9 0.010	
thermalfile21	SC73-10 a-norm 100C 130rot	Thursday, September 28, 2000 10:19 PM
21 100	130 34 2.916 0.046 1.6 0.009	
thermalfile22	SC73-10 a-norm 100C 110rot	Thursday, September 28, 2000 10:26 PM
22 100	110 58 2.854 0.022 0.8 0.007	
thermalfile25	SC73-10 a-norm 200C 110rot	Thursday, September 28, 2000 11:54 PM
25 200	110 47 2.329 0.009 0.5 0.007	

thermalfile26	SC73-10 a-norm 200C 130rot	Friday, September 29, 2000 12:03 AM
26 200	130 38 2.386 0.025 1.0 0.007	
thermalfile27	SC73-10 a-norm 200C 150rot	Friday, September 29, 2000 12:12 AM
27 200	150 42 2.472 0.038 1.6 0.007	
thermalfile28	SC73-10 a-norm 200C 170rot	Friday, September 29, 2000 12:21 AM
28 200	170 42 2.466 0.045 1.8 0.008	
thermalfile29	SC73-10 a-norm 200C 190rot	Friday, September 29, 2000 12:27 AM
29 200	190 35 2.460 0.015 0.6 0.007	
thermalfile30	SC73-10 a-norm 200C 210rot	Friday, September 29, 2000 12:32 AM
30 200	210 28 2.388 0.012 0.5 0.007	
thermalfile31	SC73-10 a-norm 200C 230rot	Friday, September 29, 2000 12:41 AM
31 200	230 65 2.274 0.008 0.5 0.008	
thermalfile32	SC73-10 a-norm 200C 250rot	Friday, September 29, 2000 12:48 AM
32 200	250 36 2.181 0.029 1.3 0.008	
thermalfile33	SC73-10 a-norm 200C 270rot	Friday, September 29, 2000 12:56 AM
33 200	270 51 2.244 0.011 0.5 0.006	
thermalfile12	methanol 24.2C	Thursday, September 28, 2000 7:08 PM
12 24.2	1105.6 15.233	
thermalfile2	methanol 23.7C	Thursday, September 28, 2000 5:31 PM
2 23.7	1107.2 15.235	
thermalfile13	methanol 25.1C	Thursday, September 28, 2000 9:04 PM
13 25.1	1102.7 15.268	
thermalfile23	methanol 24.9C	Thursday, September 28, 2000 10:34 PM
23 24.9	1103.3 15.257	
thermalfile24	methanol 25.2C	Thursday, September 28, 2000 11:43 PM
24 25.2	1102.4 15.272	
thermalfile35	methanol 25.2C	Friday, September 29, 2000 1:08 AM
35 25.2	1102.4 15.274	

2 October 2000

thermalfile1	SC73-10 b-norm RT 110rot	Monday, October 2, 2000 7:06 PM
1 27	110 44 3.691 0.024 0.6 0.009	
thermalfile2	SC73-10 b-norm RT 130rot	Monday, October 2, 2000 7:20 PM
2 27	130 43 3.672 0.024 0.6 0.009	
thermalfile3	SC73-10 b-norm RT 150rot	Monday, October 2, 2000 7:29 PM
3 27	150 67 3.718 0.032 0.9 0.008	
thermalfile4	SC73-10 b-norm RT 170rot	Monday, October 2, 2000 7:39 PM
4 27	170 61 3.887 0.033 0.8 0.009	
thermalfile5	SC73-10 b-norm RT 190rot	Monday, October 2, 2000 7:47 PM
5 27	190 44 3.923 0.073 1.9 0.014	
thermalfile6	SC73-10 b-norm RT 210rot	Monday, October 2, 2000 7:54 PM

6	27	210	37	3.929	0.153	3.9	0.018
thermalfile7	SC73-10 b-norm RT 230rot						Monday, October 2, 2000 8:01 PM
7	27	230	36	3.910	0.133	3.4	0.019
thermalfile8	SC73-10 b-norm RT 250rot						Monday, October 2, 2000 8:11 PM
8	27	250	39	3.932	0.057	1.4	0.012
thermalfile9	SC73-10 b-norm RT 270rot						Monday, October 2, 2000 8:18 PM
9	27	270	59	3.787	0.050	1.3	0.011
thermalfile12	SC73-10 b-norm 100C 270rot						Monday, October 2, 2000 11:42 PM
12	100	270	107	2.938	0.046	1.6	0.006
thermalfile13	SC73-10 b-norm 100C 250rot						Monday, October 2, 2000 11:52 PM
13	100	250	79	3.087	0.045	1.5	0.008
thermalfile14	SC73-10 b-norm 100C 230rot						Tuesday, October 3, 2000 12:00 AM
14	100	230	45	3.170	0.059	1.9	0.011
thermalfile15	SC73-10 b-norm 100C 210rot						Tuesday, October 3, 2000 12:07 AM
15	100	210	38	3.201	0.079	2.5	0.012
thermalfile16	SC73-10 b-norm 100C 190rot						Tuesday, October 3, 2000 12:15 AM
16	100	190	45	3.131	0.064	2.0	0.011
thermalfile17	SC73-10 b-norm 100C 170rot						Tuesday, October 3, 2000 12:23 AM
17	100	170	68	3.057	0.043	1.4	0.008
thermalfile18	SC73-10 b-norm 100C 150rot						Tuesday, October 3, 2000 12:31 AM
18	100	150	63	2.962	0.039	1.3	0.009
thermalfile19	SC73-10 b-norm 100C 130rot						Tuesday, October 3, 2000 12:41 AM
19	100	130	33	2.961	0.018	0.6	0.008
thermalfile20	SC73-10 b-norm 100C 110rot						Tuesday, October 3, 2000 12:49 AM
20	100	110	30	2.970	0.019	0.6	0.008
thermalfile23	SC73-10 b-norm 200C 110rot						Tuesday, October 3, 2000 2:56 AM
23	200	110	55	2.386	0.019	0.8	0.007
thermalfile24	SC73-10 b-norm 200C 130rot						Tuesday, October 3, 2000 3:02 AM
24	200	130	58	2.379	0.021	0.9	0.006
thermalfile25	SC73-10 b-norm 200C 150rot						Tuesday, October 3, 2000 3:08 AM
25	200	150	107	2.456	0.013	0.5	0.008
thermalfile26	SC73-10 b-norm 200C 170rot						Tuesday, October 3, 2000 3:19 AM
26	200	170	83	2.506	0.018	0.7	0.006
thermalfile27	SC73-10 b-norm 200C 190rot						Tuesday, October 3, 2000 3:27 AM
27	200	190	81	2.643	0.013	0.5	0.005
thermalfile28	SC73-10 b-norm 200C 210rot						Tuesday, October 3, 2000 3:36 AM
28	200	210	47	2.663	0.035	1.3	0.007
thermalfile29	SC73-10 b-norm 200C 230rot						Tuesday, October 3, 2000 3:44 AM
29	200	230	33	2.703	0.015	0.5	0.005
thermalfile30	SC73-10 b-norm 200C 250rot						Tuesday, October 3, 2000 3:54 AM
30	200	250	68	2.608	0.013	0.5	0.006
thermalfile31	SC73-10 b-norm 200C 270rot						Tuesday, October 3, 2000 4:00 AM
31	200	270	59	2.486	0.015	0.6	0.006
thermalfile34	SC73-10 b-norm 300C 270rot						Tuesday, October 3, 2000 5:09 AM

34	300	270	80	2.180	0.010	0.5	0.007
thermalfile35	SC73-10	b-norm	300C	250rot			Tuesday, October 3, 2000 5:19 AM
35	300	250	78	2.269	0.007	0.5	0.007
thermalfile36	SC73-10	b-norm	300C	230rot			Tuesday, October 3, 2000 5:26 AM
36	300	230	54	2.327	0.028	1.2	0.006
thermalfile37	SC73-10	b-norm	300C	210rot			Tuesday, October 3, 2000 5:31 AM
37	300	210	50	2.339	0.025	1.1	0.006
thermalfile38	SC73-10	b-norm	300C	190rot			Tuesday, October 3, 2000 5:38 AM
38	300	190	63	2.294	0.013	0.6	0.006
thermalfile39	SC73-10	b-norm	300C	170rot			Tuesday, October 3, 2000 5:45 AM
39	300	170	85	2.224	0.013	0.6	0.008
thermalfile40	SC73-10	b-norm	300C	150rot			Tuesday, October 3, 2000 5:50 AM
40	300	150	92	2.144	0.008	0.5	0.009
thermalfile41	SC73-10	b-norm	300C	130rot			Tuesday, October 3, 2000 5:55 AM
41	300	130	62	2.076	0.015	0.7	0.007
thermalfile42	SC73-10	b-norm	300C	110rot			Tuesday, October 3, 2000 6:01 AM
42	300	110	69	2.109	0.008	0.5	0.008
thermalfile45	SC73-10	b-norm	400C	110rot			Tuesday, October 3, 2000 7:21 AM
45	400	110	45	1.880	0.016	0.8	0.008
thermalfile46	SC73-10	b-norm	400C	130rot			Tuesday, October 3, 2000 7:34 AM
46	400	130	55	1.876	0.015	0.8	0.008
thermalfile47	SC73-10	b-norm	400C	150rot			Tuesday, October 3, 2000 7:42 AM
47	400	150	75	1.940	0.007	0.5	0.009
thermalfile48	SC73-10	b-norm	400C	170rot			Tuesday, October 3, 2000 7:50 AM
48	400	170	80	2.017	0.012	0.6	0.009
thermalfile49	SC73-10	b-norm	400C	190rot			Tuesday, October 3, 2000 7:56 AM
49	400	190	62	2.083	0.016	0.8	0.006
thermalfile50	SC73-10	b-norm	400C	210rot			Tuesday, October 3, 2000 8:06 AM
50	400	210	54	2.135	0.015	0.7	0.006
thermalfile51	SC73-10	b-norm	400C	230rot			Tuesday, October 3, 2000 8:12 AM
51	400	230	57	2.120	0.009	0.5	0.007
thermalfile52	SC73-10	b-norm	400C	250rot			Tuesday, October 3, 2000 8:18 AM
52	400	250	64	2.049	0.010	0.5	0.008
thermalfile53	SC73-10	b-norm	400C	270rot			Tuesday, October 3, 2000 8:24 AM
53	400	270	99	1.973	0.009	0.5	0.010
thermalfile57	SC73-10	b-norm	500C	270rot			Tuesday, October 3, 2000 9:43 AM
57	500	270	126	1.833	0.018	1.0	0.015
thermalfile58	SC73-10	b-norm	500C	250rot			Tuesday, October 3, 2000 9:49 AM
58	500	250	114	1.913	0.015	0.8	0.012
thermalfile59	SC73-10	b-norm	500C	230rot			Tuesday, October 3, 2000 9:56 AM
59	500	230	82	1.983	0.014	0.7	0.009
thermalfile60	SC73-10	b-norm	500C	210rot			Tuesday, October 3, 2000 10:02 AM
60	500	210	75	2.000	0.014	0.7	0.010
thermalfile61	SC73-10	b-norm	500C	190rot			Tuesday, October 3, 2000 10:07 AM

61	500	190	78	1.951	0.015	0.8	0.010
thermalfile62	SC73-10 b-norm 500C 170rot						Tuesday, October 3, 2000 10:12 AM
62	500	170	100	1.873	0.017	0.9	0.012
thermalfile63	SC73-10 b-norm 500C 150rot						Tuesday, October 3, 2000 10:20 AM
63	500	150	77	1.807	0.017	0.9	0.013
thermalfile64	SC73-10 b-norm 500C 130rot						Tuesday, October 3, 2000 10:27 AM
64	500	130	71	1.771	0.019	1.1	0.013
thermalfile65	SC73-10 b-norm 500C 110rot						Tuesday, October 3, 2000 10:33 AM
65	500	110	88	1.764	0.009	0.5	0.012
thermalfile68	SC73-10 b-norm 600C 110rot						Tuesday, October 3, 2000 11:39 AM
68	600	110	97	1.675	0.022	1.3	0.015
thermalfile69	SC73-10 b-norm 600C 130rot						Tuesday, October 3, 2000 11:46 AM
69	600	130	81	1.657	0.024	1.5	0.016
thermalfile70	SC73-10 b-norm 600C 150rot						Tuesday, October 3, 2000 11:51 AM
70	600	150	131	1.682	0.021	1.2	0.018
thermalfile71	SC73-10 b-norm 600C 170rot						Tuesday, October 3, 2000 11:59 AM
71	600	170	126	1.756	0.025	1.4	0.018
thermalfile72	SC73-10 b-norm 600C 190rot						Tuesday, October 3, 2000 12:05 PM
72	600	190	78	1.844	0.023	1.2	0.018
thermalfile73	SC73-10 b-norm 600C 210rot						Tuesday, October 3, 2000 12:14 PM
73	600	210	67	1.881	0.024	1.3	0.012
thermalfile74	SC73-10 b-norm 600C 230rot						Tuesday, October 3, 2000 12:20 PM
74	600	230	84	1.811	0.017	0.9	0.008
thermalfile75	SC73-10 b-norm 600C 250rot						Tuesday, October 3, 2000 12:27 PM
75	600	250	104	1.761	0.010	0.5	0.011
thermalfile76	SC73-10 b-norm 600C 270rot						Tuesday, October 3, 2000 12:31 PM
76	600	270	107	1.687	0.011	0.6	0.011
thermalfile79	SC73-10 b-norm RT 270rot						Tuesday, October 3, 2000 5:00 PM
79	27	270	67	3.686	0.046	1.2	0.009
thermalfile80	SC73-10 b-norm RT 250rot						Tuesday, October 3, 2000 5:09 PM
80	27	250	50	3.822	0.039	1.0	0.010
thermalfile81	SC73-10 b-norm RT 230rot						Tuesday, October 3, 2000 5:18 PM
81	27	230	36	4.034	0.017	0.5	0.010
thermalfile82	SC73-10 b-norm RT 210rot						Tuesday, October 3, 2000 5:26 PM
82	27	210	33	3.933	0.075	1.9	0.013
thermalfile83	SC73-10 b-norm RT 190rot						Tuesday, October 3, 2000 5:33 PM
83	27	190	43	3.950	0.013	0.5	0.010
thermalfile84	SC73-10 b-norm RT 170rot						Tuesday, October 3, 2000 5:41 PM
84	27	170	67	3.783	0.027	0.7	0.007
thermalfile85	SC73-10 b-norm RT 150rot						Tuesday, October 3, 2000 5:46 PM
85	27	150	63	3.643	0.031	0.9	0.008
thermalfile86	SC73-10 b-norm RT 130rot						Tuesday, October 3, 2000 5:52 PM
86	27	130	40	3.533	0.034	1.0	0.010
thermalfile87	SC73-10 b-norm RT 110rot						Tuesday, October 3, 2000 5:59 PM

87	27	110	34	3.569	0.050	1.4	0.009
thermalfile0	methanol	23.4C					Monday, October 2, 2000 6:54 PM
0	23.4	1108.1		15.245			
thermalfile10	methanol	23.0C					Monday, October 2, 2000 8:25 PM
10	23.0	1109.4		15.297			
thermalfile11	methanol	23.0C					Monday, October 2, 2000 11:25 PM
11	23.0	1109.4		15.235			
thermalfile21	methanol	22.6C					Tuesday, October 3, 2000 12:55 AM
21	22.6	1110.7		15.289			
thermalfile22	methanol	22.8C					Tuesday, October 3, 2000 2:35 AM
22	22.8	1110.0		15.253			
thermalfile32	methanol	22.7C					Tuesday, October 3, 2000 4:07 AM
32	22.7	1110.4		15.256			
thermalfile33	methanol	22.6C					Tuesday, October 3, 2000 4:57 AM
33	22.6	1110.7		15.253			
thermalfile43	methanol	22.6C					Tuesday, October 3, 2000 6:07 AM
43	22.6	1110.7		15.257			
thermalfile44	methanol	22.4C					Tuesday, October 3, 2000 7:13 AM
44	22.4	1111.3		15.272			
thermalfile54	methanol	22.7C					Tuesday, October 3, 2000 8:33 AM
54	22.7	1110.4		15.273			
thermalfile55	methanol	23.2C					Tuesday, October 3, 2000 9:27 AM
55	23.2	1108.8		15.294			
thermalfile66	methanol	23.4C					Tuesday, October 3, 2000 10:43 AM
66	23.4	1108.1		15.268			
thermalfile67	methanol	23.5C					Tuesday, October 3, 2000 11:30 AM
67	23.5	1107.8		15.287			
thermalfile77	methanol	23.8C					Tuesday, October 3, 2000 12:36 PM
77	23.8	1106.8		15.257			
thermalfile78	methanol	23.0C					Tuesday, October 3, 2000 4:51 PM
78	23.0	1109.4		15.293			
thermalfile89	methanol	23.6C					Tuesday, October 3, 2000 6:11 PM
89	23.6	1107.5		15.283			

FA-147337*29 March 2000*

thermalfile1	fa147337	a-norm	RT	0deg			Wednesday, March 29, 2000 6:53 PM
1	27	0	39	1.856	0.007	0.5	0.008
thermalfile101	fa147337	a-norm	RT	0deg			Wednesday, March 29, 2000 6:53 PM

101	27	0	39	1.851	0.007	0.5	0.008	
thermalfile102	fa147337	a-norm	RT 20deg	Wednesday, March 29, 2000 7:06 PM				
102	27	20	40	2.347	0.017	0.7	0.008	
thermalfile103	fa147337	a-norm	RT 40deg	Wednesday, March 29, 2000 7:17 PM				
103	27	40	61	2.791	0.028	1.0	0.006	
thermalfile104	fa147337	a-norm	RT 60deg	Wednesday, March 29, 2000 7:28 PM				
104	27	60	85	2.888	0.048	1.7	0.006	
thermalfile105	fa147337	a-norm	RT 80deg	Wednesday, March 29, 2000 7:39 PM				
105	27	80	66	2.798	0.024	0.9	0.005	
thermalfile106	fa147337	a-norm	RT 100deg	Wednesday, March 29, 2000 7:49 PM				
106	27	100	74	2.505	0.043	1.7	0.013	
thermalfile107	fa147337	a-norm	RT 120deg	Wednesday, March 29, 2000 7:59 PM				
107	27	120	56	1.956	0.025	1.3	0.013	
thermalfile108	fa147337	a-norm	RT 140deg	Wednesday, March 29, 2000 8:09 PM				
108	27	140	46	1.622	0.009	0.6	0.012	
thermalfile2	fa147337	a-norm	RT 20deg	Wednesday, March 29, 2000 7:06 PM				
2	27	20	40	2.351	0.021	0.9	0.009	
thermalfile3	fa147337	a-norm	RT 40deg	Wednesday, March 29, 2000 7:17 PM				
3	27	40	61	2.794	0.030	1.1	0.007	
thermalfile4	fa147337	a-norm	RT 60deg	Wednesday, March 29, 2000 7:28 PM				
4	27	60	84	2.889	0.048	1.7	0.006	
thermalfile5	fa147337	a-norm	RT 80deg	Wednesday, March 29, 2000 7:39 PM				
5	27	80	66	2.800	0.024	0.9	0.005	
thermalfile6	fa147337	a-norm	RT 100deg	Wednesday, March 29, 2000 7:49 PM				
6	27	100	74	2.507	0.046	1.8	0.014	
thermalfile7	fa147337	a-norm	RT 120deg	Wednesday, March 29, 2000 7:59 PM				
7	27	120	56	1.959	0.027	1.4	0.014	
thermalfile8	fa147337	a-norm	RT 140deg	Wednesday, March 29, 2000 8:09 PM				
8	27	140	46	1.625	0.011	0.7	0.012	
thermalfile0	methanol 25.3C			Wednesday, March 29, 2000 6:36 PM				
0	25.3	1102.0	14.317					
thermalfile10	methanol 24.4C			Wednesday, March 29, 2000 8:26 PM				
10	24.4	1104.9	14.283					

30 March 2000

thermalfile1	Fa147337	c-norm	RT 0deg	Thursday, March 30, 2000 3:07 PM				
1	27	0	15	1.472	0.008	0.5	0.015	
thermalfile2	Fa147337	c-norm	RT 20deg	Thursday, March 30, 2000 3:25 PM				
2	27	20	24	1.672	0.021	1.2	0.017	
thermalfile3	Fa147337	c-norm	RT 40deg	Thursday, March 30, 2000 3:46 PM				
3	27	40	35	2.127	0.019	0.9	0.014	

thermalfile4 Fa147337 c-norm RT 60deg Thursday, March 30, 2000 3:56 PM
 4 27 60 66 2.645 0.020 0.8 0.006
 thermalfile5 Fa147337 c-norm RT 80deg Thursday, March 30, 2000 4:07 PM
 5 27 80 99 2.842 0.040 1.4 0.005
 thermalfile6 Fa147337 c-norm RT 100deg Thursday, March 30, 2000 4:14 PM
 6 27 100 107 2.792 0.034 1.2 0.004
 thermalfile7 Fa147337 c-norm RT 120deg Thursday, March 30, 2000 4:21 PM
 7 27 120 80 2.442 0.029 1.2 0.005
 thermalfile8 Fa147337 c-norm RT 140deg Thursday, March 30, 2000 4:35 PM
 8 27 140 23 2.026 0.010 0.5 0.009
 thermalfile9 Fa147337 c-norm RT 160deg Thursday, March 30, 2000 4:50 PM
 9 27 160 21 1.593 0.017 1.0 0.018
 thermalfile0 methanol 25.2C Thursday, March 30, 2000 2:45 PM
 0 25.2 1102.4 14.543
 thermalfile11 methanol 25.9C Thursday, March 30, 2000 5:13 PM
 11 25.9 1100.1 14.578

31 March 2000

thermalfile1 Fa147337 a-norm RT 260rot Friday, March 31, 2000 2:49 PM
 1 27 260 19 2.491 0.013 0.5 0.006
 thermalfile10 Fa147337 a-norm RT 140rot Friday, March 31, 2000 5:00 PM
 10 27 140 39 1.827 0.031 1.7 0.014
 thermalfile11 Fa147337 a-norm RT 120rot Friday, March 31, 2000 5:12 PM
 11 27 120 44 2.063 0.015 0.7 0.006
 thermalfile12 Fa147337 a-norm RT 110rot Friday, March 31, 2000 5:23 PM
 12 27 110 13 2.266 0.012 0.5 0.010
 thermalfile13 Fa147337 a-norm RT 160rot Friday, March 31, 2000 5:47 PM
 13 27 160 17 1.426 0.006 0.5 0.012
 thermalfile14 Fa147337 a-norm RT 180rot Friday, March 31, 2000 5:54 PM
 14 27 180 6 1.304 0.044 3.4 0.030
 thermalfile2 Fa147337 a-norm RT 240rot Friday, March 31, 2000 3:14 PM
 2 27 240 28 1.996 0.022 1.1 0.013
 thermalfile3 Fa147337 a-norm RT 220rot Friday, March 31, 2000 3:22 PM
 3 27 220 16 1.545 0.031 2.0 0.022
 thermalfile4 Fa147337 a-norm RT 200rot Friday, March 31, 2000 3:34 PM
 4 27 200 8 1.279 0.034 2.6 0.029
 thermalfile5 Fa147337 a-norm RT 180rot Friday, March 31, 2000 3:47 PM
 5 27 180 6 1.210 0.029 2.4 0.024
 thermalfile0 methanol 25.4C Friday, March 31, 2000 2:09 PM
 0 25.4 1101.7 14.586
 thermalfile15 methanol 26.1C Friday, March 31, 2000 6:03 PM

15	26.1	1099.5	14.615	
thermalfile6	methanol 26.6C			Friday, March 31, 2000 3:58 PM
6	26.6	1097.9	14.678	
thermalfile7	methanol 26.7C			Friday, March 31, 2000 4:08 PM
7	26.7	1097.6	14.388	
thermalfile8	methanol 26.7C			Friday, March 31, 2000 4:23 PM
8	26.7	1097.6	14.484	

5 April 2000

thermalfile2	Fa147337 a-norm RT 110rot				Wednesday, April 5, 2000 2:40 PM
2	27	110	17	1.639	0.014 0.9 0.015
thermalfile3	Fa147337 a-norm RT 130rot				Wednesday, April 5, 2000 2:59 PM
3	27	130	58	2.010	0.032 1.6 0.012
thermalfile4	Fa147337 a-norm RT 150rot				Wednesday, April 5, 2000 3:23 PM
4	27	150	85	2.335	0.029 1.2 0.006
thermalfile5	Fa147337 a-norm RT 170rot				Wednesday, April 5, 2000 3:55 PM
5	27	170	53	2.829	0.021 0.8 0.007
thermalfile6	Fa147337 a-norm RT 190rot				Wednesday, April 5, 2000 4:05 PM
6	27	190	83	2.901	0.056 1.9 0.006
thermalfile7	Fa147337 a-norm RT 210rot				Wednesday, April 5, 2000 4:22 PM
7	27	210	47	2.839	0.026 0.9 0.008
thermalfile8	Fa147337 a-norm RT 230rot				Wednesday, April 5, 2000 4:32 PM
8	27	230	45	2.441	0.031 1.3 0.009
thermalfile2	Fa147337 a-norm RT 110rot				Wednesday, April 5, 2000 2:40 PM
2	27	110	17	1.639	0.014 0.9 0.015
thermalfile3	Fa147337 a-norm RT 130rot				Wednesday, April 5, 2000 2:59 PM
3	27	130	58	2.010	0.032 1.6 0.012
thermalfile4	Fa147337 a-norm RT 150rot				Wednesday, April 5, 2000 3:23 PM
4	27	150	85	2.335	0.029 1.2 0.006
thermalfile5	Fa147337 a-norm RT 170rot				Wednesday, April 5, 2000 3:55 PM
5	27	170	53	2.829	0.021 0.8 0.007
thermalfile6	Fa147337 a-norm RT 190rot				Wednesday, April 5, 2000 4:05 PM
6	27	190	83	2.901	0.056 1.9 0.006
thermalfile7	Fa147337 a-norm RT 210rot				Wednesday, April 5, 2000 4:22 PM
7	27	210	47	2.839	0.026 0.9 0.008
thermalfile8	Fa147337 a-norm RT 230rot				Wednesday, April 5, 2000 4:32 PM
8	27	230	45	2.441	0.031 1.3 0.009
thermalfile0	methanol 23.1C				Wednesday, April 5, 2000 1:56 PM
0	23.1	1109.1	14.581		
thermalfile9	methanol 23.8C				Wednesday, April 5, 2000 5:01 PM
9	23.8	1106.8	14.630		

6 April 2000

thermalfile13	Fa147337 a-norm 200C 120rot	Thursday, April 6, 2000 6:18 PM
13 200	120 260 1.650 0.035 2.1	0.035
thermalfile14	Fa147337 a-norm 200C 120rot	Thursday, April 6, 2000 6:28 PM
14 200	120 272 1.637 0.032 2.0	0.025
thermalfile15	Fa147337 a-norm 200C 130rot	Thursday, April 6, 2000 6:42 PM
15 200	130 187 1.728 0.044 2.6	0.027
thermalfile16	Fa147337 a-norm 200C 130rot	Thursday, April 6, 2000 6:48 PM
16 200	130 178 1.728 0.040 2.3	0.018
thermalfile17	Fa147337 a-norm 200C 160rot	Thursday, April 6, 2000 6:56 PM
17 200	160 188 1.540 0.037 2.4	0.021
thermalfile18	Fa147337 a-norm 200C 180rot	Thursday, April 6, 2000 7:07 PM
18 200	180 153 1.295 0.027 2.1	0.023
thermalfile19	Fa147337 a-norm 200C 200rot	Thursday, April 6, 2000 7:15 PM
19 200	200 81 1.037 0.006 0.6	0.027
thermalfile2	Fa147337 a-norm 100C 240rot	Thursday, April 6, 2000 3:38 PM
2 100	240 41 1.210 0.009 0.8	0.014
thermalfile20	Fa147337 a-norm 200C 220rot	Thursday, April 6, 2000 7:24 PM
20 200	220 54 0.950 0.016 1.7	0.018
thermalfile21	Fa147337 a-norm 200C 240rot	Thursday, April 6, 2000 7:32 PM
21 200	240 71 1.024 0.016 1.6	0.022
thermalfile26	Fa147337 a-norm 300C 120rot	Thursday, April 6, 2000 10:18 PM
26 300	120 174 1.447 0.025 1.7	0.018
thermalfile27	Fa147337 a-norm 300C 130rot	Thursday, April 6, 2000 10:27 PM
27 300	130 149 1.476 0.029 1.9	0.019
thermalfile28	Fa147337 a-norm 300C 160rot	Thursday, April 6, 2000 10:36 PM
28 300	160 122 1.270 0.012 1.0	0.011
thermalfile29	Fa147337 a-norm 300C 180rot	Thursday, April 6, 2000 10:48 PM
29 300	180 61 1.079 0.009 0.8	0.009
thermalfile3	Fa147337 a-norm 100C 220rot	Thursday, April 6, 2000 3:46 PM
3 100	220 53 1.131 0.007 0.6	0.018
thermalfile4	Fa147337 a-norm 100C 200rot	Thursday, April 6, 2000 4:01 PM
4 100	200 61 1.255 0.009 0.7	0.016
thermalfile5	Fa147337 a-norm 100C 180rot	Thursday, April 6, 2000 4:13 PM
5 100	180 46 1.559 0.018 1.2	0.014
thermalfile6	Fa147337 a-norm 100C 160rot	Thursday, April 6, 2000 4:24 PM
6 100	160 109 1.906 0.028 1.5	0.015
thermalfile7	Fa147337 a-norm 100C 140rot	Thursday, April 6, 2000 4:32 PM
7 100	140 112 2.070 0.025 1.2	0.012
thermalfile8	Fa147337 a-norm 100C 120rot	Thursday, April 6, 2000 4:39 PM

8	100	120	108	2.057	0.025	1.2	0.012	
thermalfile0	methanol	23.4C						Thursday, April 6, 2000 3:10 PM
0	23.4	1108.1		14.495				
thermalfile10	methanol	23.6C						Thursday, April 6, 2000 4:58 PM
10	23.6	1107.5		14.612				
thermalfile11	methanol	23.7C						Thursday, April 6, 2000 5:51 PM
11	23.7	1107.2		14.526				
thermalfile23	methanol	24.0C						Thursday, April 6, 2000 7:48 PM
23	24.0	1106.2		14.733				
thermalfile24	methanol	23.8C						Thursday, April 6, 2000 9:54 PM
24	23.8	1106.8		14.564				
thermalfile30	methanol	23.5C						Thursday, April 6, 2000 11:20 PM
30	23.5	1107.8		14.602				

7 April 2000

thermalfile10	Fa147337	a-norm	300C	200rot				Friday, April 7, 2000 7:16 PM
10	300	200	32	0.887	0.003	0.5	0.019	
thermalfile11	Fa147337	a-norm	300C	180rot				Friday, April 7, 2000 7:25 PM
11	300	180	30	1.075	0.007	0.7	0.017	
thermalfile12	Fa147337	a-norm	300C	160rot				Friday, April 7, 2000 7:36 PM
12	300	160	22	1.305	0.008	0.6	0.014	
thermalfile13	Fa147337	a-norm	300C	140rot				Friday, April 7, 2000 7:44 PM
13	300	140	94	1.441	0.015	1.1	0.017	
thermalfile14	Fa147337	a-norm	300C	120rot				Friday, April 7, 2000 7:53 PM
14	300	120	46	1.459	0.015	1.0	0.015	
thermalfile18	Fa147337	a-norm	400C	120rot				Friday, April 7, 2000 9:37 PM
18	400	120	141	1.271	0.010	0.8	0.014	
thermalfile19	Fa147337	a-norm	400C	140rot				Friday, April 7, 2000 9:44 PM
19	400	140	114	1.268	0.008	0.6	0.012	
thermalfile2	Fa147337	a-norm	RT	120rot				Friday, April 7, 2000 3:12 PM
2	27	120	127	2.343	0.019	0.8	0.012	
thermalfile20	Fa147337	a-norm	400C	160rot				Friday, April 7, 2000 9:59 PM
20	400	160	66	1.153	0.007	0.6	0.010	
thermalfile21	Fa147337	a-norm	400C	180rot				Friday, April 7, 2000 10:06 PM
21	400	180	49	0.988	0.011	1.1	0.014	
thermalfile22	Fa147337	a-norm	400C	200rot				Friday, April 7, 2000 10:13 PM
22	400	200	49	0.817	0.004	0.5	0.015	
thermalfile23	Fa147337	a-norm	400C	220rot				Friday, April 7, 2000 10:21 PM
23	400	220	27	0.753	0.004	0.5	0.015	
thermalfile24	Fa147337	a-norm	400C	240rot				Friday, April 7, 2000 10:30 PM
24	400	240	30	0.821	0.005	0.6	0.017	

thermalfile28	Fa147337 a-norm 500C 240rot	Saturday, April 8, 2000 12:03 AM
28 500	240 16 0.747 0.006 0.9	0.011
thermalfile29	Fa147337 a-norm 500C 220rot	Saturday, April 8, 2000 12:10 AM
29 500	220 23 0.706 0.004 0.6	0.017
thermalfile3	Fa147337 a-norm RT 130rot	Friday, April 7, 2000 3:28 PM
3 27	130 50 2.360 0.011 0.5	0.009
thermalfile30	Fa147337 a-norm 500C 200rot	Saturday, April 8, 2000 12:17 AM
30 500	200 16 0.782 0.006 0.7	0.015
thermalfile31	Fa147337 a-norm 500C 180rot	Saturday, April 8, 2000 12:26 AM
31 500	180 16 0.931 0.003 0.5	0.012
thermalfile32	Fa147337 a-norm 500C 160rot	Saturday, April 8, 2000 12:33 AM
32 500	160 77 1.104 0.023 2.1	0.019
thermalfile33	Fa147337 a-norm 500C 140rot	Saturday, April 8, 2000 12:39 AM
33 500	140 37 1.196 0.014 1.2	0.012
thermalfile34	Fa147337 a-norm 500C 120rot	Saturday, April 8, 2000 12:47 AM
34 500	120 39 1.175 0.008 0.7	0.013
thermalfile38	Fa147337 a-norm 600C 120rot	Saturday, April 8, 2000 2:09 AM
38 600	120 32 1.089 0.007 0.6	0.020
thermalfile39	Fa147337 a-norm 600C 140rot	Saturday, April 8, 2000 2:16 AM
39 600	140 32 1.100 0.010 0.9	0.022
thermalfile4	Fa147337 a-norm RT 220rot	Friday, April 7, 2000 3:44 PM
4 27	220 105 1.393 0.014 1.0	0.020
thermalfile40	Fa147337 a-norm 600C 160rot	Saturday, April 8, 2000 2:24 AM
40 600	160 22 0.993 0.006 0.6	0.014
thermalfile41	Fa147337 a-norm 600C 180rot	Saturday, April 8, 2000 2:32 AM
41 600	180 19 0.848 0.008 1.0	0.026
thermalfile42	Fa147337 a-norm 600C 200rot	Saturday, April 8, 2000 2:39 AM
42 600	200 10 0.712 0.007 0.9	0.024
thermalfile43	Fa147337 a-norm 600C 220rot	Saturday, April 8, 2000 2:46 AM
43 600	220 8 0.647 0.008 1.2	0.021
thermalfile44	Fa147337 a-norm 600C 240rot	Saturday, April 8, 2000 2:52 AM
44 600	240 12 0.705 0.003 0.5	0.023
thermalfile5	Fa147337 a-norm RT 240rot	Friday, April 7, 2000 3:51 PM
5 27	240 77 1.322 0.016 1.2	0.031
thermalfile8	Fa147337 a-norm 300C 240rot	Friday, April 7, 2000 6:55 PM
8 300	240 51 0.900 0.004 0.5	0.018
thermalfile9	Fa147337 a-norm 300C 220rot	Friday, April 7, 2000 7:06 PM
9 300	220 18 0.818 0.005 0.6	0.031
thermalfile0	methanol 24.1C	Friday, April 7, 2000 2:45 PM
0 24.1	1105.9 14.614	
thermalfile16	methanol 24.6C	Friday, April 7, 2000 8:15 PM
16 24.6	1104.3 14.654	
thermalfile17	methanol 24.3C	Friday, April 7, 2000 9:20 PM
17 24.3	1105.2 14.583	

thermalfile26	methanol 24.0C	Friday, April 7, 2000 10:48 PM
26	24.0 1106.2 14.608	
thermalfile27	methanol 23.8C	Friday, April 7, 2000 11:50 PM
27	23.8 1106.8 14.622	
thermalfile36	methanol 23.5C	Saturday, April 8, 2000 1:01 AM
36	23.5 1107.8 14.641	
thermalfile37	methanol 23.4C	Saturday, April 8, 2000 1:59 AM
37	23.4 1108.1 14.527	
thermalfile46	methanol 23.3C	Saturday, April 8, 2000 3:07 AM
46	23.3 1108.4 14.591	
thermalfile6	methanol 24.9C	Friday, April 7, 2000 4:02 PM
6	24.9 1103.3 14.592	
thermalfile7	methanol 25.1C	Friday, April 7, 2000 6:35 PM
7	25.1 1102.7 14.491	

10 April 2000

thermalfile0	Fa147337 c-norm RT 260rot	Monday, April 10, 2000 6:36 PM
0	27 260 30 1.477 0.017 1.2 0.020	
thermalfile1	Fa147337 c-norm RT 240rot	Monday, April 10, 2000 6:52 PM
1	27 240 34 1.731 0.017 1.0 0.017	
thermalfile10	Fa147337 c-norm RT 140rot	Monday, April 10, 2000 8:45 PM
10	27 140 21 2.176 0.012 0.6 0.012	
thermalfile11	Fa147337 c-norm RT 120rot	Monday, April 10, 2000 8:54 PM
11	27 120 23 1.703 0.027 1.6 0.017	
thermalfile2	Fa147337 c-norm RT 220rot	Monday, April 10, 2000 7:00 PM
2	27 220 54 2.222 0.032 1.4 0.010	
thermalfile3	Fa147337 c-norm RT 200rot	Monday, April 10, 2000 7:11 PM
3	27 200 28 2.570 0.017 0.7 0.007	
thermalfile4	Fa147337 c-norm RT 180rot	Monday, April 10, 2000 7:21 PM
4	27 180 30 2.743 0.007 0.5 0.007	
thermalfile5	Fa147337 c-norm RT 160rot	Monday, April 10, 2000 7:35 PM
5	27 160 8 2.572 0.015 0.6 0.020	
thermalfile9	Fa147337 c-norm RT 160rot	Monday, April 10, 2000 8:34 PM
9	27 160 48 2.577 0.031 1.2 0.009	
thermalfile13	methanol 25.0C	Monday, April 10, 2000 9:15 PM
13	25.0 1103.0 14.642	
thermalfile6	methanol 25.4C	Monday, April 10, 2000 7:56 PM
6	25.4 1101.7 14.646	
thermalfile7	methanol 25.4C	Monday, April 10, 2000 8:06 PM
7	25.4 1101.7 14.597	

17 April 2000

thermalfile10	Fa147337	c-norm	100C	140rot	Monday, April 17, 2000 10:50 PM
10	100	140	65	1.845 0.006 0.5	0.014
thermalfile11	Fa147337	c-norm	100C	120rot	Monday, April 17, 2000 10:59 PM
11	100	120	20	2.135 0.024 1.1	0.011
thermalfile15	Fa147337	c-norm	200C	120rot	Tuesday, April 18, 2000 12:51 AM
15	200	120	72	1.766 0.020 1.1	0.012
thermalfile16	Fa147337	c-norm	200C	110rot	Tuesday, April 18, 2000 12:58 AM
16	200	110	43	1.708 0.008 0.5	0.007
thermalfile17	Fa147337	c-norm	200C	140rot	Tuesday, April 18, 2000 1:11 AM
17	200	140	109	1.526 0.009 0.6	0.011
thermalfile18	Fa147337	c-norm	200C	160rot	Tuesday, April 18, 2000 1:19 AM
18	200	160	118	1.300 0.011 0.9	0.015
thermalfile19	Fa147337	c-norm	200C	180rot	Tuesday, April 18, 2000 1:27 AM
19	200	180	78	1.062 0.006 0.6	0.019
thermalfile20	Fa147337	c-norm	200C	200rot	Tuesday, April 18, 2000 1:37 AM
20	200	200	86	0.950 0.019 2.0	0.021
thermalfile21	Fa147337	c-norm	200C	220rot	Tuesday, April 18, 2000 1:49 AM
21	200	220	88	1.008 0.008 0.8	0.016
thermalfile25	Fa147337	c-norm	300C	220rot	Tuesday, April 18, 2000 3:33 AM
25	300	220	30	0.887 0.005 0.6	0.016
thermalfile26	Fa147337	c-norm	300C	200rot	Tuesday, April 18, 2000 3:39 AM
26	300	200	29	0.814 0.003 0.5	0.014
thermalfile27	Fa147337	c-norm	300C	180rot	Tuesday, April 18, 2000 3:49 AM
27	300	180	55	0.888 0.010 1.2	0.011
thermalfile28	Fa147337	c-norm	300C	160rot	Tuesday, April 18, 2000 3:57 AM
28	300	160	54	1.120 0.006 0.5	0.011
thermalfile29	Fa147337	c-norm	300C	140rot	Tuesday, April 18, 2000 4:07 AM
29	300	140	35	1.352 0.009 0.6	0.013
thermalfile30	Fa147337	c-norm	300C	120rot	Tuesday, April 18, 2000 4:17 AM
30	300	120	17	1.465 0.009 0.6	0.010
thermalfile31	Fa147337	c-norm	300C	110rot	Tuesday, April 18, 2000 4:26 AM
31	300	110	26	1.465 0.008 0.5	0.010
thermalfile35	Fa147338	c-norm	400C	110rot	Tuesday, April 18, 2000 5:37 AM
35	400	110	18	1.138 0.026 2.3	0.036
thermalfile36	Fa147338	c-norm	400C	120rot	Tuesday, April 18, 2000 5:44 AM
36	400	120	18	1.282 0.010 0.8	0.022
thermalfile37	Fa147338	c-norm	400C	140rot	Tuesday, April 18, 2000 5:53 AM
37	400	140	22	1.214 0.012 1.0	0.019
thermalfile38	Fa147338	c-norm	400C	160rot	Tuesday, April 18, 2000 5:59 AM
38	400	160	39	1.063 0.009 0.8	0.016

thermalfile39	Fa147338 c-norm 400C 180rot	Tuesday, April 18, 2000 6:06 AM
39 400	180 42 0.846 0.011 1.3	0.015
thermalfile4	Fa147337 c-norm 100C 260rot	Monday, April 17, 2000 9:51 PM
4 100	260 60 1.811 0.017 1.0	0.014
thermalfile40	Fa147338 c-norm 400C 200rot	Tuesday, April 18, 2000 6:15 AM
40 400	200 42 0.750 0.010 1.4	0.015
thermalfile41	Fa147338 c-norm 400C 220rot	Tuesday, April 18, 2000 6:23 AM
41 400	220 28 0.823 0.010 1.2	0.023
thermalfile5	Fa147337 c-norm 100C 240rot	Monday, April 17, 2000 10:04 PM
5 100	240 29 1.474 0.020 1.4	0.018
thermalfile6	Fa147337 c-norm 100C 220rot	Monday, April 17, 2000 10:15 PM
6 100	220 57 1.233 0.018 1.4	0.026
thermalfile7	Fa147337 c-norm 100C 200rot	Monday, April 17, 2000 10:24 PM
7 100	200 74 1.081 0.012 1.1	0.027
thermalfile8	Fa147337 c-norm 100C 180rot	Monday, April 17, 2000 10:32 PM
8 100	180 51 1.207 0.014 1.2	0.025
thermalfile9	Fa147337 c-norm 100C 160rot	Monday, April 17, 2000 10:41 PM
9 100	160 45 1.513 0.007 0.5	0.013
thermalfile0	methanol 25.3C	Monday, April 17, 2000 7:01 PM
0 25.3	1102.0 14.570	
thermalfile13	methanol 24.0C	Monday, April 17, 2000 11:11 PM
13 24.0	1106.2 14.668	
thermalfile14	methanol 23.9C	Tuesday, April 18, 2000 12:41 AM
14 23.9	1106.5 14.649	
thermalfile2	methanol 24.8C	Monday, April 17, 2000 9:13 PM
2 24.8	1103.6 14.569	
thermalfile23	methanol 23.6C	Tuesday, April 18, 2000 2:03 AM
23 23.6	1107.5 14.666	
thermalfile24	methanol 23.4C	Tuesday, April 18, 2000 3:24 AM
24 23.4	1108.1 14.646	
thermalfile33	methanol 23.1C	Tuesday, April 18, 2000 4:38 AM
33 23.1	1109.1 14.696	
thermalfile34	methanol 23.0C	Tuesday, April 18, 2000 5:23 AM
34 23.0	1109.4 14.685	
thermalfile43	methanol 23.2C	Tuesday, April 18, 2000 6:36 AM
43 23.2	1108.8 14.725	

18 April 2000

thermalfile1	Fa147337 a-norm RT 300rot	Tuesday, April 18, 2000 10:38 PM
1 27	300 108 3.074 0.027 0.9 0.007	
thermalfile2	Fa147337 a-norm RT 280rot	Tuesday, April 18, 2000 10:51 PM

2	27	280	79	2.592	0.048	1.9	0.006	
thermalfile3		Fa147337 a-norm RT 260rot				Tuesday, April 18, 2000 11:01 PM		
3	27	260	69	2.182	0.017	0.8	0.009	
thermalfile4		Fa147337 a-norm RT 240rot				Tuesday, April 18, 2000 11:14 PM		
4	27	240	65	1.822	0.028	1.6	0.014	
thermalfile5		Fa147337 a-norm RT 220rot				Tuesday, April 18, 2000 11:25 PM		
5	27	220	60	1.680	0.030	1.8	0.016	
thermalfile6		Fa147337 a-norm RT 200rot				Tuesday, April 18, 2000 11:33 PM		
6	27	200	72	1.907	0.018	1.0	0.012	
thermalfile7		Fa147337 a-norm RT 180rot				Tuesday, April 18, 2000 11:41 PM		
7	27	180	96	2.308	0.019	0.8	0.007	
thermalfile8		Fa147337 a-norm RT 320rot				Tuesday, April 18, 2000 11:49 PM		
8	27	320	105	2.984	0.044	1.5	0.007	
thermalfile0		methanol 24.5C				Tuesday, April 18, 2000 10:12 PM		
0	24.5	1104.6		14.687				
thermalfile10		methanol 24.1C				Wednesday, April 19, 2000 12:24 AM		
10	24.1	1105.9		14.691				

KH-OPX*20 October 1999*

thermalfile1		KH OPX a-norm RT 170rot				Wednesday, October 20, 1999 3:01 PM		
1	27	170	44	3.236	0.051	1.6	0.013	
thermalfile10		KH OPX a-norm 100C 115rot				Wednesday, October 20, 1999 7:43 PM		
10	100	115	104	2.953	0.021	0.7	0.008	
thermalfile101		KH OPX a-norm RT 170rot				Wednesday, October 20, 1999 3:01 PM		
101	27	170	44	3.234	0.053	1.6	0.013	
thermalfile102		KH OPX a-norm RT 190rot				Wednesday, October 20, 1999 3:08 PM		
102	27	190	14	2.818	0.014	0.5	0.015	
thermalfile103		KH OPX a-norm RT 210rot				Wednesday, October 20, 1999 3:22 PM		
103	27	210	11	2.532	0.014	0.6	0.019	
thermalfile104		KH OPX a-norm RT 150rot				Wednesday, October 20, 1999 4:03 PM		
104	27	150	76	3.558	0.052	1.5	0.012	
thermalfile105		KH OPX a-norm RT 130rot				Wednesday, October 20, 1999 4:12 PM		
105	27	130	50	3.624	0.027	0.7	0.011	
thermalfile106		KH OPX a-norm RT 110rot				Wednesday, October 20, 1999 4:32 PM		
106	27	110	35	3.319	0.037	1.1	0.011	
thermalfile11		KH OPX a-norm 100C 135rot				Wednesday, October 20, 1999 7:52 PM		
11	100	135	53	3.044	0.047	1.5	0.012	
thermalfile110		KH OPX a-norm 100C 115rot				Wednesday, October 20, 1999 7:43 PM		

110 100 115 103 2.949 0.022 0.8 0.008
 thermalfile111 KH OPX a-norm 100C 135rot Wednesday, October 20, 1999 7:52 PM
 111 100 135 53 3.038 0.050 1.7 0.012
 thermalfile112 KH OPX a-norm 100C 155rot Wednesday, October 20, 1999 7:59 PM
 112 100 155 37 2.959 0.014 0.5 0.011
 thermalfile113 KH OPX a-norm 100C 175rot Wednesday, October 20, 1999 8:11 PM
 113 100 175 32 2.725 0.033 1.2 0.011
 thermalfile114 KH OPX a-norm 100C 195rot Wednesday, October 20, 1999 8:21 PM
 114 100 195 8 2.335 0.032 1.4 0.023
 thermalfile115 KH OPX a-norm 100C 215rot Wednesday, October 20, 1999 8:39 PM
 115 100 215 9 1.946 0.020 1.0 0.049
 thermalfile12 KH OPX a-norm 100C 155rot Wednesday, October 20, 1999 7:59 PM
 12 100 155 37 2.969 0.012 0.5 0.010
 thermalfile120 KH OPX a-norm 200C 135rot Wednesday, October 20, 1999 9:31 PM
 120 200 135 148 2.578 0.017 0.7 0.012
 thermalfile121 KH OPX a-norm 200C 135rot Wednesday, October 20, 1999 9:31 PM
 121 200 135 148 2.576 0.017 0.7 0.012
 thermalfile122 KH OPX a-norm 200C 155rot Wednesday, October 20, 1999 9:39 PM
 122 200 155 205 2.464 0.014 0.6 0.015
 thermalfile123 KH OPX a-norm 200C 175rot Wednesday, October 20, 1999 9:47 PM
 123 200 175 181 2.210 0.018 0.8 0.016
 thermalfile124 KH OPX a-norm 200C 195rot Wednesday, October 20, 1999 9:53 PM
 124 200 195 54 1.920 0.014 0.7 0.015
 thermalfile125 KH OPX a-norm 200C 215rot Wednesday, October 20, 1999 10:04 PM
 125 200 215 4 1.638 0.029 1.8 0.046
 thermalfile129 KH OPX a-norm 300C 115rot Wednesday, October 20, 1999 10:46 PM
 129 300 115 302 2.128 0.033 1.6 0.028
 thermalfile13 KH OPX a-norm 100C 175rot Wednesday, October 20, 1999 8:11 PM
 13 100 175 32 2.731 0.034 1.2 0.010
 thermalfile130 KH OPX a-norm 300C 135rot Wednesday, October 20, 1999 10:52 PM
 130 300 135 236 2.268 0.028 1.2 0.020
 thermalfile131 KH OPX a-norm 300C 155rot Wednesday, October 20, 1999 10:58 PM
 131 300 155 98 2.207 0.012 0.5 0.010
 thermalfile132 KH OPX a-norm 300C 175rot Wednesday, October 20, 1999 11:06 PM
 132 300 175 58 1.971 0.019 0.9 0.013
 thermalfile133 KH OPX a-norm 300C 195rot Wednesday, October 20, 1999 11:12 PM
 133 300 195 37 1.711 0.025 1.5 0.018
 thermalfile134 KH OPX a-norm 300C 215rot Wednesday, October 20, 1999 11:27 PM
 134 300 215 3 1.409 0.041 2.9 0.077
 thermalfile139 KH OPX a-norm 400C 115rot Thursday, October 21, 1999 12:08 AM
 139 400 115 31 2.106 0.060 2.9 0.017
 thermalfile14 KH OPX a-norm 100C 195rot Wednesday, October 20, 1999 8:21 PM
 14 100 195 8 2.358 0.041 1.8 0.023
 thermalfile140 KH OPX a-norm 400C 135rot Thursday, October 21, 1999 12:17 AM

140 400 135 47 2.239 0.048 2.2 0.013
 thermalfile141 KH OPX a-norm 400C 155rot Thursday, October 21, 1999 12:25 AM
 141 400 155 175 2.129 0.027 1.3 0.016
 thermalfile142 KH OPX a-norm 400C 175rot Thursday, October 21, 1999 12:34 AM
 142 400 175 159 1.862 0.012 0.6 0.012
 thermalfile143 KH OPX a-norm 400C 195rot Thursday, October 21, 1999 12:42 AM
 143 400 195 8 1.501 0.005 0.5 0.027
 thermalfile144 KH OPX a-norm 400C 215rot Thursday, October 21, 1999 12:53 AM
 144 400 215 28 1.373 0.012 0.9 0.020
 thermalfile15 KH OPX a-norm 100C 215rot Wednesday, October 20, 1999 8:39 PM
 15 100 215 9 1.965 0.030 1.5 0.041
 thermalfile2 KH OPX a-norm RT 190rot Wednesday, October 20, 1999 3:08 PM
 2 27 190 14 2.830 0.015 0.5 0.015
 thermalfile20 KH OPX a-norm 200C 115rot Wednesday, October 20, 1999 9:22 PM
 20 200 115 30 2.430 0.021 0.9 0.013
 thermalfile21 KH OPX a-norm 200C 135rot Wednesday, October 20, 1999 9:31 PM
 21 200 135 148 2.578 0.017 0.7 0.012
 thermalfile22 KH OPX a-norm 200C 155rot Wednesday, October 20, 1999 9:39 PM
 22 200 155 205 2.465 0.014 0.6 0.015
 thermalfile23 KH OPX a-norm 200C 175rot Wednesday, October 20, 1999 9:47 PM
 23 200 175 181 2.211 0.018 0.8 0.016
 thermalfile24 KH OPX a-norm 200C 195rot Wednesday, October 20, 1999 9:53 PM
 24 200 195 54 1.923 0.016 0.8 0.015
 thermalfile25 KH OPX a-norm 200C 215rot Wednesday, October 20, 1999 10:04 PM
 25 200 215 4 1.661 0.027 1.6 0.044
 thermalfile29 KH OPX a-norm 300C 115rot Wednesday, October 20, 1999 10:46 PM
 29 300 115 302 2.128 0.033 1.6 0.029
 thermalfile3 KH OPX a-norm RT 210rot Wednesday, October 20, 1999 3:22 PM
 3 27 210 11 2.545 0.020 0.8 0.020
 thermalfile30 KH OPX a-norm 300C 135rot Wednesday, October 20, 1999 10:52 PM
 30 300 135 236 2.268 0.028 1.2 0.020
 thermalfile31 KH OPX a-norm 300C 155rot Wednesday, October 20, 1999 10:58 PM
 31 300 155 98 2.207 0.011 0.5 0.011
 thermalfile32 KH OPX a-norm 300C 175rot Wednesday, October 20, 1999 11:06 PM
 32 300 175 59 1.971 0.018 0.9 0.013
 thermalfile33 KH OPX a-norm 300C 195rot Wednesday, October 20, 1999 11:12 PM
 33 300 195 37 1.709 0.025 1.4 0.018
 thermalfile34 KH OPX a-norm 300C 215rot Wednesday, October 20, 1999 11:27 PM
 34 300 215 3 1.405 0.038 2.7 0.064
 thermalfile39 KH OPX a-norm 400C 115rot Thursday, October 21, 1999 12:08 AM
 39 400 115 31 2.105 0.057 2.7 0.016
 thermalfile4 KH OPX a-norm RT 150rot Wednesday, October 20, 1999 4:03 PM
 4 27 150 76 3.559 0.051 1.4 0.011
 thermalfile40 KH OPX a-norm 400C 135rot Thursday, October 21, 1999 12:17 AM

40 400 135 47 2.238 0.045 2.0 0.013
 thermalfile41 KH OPX a-norm 400C 155rot Thursday, October 21, 1999 12:25 AM
 41 400 155 175 2.129 0.026 1.2 0.016
 thermalfile42 KH OPX a-norm 400C 175rot Thursday, October 21, 1999 12:34 AM
 42 400 175 159 1.861 0.012 0.6 0.012
 thermalfile43 KH OPX a-norm 400C 195rot Thursday, October 21, 1999 12:42 AM
 43 400 195 7 1.498 0.009 0.6 0.024
 thermalfile44 KH OPX a-norm 400C 215rot Thursday, October 21, 1999 12:53 AM
 44 400 215 28 1.375 0.011 0.8 0.020
 thermalfile5 KH OPX a-norm RT 130rot Wednesday, October 20, 1999 4:12 PM
 5 27 130 50 3.625 0.027 0.7 0.011
 thermalfile6 KH OPX a-norm RT 110rot Wednesday, October 20, 1999 4:32 PM
 6 27 110 35 3.322 0.036 1.1 0.010
 thermalfile0 methanol 26.3C Wednesday, October 20, 1999 2:43 PM
 0 26.3 1098.8 14.968
 thermalfile18 methanol 27.7C Wednesday, October 20, 1999 8:50 PM
 18 27.7 1094.4 14.914
 thermalfile19 methanol 27.6C Wednesday, October 20, 1999 9:05 PM
 19 27.6 1094.7 14.941
 thermalfile27 methanol 27.1C Wednesday, October 20, 1999 10:16 PM
 27 27.1 1096.3 14.958
 thermalfile28 methanol 27.0C Wednesday, October 20, 1999 10:31 PM
 28 27.0 1096.6 14.955
 thermalfile37 methanol 26.6C Wednesday, October 20, 1999 11:43 PM
 37 26.6 1097.9 15.017
 thermalfile38 methanol 26.7C Wednesday, October 20, 1999 11:54 PM
 38 26.7 1097.6 14.996
 thermalfile46 methanol 26.5C Thursday, October 21, 1999 1:05 AM
 46 26.5 1098.2 14.958
 thermalfile8 methanol 27.4C Wednesday, October 20, 1999 4:50 PM
 8 27.4 1095.3 14.971
 thermalfile9 methanol 27.5C Wednesday, October 20, 1999 6:57 PM
 9 27.5 1095.0 14.905

21 October 1999

thermalfile1 KH OPX a-norm 500C 115rot Thursday, October 21, 1999 1:35 AM
 1 500 115 362 1.909 0.047 2.4 0.040
 thermalfile101 KH OPX a-norm 500C 115rot Thursday, October 21, 1999 1:35 AM
 101 500 115 362 1.909 0.047 2.4 0.040
 thermalfile102 KH OPX a-norm 500C 135rot Thursday, October 21, 1999 1:41 AM
 102 500 135 348 2.064 0.063 3.1 0.040

thermalfile103 KH OPX a-norm 500C 155rot Thursday, October 21, 1999 1:47 AM
 103 500 155 246 2.026 0.039 1.9 0.027
 thermalfile104 KH OPX a-norm 500C 175rot Thursday, October 21, 1999 1:57 AM
 104 500 175 27 1.774 0.022 1.2 0.015
 thermalfile105 KH OPX a-norm 500C 195rot Thursday, October 21, 1999 2:05 AM
 105 500 195 8 1.439 0.026 1.8 0.037
 thermalfile106 KH OPX a-norm 500C 215rot Thursday, October 21, 1999 2:20 AM
 106 500 215 4 1.340 0.033 2.5 0.071
 thermalfile11 KH OPX a-norm 600C 115rot Thursday, October 21, 1999 3:17 AM
 11 600 115 368 1.796 0.034 1.9 0.040
 thermalfile111 KH OPX a-norm 600C 115rot Thursday, October 21, 1999 3:17 AM
 111 600 115 368 1.796 0.034 1.9 0.040
 thermalfile112 KH OPX a-norm 600C 135rot Thursday, October 21, 1999 3:24 AM
 112 600 135 321 1.982 0.059 3.0 0.039
 thermalfile113 KH OPX a-norm 600C 155rot Thursday, October 21, 1999 3:30 AM
 113 600 155 254 1.901 0.027 1.4 0.027
 thermalfile114 KH OPX a-norm 600C 175rot Thursday, October 21, 1999 3:36 AM
 114 600 175 139 1.739 0.037 2.1 0.022
 thermalfile115 KH OPX a-norm 600C 195rot Thursday, October 21, 1999 3:42 AM
 115 600 195 24 1.434 0.014 1.0 0.019
 thermalfile116 KH OPX a-norm 600C 210rot Thursday, October 21, 1999 3:54 AM
 116 600 210 12 1.291 0.026 2.0 0.027
 thermalfile12 KH OPX a-norm 600C 135rot Thursday, October 21, 1999 3:24 AM
 12 600 135 321 1.982 0.058 2.9 0.039
 thermalfile120 KH OPX a-norm 700C 115rot Thursday, October 21, 1999 4:28 AM
 120 700 115 205 1.752 0.015 0.9 0.019
 thermalfile121 KH OPX a-norm 700C 135rot Thursday, October 21, 1999 4:34 AM
 121 700 135 126 1.929 0.031 1.6 0.017
 thermalfile122 KH OPX a-norm 700C 155rot Thursday, October 21, 1999 4:41 AM
 122 700 155 73 1.890 0.040 2.1 0.018
 thermalfile123 KH OPX a-norm 700C 175rot Thursday, October 21, 1999 4:49 AM
 123 700 175 44 1.617 0.005 0.5 0.014
 thermalfile124 KH OPX a-norm 700C 195rot Thursday, October 21, 1999 4:55 AM
 124 700 195 9 1.370 0.020 1.4 0.029
 thermalfile125 KH OPX a-norm 700C 210rot Thursday, October 21, 1999 5:05 AM
 125 700 210 3 1.128 0.012 1.1 0.088
 thermalfile13 KH OPX a-norm 600C 155rot Thursday, October 21, 1999 3:30 AM
 13 600 155 254 1.901 0.027 1.4 0.027
 thermalfile130 KH OPX a-norm 800C 115rot Thursday, October 21, 1999 5:42 AM
 130 800 115 251 1.734 0.041 2.4 0.032
 thermalfile131 KH OPX a-norm 800C 135rot Thursday, October 21, 1999 5:49 AM
 131 800 135 161 1.861 0.038 2.0 0.021
 thermalfile132 KH OPX a-norm 800C 155rot Thursday, October 21, 1999 5:55 AM
 132 800 155 105 1.781 0.016 0.9 0.015

thermalfile133 KH OPX a-norm 800C 175rot Thursday, October 21, 1999 6:01 AM
 133 800 175 48 1.579 0.008 0.5 0.017
 thermalfile134 KH OPX a-norm 800C 195rot Thursday, October 21, 1999 6:09 AM
 134 800 195 45 1.350 0.022 1.7 0.021
 thermalfile135 KH OPX a-norm 800C 210rot Thursday, October 21, 1999 6:15 AM
 135 800 210 13 1.182 0.015 1.3 0.024
 thermalfile139 KH OPX a-norm 900C 115rot Thursday, October 21, 1999 6:53 AM
 139 900 115 109 1.702 0.032 1.9 0.020
 thermalfile14 KH OPX a-norm 600C 175rot Thursday, October 21, 1999 3:36 AM
 14 600 175 139 1.739 0.036 2.1 0.022
 thermalfile140 KH OPX a-norm 900C 135rot Thursday, October 21, 1999 7:01 AM
 140 900 135 37 1.717 0.013 0.7 0.012
 thermalfile141 KH OPX a-norm 900C 155rot Thursday, October 21, 1999 7:06 AM
 141 900 155 45 1.644 0.004 0.5 0.012
 thermalfile142 KH OPX a-norm 900C 175rot Thursday, October 21, 1999 7:10 AM
 142 900 175 195 1.465 0.027 1.8 0.030
 thermalfile143 KH OPX a-norm 900C 195rot Thursday, October 21, 1999 7:15 AM
 143 900 195 120 1.218 0.017 1.4 0.024
 thermalfile144 KH OPX a-norm 900C 210rot Thursday, October 21, 1999 7:22 AM
 144 900 210 23 1.052 0.006 0.6 0.023
 thermalfile148 KH OPX a-norm 1000C 115rot Thursday, October 21, 1999 7:56 AM
 148 1000 115 18 1.577 0.006 0.5 0.017
 thermalfile149 KH OPX a-norm 1000C 135rot Thursday, October 21, 1999 8:02 AM
 149 1000 135 118 1.672 0.011 0.7 0.013
 thermalfile15 KH OPX a-norm 600C 195rot Thursday, October 21, 1999 3:42 AM
 15 600 195 25 1.431 0.013 0.9 0.019
 thermalfile150 KH OPX a-norm 1000C 155rot Thursday, October 21, 1999 8:06 AM
 150 1000 155 133 1.598 0.009 0.5 0.015
 thermalfile151 KH OPX a-norm 1000C 175rot Thursday, October 21, 1999 8:12 AM
 151 1000 175 164 1.369 0.013 0.9 0.018
 thermalfile152 KH OPX a-norm 1000C 195rot Thursday, October 21, 1999 8:16 AM
 152 1000 195 99 1.171 0.010 0.9 0.023
 thermalfile153 KH OPX a-norm 1000C 210rot Thursday, October 21, 1999 8:21 AM
 153 1000 210 63 1.041 0.010 0.9 0.022
 thermalfile16 KH OPX a-norm 600C 210rot Thursday, October 21, 1999 3:54 AM
 16 600 210 12 1.287 0.025 2.0 0.027
 thermalfile2 KH OPX a-norm 500C 135rot Thursday, October 21, 1999 1:41 AM
 2 500 135 349 2.064 0.063 3.1 0.040
 thermalfile20 KH OPX a-norm 700C 115rot Thursday, October 21, 1999 4:28 AM
 20 700 115 205 1.752 0.015 0.9 0.019
 thermalfile21 KH OPX a-norm 700C 135rot Thursday, October 21, 1999 4:34 AM
 21 700 135 127 1.929 0.031 1.6 0.018
 thermalfile22 KH OPX a-norm 700C 155rot Thursday, October 21, 1999 4:41 AM
 22 700 155 74 1.890 0.040 2.1 0.018

thermalfile23 KH OPX a-norm 700C 175rot Thursday, October 21, 1999 4:49 AM
 23 700 175 44 1.617 0.005 0.5 0.014
 thermalfile24 KH OPX a-norm 700C 195rot Thursday, October 21, 1999 4:55 AM
 24 700 195 9 1.368 0.019 1.4 0.028
 thermalfile25 KH OPX a-norm 700C 210rot Thursday, October 21, 1999 5:05 AM
 25 700 210 3 1.137 0.017 1.5 0.069
 thermalfile3 KH OPX a-norm 500C 155rot Thursday, October 21, 1999 1:47 AM
 3 500 155 247 2.027 0.039 1.9 0.028
 thermalfile30 KH OPX a-norm 800C 115rot Thursday, October 21, 1999 5:42 AM
 30 800 115 251 1.734 0.041 2.4 0.033
 thermalfile31 KH OPX a-norm 800C 135rot Thursday, October 21, 1999 5:49 AM
 31 800 135 161 1.861 0.038 2.0 0.021
 thermalfile32 KH OPX a-norm 800C 155rot Thursday, October 21, 1999 5:55 AM
 32 800 155 106 1.781 0.016 0.9 0.015
 thermalfile33 KH OPX a-norm 800C 175rot Thursday, October 21, 1999 6:01 AM
 33 800 175 48 1.580 0.008 0.5 0.017
 thermalfile34 KH OPX a-norm 800C 195rot Thursday, October 21, 1999 6:09 AM
 34 800 195 45 1.350 0.022 1.6 0.021
 thermalfile35 KH OPX a-norm 800C 210rot Thursday, October 21, 1999 6:15 AM
 35 800 210 13 1.182 0.016 1.3 0.025
 thermalfile39 KH OPX a-norm 900C 115rot Thursday, October 21, 1999 6:53 AM
 39 900 115 110 1.703 0.033 1.9 0.020
 thermalfile4 KH OPX a-norm 500C 175rot Thursday, October 21, 1999 1:57 AM
 4 500 175 27 1.774 0.021 1.2 0.015
 thermalfile40 KH OPX a-norm 900C 135rot Thursday, October 21, 1999 7:01 AM
 40 900 135 37 1.718 0.012 0.7 0.013
 thermalfile41 KH OPX a-norm 900C 155rot Thursday, October 21, 1999 7:06 AM
 41 900 155 45 1.645 0.004 0.5 0.013
 thermalfile42 KH OPX a-norm 900C 175rot Thursday, October 21, 1999 7:10 AM
 42 900 175 195 1.465 0.027 1.8 0.030
 thermalfile43 KH OPX a-norm 900C 195rot Thursday, October 21, 1999 7:15 AM
 43 900 195 119 1.219 0.017 1.4 0.025
 thermalfile44 KH OPX a-norm 900C 210rot Thursday, October 21, 1999 7:22 AM
 44 900 210 23 1.054 0.006 0.5 0.023
 thermalfile48 KH OPX a-norm 1000C 115rot Thursday, October 21, 1999 7:56 AM
 48 1000 115 18 1.582 0.009 0.6 0.016
 thermalfile49 KH OPX a-norm 1000C 135rot Thursday, October 21, 1999 8:02 AM
 49 1000 135 118 1.673 0.011 0.7 0.013
 thermalfile5 KH OPX a-norm 500C 195rot Thursday, October 21, 1999 2:05 AM
 5 500 195 8 1.444 0.029 2.0 0.035
 thermalfile50 KH OPX a-norm 1000C 155rot Thursday, October 21, 1999 8:06 AM
 50 1000 155 133 1.598 0.009 0.5 0.015
 thermalfile51 KH OPX a-norm 1000C 175rot Thursday, October 21, 1999 8:12 AM
 51 1000 175 164 1.369 0.013 0.9 0.018

thermalfile52 KH OPX a-norm 1000C 195rot Thursday, October 21, 1999 8:16 AM
 52 1000 195 99 1.171 0.010 0.9 0.023
 thermalfile53 KH OPX a-norm 1000C 210rot Thursday, October 21, 1999 8:21 AM
 53 1000 210 63 1.041 0.009 0.8 0.022
 thermalfile6 KH OPX a-norm 500C 215rot Thursday, October 21, 1999 2:20 AM
 6 500 215 3 1.357 0.043 3.2 0.069
 thermalfile0 methanol 26.4C Thursday, October 21, 1999 1:22 AM
 0 26.4 1098.5 14.975
 thermalfile10 methanol 26.2C Thursday, October 21, 1999 3:03 AM
 10 26.2 1099.2 14.951
 thermalfile18 methanol 26.2C Thursday, October 21, 1999 4:03 AM
 18 26.2 1099.2 14.963
 thermalfile19 methanol 26.1C Thursday, October 21, 1999 4:17 AM
 19 26.1 1099.5 14.988
 thermalfile28 methanol 25.9C Thursday, October 21, 1999 5:18 AM
 28 25.9 1100.1 14.966
 thermalfile29 methanol 25.9C Thursday, October 21, 1999 5:31 AM
 29 25.9 1100.1 15.063
 thermalfile37 methanol 26.4C Thursday, October 21, 1999 6:26 AM
 37 26.4 1098.5 15.094
 thermalfile38 methanol 26.7C Thursday, October 21, 1999 6:43 AM
 38 26.7 1097.6 15.014
 thermalfile46 methanol 27.0C Thursday, October 21, 1999 7:32 AM
 46 27.0 1096.6 15.074
 thermalfile47 methanol 27.1C Thursday, October 21, 1999 7:43 AM
 47 27.1 1096.3 14.992
 thermalfile55 methanol 27.1C Thursday, October 21, 1999 8:28 AM
 55 27.1 1096.3 14.971
 thermalfile9 methanol 26.2C Thursday, October 21, 1999 2:35 AM
 9 26.2 1099.2 14.985

26 October 1999

thermalfile1 KH OPX b-norm RT 210rot Tuesday, October 26, 1999 1:32 PM
 1 27 210 7 2.940 0.031 1.0 0.023
 thermalfile2 KH OPX b-norm RT 230rot Tuesday, October 26, 1999 1:43 PM
 2 27 230 13 2.994 0.043 1.4 0.019
 thermalfile3 KH OPX b-norm RT 250rot Tuesday, October 26, 1999 1:53 PM
 3 27 250 32 3.312 0.054 1.6 0.013
 thermalfile4 KH OPX b-norm RT 270rot Tuesday, October 26, 1999 2:04 PM
 4 27 270 27 3.640 0.086 2.4 0.015
 thermalfile0 methanol 24.5C Tuesday, October 26, 1999 12:55 PM

0 24.5 1104.6 15.078

28 October 1999

thermalfile1	KH OPX b-norm RT 150rot	Thursday, October 28, 1999 4:47 PM
1 27	150 37 2.894 0.024 0.8 0.011	
thermalfile101	KH OPX b-norm RT 150rot	Thursday, October 28, 1999 4:47 PM
101 27	150 36 2.896 0.026 0.9 0.011	
thermalfile102	KH OPX b-norm RT 170rot	Thursday, October 28, 1999 4:58 PM
102 27	170 42 2.866 0.018 0.6 0.010	
thermalfile103	KH OPX b-norm RT 190rot	Thursday, October 28, 1999 5:06 PM
103 27	190 19 3.074 0.020 0.7 0.012	
thermalfile104	KH OPX b-norm RT 210rot	Thursday, October 28, 1999 5:12 PM
104 27	210 43 3.403 0.034 1.0 0.013	
thermalfile105	KH OPX b-norm RT 230rot	Thursday, October 28, 1999 5:19 PM
105 27	230 27 3.591 0.081 2.2 0.016	
thermalfile106	KH OPX b-norm RT 250rot	Thursday, October 28, 1999 5:29 PM
106 27	250 19 3.788 0.052 1.4 0.016	
thermalfile107	KH OPX b-norm RT 270rot	Thursday, October 28, 1999 5:37 PM
107 27	270 23 3.608 0.075 2.1 0.015	
thermalfile2	KH OPX b-norm RT 170rot	Thursday, October 28, 1999 4:58 PM
2 27	170 43 2.864 0.017 0.6 0.011	
thermalfile3	KH OPX b-norm RT 190rot	Thursday, October 28, 1999 5:06 PM
3 27	190 20 3.073 0.029 0.9 0.013	
thermalfile4	KH OPX b-norm RT 210rot	Thursday, October 28, 1999 5:12 PM
4 27	210 43 3.400 0.038 1.1 0.013	
thermalfile5	KH OPX b-norm RT 230rot	Thursday, October 28, 1999 5:19 PM
5 27	230 28 3.589 0.081 2.2 0.016	
thermalfile6	KH OPX b-norm RT 250rot	Thursday, October 28, 1999 5:29 PM
6 27	250 19 3.778 0.059 1.6 0.018	
thermalfile7	KH OPX b-norm RT 270rot	Thursday, October 28, 1999 5:37 PM
7 27	270 24 3.605 0.073 2.0 0.017	
thermalfile0	methanol 24.6C	Thursday, October 28, 1999 4:27 PM
0 24.6	1104.3 15.087	
thermalfile9	methanol 25.3C	Thursday, October 28, 1999 5:57 PM
9 25.3	1102.0 15.024	

29 October 1999

thermalfile1 KH OPX b-norm 100C 140rot Friday, October 29, 1999 12:16 PM

1	100	140	49	2.362	0.011	0.5	0.011
thermalfile101	KH OPX b-norm 100C 140rot						Friday, October 29, 1999 12:16 PM
101	100	140	49	2.363	0.011	0.5	0.010
thermalfile102	KH OPX b-norm 100C 160rot						Friday, October 29, 1999 12:25 PM
102	100	160	55	2.332	0.020	0.8	0.011
thermalfile103	KH OPX b-norm 100C 180rot						Friday, October 29, 1999 12:34 PM
103	100	180	25	2.460	0.014	0.6	0.012
thermalfile104	KH OPX b-norm 100C 200rot						Friday, October 29, 1999 12:44 PM
104	100	200	14	2.755	0.035	1.3	0.014
thermalfile105	KH OPX b-norm 100C 220rot						Friday, October 29, 1999 12:58 PM
105	100	220	11	2.942	0.039	1.3	0.018
thermalfile106	KH OPX b-norm 100C 240rot						Friday, October 29, 1999 1:08 PM
106	100	240	22	3.163	0.048	1.5	0.014
thermalfile107	KH OPX b-norm 100C 260rot						Friday, October 29, 1999 1:15 PM
107	100	260	21	3.185	0.047	1.5	0.014
thermalfile11	KH OPX b-norm 200C 140rot						Friday, October 29, 1999 1:46 PM
11	200	140	86	1.950	0.010	0.5	0.009
thermalfile111	KH OPX b-norm 200C 140rot						Friday, October 29, 1999 1:46 PM
111	200	140	86	1.949	0.010	0.5	0.009
thermalfile112	KH OPX b-norm 200C 160rot						Friday, October 29, 1999 1:54 PM
112	200	160	77	1.898	0.013	0.7	0.013
thermalfile113	KH OPX b-norm 200C 180rot						Friday, October 29, 1999 2:05 PM
113	200	180	48	1.983	0.011	0.5	0.010
thermalfile114	KH OPX b-norm 200C 200rot						Friday, October 29, 1999 2:11 PM
114	200	200	43	2.214	0.007	0.5	0.008
thermalfile115	KH OPX b-norm 200C 220rot						Friday, October 29, 1999 2:16 PM
115	200	220	55	2.528	0.011	0.5	0.009
thermalfile116	KH OPX b-norm 200C 240rot						Friday, October 29, 1999 2:20 PM
116	200	240	47	2.621	0.037	1.4	0.009
thermalfile117	KH OPX b-norm 200C 260rot						Friday, October 29, 1999 2:24 PM
117	200	260	49	2.611	0.029	1.1	0.008
thermalfile12	KH OPX b-norm 200C 160rot						Friday, October 29, 1999 1:54 PM
12	200	160	77	1.899	0.014	0.7	0.013
thermalfile120	KH OPX b-norm 300C 140rot						Friday, October 29, 1999 2:45 PM
120	300	140	84	1.784	0.035	1.9	0.018
thermalfile121	KH OPX b-norm 300C 160rot						Friday, October 29, 1999 2:51 PM
121	300	160	94	1.646	0.011	0.7	0.015
thermalfile122	KH OPX b-norm 300C 180rot						Friday, October 29, 1999 2:56 PM
122	300	180	41	1.741	0.003	0.5	0.013
thermalfile123	KH OPX b-norm 300C 200rot						Friday, October 29, 1999 3:00 PM
123	300	200	62	1.960	0.010	0.5	0.013
thermalfile124	KH OPX b-norm 300C 220rot						Friday, October 29, 1999 3:05 PM
124	300	220	28	2.227	0.014	0.6	0.012
thermalfile125	KH OPX b-norm 300C 240rot						Friday, October 29, 1999 3:12 PM

125	300	240	41	2.333	0.013	0.6	0.010
thermalfile126	KH OPX b-norm 300C 260rot						Friday, October 29, 1999 3:19 PM
126	300	260	57	2.346	0.014	0.6	0.008
thermalfile129	KH OPX b-norm 400C 140rot						Friday, October 29, 1999 3:42 PM
129	400	140	106	1.599	0.013	0.8	0.017
thermalfile13	KH OPX b-norm 200C 180rot						Friday, October 29, 1999 2:05 PM
13	200	180	48	1.984	0.011	0.5	0.010
thermalfile130	KH OPX b-norm 400C 160rot						Friday, October 29, 1999 3:49 PM
130	400	160	89	1.507	0.007	0.5	0.015
thermalfile131	KH OPX b-norm 400C 180rot						Friday, October 29, 1999 3:54 PM
131	400	180	108	1.627	0.017	1.0	0.017
thermalfile132	KH OPX b-norm 400C 200rot						Friday, October 29, 1999 3:58 PM
132	400	200	54	1.794	0.011	0.6	0.010
thermalfile133	KH OPX b-norm 400C 220rot						Friday, October 29, 1999 4:05 PM
133	400	220	59	2.024	0.018	0.9	0.010
thermalfile134	KH OPX b-norm 400C 240rot						Friday, October 29, 1999 4:11 PM
134	400	240	46	2.157	0.022	1.0	0.009
thermalfile135	KH OPX b-norm 400C 260rot						Friday, October 29, 1999 4:14 PM
135	400	260	61	2.202	0.016	0.7	0.008
thermalfile139	KH OPX b-norm 500C 140rot						Friday, October 29, 1999 4:43 PM
139	500	140	106	1.512	0.023	1.5	0.020
thermalfile14	KH OPX b-norm 200C 200rot						Friday, October 29, 1999 2:11 PM
14	200	200	43	2.214	0.008	0.5	0.009
thermalfile140	KH OPX b-norm 500C 160rot						Friday, October 29, 1999 4:50 PM
140	500	160	92	1.451	0.025	1.7	0.021
thermalfile141	KH OPX b-norm 500C 180rot						Friday, October 29, 1999 4:55 PM
141	500	180	55	1.534	0.015	1.0	0.017
thermalfile142	KH OPX b-norm 500C 200rot						Friday, October 29, 1999 4:59 PM
142	500	200	34	1.741	0.018	1.0	0.021
thermalfile143	KH OPX b-norm 500C 220rot						Friday, October 29, 1999 5:08 PM
143	500	220	93	1.927	0.016	0.8	0.010
thermalfile144	KH OPX b-norm 500C 240rot						Friday, October 29, 1999 5:13 PM
144	500	240	63	2.095	0.015	0.7	0.012
thermalfile145	KH OPX b-norm 500C 260rot						Friday, October 29, 1999 5:17 PM
145	500	260	74	2.105	0.010	0.5	0.014
thermalfile148	KH OPX b-norm 600C 140rot						Friday, October 29, 1999 5:35 PM
148	600	140	119	1.429	0.023	1.6	0.022
thermalfile149	KH OPX b-norm 600C 160rot						Friday, October 29, 1999 5:42 PM
149	600	160	103	1.372	0.022	1.6	0.023
thermalfile15	KH OPX b-norm 200C 220rot						Friday, October 29, 1999 2:16 PM
15	200	220	56	2.529	0.012	0.5	0.009
thermalfile150	KH OPX b-norm 600C 180rot						Friday, October 29, 1999 5:48 PM
150	600	180	111	1.458	0.021	1.5	0.021
thermalfile151	KH OPX b-norm 600C 200rot						Friday, October 29, 1999 5:52 PM

151	600	200	113	1.655	0.020	1.2	0.018
thermalfile152	KH OPX b-norm 600C 220rot						Friday, October 29, 1999 5:57 PM
152	600	220	78	1.804	0.023	1.3	0.008
thermalfile153	KH OPX b-norm 600C 240rot						Friday, October 29, 1999 6:01 PM
153	600	240	104	1.949	0.017	0.8	0.009
thermalfile154	KH OPX b-norm 600C 260rot						Friday, October 29, 1999 6:05 PM
154	600	260	153	2.003	0.024	1.2	0.016
thermalfile157	KH OPX b-norm 700C 140rot						Friday, October 29, 1999 6:24 PM
157	700	140	76	1.388	0.040	2.9	0.026
thermalfile158	KH OPX b-norm 700C 160rot						Friday, October 29, 1999 6:28 PM
158	700	160	75	1.300	0.022	1.7	0.023
thermalfile159	KH OPX b-norm 700C 180rot						Friday, October 29, 1999 6:32 PM
159	700	180	85	1.376	0.016	1.1	0.020
thermalfile16	KH OPX b-norm 200C 240rot						Friday, October 29, 1999 2:20 PM
16	200	240	48	2.621	0.035	1.3	0.009
thermalfile160	KH OPX b-norm 700C 200rot						Friday, October 29, 1999 6:36 PM
160	700	200	62	1.553	0.014	0.9	0.016
thermalfile161	KH OPX b-norm 700C 220rot						Friday, October 29, 1999 6:41 PM
161	700	220	65	1.754	0.011	0.6	0.013
thermalfile162	KH OPX b-norm 700C 240rot						Friday, October 29, 1999 6:45 PM
162	700	240	98	1.888	0.005	0.5	0.011
thermalfile163	KH OPX b-norm 700C 260rot						Friday, October 29, 1999 6:49 PM
163	700	260	139	1.920	0.029	1.5	0.018
thermalfile166	KH OPX b-norm 800C 140rot						Friday, October 29, 1999 7:19 PM
166	800	140	100	1.284	0.013	1.0	0.021
thermalfile167	KH OPX b-norm 800C 160rot						Friday, October 29, 1999 7:25 PM
167	800	160	67	1.221	0.011	0.9	0.020
thermalfile168	KH OPX b-norm 800C 180rot						Friday, October 29, 1999 7:29 PM
168	800	180	77	1.307	0.010	0.7	0.019
thermalfile169	KH OPX b-norm 800C 200rot						Friday, October 29, 1999 7:36 PM
169	800	200	84	1.496	0.017	1.1	0.019
thermalfile17	KH OPX b-norm 200C 260rot						Friday, October 29, 1999 2:24 PM
17	200	260	49	2.611	0.026	1.0	0.008
thermalfile170	KH OPX b-norm 800C 220rot						Friday, October 29, 1999 7:40 PM
170	800	220	69	1.699	0.019	1.1	0.019
thermalfile171	KH OPX b-norm 800C 240rot						Friday, October 29, 1999 7:44 PM
171	800	240	94	1.823	0.010	0.5	0.014
thermalfile172	KH OPX b-norm 800C 260rot						Friday, October 29, 1999 7:49 PM
172	800	260	97	1.810	0.010	0.5	0.014
thermalfile176	KH OPX b-norm 900C 140rot						Friday, October 29, 1999 8:18 PM
176	900	140	57	1.225	0.012	1.0	0.021
thermalfile177	KH OPX b-norm 900C 160rot						Friday, October 29, 1999 8:23 PM
177	900	160	37	1.164	0.013	1.1	0.037
thermalfile178	KH OPX b-norm 900C 180rot						Friday, October 29, 1999 8:27 PM

178	900	180	48	1.272	0.031	2.4	0.025
thermalfile179	KH OPX b-norm 900C 200rot						Friday, October 29, 1999 8:31 PM
179	900	200	43	1.472	0.040	2.7	0.023
thermalfile180	KH OPX b-norm 900C 220rot						Friday, October 29, 1999 8:36 PM
180	900	220	26	1.622	0.012	0.7	0.019
thermalfile181	KH OPX b-norm 900C 240rot						Friday, October 29, 1999 8:41 PM
181	900	240	39	1.802	0.051	2.8	0.020
thermalfile182	KH OPX b-norm 900C 260rot						Friday, October 29, 1999 8:45 PM
182	900	260	39	1.794	0.051	2.8	0.020
thermalfile185	KH OPX b-norm 1000C 140rot						Friday, October 29, 1999 9:07 PM
185	1000	140	49	1.188	0.021	1.7	0.025
thermalfile186	KH OPX b-norm 1000C 160rot						Friday, October 29, 1999 9:12 PM
186	1000	160	35	1.127	0.018	1.6	0.026
thermalfile187	KH OPX b-norm 1000C 180rot						Friday, October 29, 1999 9:16 PM
187	1000	180	31	1.195	0.016	1.3	0.028
thermalfile188	KH OPX b-norm 1000C 200rot						Friday, October 29, 1999 9:21 PM
188	1000	200	34	1.377	0.020	1.4	0.029
thermalfile189	KH OPX b-norm 1000C 220rot						Friday, October 29, 1999 9:28 PM
189	1000	220	19	1.583	0.029	1.9	0.021
thermalfile190	KH OPX b-norm 1000C 240rot						Friday, October 29, 1999 9:33 PM
190	1000	240	20	1.689	0.020	1.2	0.016
thermalfile191	KH OPX b-norm 1000C 260rot						Friday, October 29, 1999 9:38 PM
191	1000	260	21	1.683	0.018	1.0	0.015
thermalfile2	KH OPX b-norm 100C 160rot						Friday, October 29, 1999 12:25 PM
2	100	160	55	2.331	0.019	0.8	0.011
thermalfile20	KH OPX b-norm 300C 140rot						Friday, October 29, 1999 2:45 PM
20	300	140	85	1.785	0.036	2.0	0.018
thermalfile21	KH OPX b-norm 300C 160rot						Friday, October 29, 1999 2:51 PM
21	300	160	94	1.647	0.011	0.7	0.015
thermalfile22	KH OPX b-norm 300C 180rot						Friday, October 29, 1999 2:56 PM
22	300	180	41	1.743	0.004	0.5	0.013
thermalfile23	KH OPX b-norm 300C 200rot						Friday, October 29, 1999 3:00 PM
23	300	200	62	1.962	0.013	0.6	0.013
thermalfile24	KH OPX b-norm 300C 220rot						Friday, October 29, 1999 3:05 PM
24	300	220	29	2.228	0.015	0.7	0.012
thermalfile25	KH OPX b-norm 300C 240rot						Friday, October 29, 1999 3:12 PM
25	300	240	41	2.331	0.011	0.5	0.010
thermalfile26	KH OPX b-norm 300C 260rot						Friday, October 29, 1999 3:19 PM
26	300	260	57	2.345	0.016	0.7	0.008
thermalfile29	KH OPX b-norm 400C 140rot						Friday, October 29, 1999 3:42 PM
29	400	140	106	1.598	0.013	0.8	0.017
thermalfile3	KH OPX b-norm 100C 180rot						Friday, October 29, 1999 12:34 PM
3	100	180	25	2.456	0.011	0.5	0.013
thermalfile30	KH OPX b-norm 400C 160rot						Friday, October 29, 1999 3:49 PM

30	400	160	90	1.507	0.007	0.5	0.015
thermalfile31	KH OPX b-norm 400C 180rot						Friday, October 29, 1999 3:54 PM
31	400	180	108	1.627	0.017	1.0	0.017
thermalfile32	KH OPX b-norm 400C 200rot						Friday, October 29, 1999 3:58 PM
32	400	200	55	1.794	0.011	0.6	0.010
thermalfile33	KH OPX b-norm 400C 220rot						Friday, October 29, 1999 4:05 PM
33	400	220	60	2.024	0.015	0.7	0.010
thermalfile34	KH OPX b-norm 400C 240rot						Friday, October 29, 1999 4:11 PM
34	400	240	46	2.156	0.022	1.0	0.009
thermalfile35	KH OPX b-norm 400C 260rot						Friday, October 29, 1999 4:14 PM
35	400	260	61	2.201	0.016	0.7	0.009
thermalfile39	KH OPX b-norm 500C 140rot						Friday, October 29, 1999 4:43 PM
39	500	140	106	1.511	0.022	1.5	0.020
thermalfile4	KH OPX b-norm 100C 200rot						Friday, October 29, 1999 12:44 PM
4	100	200	15	2.746	0.021	0.8	0.016
thermalfile40	KH OPX b-norm 500C 160rot						Friday, October 29, 1999 4:50 PM
40	500	160	92	1.451	0.024	1.7	0.021
thermalfile41	KH OPX b-norm 500C 180rot						Friday, October 29, 1999 4:55 PM
41	500	180	55	1.534	0.015	1.0	0.017
thermalfile42	KH OPX b-norm 500C 200rot						Friday, October 29, 1999 4:59 PM
42	500	200	34	1.742	0.017	1.0	0.021
thermalfile43	KH OPX b-norm 500C 220rot						Friday, October 29, 1999 5:08 PM
43	500	220	93	1.926	0.015	0.8	0.011
thermalfile44	KH OPX b-norm 500C 240rot						Friday, October 29, 1999 5:13 PM
44	500	240	63	2.097	0.016	0.8	0.012
thermalfile45	KH OPX b-norm 500C 260rot						Friday, October 29, 1999 5:17 PM
45	500	260	74	2.107	0.012	0.6	0.014
thermalfile48	KH OPX b-norm 600C 140rot						Friday, October 29, 1999 5:35 PM
48	600	140	119	1.430	0.023	1.6	0.022
thermalfile49	KH OPX b-norm 600C 160rot						Friday, October 29, 1999 5:42 PM
49	600	160	103	1.372	0.022	1.6	0.023
thermalfile5	KH OPX b-norm 100C 220rot						Friday, October 29, 1999 12:58 PM
5	100	220	11	2.929	0.056	1.9	0.019
thermalfile50	KH OPX b-norm 600C 180rot						Friday, October 29, 1999 5:48 PM
50	600	180	111	1.458	0.021	1.5	0.021
thermalfile51	KH OPX b-norm 600C 200rot						Friday, October 29, 1999 5:52 PM
51	600	200	113	1.655	0.020	1.2	0.019
thermalfile52	KH OPX b-norm 600C 220rot						Friday, October 29, 1999 5:57 PM
52	600	220	78	1.805	0.023	1.3	0.009
thermalfile53	KH OPX b-norm 600C 240rot						Friday, October 29, 1999 6:01 PM
53	600	240	104	1.949	0.016	0.8	0.009
thermalfile54	KH OPX b-norm 600C 260rot						Friday, October 29, 1999 6:05 PM
54	600	260	153	2.003	0.024	1.2	0.016
thermalfile57	KH OPX b-norm 700C 140rot						Friday, October 29, 1999 6:24 PM

57	700	140	76	1.388	0.039	2.8	0.027
thermalfile58	KH OPX b-norm 700C 160rot						Friday, October 29, 1999 6:28 PM
58	700	160	76	1.300	0.022	1.7	0.023
thermalfile59	KH OPX b-norm 700C 180rot						Friday, October 29, 1999 6:32 PM
59	700	180	85	1.377	0.016	1.1	0.020
thermalfile6	KH OPX b-norm 100C 240rot						Friday, October 29, 1999 1:08 PM
6	100	240	23	3.155	0.055	1.8	0.015
thermalfile60	KH OPX b-norm 700C 200rot						Friday, October 29, 1999 6:36 PM
60	700	200	62	1.554	0.014	0.9	0.017
thermalfile61	KH OPX b-norm 700C 220rot						Friday, October 29, 1999 6:41 PM
61	700	220	65	1.755	0.012	0.7	0.014
thermalfile62	KH OPX b-norm 700C 240rot						Friday, October 29, 1999 6:45 PM
62	700	240	98	1.889	0.007	0.5	0.012
thermalfile63	KH OPX b-norm 700C 260rot						Friday, October 29, 1999 6:49 PM
63	700	260	139	1.921	0.029	1.5	0.018
thermalfile66	KH OPX b-norm 800C 140rot						Friday, October 29, 1999 7:19 PM
66	800	140	100	1.285	0.014	1.1	0.021
thermalfile67	KH OPX b-norm 800C 160rot						Friday, October 29, 1999 7:25 PM
67	800	160	67	1.224	0.011	0.9	0.020
thermalfile68	KH OPX b-norm 800C 180rot						Friday, October 29, 1999 7:29 PM
68	800	180	77	1.308	0.010	0.8	0.019
thermalfile69	KH OPX b-norm 800C 200rot						Friday, October 29, 1999 7:36 PM
69	800	200	84	1.495	0.016	1.0	0.019
thermalfile7	KH OPX b-norm 100C 260rot						Friday, October 29, 1999 1:15 PM
7	100	260	21	3.181	0.055	1.7	0.015
thermalfile70	KH OPX b-norm 800C 220rot						Friday, October 29, 1999 7:40 PM
70	800	220	69	1.697	0.017	1.0	0.018
thermalfile71	KH OPX b-norm 800C 240rot						Friday, October 29, 1999 7:44 PM
71	800	240	94	1.822	0.009	0.5	0.013
thermalfile72	KH OPX b-norm 800C 260rot						Friday, October 29, 1999 7:49 PM
72	800	260	98	1.809	0.008	0.5	0.014
thermalfile76	KH OPX b-norm 900C 140rot						Friday, October 29, 1999 8:18 PM
76	900	140	57	1.225	0.012	1.0	0.022
thermalfile77	KH OPX b-norm 900C 160rot						Friday, October 29, 1999 8:23 PM
77	900	160	37	1.165	0.014	1.2	0.038
thermalfile78	KH OPX b-norm 900C 180rot						Friday, October 29, 1999 8:27 PM
78	900	180	48	1.273	0.030	2.4	0.025
thermalfile79	KH OPX b-norm 900C 200rot						Friday, October 29, 1999 8:31 PM
79	900	200	44	1.474	0.041	2.8	0.024
thermalfile80	KH OPX b-norm 900C 220rot						Friday, October 29, 1999 8:36 PM
80	900	220	26	1.624	0.012	0.8	0.019
thermalfile81	KH OPX b-norm 900C 240rot						Friday, October 29, 1999 8:41 PM
81	900	240	39	1.805	0.053	2.9	0.021
thermalfile82	KH OPX b-norm 900C 260rot						Friday, October 29, 1999 8:45 PM

82	900	260	40	1.796	0.052	2.9	0.020	
thermalfile85	KH OPX b-norm 1000C 140rot						Friday, October 29, 1999 9:07 PM	
85	1000	140	50	1.189	0.021	1.8	0.025	
thermalfile86	KH OPX b-norm 1000C 160rot						Friday, October 29, 1999 9:12 PM	
86	1000	160	35	1.127	0.018	1.6	0.026	
thermalfile87	KH OPX b-norm 1000C 180rot						Friday, October 29, 1999 9:16 PM	
87	1000	180	32	1.196	0.016	1.3	0.028	
thermalfile88	KH OPX b-norm 1000C 200rot						Friday, October 29, 1999 9:21 PM	
88	1000	200	34	1.378	0.020	1.5	0.029	
thermalfile89	KH OPX b-norm 1000C 220rot						Friday, October 29, 1999 9:28 PM	
89	1000	220	19	1.583	0.030	1.9	0.021	
thermalfile90	KH OPX b-norm 1000C 240rot						Friday, October 29, 1999 9:33 PM	
90	1000	240	20	1.690	0.021	1.3	0.016	
thermalfile91	KH OPX b-norm 1000C 260rot						Friday, October 29, 1999 9:38 PM	
91	1000	260	21	1.684	0.018	1.1	0.016	
thermalfile0	methanol 23.9C							Friday, October 29, 1999 12:05 PM
0	23.9	1106.5	15.141					
thermalfile10	methanol 24.9C							Friday, October 29, 1999 1:38 PM
10	24.9	1103.3	15.027					
thermalfile19	methanol 25.3C							Friday, October 29, 1999 2:31 PM
19	25.3	1102.0	15.028					
thermalfile28	methanol 25.6C							Friday, October 29, 1999 3:30 PM
28	25.6	1101.1	15.013					
thermalfile37	methanol 25.9C							Friday, October 29, 1999 4:22 PM
37	25.9	1100.1	14.986					
thermalfile38	methanol 26.0C							Friday, October 29, 1999 4:34 PM
38	26.0	1099.8	14.953					
thermalfile47	methanol 26.0C							Friday, October 29, 1999 5:25 PM
47	26.0	1099.8	15.001					
thermalfile56	methanol 26.2C							Friday, October 29, 1999 6:13 PM
56	26.2	1099.2	14.978					
thermalfile65	methanol 26.4C							Friday, October 29, 1999 6:57 PM
65	26.4	1098.5	15.009					
thermalfile74	methanol 26.5C							Friday, October 29, 1999 7:56 PM
74	26.5	1098.2	15.007					
thermalfile75	methanol 26.6C							Friday, October 29, 1999 8:08 PM
75	26.6	1097.9	14.986					
thermalfile84	methanol 26.7C							Friday, October 29, 1999 8:53 PM
84	26.7	1097.6	14.935					
thermalfile9	methanol 24.8C							Friday, October 29, 1999 1:26 PM
9	24.8	1103.6	15.012					
thermalfile93	methanol 26.3C							Friday, October 29, 1999 9:45 PM
93	26.3	1098.8	14.910					

KH-CPX*26 March 1998, first set (a)*

thermalfile0	KH CPX a*-norm RT 20rot	Thursday, March 26, 1998 1:45 PM
0 27	20 33 4.876 0.080 1.6 0.029	
thermalfile10	KH CPX a*-norm RT 60rot	Thursday, March 26, 1998 2:47 PM
10 27	60 202 5.293 0.162 3.1 0.022	
thermalfile3	KH CPX a*-norm RT 40rot	Thursday, March 26, 1998 2:21 PM
3 27	40 93 5.282 0.103 2.0 0.019	
thermalfile4	KH CPX a*-norm RT 40rot	Thursday, March 26, 1998 2:47 PM
4 27	40 229 5.333 0.123 2.3 0.036	
thermalfile6	KH CPX a*-norm RT 60rot	Thursday, March 26, 1998 2:47 PM
6 27	60 202 5.293 0.162 3.1 0.022	
thermalfile9	KH CPX a*-norm RT 80rot	Thursday, March 26, 1998 3:46 PM
9 27	80 22 5.161 0.115 2.2 0.037	
Dummy entry, angle determined by retroreflection.		
-0.5	0 0 20.217	
Dummy entry, angle determined by retroreflection.		
8.5	0 0 20.133	

26 March 1998, second set (b)

thermalfile0	KH CPX a*-norm RT 100rot	Thursday, March 26, 1998 4:34 PM
0 27	100 34 4.466 0.138 3.1 0.030	
thermalfile1	KH CPX a*-norm RT 120rot	Thursday, March 26, 1998 5:05 PM
1 27	120 8 3.898 0.182 4.7 0.091	
thermalfile2	KH CPX a*-norm RT 140rot	Thursday, March 26, 1998 5:57 PM
2 27	140 9 3.618 0.128 3.5 0.073	
thermalfile3	KH CPX a*-norm RT 160rot	Thursday, March 26, 1998 7:02 PM
3 27	160 12 3.645 0.118 3.2 0.047	
Dummy entry, angle determined by retroreflection.		
1.5	0 0 20.317	

27 March 1998

thermalfile0	KH CPX a*-norm RT 80rot	Friday, March 27, 1998 1:28 PM
--------------	-------------------------	--------------------------------

0	27	80	47	5.256	0.129	2.5	0.025
thermalfile1	KH CPX a*-norm RT 0rot						Friday, March 27, 1998 1:58 PM
1	27	0	15	4.232	0.092	2.2	0.045
thermalfile2	KH CPX b-norm RT 90rot						Friday, March 27, 1998 3:05 PM
2	27	90	10	5.600	0.346	6.2	0.068
thermalfile3	KH CPX b-norm RT 45rot						Friday, March 27, 1998 3:53 PM
3	27	45	7	5.258	0.232	4.4	0.080
thermalfile4	KH CPX a*-norm RT 60rot						Friday, March 27, 1998 4:42 PM
4	27	60	53	5.481	0.137	2.5	0.022
thermalfile5	KH CPX a*-norm RT 90rot						Friday, March 27, 1998 5:27 PM
5	27	90	22	4.819	0.201	4.2	0.020
thermalfile6	KH CPX a*-norm RT 40rot						Saturday, March 28, 1998 3:12 PM
6	27	40	32	5.449	0.073	1.3	0.027
thermalfile7	KH CPX a*-norm RT 20rot						Saturday, March 28, 1998 3:55 PM
7	27	20	59	4.961	0.087	1.8	0.016
thermalfile8	KH CPX b-norm RT 20rot						Saturday, March 28, 1998 5:09 PM
8	27	20	18	4.506	0.173	3.8	0.053
Dummy entry, angle determined by retroreflection.							
1.5	0	0	20.15				
Dummy entry, angle determined by retroreflection.							
5.5	0	0	20.15				

31 March 1998

thermalfile0	KH CPX a*-norm RT 0rot						Tuesday, March 31, 1998 4:46 PM
0	27	0	19	4.362	0.085	1.9	0.043
thermalfile1	KH CPX a*-norm RT 0rot						Tuesday, March 31, 1998 5:16 PM
1	27	0	37	4.315	0.054	1.2	0.023
thermalfile2	KH CPX a*-norm RT 50rot						Tuesday, March 31, 1998 5:58 PM
2	27	50	117	5.550	0.113	2.0	0.019
thermalfile3	KH CPX a*-norm RT 100rot						Tuesday, March 31, 1998 6:29 PM
3	27	100	22	4.636	0.135	2.9	0.040
thermalfile4	KH CPX a*-norm RT 150rot						Tuesday, March 31, 1998 7:42 PM
4	27	150	21	3.877	0.069	1.8	0.057
thermalfile5	KH CPX a*-norm RT 50rot						Tuesday, March 31, 1998 8:14 PM
5	27	50	57	5.612	0.113	2.0	0.025
thermalfile6	KH CPX a*-norm RT 150rot						Tuesday, March 31, 1998 9:02 PM
6	27	150	29	3.859	0.083	2.2	0.045
Dummy entry, angle determined by retroreflection.							
1.5	0	0	20.383				
Dummy entry, angle determined by retroreflection.							
3.5	0	0	20.3875				

Dummy entry, angle determined by retroreflection.

5.5 0 0 20.422

1 April 1998

thermalfile0 KH CPX a*-norm RT 150rot Wednesday, April 1, 1998 2:28 PM
0 27 150 26 3.838 0.087 2.3 0.050

thermalfile1 KH CPX a*-norm RT 140rot Wednesday, April 1, 1998 3:18 PM
1 27 140 16 3.866 0.103 2.7 0.072

thermalfile2 KH CPX a*-norm RT 90rot Wednesday, April 1, 1998 4:11 PM
2 27 90 27 5.015 0.117 2.3 0.025

thermalfile3 KH CPX a*-norm RT 90rot Wednesday, April 1, 1998 5:07 PM
3 27 90 15 4.972 0.111 2.2 0.029

Dummy entry, angle determined by retroreflection.

0.5 0 0 20.433

Dummy entry, angle determined by retroreflection.

1.5 0 0 20.383

Dummy entry, angle determined by retroreflection.

2.5 0 0 20.283

Dummy entry, angle determined by retroreflection.

3.5 0 0 20.367

15 April 1998, a-normal*

thermalfile0 KH CPX a*-norm RT 0rot Wednesday, April 15, 1998 11:47 AM
0 27 0 16 3.639 0.044 1.2 0.018

thermalfile1 KH CPX a*-norm RT 20rot Wednesday, April 15, 1998 12:15 PM
1 27 20 19 3.946 0.057 1.4 0.018

thermalfile10 KH CPX a*-norm RT 180rot Wednesday, April 15, 1998 6:42 PM
10 27 180 12 3.872 0.112 2.9 0.036

thermalfile11 KH CPX a*-norm RT 160rot Wednesday, April 15, 1998 7:04 PM
11 27 160 9 4.024 0.081 2.0 0.039

thermalfile12 KH CPX a*-norm RT 0rot Wednesday, April 15, 1998 7:44 PM
12 27 0 16 3.594 0.051 1.4 0.018

thermalfile2 KH CPX a*-norm RT 40rot Wednesday, April 15, 1998 12:34 PM
2 27 40 39 4.517 0.055 1.2 0.016

thermalfile3 KH CPX a*-norm RT 60rot Wednesday, April 15, 1998 1:01 PM
3 27 60 71 5.159 0.091 1.8 0.020

thermalfile4 KH CPX a*-norm RT 80rot Wednesday, April 15, 1998 2:20 PM
4 27 80 24 5.506 0.133 2.4 0.024

thermalfile5 KH CPX a*-norm RT 100rot Wednesday, April 15, 1998 2:41 PM
 5 27 100 11 5.423 0.166 3.1 0.032
 thermalfile6 KH CPX a*-norm RT 120rot Wednesday, April 15, 1998 3:10 PM
 6 27 120 45 4.963 0.136 2.7 0.024
 thermalfile7 KH CPX a*-norm RT 140rot Wednesday, April 15, 1998 3:35 PM
 7 27 140 23 4.394 0.116 2.6 0.027
 thermalfile8 KH CPX a*-norm RT 160rot Wednesday, April 15, 1998 5:15 PM
 8 27 160 3 4.112 0.186 4.5 0.056
 thermalfile9 KH CPX a*-norm RT 180rot Wednesday, April 15, 1998 5:39 PM
 9 27 180 6 3.749 0.091 2.4 0.042
 Dummy entry, angle determined by retroreflection.
 2.5 0 0 20.317
 Dummy entry, angle determined by retroreflection.
 3.5 0 0 20.35
 Dummy entry, angle determined by retroreflection.
 5.5 0 0 20.417
 Dummy entry, angle determined by retroreflection.
 7.5 0 0 20.45
 Dummy entry, angle determined by retroreflection.
 9.5 0 0 20.4
 Dummy entry, angle determined by retroreflection.
 11.5 0 0 20.4

15 April 1998, b-normal

thermalfile0 KH CPX b-norm RT 0rot Wednesday, April 15, 1998 8:19 PM
 0 27 0 23 5.431 0.142 2.6 0.027
 thermalfile1 KH CPX b-norm RT 20rot Wednesday, April 15, 1998 8:36 PM
 1 27 20 25 4.885 0.127 2.6 0.022
 thermalfile10 KH CPX b-norm RT 160rot Thursday, April 16, 1998 12:45 AM
 10 27 160 11 5.759 0.196 3.4 0.023
 thermalfile2 KH CPX b-norm RT 40rot Wednesday, April 15, 1998 9:37 PM
 2 27 40 20 4.285 0.064 1.5 0.022
 thermalfile3 KH CPX b-norm RT 60rot Wednesday, April 15, 1998 9:54 PM
 3 27 60 22 3.879 0.070 1.8 0.021
 thermalfile4 KH CPX b-norm RT 80rot Wednesday, April 15, 1998 10:19 PM
 4 27 80 11 3.882 0.081 2.1 0.023
 thermalfile5 KH CPX b-norm RT 100rot Wednesday, April 15, 1998 10:37 PM
 5 27 100 12 4.320 0.069 1.6 0.023
 thermalfile6 KH CPX b-norm RT 120rot Wednesday, April 15, 1998 11:01 PM
 6 27 120 12 4.920 0.155 3.2 0.023
 thermalfile7 KH CPX b-norm RT 140rot Wednesday, April 15, 1998 11:23 PM

7	27	140	13	5.502	0.176	3.2	0.017
thermalfile8	KH CPX b-norm RT 160rot			Wednesday, April 15, 1998 11:43 PM			
8	27	160	15	5.768	0.172	3.0	0.032
thermalfile9	KH CPX b-norm RT 180rot			Thursday, April 16, 1998 12:09 AM			
9	27	180	10	5.348	0.177	3.3	0.025
Dummy entry, angle determined by retroreflection.							
-0.5	0	0	20.4				
Dummy entry, angle determined by retroreflection.							
1.5	0	0	20.517				
Dummy entry, angle determined by retroreflection.							
3.5	0	0	20.5				
Dummy entry, angle determined by retroreflection.							
6.5	0	0	20.5				
Dummy entry, angle determined by retroreflection.							
9.5	0	0	20.483				
Dummy entry, angle determined by retroreflection.							
10.5	0	0	20.45				

16 July 1998

thermalfile0	KH CPX b-norm RT 0rot			Thursday, July 16, 1998 4:11 PM			
0	27	0	11	2.427	0.012	0.5	0.017
thermalfile1	KH CPX b-norm RT 20rot			Thursday, July 16, 1998 4:45 PM			
1	27	20	6	2.769	0.029	1.0	0.025
thermalfile2	KH CPX b-norm RT 40rot			Thursday, July 16, 1998 5:06 PM			
2	27	40	4	3.068	0.050	1.6	0.031
thermalfile3	KH CPX b-norm RT 60rot			Thursday, July 16, 1998 6:18 PM			
3	27	60	2	3.178	0.079	2.5	0.062
thermalfile4	KH CPX b-norm RT 80rot			Thursday, July 16, 1998 7:09 PM			
4	27	80	8	3.103	0.037	1.2	0.021
thermalfile5	KH CPX b-norm RT 100rot			Thursday, July 16, 1998 7:31 PM			
5	27	100	7	2.742	0.014	0.5	0.023
thermalfile6	KH CPX b-norm RT 120rot			Thursday, July 16, 1998 8:06 PM			
6	27	120	3	2.361	0.050	2.1	0.044
thermalfile7	KH CPX b-norm RT 140rot			Thursday, July 16, 1998 8:30 PM			
7	27	140	2	2.148	0.037	1.7	0.055
thermalfile8	KH CPX b-norm RT 160rot			Thursday, July 16, 1998 8:55 PM			
8	27	160	3	2.146	0.068	3.2	0.044
thermalfile9	KH CPX b-norm RT 180rot			Thursday, July 16, 1998 9:18 PM			
9	27	180	6	2.405	0.011	0.5	0.025
Dummy entry, angle determined by retroreflection.							
-0.5	0	0	14.883				

Dummy entry, angle determined by retroreflection.

1.5 0 0 14.983

Dummy entry, angle determined by retroreflection.

5.5 0 0 14.967

Dummy entry, angle determined by retroreflection.

9.5 0 0 15.017

17 July 1998

thermalfile0 KH CPX a*-norm RT 0rot Friday, July 17, 1998 2:00 PM

0 27 0 4 2.503 0.039 1.6 0.032

thermalfile1 KH CPX a*-norm RT 20rot Friday, July 17, 1998 2:32 PM

1 27 20 4 2.175 0.017 0.8 0.028

thermalfile2 KH CPX a*-norm RT 40rot Friday, July 17, 1998 2:54 PM

2 27 40 4 2.033 0.021 1.0 0.032

thermalfile3 KH CPX a*-norm RT 60rot Friday, July 17, 1998 3:29 PM

3 27 60 3 2.180 0.022 1.0 0.037

thermalfile4 KH CPX a*-norm RT 80rot Friday, July 17, 1998 4:09 PM

4 27 80 6 2.488 0.024 1.0 0.027

thermalfile5 KH CPX a*-norm RT 100rot Friday, July 17, 1998 4:29 PM

5 27 100 5 2.806 0.049 1.7 0.028

thermalfile6 KH CPX a*-norm RT 120rot Friday, July 17, 1998 5:04 PM

6 27 120 8 2.971 0.030 1.0 0.016

thermalfile7 KH CPX a*-norm RT 140rot Friday, July 17, 1998 5:25 PM

7 27 140 13 3.000 0.035 1.2 0.015

thermalfile8 KH CPX a*-norm RT 160rot Friday, July 17, 1998 5:44 PM

8 27 160 12 2.786 0.035 1.3 0.017

thermalfile9 KH CPX a*-norm RT 180rot Friday, July 17, 1998 6:06 PM

9 27 180 16 2.466 0.049 2.0 0.021

Dummy entry, angle determined by retroreflection.

-0.5 0 0 15.0

Dummy entry, angle determined by retroreflection.

2.5 0 0 14.967

Dummy entry, angle determined by retroreflection.

5.5 0 0 15.1

Dummy entry, angle determined by retroreflection.

9.5 0 0 14.917

22 July 1998

thermalfile0	KH CPX b-norm RT 0rot	Wednesday, July 22, 1998 11:19 AM
0 27	0 9 10.737	1.198 11.2 0.048
thermalfile1	KH CPX b-norm RT 20rot	Wednesday, July 22, 1998 11:43 AM
1 27	20 4 8.766 1.068	12.2 0.079
thermalfile10	KH CPX b-norm RT 120rot	Wednesday, July 22, 1998 6:06 PM
10 27	120 7 9.332 1.237	13.3 0.067
thermalfile11	KH CPX b-norm RT 140rot	Wednesday, July 22, 1998 6:40 PM
11 27	140 8 10.924	1.281 11.7 0.053
thermalfile12	KH CPX b-norm RT 160rot	Wednesday, July 22, 1998 7:00 PM
12 27	160 6 11.440	1.388 12.1 0.058
thermalfile13	KH CPX b-norm RT 180rot	Wednesday, July 22, 1998 7:23 PM
13 27	180 4 10.753	1.438 13.4 0.072
thermalfile3	KH CPX b-norm RT 0rot	Wednesday, July 22, 1998 2:09 PM
3 27	0 9 10.685	1.178 11.0 0.053
thermalfile4	KH CPX b-norm RT 20rot	Wednesday, July 22, 1998 2:29 PM
4 27	20 7 9.182 0.938	10.2 0.056
thermalfile5	KH CPX b-norm RT 40rot	Wednesday, July 22, 1998 3:07 PM
5 27	40 8 8.054 0.481	6.0 0.058
thermalfile6	KH CPX b-norm RT 60rot	Wednesday, July 22, 1998 3:31 PM
6 27	60 4 7.265 0.377	5.2 0.072
thermalfile7	KH CPX b-norm RT 80rot	Wednesday, July 22, 1998 4:14 PM
7 27	80 4 7.180 0.544	7.6 0.071
thermalfile8	KH CPX b-norm RT 80rot	Wednesday, July 22, 1998 5:24 PM
8 27	80 12 7.468 0.492	6.6 0.055
thermalfile9	KH CPX b-norm RT 100rot	Wednesday, July 22, 1998 5:46 PM
9 27	100 6 8.104 0.706	8.7 0.061
Dummy entry, angle determined by retroreflection.		
1.5	0 0 29.667	
Dummy entry, angle determined by retroreflection.		
4.5	0 0 29.65	
Dummy entry, angle determined by retroreflection.		
6.5	0 0 29.783	
Dummy entry, angle determined by retroreflection.		
10.5	0 0 29.967	
Dummy entry, angle determined by retroreflection.		
13.5	0 0 29.933	

23 July 1998

thermalfile0	KH CPX a*-norm RT 0rot	Thursday, July 23, 1998 1:44 PM
0 27	0 8 6.729 0.439	6.5 0.058
thermalfile1	KH CPX a*-norm RT 20rot	Thursday, July 23, 1998 2:10 PM

1	27	20	7	7.469	0.369	4.9	0.053	
thermalfile2	KH CPX a*-norm RT 40rot						Thursday, July 23, 1998 2:29 PM	
2	27	40	16	8.552	0.835	9.8	0.056	
thermalfile3	KH CPX a*-norm RT 60rot						Thursday, July 23, 1998 3:12 PM	
3	27	60	11	10.066		1.063	10.6 0.044	
thermalfile4	KH CPX a*-norm RT 80rot						Thursday, July 23, 1998 3:34 PM	
4	27	80	21	10.857		1.195	11.0 0.044	
thermalfile5	KH CPX a*-norm RT 100rot						Thursday, July 23, 1998 3:53 PM	
5	27	100	24	10.523		1.333	12.7 0.050	
thermalfile6	KH CPX a*-norm RT 120rot						Thursday, July 23, 1998 4:17 PM	
6	27	120	10	9.583	1.016	10.6	0.048	
thermalfile7	KH CPX a*-norm RT 140rot						Thursday, July 23, 1998 4:49 PM	
7	27	140	5	8.186	0.765	9.3	0.068	
thermalfile8	KH CPX a*-norm RT 160rot						Thursday, July 23, 1998 5:24 PM	
8	27	160	3	7.732	0.468	6.1	0.091	
thermalfile9	KH CPX a*-norm RT 180rot						Thursday, July 23, 1998 5:44 PM	
9	27	180	4	6.969	0.261	3.7	0.081	
Dummy entry, angle determined by retroreflection.								
-0.5	0	0	29.933					
Dummy entry, angle determined by retroreflection.								
2.5	0	0	29.883					
Dummy entry, angle determined by retroreflection.								
6.5	0	0	29.917					
Dummy entry, angle determined by retroreflection.								
9.5	0	0	29.917					

SCchai

10 October 2000, room pressure

thermalfile28	SCchai c-norm RT 005rot						Tue, Oct 10, 2000 11:09:37 PM	
28	27	5	297	3.159	0.065	2.1	0.014	
thermalfile29	SCchai c-norm RT 025rot						Tue, Oct 10, 2000 11:18:00 PM	
29	27	25	702	3.177	0.094	3.0	0.012	
thermalfile30	SCchai c-norm RT 025rot						Tue, Oct 10, 2000 11:24:38 PM	
30	27	25	1302	3.494	0.146	4.2	0.065	
thermalfile31	SCchai c-norm RT 045rot						Tue, Oct 10, 2000 11:34:07 PM	
31	27	45	811	4.129	0.071	1.7	0.017	
thermalfile32	SCchai c-norm RT 065rot						Tue, Oct 10, 2000 11:41:52 PM	
32	27	65	637	4.975	0.057	1.1	0.009	
thermalfile33	SCchai c-norm RT 085rot						Tue, Oct 10, 2000 11:50:11 PM	

33	27	85	710	4.711	0.188	4.0	0.015	
thermalfile34	SCchai	c-norm	RT 105rot					Tue, Oct 10, 2000 11:57:22 PM
34	27	105	785	5.265	0.038	0.7	0.018	
thermalfile36	SCchai	c-norm	RT 125rot					Wed, Oct 11, 2000 12:28:59 AM
36	27	125	650	5.649	0.231	4.1	0.033	
thermalfile37	SCchai	c-norm	RT 125rot					Wed, Oct 11, 2000 12:36:38 AM
37	27	125	870	4.629	0.062	1.3	0.029	
thermalfile38	SCchai	c-norm	RT 145rot					Wed, Oct 11, 2000 12:45:56 AM
38	27	145	1761	3.468	0.293	8.4	0.111	
thermalfile40	SCchai	c-norm	RT 165rot					Wed, Oct 11, 2000 1:05:40 AM
40	27	165	1796	3.388	0.462	13.6	0.148	
thermalfile41	SCchai	c-norm	RT 165rot					Wed, Oct 11, 2000 1:11:44 AM
41	27	165	322	3.753	0.062	1.7	0.016	
thermalfile42	SCchai	c-norm	RT 145rot					Wed, Oct 11, 2000 1:25:15 AM
42	27	145	303	3.974	0.029	0.7	0.008	
thermalfile43	SCchai	c-norm	RT 125rot					Wed, Oct 11, 2000 1:33:07 AM
43	27	125	117	5.572	0.135	2.4	0.018	
thermalfile44	SCchai	c-norm	RT 125rot					Wed, Oct 11, 2000 1:38:59 AM
44	27	125	494	5.506	0.166	3.0	0.025	
thermalfile25	methanol	22.6C						Tue, Oct 10, 2000 9:40:01 PM
25	22.6	1110.7		15.325				
thermalfile35	methanol	22.8C						Wed, Oct 11, 2000 12:14:53 AM
35	22.8	1110.0		15.298				

10 October 2000, P1(R1) 3.22, P1(R2) 3.24, P2(R1) 3.21, P2(R2) 3.23 GPa

thermalfile12	SCchai3GPa	c-norm	RT 245rot					Tue, Oct 10, 2000 1:38:24 PM
12	27	245	507	4.131	0.055	1.3	0.018	
thermalfile13	SCchai3GPa	c-norm	RT 265rot					Tue, Oct 10, 2000 2:16:13 PM
13	27	265	171	4.509	0.041	0.9	0.013	
thermalfile15	SCchai3GPa	c-norm	RT 285rot					Tue, Oct 10, 2000 3:09:24 PM
15	27	285	528	5.249	0.043	0.8	0.012	
thermalfile16	SCchai3GPa	c-norm	RT 305rot					Tue, Oct 10, 2000 3:59:58 PM
16	27	305	544	6.220	0.064	1.0	0.016	
thermalfile17	SCchai3GPa	c-norm	RT 325rot					Tue, Oct 10, 2000 4:43:17 PM
17	27	325	236	7.053	0.092	1.3	0.012	
thermalfile19	SCchai3GPa	c-norm	RT 345rot					Tue, Oct 10, 2000 5:47:54 PM
19	27	345	322	7.134	0.095	1.3	0.014	
thermalfile2	SCchai3GPa	c-norm	RT 000rot					Mon, Oct 9, 2000 3:49:30 PM
2	27	180	209	8.803	0.296	3.4	0.114	
thermalfile20	SCchai3GPa	c-norm	RT 005rot					Tue, Oct 10, 2000 6:37:40 PM
20	27	185	260	6.163	0.193	3.1	0.034	

thermalfile21	SCchai3GPa c-norm RT 025rot	Tue, Oct 10, 2000 7:24:24 PM
21 27	205 500 5.706 0.233 4.1	0.034
thermalfile22	SCchai3GPa c-norm RT 205rot	Tue, Oct 10, 2000 8:07:41 PM
22 27	205 730 5.485 0.078 1.4	0.023
thermalfile23	SCchai3GPa c-norm RT 205rot	Tue, Oct 10, 2000 8:42:50 PM
23 27	205 725 5.410 0.067 1.2	0.019
thermalfile24	SCchai3GPa c-norm RT 225rot	Tue, Oct 10, 2000 9:33:26 PM
24 27	225 833 4.549 0.133 2.9	0.032
thermalfile27	SCchai3GPa c-norm RT 225rot	Tue, Oct 10, 2000 10:30:13 PM
27 27	225 402 3.620 0.146 4.0	0.020
thermalfile3	SCchai3GPa c-norm RT 000rot	Mon, Oct 9, 2000 3:58:54 PM
3 27	180 208 7.115 0.253 3.6	0.033
thermalfile4	SCchai3GPa c-norm RT 000rot	Mon, Oct 9, 2000 4:17:01 PM
4 27	180 220 6.706 0.103 1.5	0.020
thermalfile5	SCchai3GPa c-norm RT 245rot	Mon, Oct 9, 2000 4:56:31 PM
5 27	245 73 4.332 0.048 1.1	0.020
thermalfile6	SCchai3GPa c-norm RT 245rot	Mon, Oct 9, 2000 5:12:27 PM
6 27	245 64 4.335 0.054 1.3	0.018
thermalfile9	SCchai3GPa c-norm RT 017rot	Mon, Oct 9, 2000 6:43:28 PM
9 27	197 162 6.208 0.054 0.9	0.015
thermalfile0	methanol 22.4C	Mon, Oct 9, 2000 3:20:00 PM
0 22.4	1111.3 15.261	
thermalfile10	methanol 21.6C	Tue, Oct 10, 2000 12:15:37 PM
10 21.6	1113.9 15.308	
thermalfile14	methanol 22.4C	Tue, Oct 10, 2000 2:31:13 PM
14 22.4	1111.3 15.322	
thermalfile18	methanol 22.6C	Tue, Oct 10, 2000 5:08:06 PM
18 22.6	1110.7 15.308	
thermalfile25	methanol 22.6C	Tue, Oct 10, 2000 9:40:01 PM
25 22.6	1110.7 15.324	
thermalfile7	methanol 23.2C	Mon, Oct 9, 2000 5:37:22 PM
7 23.2	1108.8 15.251	
thermalfile8	methanol 23.3C	Mon, Oct 9, 2000 6:19:34 PM
8 23.3	1108.4 15.264	

11 October 2000, room pressure

thermalfile1	SCchai c-norm RT 120rot	Wed, Oct 11, 2000 11:48:38 AM
1 27	120 193 5.301 0.023 0.5 0.010	
thermalfile10	SCchai c-norm RT 280rot	Wed, Oct 11, 2000 1:20:09 PM
10 27	280 269 5.912 0.065 1.1 0.010	
thermalfile11	SCchai c-norm RT 300rot	Wed, Oct 11, 2000 1:28:04 PM

11	27	300	187	5.351	0.055	1.0	0.011
thermalfile2	SCchai c-norm RT 140rot						Wed, Oct 11, 2000 11:55:25 AM
2	27	140	361	4.431	0.019	0.5	0.013
thermalfile3	SCchai c-norm RT 160rot						Wed, Oct 11, 2000 12:03:40 PM
3	27	160	133	3.616	0.052	1.4	0.015
thermalfile4	SCchai c-norm RT 180rot						Wed, Oct 11, 2000 12:14:06 PM
4	27	180	308	3.476	0.053	1.5	0.011
thermalfile5	SCchai c-norm RT 200rot						Wed, Oct 11, 2000 12:26:24 PM
5	27	200	230	3.758	0.008	0.5	0.009
thermalfile7	SCchai c-norm RT 220rot						Wed, Oct 11, 2000 12:51:56 PM
7	27	220	147	4.539	0.024	0.5	0.012
thermalfile8	SCchai c-norm RT 240rot						Wed, Oct 11, 2000 12:58:25 PM
8	27	240	149	5.468	0.033	0.6	0.011
thermalfile9	SCchai c-norm RT 260rot						Wed, Oct 11, 2000 1:07:34 PM
9	27	260	192	6.071	0.062	1.0	0.011
thermalfile0	methanol 21.7C		Wed, Oct 11, 2000 11:37:51 AM				
0	21.7	1113.6	15.249				
thermalfile6	methanol 22.2C		Wed, Oct 11, 2000 12:43:48 PM				
6	22.2	1112.0	15.291				

18 October 2000, 3.22 GPa

thermalfile10	SCchai3GPa c-norm RT 080rot						Wed, Oct 18, 2000 4:53:42 PM
10	27	80	180	7.355	0.133	1.8	0.018
thermalfile11	SCchai3GPa c-norm RT 100rot						Wed, Oct 18, 2000 5:07:04 PM
11	27	100	188	8.608	0.090	1.0	0.011
thermalfile12	SCchai3GPa c-norm RT 060rot						Wed, Oct 18, 2000 5:20:09 PM
12	27	60	253	7.854	0.097	1.2	0.013
thermalfile13	SCchai3GPa c-norm RT 040rot						Wed, Oct 18, 2000 5:37:14 PM
13	27	40	197	8.707	0.054	0.6	0.011
thermalfile14	SCchai3GPa c-norm RT 020rot						Wed, Oct 18, 2000 6:15:31 PM
14	27	20	178	9.759	0.048	0.5	0.015
thermalfile16	SCchai3GPa c-norm RT 000rot						Wed, Oct 18, 2000 7:02:08 PM
16	27	0	102	10.891	0.122	1.1	0.017
thermalfile17	SCchai3GPa c-norm RT 340rot						Wed, Oct 18, 2000 7:26:25 PM
17	27	160	72	11.808	0.198	1.7	0.027
thermalfile15	methanol 24.0C		Wed, Oct 18, 2000 6:34:31 PM				
15	24.0	1106.2	20.304				
thermalfile8	methanol 23.6C		Wed, Oct 18, 2000 3:38:21 PM				
8	23.6	1107.5	20.292				

18 October 2000, P(R1) 5.09, P(R2) 5.08 GPa

thermalfile19	SCchai5GPa c-norm RT 340rot	Wed, Oct 18, 2000 8:54:53 PM
19 27	340 199 12.367 0.085 0.7 0.010	
thermalfile20	SCchai5GPa c-norm RT 320rot	Wed, Oct 18, 2000 9:23:10 PM
20 27	320 143 10.468 0.241 2.3 0.015	
thermalfile21	SCchai5GPa c-norm RT 300rot	Wed, Oct 18, 2000 9:57:03 PM
21 27	300 407 8.766 0.338 3.9 0.021	
thermalfile18	methanol 23.9C	Wed, Oct 18, 2000 8:37:36 PM
18 23.9	1106.5 20.295	

19 October 2000, P(R1) 5.09, P(R2) 5.13 GPa

thermalfile11	SCchai5GPa c-norm RT 250rot	Thu, Oct 19, 2000 6:03:07 PM
11 27	250 165 7.380 0.158 2.1 0.019	
thermalfile2	SCchai5GPa c-norm RT 340rot	Thu, Oct 19, 2000 3:48:37 PM
2 27	340 193 12.189 0.052 0.5 0.018	
thermalfile3	SCchai5GPa c-norm RT 320rot	Thu, Oct 19, 2000 4:02:14 PM
3 27	320 228 12.178 0.270 2.2 0.017	
thermalfile4	SCchai5GPa c-norm RT 300rot	Thu, Oct 19, 2000 4:21:12 PM
4 27	300 232 10.462 0.037 0.5 0.007	
thermalfile5	SCchai5GPa c-norm RT 280rot	Thu, Oct 19, 2000 4:36:57 PM
5 27	280 247 9.040 0.080 0.9 0.013	
thermalfile6	SCchai5GPa c-norm RT 260rot	Thu, Oct 19, 2000 4:50:40 PM
6 27	260 309 7.983 0.078 1.0 0.009	
thermalfile7	SCchai5GPa c-norm RT 240rot	Thu, Oct 19, 2000 5:04:58 PM
7 27	240 303 7.662 0.033 0.5 0.008	
thermalfile8	SCchai5GPa c-norm RT 220rot	Thu, Oct 19, 2000 5:20:04 PM
8 27	220 228 8.673 0.022 0.5 0.010	
thermalfile0	methanol 22.9C	Thu, Oct 19, 2000 2:57:51 PM
0 22.9	1109.7 20.288	
thermalfile10	methanol 23.8C	Thu, Oct 19, 2000 5:42:41 PM
10 23.8	1106.8 20.284	
thermalfile9	methanol 23.8C	Thu, Oct 19, 2000 5:33:50 PM
9 23.8	1106.8 20.282	

19 October 2000, room pressure

thermalfile12	SCchai c-norm RT 090rot	Thu, Oct 19, 2000 6:26:17 PM
---------------	-------------------------	------------------------------

12	27	90	139	7.597	0.061	0.8	0.009
thermalfile13	SCchai c-norm	RT 070rot				Thu, Oct 19, 2000 6:32:47 PM	
13	27	70	348	6.346	0.036	0.6	0.008
thermalfile14	SCchai c-norm	RT 070rot				Thu, Oct 19, 2000 6:35:59 PM	
14	27	70	355	6.282	0.058	0.9	0.009
thermalfile15	SCchai c-norm	RT 050rot				Thu, Oct 19, 2000 6:40:39 PM	
15	27	50	351	5.792	0.028	0.5	0.010
thermalfile16	SCchai c-norm	RT 030rot				Thu, Oct 19, 2000 6:49:49 PM	
16	27	30	296	6.591	0.038	0.6	0.009
thermalfile17	SCchai c-norm	RT 010rot				Thu, Oct 19, 2000 6:56:46 PM	
17	27	10	201	7.852	0.088	1.1	0.014
thermalfile18	SCchai c-norm	RT 110rot				Thu, Oct 19, 2000 7:02:24 PM	
18	27	110	227	9.319	0.154	1.7	0.015
thermalfile19	SCchai c-norm	RT 130rot				Thu, Oct 19, 2000 7:08:51 PM	
19	27	130	163	9.944	0.105	1.1	0.014
thermalfile20	SCchai c-norm	RT 150rot				Thu, Oct 19, 2000 7:15:08 PM	
20	27	150	163	9.907	0.120	1.2	0.015
thermalfile21	SCchai c-norm	RT 140rot				Thu, Oct 19, 2000 7:21:16 PM	
21	27	140	185	10.333		0.130 1.3	0.012
thermalfile10	methanol 23.8C					Thu, Oct 19, 2000 5:42:41 PM	
10	23.8	1106.8		20.285			

Appendix B: MATLAB Files Used in Processing the Data

"The sign as the mark of a lack refers to the necessary absence of that which the sign refers to [*sic*]. If I want to make reference to a cow, I can say the word 'cow,' draw a picture of a cow, or pantomime a cow. Each of these are signs representing the cow, but the cow to which the sign refers is not actually present in any of the signs."

(Westlind, 1996, p. 64)

The following MATLAB routines were written for the purpose of processing the impulsive stimulated light scattering data gathered in the course of this work. In several cases some of the code was copied from routines written and modified by members of the High Pressure Mineral Physics Laboratory over a period of several years, though no previous versions were designed to process large batches of files automatically. In order to use these routines, the format for comments, as entered in LabVIEW before the raw data are saved, must match that shown in the first line of each entry in Appendix A. If necessary, comments may be modified with `edit_comments.m`.

An entire folder of thermalfiles may be fit at once with `fit_entire_folder.m` and `fit_entire_folder_standards.m`. Each will call several other m-files (located in the same folder as these two routines) and each will place into the folder of data a text file, for the former called "decays" and for the latter "standards" to be used in the next step. For the materials in this study, the contents of these files constitute the entries in Appendix A.

The routine `reading_decays.m` will open "decays" and "standards" for a specified folder, parse the contents, sort the data by temperature and match each entry with the appropriate standard(s), then fit each round of data with both variable and fixed offsets. It will save the results, again in the data folder, to a file called "diffusivities" and plot the results at each temperature as well as the tensor values as a function of temperature. It also calls several other routines that are located with it.

The conductivity model is executed in several steps: First, the routine `schatz.m` is run, followed by a file containing the appropriate isotropic diffusivities and material properties for the desired composition. `SCOLV.m` is an example of the format. Next, `conductivity_data.m` is executed, and finally the appropriately modified `meanfreepath.m` routine, such as `meanfreepathSCOLV.m`. Much of this should be rewritten before put into general use.

These routines are archived on several computers in the High Pressure Mineral Physics Laboratory.

Vita

Michael Damian Harrell

Doctor of Philosophy, 2002, University of Washington, Seattle, Washington

Master of Science, 1994, University of Oregon, Eugene, Oregon

**Bachelor of Arts, 1991, Robert Donald Clark Honors College, University of Oregon,
Eugene, Oregon**